

**Genetic and epigenetic regulation of candidate genes  
associated with pseudoexfoliation**

*By*

**KAPUGANTI RAMANI SHYAM**

**Enrolment No. LIFE11201604014**

**NATIONAL INSTITUTE OF SCIENCE EDUCATION AND RESEARCH  
BHUBANESWAR**

*A thesis submitted to the*

*Board of Studies in Life Sciences*

*In partial fulfilment of requirements*

*For the Degree of*

**DOCTOR OF PHILOSOPHY**

*of*

**HOMI BHABHA NATIONAL INSTITUTE**



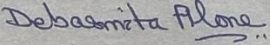
**September, 2023**

Homi Bhaba National Institute

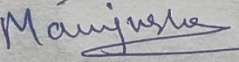
Recommendations of the Viva Voce Committee

As members of the Viva Voce Committee, we certify that we have read the dissertation prepared by **Kapuganti Ramani Shyam** entitled "**Genetic and epigenetic regulation of candidate genes associated with pseudoexfoliation**" and recommend that it may be accepted as fulfilling the thesis requirement for the award of Degree of Doctor of Philosophy.

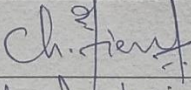
Chairman – Dr. Chandan Goswami  Date: 18/09/2023

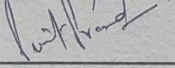
Guide / Convener – Dr. Debasmita P. Alone  Date: 18/9/2023

Examiner – Prof. Jayandharan G. Rao  Date: 18.9.23

Member 1 – Dr. Manjusha Dixit  Date: 18.9.23

Member 2 – Dr. Pankaj V. Alone  Date: 18/9/2023

Member 3 – Dr. Tirumala K. Chowdary  Date: 18/9/2023

Member 4 – Dr. Punit Prasad  Date: 18/09/2023

Final approval and acceptance of this thesis is contingent upon the candidate's submission of the final copies of the thesis to HBNI.

I/We hereby certify that I/we have read this thesis prepared under my/our direction and recommend that it may be accepted as fulfilling the thesis requirement.

Date: 18/9/2023

Place: Jaboti

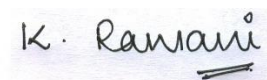
Signature

Guide DEBASMITA P. ALONE

## **STATEMENT BY AUTHOR**

This dissertation has been submitted in partial fulfilment of requirements for an advanced degree at Homi Bhabha National Institute (HBNI) and is deposited in the library to be made available to borrowers under rules of the HBNI.

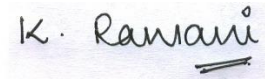
Brief quotations from this dissertation are allowable without any special permission, provided accurate acknowledgement of the source is made. Requests for permission for extended quotation from or reproduction of this manuscript in whole or in part may be granted by the competent authority of HBNI when in his or her judgment the proposed use of the material is in the interests of the scholarship. In all other instances, however, permission must be obtained from the author.

A handwritten signature in black ink that reads "K. Ramani Shyam". The signature is written in a cursive style with a small circle above the 'i' in "Shyam". There are two horizontal lines drawn below the signature.

**K. Ramani Shyam**

## **DECLARATION**

I, hereby, declare that the investigation presented in the thesis has been carried out by me. The work is original and has not been submitted earlier as a whole or in part for a degree/diploma at this or any other Institution/ University.

A handwritten signature in black ink that reads "K. Ramani Shyam". The signature is written in a cursive style with a small flourish at the end.

**K. Ramani Shyam**

## List of Publications arising from the thesis

### Publications in Refereed Journals:

a) Published:

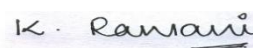
1. **Kapuganti Ramani Shyam**, Pranjya Paramita Mohanty, Debasmita Pankaj Alone. Quantitative analysis of circulating levels of vimentin, clusterin and fibulin-5 in patients with pseudoexfoliation syndrome and glaucoma. *Experimental Eye Research*. Nov 2022; 224:109236 (pg 1-9). 10.1016/j.exer.2022.109236.
2. **Kapuganti Ramani Shyam**, Barsha Bharati, Pranjya Paramita Mohanty, Debasmita Pankaj Alone. Genetic variants and haplotypes in fibulin-5 (*FBLN5*) are associated with pseudoexfoliation glaucoma but not with pseudoexfoliation syndrome. Mar 2023; 43(3):BSR20221622 (pg 1-12). 10.1042/BSR20221622.
3. **Kapuganti Ramani Shyam**, Bushra Hayat, Pranjya Paramita Mohanty, Debasmita Pankaj Alone. Dickkopf-1 and ROCK2 upregulation and associated protein aggregation in pseudoexfoliation syndrome and glaucoma. *Life Sciences*. Aug 2023; 326:121797 (pg 1-14). 10.1016/j.lfs.2023.121797.
4. **Kapuganti Ramani Shyam**, Bushra Hayat, Pranjya Paramita Mohanty, Debasmita Pankaj Alone. Role of clusterin gene 3'-UTR polymorphisms and promoter hypomethylation in the pathogenesis of pseudoexfoliation syndrome and pseudoexfoliation glaucoma. *BBA-Gene Regulatory Mechanisms*. Aug 2023; 1866(4):194980 (pg 1-15). 10.1016/j.bbagr.2023.194980.
5. **Kapuganti Ramani Shyam** and Debasmita Pankaj Alone. Current understanding of genetics and epigenetics in pseudoexfoliation syndrome and glaucoma. *Molecular Aspects of Medicine*. (*Accepted*)

b) Manuscript under preparation:

1. **Kapuganti Ramani Shyam**, Pranjya Paramita Mohanty, Debasmita Pankaj Alone. Expression profile of glutathione-S-transferases and their regulation in pseudoexfoliation syndrome and glaucoma.

### Conference proceedings:

1. **Kapuganti Ramani Shyam**, Bushra Hayat, Biswajit Padhy, Pranjya Paramita Mohanty, Debasmita Pankaj Alone. Genetic and epigenetic regulation of chaperones in the pathogenesis of pseudoexfoliation syndrome and glaucoma. European Conference on Human Genetics, ESHG 2020.2 Jun 6-9, 2020, Poster Presentation.
2. **Kapuganti Ramani Shyam**, Biswajit Padhy, Bushra Hayat, Pranjya Paramita Mohanty, Debasmita Pankaj Alone. Fibulin-5, a matricellular protein in the progression of pseudoexfoliation. Indian Eye Research Group (IERG) ARVO International Conference 2018, LV Prasad Eye Institute, Hyderabad, Oral Presentation.



**K. Ramani Shyam**

## **Dedication**

*This thesis is dedicated to my dear grandmother and soulmate, Krishnakumari.*

## **Acknowledgements**

First and foremost, I thank the Lord Almighty for being the pillars of cloud and fire all throughout my PhD journey.

I extend my profound gratitude to my supervisor, Dr. Debasmita P. Alone for her endless support, guidance and love. I thank the Director, Prof. Sudhakar Panda for providing necessary lab amenities and instrumentation facilities and NISER DAE for the fellowship during my PhD tenure.

I acknowledge my Doctoral Committee members, Dr. Chandan Goswami, Dr. Manjusha Dixit, Dr. Pankaj V. Alone, Dr. Punit Prasad and Dr. Tirumala K. Chowdary for their critical comments, valuable suggestions and feedback in my Thesis. I extend my deepest gratitude to our clinical collaborators, Dr Pranjya P Mohanty and Dr. Sucheta Parija and the volunteers without whom this thesis wouldn't have been possible.

I sincerely thank the past and current lab mates namely, Dr. Gargi, Dr. Biswajit, Dr. Bushra, Mr. Maynak and my dear chingus Sushree, Lipsa, Sushmita, Sravani, Swag, Rudra, Dr. Haritha, Subhadra, Punya, Barsha, Deepak, Archita, DJ, Rajesh, Senjit, Anup, Bala, Akash, Akhil, Abhijit, and a special thanks to Bhagyashree and Pragnya for collection of patient samples.

I am grateful to my friends and batchmates, Aranya, Bratati, Chandan, Prerna, Ram, Saptarshi, Tatha, Vinay for their help and keeping up with my tantrums. A special thanks to my friends Mukesh and Trisha for the research-related discussions and a friendly chat after a long day. I am grateful to my 'badminton friends' for infusing me with energy on a dull day.

I am forever indebted to my family and relatives for their blessings, prayers and patience.

# Contents

<b>Abstract.....</b>	<b>1</b>
<b>List of Figures.....</b>	<b>3</b>
<b>List of Tables .....</b>	<b>6</b>
<b>List of Abbreviations .....</b>	<b>7</b>
<b>1. Introduction and review of literature .....</b>	<b>11</b>
1.1. Composition of exfoliative material .....	12
1.2. Pathology of pseudoexfoliation syndrome .....	13
1.3. Pathology of pseudoexfoliation glaucoma .....	14
1.4. Demographics and prevalence of pseudoexfoliation.....	15
1.5. Theories associated with causation and progression of pseudoexfoliation .....	17
1.6. Ocular and non-ocular complications associated with pseudoexfoliation.....	18
1.7. Risk factors involved in pseudoexfoliation progression.....	19
1.8. Molecular and cellular pathways implicated in pseudoexfoliation pathology .....	32
1.9. Lacunae and unanswered questions in the field .....	36
<b>2. Association of genetic variants within fibulin-5 with PEX .....</b>	<b>39</b>
2.1. Introduction .....	39
2.2. Materials and methods.....	41
2.2.1. Study subjects' recruitment and sample collection.....	41
2.2.2. DNA isolation from blood .....	42
2.2.3. Taqman SNP genotyping assay .....	43
2.2.4. Cloning techniques.....	44
2.2.5. Plasmid isolation.....	45
2.2.6. Cell culture.....	46
2.2.7. Luciferase assay .....	46
2.2.8. Electrophoretic mobility shift assay (EMSA).....	47
2.2.9. <i>In silico</i> analysis.....	48
2.2.10. Genetic and statistical analysis .....	48
2.3. Results .....	49
2.3.1. Demographics of the study subjects .....	49
2.3.2. Intronic variants, rs72705342 and rs17732466, within <i>FBLN5</i> are genetically associated with PEXG.....	49
2.3.3. Haplotypes in the Tag SNPs of <i>FBLN5</i> are associated with PEXG .....	54

2.3.4. Haplotypes of Tag SNPs and previously reported SNPs in <i>FBLN5</i> gene are associated with PEXS and PEXG .....	56
2.3.5. rs72705342 shows an allele-specific regulatory effect.....	61
2.3.6. Risk allele ‘C’ at rs72705342 showed greater protein binding affinity compared to the ‘T’ allele.....	63
2.4. Discussion.....	66
<b>3. Mechanism of regulation of clusterin in the pathogenesis of PEX.....</b>	<b>71</b>
3.1. Introduction .....	71
3.2. Materials and methods.....	73
3.2.1. Study subjects’ selection, recruitment, and sample collection .....	73
3.2.2. DNA isolation from blood .....	73
3.2.3. Polymerase Chain Reaction .....	74
3.2.4. Gel elution.....	75
3.2.5. Bisulfite conversion .....	75
3.2.6. Sequencing PCR, Clean up, and Sequencing.....	76
3.2.7. RNA extraction, cDNA conversion, and quantitative real-time PCR .....	78
3.2.8. Protein isolation .....	79
3.2.9. Western blotting.....	80
3.2.10. Cell culture.....	81
3.2.11. Plasmid construction and luciferase assay .....	81
3.2.12. <i>In silico</i> analysis.....	82
3.2.13. Chromatin immunoprecipitation.....	82
3.2.14. Genetic and Statistical analysis.....	83
3.3. Results .....	84
3.3.1. Demographics of the study subjects .....	84
3.3.2. 3’-UTR variants of <i>CLU</i> , rs9331942 and rs9331949 are genetically associated with PEX.....	84
3.3.3. Genotypic association of 3’-UTR SNPs in <i>CLU</i> with PEX.....	86
3.3.4. Haplotypes at ‘rs9331942-rs9331949-rs9331950’ are associated with PEX .....	86
3.3.5. Bioinformatic analysis- binding sites of miRNAs are predicted to be affected by the 3’-UTR variants .....	91
3.3.6. Risk variants at rs9331942 and rs9331949 have a functional significance .....	92
3.3.7. <i>CLU</i> promoter is hypomethylated in pseudoexfoliation patients .....	94
3.3.8. Clusterin promoter hypomethylation corroborates with decreased <i>DNMT1</i> .....	98
3.3.9. DNA methylation inhibitor, 5-aza-dC induced increased Sp-1 binding to hypomethylated region in the promoter and higher expression of <i>CLU</i> .....	100

3.4. Discussion.....	103
<b>4. Protein aggregation and vimentin in PEX pathology.....</b>	<b>110</b>
4.1. Introduction .....	110
4.2. Materials and Methods .....	112
4.2.1. Study subjects' selection, recruitment, and sample collection .....	112
4.2.2. Quantitative Real time-PCR (qRT- PCR) for mRNA expression studies .....	112
4.2.3. Western blotting.....	113
4.2.4. Immunostaining .....	113
4.2.5. Cell culture.....	114
4.2.6. Plasmid construction and transfection for DKK1 overexpression and knockdown experiments .....	114
4.2.7. Aggresome detection and double labelling.....	115
4.2.8. Statistical analysis.....	116
4.3. Results .....	116
4.3.1. Vimentin is upregulated in the lens capsule and the aqueous humor of pseudoexfoliation.....	116
4.3.2. Increased formation of protein aggregates in the lens capsule of pseudoexfoliation and DKK1 overexpressed human lens epithelial cells .....	119
4.3.3. DKK1 regulates the Wnt pathway gene, ROCK2 and vimentin in HLE B-3 cells .....	122
4.3.4. DKK1 regulates vimentin expression and protein aggregation via ROCK2 in HLE B-3 cells .....	123
4.4. Discussion.....	126
<b>5. Regulation of glutathione-S-transferases in PEX.....</b>	<b>130</b>
5.1. Introduction .....	130
5.2. Materials and Methods .....	132
5.2.1. Study subjects' selection, recruitment, and sample collection .....	132
5.2.2. Quantitative Real time-PCR (qRT- PCR) for mRNA expression studies .....	133
5.2.3. Protein isolation and western blotting.....	134
5.2.4. Immunostaining .....	134
5.2.5. DNA extraction and bisulfite sequencing.....	135
5.2.6. Statistical analysis.....	135
5.3. Results .....	135
5.3.1. Differential expression of <i>GST</i> genes in PEXS compared to controls.....	135
5.3.2. <i>GSTP1</i> is downregulation in PEXS patients.....	136
5.3.3. <i>In silico</i> identification of CpG islands in <i>GSTP1</i> .....	137

5.3.4. DNA methylation status of <i>GSTP1</i> in PEXS individuals .....	138
5.4. Discussion.....	141
<b>6. Potential biomarkers and novel genetic variants for PEX.....</b>	<b>146</b>
6.1. Introduction .....	146
6.2. Materials and Methods .....	148
6.2.1. Study subjects' selection, recruitment, and sample collection .....	148
6.2.2. Enzyme-linked immunosorbent assay (ELISA) .....	148
6.2.2.1. ELISA of fibulin-5 and vimentin .....	148
6.2.2.2. ELISA of clusterin .....	149
6.2.3. Full gene sequencing of <i>FBLN5</i> , <i>CLU</i> and <i>VIM</i> genes.....	150
6.2.4. Statistical analysis .....	151
6.3. Results .....	152
6.3.1. Demographics of the study subjects .....	152
6.3.2. Plasma fibulin-5 levels did not show differences between controls and patients .....	153
6.3.3. Increased plasma levels of clusterin in PEXS.....	154
6.3.4. Increased levels of vimentin in aqueous humor of PEX affected individuals ..	157
6.3.5. Increased plasma level of vimentin has the potential to be used as a biomarker for PEX .....	159
6.3.5. Single nucleotide polymorphisms identified in <i>FBLN5</i> gene in PEX patients .	163
6.3.6. Single nucleotide polymorphisms identified in <i>CLU</i> gene in PEX patients.....	177
6.3.7. Single nucleotide polymorphisms identified in the <i>VIM</i> gene in PEX patients	181
6.4. Discussion.....	183
<b>7. Conclusions and future perspectives.....</b>	<b>192</b>
7.1. Role of fibulin-5 polymorphisms in pseudoexfoliation pathology.....	192
7.2. Regulatory mechanisms of clusterin in pseudoexfoliation pathogenesis .....	193
7.3. Regulation of glutathione-S-transferases in pseudoexfoliation.....	194
7.4. Novel association of vimentin with pseudoexfoliation .....	195
7.5. Summary at a Glance.....	196
7.6. Key findings from the study .....	197
7.7. Future perspectives .....	199
<b>8. References.....</b>	<b>201</b>
<b>APPENDIX-I.....</b>	<b>220</b>

## **Abstract**

Pseudoexfoliation (PEX) is a protein aggregopathy most commonly seen in people aged above 60 years and accounts for one of the major causes of secondary glaucoma worldwide. It is a progressive disease involving the deposition of extracellular fibrillar material throughout the body with clear ocular manifestation. The early stage of the disease is termed pseudoexfoliation syndrome (PEXS), and the advanced stage is known as pseudoexfoliation glaucoma (PEXG). PEX causation and progression involve a complex interplay of genetic and epigenetic factors. Despite extensive research in this field over the last three decades, the exact etiology of PEX remains elusive with limited availability of biomarkers for early disease detection. This warrants the identification of novel risk factors and pathways in its pathogenesis.

For the work detailed in my Thesis, the contribution of four genes, fibulin-5 (extracellular scaffold protein), clusterin (molecular chaperone), vimentin (intermediate filament), and glutathione-S-transferase (antioxidant defense enzyme) in PEX pathology has been studied.

Genetic association studies identified variants and haplotypes in the intronic region and 3'-UTR of fibulin-5 and clusterin as risk factors for PEX, and molecular assays identified functional variants within these genes. Further, promoter methylation analysis studies showed that clusterin could be regulated via promoter CpG hypomethylation in PEX which was validated through in vitro molecular assays in human lens epithelial cells. Gene expression studies revealed the downregulation of glutathione-S-transferase P1 and vimentin with PEX. We also identified a plausible role of Dickkopf-1, a Wnt signaling antagonist, in protein aggregation and vimentin regulation in PEX. Finally, we assessed the candidature of fibulin-5, clusterin, and vimentin as potential biomarkers for PEX. Our

studies revealed that plasma vimentin levels could distinguish between non-PEX control and PEX with good sensitivity and specificity and also have the potential to distinguish between the early PEXS and the advanced PEXG stages of the disease. We have also initiated a targeted search for polymorphisms in fibulin-5, clusterin, and vimentin genes that are associated with PEX in the Indian population and might have a functional role.

Overall, results from my thesis not only reiterated the involvement of both genetic and epigenetic factors in PEX pathology by identifying novel risk factors and understanding the pathogenesis but also identified a potential biomarker for early detection of PEX.

## List of Figures

Figure 1.1. Anatomy of the human eye.....	11
Figure 1.2. Clinical picture of human eye with pseudoexfoliation syndrome.....	13
Figure 1.3. Characteristic features of pseudoexfoliation glaucoma.....	14
Figure 1.4. Graphical representation of the prevalence of PEX across the globe .....	16
Figure 1.5. Role of epigenetic silencing of LOXL1 and HSP70 in PEX pathogenesis.....	29
Figure 2.1. Role of fibulin-5 in elastogenesis .....	39
Figure 2.2. Position of Tag SNPs.....	50
Figure 2.3. Linkage disequilibrium pattern and haplotype association analysis. ....	54
Figure 2.4. Putative regulatory effect of <i>FBLN5</i> variants.....	62
Figure 2.5. Binding of nuclear proteins to rs72705342 .....	63
Figure 2.6. Competitive EMSA on rs72705342. ....	64
Figure 2.7. <i>In-silico</i> prediction of transcription factors binding to rs72705342 element .....	65
Figure 2.8. Binding of specific transcription factors to rs72705342 .....	66
Figure 2.9. rs72705342 is an eQTL for <i>FBLN5</i> expression.....	68
Figure 3.1. Gene structure of clusterin with SNPs.....	85
Figure 3.2. LD block pattern generated by Haploview.....	87
Figure 3.3. Location of binding of microRNAs to 3'-UTR of <i>CLU</i> at rs9331942 and rs9331949.....	91
Figure 3.4. rs9331942 and rs9331949 showed differential luciferase activity. ....	93
Figure 3.5. Promoter methylation pattern of clusterin in the blood cells of PEX versus controls.....	95
Figure 3.6. Promoter methylation pattern of clusterin in the lens capsule of PEX versus controls.....	97
Figure 3.7. Effect of DNMT1 overexpression on clusterin in HLE B-3 cells .....	99
Figure 3.8. Effect of 5-Aza-dC on clusterin expression in HLE B-3 cells .....	101
Figure 3.9. Effect of clusterin promoter demethylation on Sp-1 binding.....	103
Figure 4.1. Vimentin is upregulated in the lens capsule of PEX-affected individuals .....	117
Figure 4.2. Increased vimentin levels in aqueous humor of PEX patients .....	118
Figure 4.3. Increased vimentin expression in lens capsule in PEX patients through immunostaining.....	118
Figure 4.4. Presence of aggresomes in the lens capsule of PEXS and PEXG.....	119

Figure 4.5. Presence of aggresomes in LC and HLE B-3 cells overexpressed with pCMV-DKK1 .....	121
Figure 4.6. Presence of protein aggregates in HLE B-3 cells overexpressed with pCMV-DKK1 .....	122
Figure 4.7. Dysregulation ROCK2 and VIM in cells transfected with DKK1-siRNA.....	123
Figure 4.8. Effect of ROCK inhibitor Y-27632 on ROCK2 and VIM expression in HLE B-3 cells .....	124
Figure 4.9. DKK1 regulates protein aggregation via ROCK2 in HLE B-3 cells.....	125
Figure 5.1. Role of glutathione-S-transferases inside the cell .....	131
Figure 5.2. <i>GSTP1</i> mRNA is downregulated in the lens capsule of PEXS-affected individuals .....	136
Figure 5.3. <i>GSTP1</i> is downregulated in the lens capsule of PEXS-affected individuals .....	137
Figure 5.4. In-silico identification of CpG islands in the promoter of <i>GSTP1</i> .....	138
Figure 5.5. Promoter methylation pattern of <i>GSTP1</i> in blood cells of PEXS versus controls .....	140
Figure 5.6. Promoter methylation pattern of <i>GSTP1</i> in the lens capsule of PEXS versus controls.....	141
Figure 6.1. Levels of plasma fibulin-5 in controls, PEXS and PEXG.....	154
Figure 6.2. Levels of plasma clusterin in controls, PEXS and PEXG and receiver operating characteristic curves.....	155
Figure 6.3. Receiver operating characteristic curves of plasma clusterin.....	156
Figure 6.4. Levels of aqueous humor vimentin in controls, PEXS and PEXG .....	157
Figure 6.5. Receiver operating characteristic curves of vimentin levels .....	158
Figure 6.6. Levels of plasma vimentin in controls, PEXS and PEXG.....	160
Figure 6.7. Levels of plasma clusterin in controls, PEXS and PEXG and receiver operating characteristic curves.....	161
Figure 6.8. Correlation between plasma and aqueous humor vimentin.....	163
Figure 6.9. Gene structure of fibulin-5 .....	164
Figure 6.10. Distribution of variants in <i>FBLN5</i> gene in controls, PEXS and PEXG .....	177
Figure 6.11. Gene structure of clusterin.....	178
Figure 6.12. Distribution of variants in <i>CLU</i> gene in controls, PEXS and PEXG .....	179
Figure 6.13. Gene structure of vimentin .....	179
Figure 6.14. Distribution of variants in <i>VIM</i> gene in controls, PEXS and PEXG.....	182
Figure 6.15. rs7982 is an eQTL for <i>CLU</i> expression.....	189

Figure 6.16. rs3758410 is an eQTL for *VIM* expression ..... 190

Figure 7.1. A hypothetical model showing the factors contributing to pseudoexfoliation pathology..... 197

## List of Tables

Table 2.1. Tag SNPs in <i>FBLN5</i> (Chr 14, hg38 build) chosen for this study.....	43
Table 2.2. List of oligos used in the study .....	47
Table 2.3. Demographic details of the study subjects .....	49
Table 2.4. Distribution of <i>FBLN5</i> variants in PEXS and PEXG compared to the controls.....	51
Table 2.5. Genotypic distribution of <i>FBLN5</i> variants in control, PEXS and PEXG .....	52
Table 2.6. Haplotype association of Tag SNPs of <i>FBLN5</i> with PEXS and PEXG .....	55
Table 2.7. Haplotype distribution of <i>FBLN5</i> variants in block 2 of controls, PEXS and PEXG.....	55
Table 2.8. Haplotype distribution of all <i>FBLN5</i> variants studied in controls, PEXS and PEXG .....	57
Table 2.9. Haplotype distribution at rs12432450-rs7149187 in controls, PEXS and PEXG ..	60
Table 2.10. Haplotype distribution at rs929608-rs72705342-rs17732466-rs7149187 in controls, PEXS and PEXG.....	60
Table 3.1. List of oligos used in the study .....	83
Table 3.2. Demographics of the study subjects .....	84
Table 3.3. Genetic association of 3'-UTR variants in PEX versus control .....	88
Table 3.4. Genetic Models and genotypic distribution of <i>CLU</i> 3'-UTR variants in PEX.....	89
Table 3.5. Haplotype distribution of the 3'UTR variants .....	90
Table 3.6. Predicted transcription factor binding sites to CpGs in <i>CLU</i> region I.....	102
Table 5.1. Oligos used in the study.....	133
Table 6.1. List of oligos used in the study .....	151
Table 6.2. Demographics of study subjects included for ELISA in aqueous humor and plasma samples of control, PEXS and PEXG .....	153
Table 6.3. ROC curve report for plasma clusterin .....	156
Table 6.4. ROC curve report for aqueous humor vimentin .....	158
Table 6.5. ROC curve report for plasma vimentin.....	161
Table 6.6. List of annotated variants observed in <i>FBLN5</i> gene.....	164
Table 6.7. List of annotated variants observed in <i>CLU</i> gene.....	177
Table 6.8. Genetic association of rs7982 with PEX, PEXS and PEXG versus control.....	180
Table 6.9. List of annotated variants identified in <i>VIM</i> gene.....	181
Table 6.10. Genetic association of rs3758410 with PEX, PEXS and PEXG versus control.	183
Table 6.11. A sub-set of molecules that are differentially regulated in PEX .....	184

## **List of Abbreviations**

5-aza-dC	5-azadeoxycytine
ACTB	$\beta$ -actin
AD	Alzheimer's disease
AH	Aqueous humor
ARC	Age-related cataract
ARMD	Age-related macular degeneration
CACNA1A	Calcium voltage-gated channel subunit alpha 1 A
CDS	Coding DNA sequence
CGI	CpG island
CL	Cutis laxa
CLU	Clusterin
CNTNAP2	Contactin Associated protein-like 2
DKK1	Dickkopf-1
DNA	Deoxyribonucleic acid
DNMTs	DNA methyl transferases
dNTPs	Deoxynucleotide triphosphates
ECM	Extracellular matrix
ELISA	Enzyme-linked
EMSA	Electrophoretic mobility shift assay
ENCODE	Encyclopaedia of DNA elements
FBLN5	Fibulin-5
GAPDH	Glyceraldehyde phosphate dehydrogenase
GSTP1	Glutathione-S-transferase P1

GWAS	Genome-wide association study
Hcy	Homocysteine
HD	Huntington's disease
HEK293	Human embryonic kidney cells 293
HLE B-3	Human lens epithelial cells B-3
IL	Interleukin
IOP	Intraocular pressure
LC	Lens capsule
LD	Linkage disequilibrium
LOXL1	Lysyl oxidase like 1
LTBP	Latent transforming growth factor binding protein
LYST	Lysosomal trafficking regulator
MAF	Minor allele frequency
miRNA	Micro-RNA
MMPs	Matrix metalloproteinases
mRNA	Messenger RNA
MTHFR	Methylenetetrahydrofolate reductase
PCR	Polymerase chain reaction
PD	Parkinson's disease
PEX	Pseudoexfoliation
PEXG	Pseudoexfoliation glaucoma
PEXS	Pseudoexfoliation syndrome
POAG	Primary open angle glaucoma
POP	Pelvic organ prolapse
qRT-PCR	Quantitative real time PCR

RNA	Ribonucleic acid
ROCK2	Rho associated coiled coil containing protein kinase 2
siRNA	Small interfering RNA
SNP	Single-nucleotide polymorphism
TGF $\beta$	Transforming growth factor beta
TIMPs	Tissue inhibitors of matrix metalloproteinases
TNF- $\alpha$	Tumor necrosis factor alpha
TSS	Transcription start site
UCSC	University of California Santa Cruz
UTR	Untranslated region
UV	Ultraviolet
VIM	Vimentin
XFM	Exfoliative material

## *Chapter 1*

# **Introduction and Review of Literature**

## 1. Introduction and review of literature

Pseudoexfoliation (PEX [MIM: 177650]) is a complex age-related systemic protein aggregopathy involving the deposition of white flaky extracellular matrix (XFM) material on the surface of tissues. The initial stage of the disease having deposition of PEX material, XFM, is termed as pseudoexfoliation syndrome (PEXS) that visibly manifests in the eye as deposition on the anterior ocular tissues.<sup>1</sup> These deposits block the aqueous humor outflow by blocking the Schlemm's canal, leading to an increase in the intraocular pressure (IOP). This increase in IOP inside the ocular chamber damages the ocular tissues leading to a degeneration of the retinal ganglion cell (RGCs) axons of the optic nerve resulting in a severe condition of irreversible blindness termed as pseudoexfoliation glaucoma (PEXG).<sup>2</sup> The anatomy of the human eye is shown in **Figure 1**. About 50% of PEXS-affected individuals progress to the advanced stage of PEXG.<sup>3</sup>

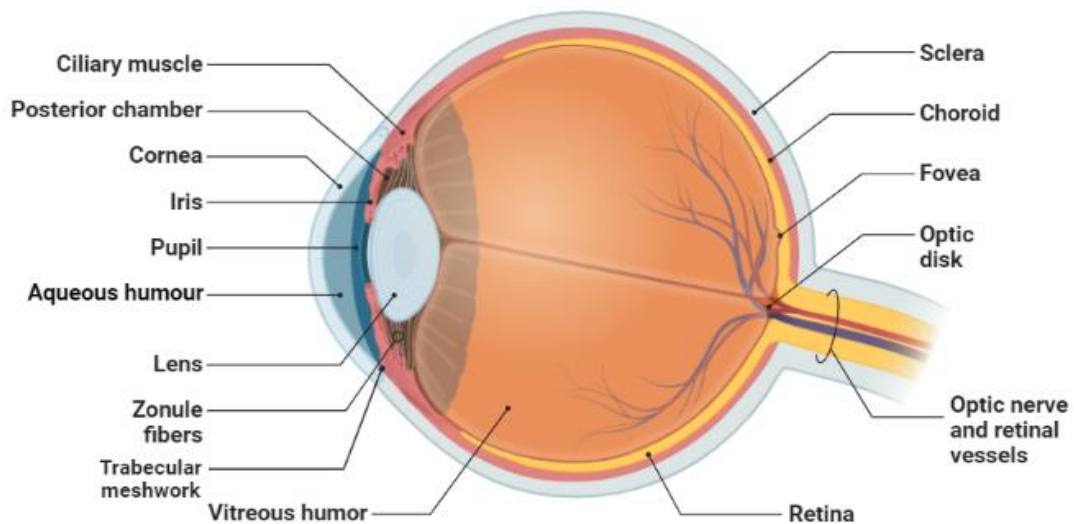


**Figure 1.1. Anatomy of the human eye.** Showing the detailed anterior and posterior structures of the eye. Template adapted from Biorender.com.

## 1.1. Composition of exfoliative material

Early studies on the amino acid analysis of the XFM showed that it comprises of the amyloid material, non-collagenous basement membrane, and elastic micro-fibril components. XFM is a highly cross-linked glycosylated structure formed of glycoproteins and glycolipids. Several carbohydrate components, such as heparin sulfate proteoglycan, chondroitin sulfate, dermatan sulfate proteoglycan, and hyaluronan, have been observed in the XFM through histochemical staining. Extensive immunohistochemical analysis showed that numerous proteins make up the XFM. The basement membrane proteins, proteins of the elastic fiber system, extracellular matrix proteins such as laminin, fibronectin, vitronectin, fibrillin, fibulins, latent TGF $\beta$  binding proteins (LTBPs), latent TGF $\beta$ 1, the extracellular molecular chaperone, clusterin, the matrix metalloproteinases (MMPs) and their inhibitors (TIMPs), tropoelastin and elastin. The presence of various complement factors such as C1q, C3, and C4 in the XFM has been reported suggesting mild inflammatory processes involved in PEX pathology.<sup>1,4-6</sup>

The XFM is thought to be produced by the various ocular cell types such as the pre-equatorial lens epithelial cells, corneal endothelial cells, non-pigmented ciliary epithelial cells, iridal cells, and trabecular endothelial cells. The XFM showed cross-banded fibrils of width varying from 250 to 2000 Å.<sup>7</sup> The fibrils are randomly arranged and are straight or slightly bent with blunt ends. Two types of fibrils were distinguished in the XFM using transmission electron microscopy. The Type-A fibrils are 1 $\mu$ m in length and 18-25 nm with a periodic banding of 50 nm. The Type-B fibrils are shorter (0.3-0.5  $\mu$ m) and stouter (30-45 nm) with the less distinct banding patterns. These fibrils are intermingled and composed of microfibril units of 3-7 nm (in diameter) and a micro periodicity of 10-12 nm that form a core by lateral aggregation of pre-existing microfibrillar subunits.<sup>8</sup>

## 1.2. Pathology of pseudoexfoliation syndrome

PEXS was first reported by the Finnish ophthalmologist John G. Lindberg in 1917. He observed ‘greyish fringes at the pupillary border that could form a membrane on the anterior lens capsule.’<sup>9</sup> Subsequent reports showed the presence of the deposits on the iris, corneal endothelium, ciliary body, zonules, trabecular meshwork, and within the conjunctiva (**Figure 2**).<sup>1,10</sup>

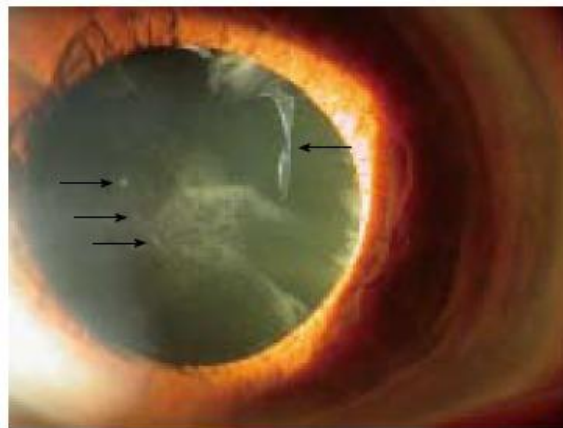


**Figure 1.2. Clinical picture of human eye with pseudoexfoliation syndrome.** Showing the presence of exfoliative material on the anterior lens surface. Black arrows show the whitish flaky deposits. (Taken from Gartaganis *et al.*, 2014).<sup>11</sup>

Although PEXS manifests prominently in the eye, these deposits have been observed in skin specimens, connective tissue portions of visceral organs, lungs, heart, brain, vessels, kidney, and bladder.<sup>1,12</sup> PEXS can cause chronic open-angle glaucoma, but also angle-closure glaucoma. The aqueous humor production is found to be reduced in PEXS-affected eyes and associated with a disrupted blood-aqueous barrier with a consequent presence of higher levels of aqueous protein concentration.<sup>13-15</sup>

### 1.3. Pathology of pseudoexfoliation glaucoma

Pseudoexfoliation glaucoma has been widely described as the result of the accumulation of exfoliative material, which obstructs the trabecular meshwork leading to an increase in IOP. PEXG is characterised by an increase in intraocular pressure, and damage to the optic nerve head leading to progressive blindness (**Figure 3**).

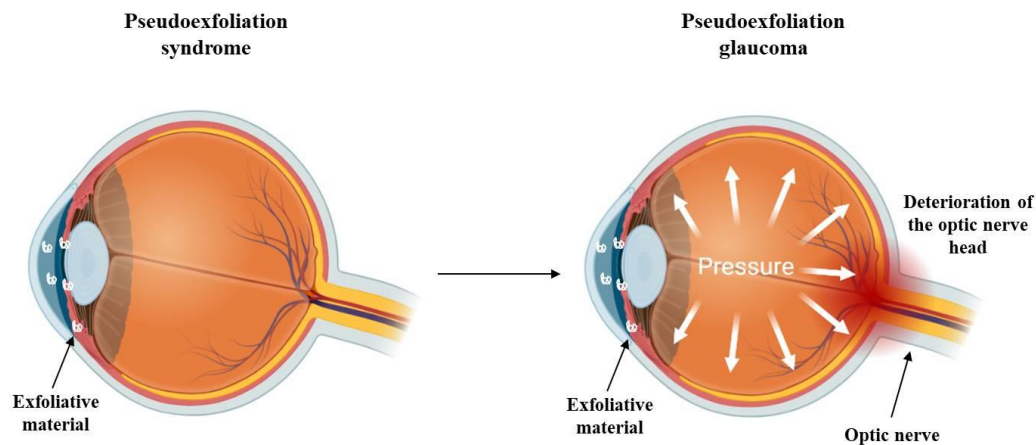


**Figure 1.3. Characteristic features of pseudoexfoliation glaucoma.** The accumulation of the exfoliative material in the anterior chamber of the eye due to pseudoexfoliation syndrome leads to increased intraocular pressure that damages the posteriorly situated optic nerve resulting in progressive irreversible blindness. Icons adapted from Biorender.com.

Also, the prevalence of PEXS in patients with glaucoma is significantly higher compared to age-matched non-glaucomatous populations. PEXG increases with age and has a higher prevalence in patients between 60 and 70 years of age. PEXG is mostly bilateral and asymmetric; compared to primary open-angle glaucoma (POAG), it presents a worse prognosis due to higher fluctuations in IOP levels and more severe optic nerve and visual field damage in affected eyes.<sup>15</sup> Furthermore, PEXG patients show higher levels of IOP compared to those affected by POAG. Many studies report a higher percentage of failure of medical management (prostaglandins, beta-blockers, adrenergic agonists, and carbonic anhydrase inhibitors) in PEXG patients. Topical drugs, such as latanoprost, travoprost, and dorzolamide-timolol combination, yield a good response in the first period of medical

treatment, but PEXS is usually recalcitrant to glaucomatous medical therapy and therefore, patients affected by PEXS or PEXG usually undergo laser or surgical therapy.<sup>16</sup>

#### **1.4. Demographics and prevalence of pseudoexfoliation**

Pseudoexfoliation has been prevalent in every part of the globe. PEX prevalence is highly variable across the globe ranging from 1.8% in USA to 39.3% in Ethiopia (**Figure 4**).<sup>17</sup> In Asia, the most populous continent, the prevalence of PEX varies across the continents. In Northern China, one study conducted on people aged above 60 years showed PEX prevalence to be as low as 0.55%.<sup>18</sup> PEX prevalence was found to be 3.6% in Russian, 3.4% in Japanese, and 2.6% in Pakistani (increased to 13.0% in individuals aged above 70 years) populations.<sup>19–</sup>  
<sup>21</sup> The Woodo study in an isolated population on a Korean island found PEX prevalence to be 10.4% which increased with age.<sup>22</sup> However, on analysing the Korean National Health and Nutrition Examination Survey data, Kim *et al.* reported that only 0.12% of South Koreans exhibit PEXS.<sup>23</sup> PEX incidence was 3.8% in the South Indian population which increased to 6.25% in people aged above 60 years.<sup>24,25</sup> In the Central India study, PEX prevalence was 1.49%, with 2.85% in the age group of 60-69 years, that increased to 12.3% in the age group 80+ years.<sup>26</sup> In extreme North India, a much higher prevalence of PEX was noted at 26.3%, of which the majority of patients were engaged in outdoor work such as agriculture.<sup>27</sup>

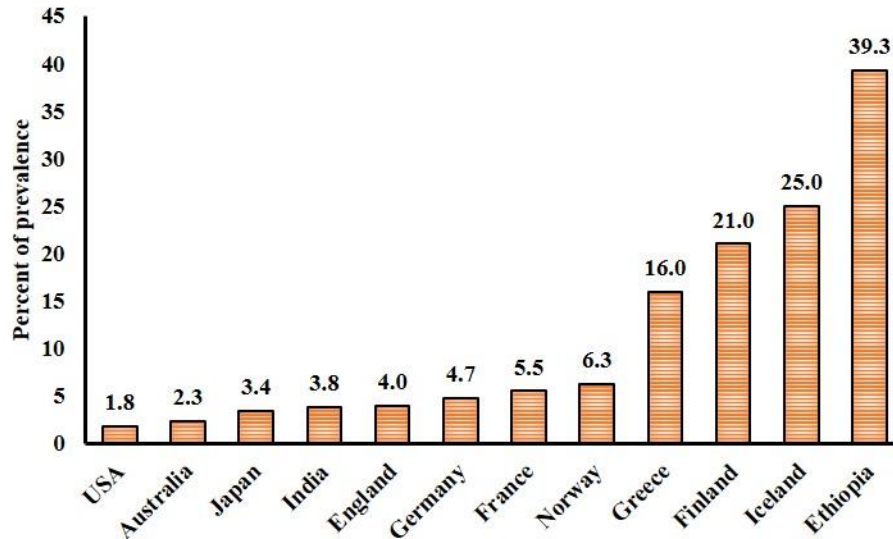


**Figure 1.4. Graphical representation of the prevalence of PEX across the globe.** The prevalence of PEX is highly variable across the countries depending on the geographical.

In the African continent, PEX prevalence varies by geographic location. Cross-sectional studies showed PEX prevalence to be 1.7% in Congo, much less than the prevalence in the South African districts, 6.0% in Temba, and 7.7% in Hlabisa.<sup>28,29</sup> The prevalence in Nigeria was more similar to that in Congo at 2.7%.<sup>30</sup> However, the highest prevalence at 39.3% was observed in tribes of Ethiopia.<sup>17,31</sup> In Australia, the prevalence was found to be 0.98% in the Visual Impairment Project study, 1.8% in the Framingham Eye study and, 2.3% in the Blue Mountains Eye Study. In the indigenous Central Australian population, PEX prevalence was found to be 4.7%.<sup>32</sup> As the population is ethnically and racially diverse in the Americas, PEX prevalence is quite varying. In the native Navajo Indian-American population of the Amazons, the prevalence is 38.0%.<sup>33</sup> However, in the South-eastern regions of the United States of America, the prevalence is only 1.6%.<sup>34</sup> In the South American countries, PEX prevalence varies from 5.0% to 24.6%.<sup>32,35</sup>

In Europe, the highest incidence of PEX has been noted in the Scandinavian countries. A study on Icelanders showed that PEX prevalence was 17.7% in individuals aged 70-79 years, which increased to 40.6% in individuals above 80 years.<sup>36</sup> In a study on the Norwegian

population, Aasved and group reported that PEX prevalence is 0.4% in the age group of 50-59 years, which increased to 7.6% in individuals above 80 years.<sup>37</sup> PEX prevalence is reported to be 20.0% in Finland, 17.0% in Greece and 23.5% in Portugal, 4.7% in Germany, and 4.0% in England.<sup>38,39</sup>

Even within the same country, based on geographic location, ethnicity, age of the individuals, and occupation- the amount of exposure to sunlight- have led to PEX prevalence of varying frequency.

### **1.5. Theories associated with causation and progression of pseudoexfoliation**

PEX is a progressive disease with a gradual accumulation of extracellular fibrillar material. Many theories have been proposed to explain the causation of the disease.

a. Ageing theory: As the development of PEX is higher in people aged above 60 years and rarely seen in individuals below 40 years, age has been attributed as an important contributor to the disease along with other pathological features.<sup>15,40</sup> It has been noted that with age, the ability of many cells to maintain proteostasis is compromised, and aging cells accumulate misfolded proteins, which is a major epidemiological risk of many protein aggregopathies such as Alzheimer's, Huntington's, including PEX.<sup>41</sup>

b. Basement membrane and elastic microfibril theory: The elastic microfibrils connect the cellular basement membranes with the stromal elastic fibre system, and the control of microfibril and basement membrane synthesis is coordinated by the same cell. However, the presence of both basement membrane components such as laminin, nidogen, and heparin sulfate proteoglycans and elastic microfibrillar components such as elastin, LTBPs, emilin, fibrillin, and vitronectin in XFM led researchers to propose that PEX could be a disease of abnormal basement membrane metabolism or a type of elastosis.<sup>3,42</sup>

c. Amyloid theory: Amyloid theory suggests involvement of amyloid-like protein in the pathogenesis of PEX. Aberrant deposition of amyloid- $\beta$ -peptide and phosphorylated tau protein in the brain tissues are responsible for the gradual deterioration of brain neurons in Alzheimer's disease (AD) affected individuals. Studies have shown the presence of amyloid  $\beta$ -peptide, serine proteinase inhibitor, alpha-1-antichymotrypsin in PEX aggregates.<sup>43</sup> Similarly, Linner *et al.* observed that there is an increased risk of PEX in AD patients compared to controls in the Norwegian population.<sup>44</sup> Further, PEXG individuals show a greater number of closely arranged myelinated fibers with decreased glial fibrillary acidic protein (GFAP) staining which is also seen in AD affected brains.<sup>45</sup> These observations suggest an involvement of amyloid-like protein in the production of PEX aggregates similar to that seen in AD patients.

d. Protein-sink theory: Lee *et al.* proposed a protein-sink model to explain the aberrant deposition of PEX material in the anterior eye tissues.<sup>46</sup> According to this model, initially, a misfolded or distorted protein complex in the aqueous humor progressively binds to or sequesters other proteins resulting in a large aggregate. Subsequently, this huge aggregate settles in the ocular tissues that come in contact with the aqueous humor. Also, a disrupted blood-aqueous barrier could aid in the transport of these aggregates to other body parts.

## **1.6. Ocular and non-ocular complications associated with pseudoexfoliation**

Pseudoexfoliation is associated with numerous co-morbidities, both ocular and non-ocular, and the XFM has been found to be deposited in various extraocular systemic tissues, such as lungs, heart, kidneys, gall bladder, liver, and meninges.<sup>47,48</sup> The occurrence of systemic comorbidities with PEX is poorly understood. Some possibilities of the plausible effect of PEX on vascular diseases include XFM deposits in the connective tissue of vessel walls leading to endothelial dysfunction. An imbalance in the MMPs and TIMPs in the ECM

affects the elasticity of the basement membrane.<sup>49</sup> Also, increased oxidative stress may play a role in the development of systemic vascular diseases in patients with PEX.

PEX is associated with an increased risk of respiratory and cardiovascular complications. Increased arterial hypertension, ischemic heart diseases, cardiac valve, and carotid artery stenosis were observed in PEX-positive groups compared to PEX negative groups.<sup>50</sup> A higher incidence of urogenital diseases, such as benign prostate hyperplasia, and renal insufficiency, was observed in PEX patients. XFM has been identified in the collagen fibres, mesenchymal cells, and blood vessels of the kidney; however, no aggregates were found in the cortical and medullary renal cortex. PEX has been associated with abdominal aortic aneurysms, erectile dysfunction, and pelvic organ prolapse.<sup>51-53</sup> Increasing evidence suggests a positive correlation between PEX and cerebrovascular diseases, including dementia and Alzheimer's. PEX is seen to be associated with ischemic brain alterations.<sup>54</sup>

PEX is often associated with an increased risk of nuclear cataracts. Age-related macular degeneration, lens subluxation, dry eye syndrome, and retinal vein occlusions are some other ocular complications manifesting due to PEXS. Lens dislocations in individuals with PEXS are much higher after cataract surgery than in individuals having surgery without PEXS.

## **1.7. Risk factors involved in pseudoexfoliation progression**

### **a. Environmental factors**

It is believed that environmental factors, such as geographic locations and climatic factors, contribute to or shape the course of pseudoexfoliation disease. UV or solar exposure contributes immensely to the risk of PEX. People who spend more time outdoors showed a higher prevalence of PEXS or PEXG. A prominent latitude effect is observed in the disease. Stein *et al.* report that solar exposure, ambient temperature, and living at more Northern

latitudes within the US could be environmental risk factors for PEXS.<sup>55</sup> A similar study by Kang *et al.* showed that residing at a middle or lower tier of latitude in the US reduced the risk of the disease.<sup>56</sup> However, people residing in the Northern tier showed increased susceptibility to developing PEX. In Greece, people living at higher altitudes exhibited a higher incidence of PEX compared to those at lower altitudes.<sup>57</sup> UV radiations alter the structure of proteins and can result in their precipitation. There exists evidence of gene-environment interactions in PEX pathogenesis. UV radiation, a pathogenic factor associated with pseudoexfoliation syndrome, leads to the upregulation of XFM components such as *LOXLI*, elastin, fibrillin-1, Transforming growth factor beta-1 (TGFβ1), Latent TGFβ binding protein-1/2 and fibulin-2/4 *in vitro* in cultured human Tenon's capsule fibroblasts.<sup>58</sup> Colder temperatures have also been associated with an increased risk of PEX. The highest prevalence of PEX has been observed in Scandinavian countries such as Finland, Iceland, and Norway. It is proposed that a precipitation reaction at colder temperatures might be responsible for the PEX deposits.

Diet is yet another important factor of lifestyle that controls the course of many diseases. Increased caffeine intake and a decreased folate intake are associated with a higher risk of PEXS. Low serum folate has been observed in patients with PEXS. Kang *et al.* found a lower risk of PEXS with increased folate intake. Decreased vitamin B12 is also noted in PEXG individuals.<sup>59</sup> Serum homocysteine (Hcy) is another factor seen to be increased in PEX individuals. Hyperhomocysteinemia contributes to vascular damage and alterations in ECM. Decreased vitamin B12 and folic acid affect the metabolism of Hcy resulting in increased plasma Hcy. Additionally, coffee consumption produces increased Hcy levels.<sup>60</sup> A study in East India reported that people with PEXS were more likely to be non-vegetarians and primarily consume fish.<sup>32</sup> This study also reported that individuals consuming higher amounts of coffee were more likely to develop PEXS and PEXG. A diet rich in fibre, fruits,

and vegetables was observed to decrease the risk of PEXS. Other lifestyle habits such as smoking, and alcohol consumption were not found to be associated with the risk of PEX.<sup>32</sup>

## **b. Genetic factors**

Early studies to understand PEX pathology were conducted to identify a genetic basis for the disease. Genome-wide and candidate gene association studies identified numerous genetic loci as risk factors for PEX.

### **Lysyl oxidase-like 1 (LOXL1)**

*LOXL1*, situated on chromosome 15q21.4 was the first gene to be associated with PEX through a genome-wide association study (GWAS). Thorleifsson *et al.* identified three single nucleotide polymorphisms (SNPs), rs2165241, rs1048661, and rs3825942 to show significant association with PEXS and PEXG in a Scandinavian population.<sup>61</sup> rs2165241 is an intronic variant and rs1048661 and rs3825942 are non-synonymous coding variants located in exon1 of *LOXL1*. rs1048661 and rs3825942 lead to amino acid changes, Arg141Leu and Gly153Asp, respectively. Subsequent studies revealed the association of these two protein-coding variants, rs1048661 and rs3825942 with PEX in various populations across the globe, including German, Austrian, Italian, Polish, Spanish, Greek, Japanese, Indian, Korean, US Caucasian, and Saudi Arabs.<sup>62,63</sup> However, the risk variants were reversed in certain populations. For example, the ‘G’ allele at rs1048661 was found to be a protective allele in Japanese and Korean populations but a risk allele in all other populations. Similarly, the ‘G’ allele at rs3825942 was associated with decreased risk of PEXS in Black South Africans but was found to be a risk allele in other populations. The ‘T’ allele at rs2165241 was found to be a risk allele in the majority of populations but was associated with low risk in Japanese, Korean, and Chinese populations. Some populations did not show any association of these variants with PEX. rs1048661 was not found to be associated with PEX in Greek and Polish

populations. Further screening of promoter and intronic regions of *LOXLI* identified the association of more variants with pseudoexfoliation which were also found to regulate the expression *LOXLI* and a long non-coding RNA, *LOXLI-AS1*. Fan *et al.* found that the ‘C’ allele at rs16958477 residing in the promoter region near the transcription start site increases the transcription activity. The ‘A’ allele is the risk allele in US-Caucasians and is associated with repressed transcription.<sup>64</sup> In a study on European and Japanese populations, an intronic variant in *LOXLI*, rs11638944, was found to alter the gene expression through altered transcription factor binding by the variants, which also enhanced alternative splicing.<sup>65</sup> Recently, Berner *et al.* observed that the non-coding variant, rs7173049 residing upstream of *LOXLI*, conferred a protective effect from PEXS and was associated with multiple populations, and did not show any allele reversal. rs7173049 was found to influence the regulation of the distally located immunoglobulin superfamily containing leucine-rich repeat protein 2 (ISLR2) and stimulated by retinoic acid receptor 6 (STRA6). PEXS is associated with decreased expression of ISLR2 and STRA6, and the protective allele ‘G’ at rs7173049 was found to increase the expression of these two proteins.<sup>66</sup> Further, Berner *et al.* showed that inhibition of the retinoic acid signaling pathway leads to an increase in PEXS-associated matrix genes *in vitro*, indicating that an impaired retinoid metabolism could be contributing to PEXS pathology.<sup>66</sup> Deep sequencing following a GWAS identified rare variants in *LOXLI* to be associated with PEXS. The ‘T’ allele at rs201011613, a coding variant in *LOXLI*, conferred a strong protective effect from PEXS, the presence of which corroborated with an increase in ECM proteins and cell-cell adhesion in human lens epithelial cells.<sup>67</sup>

*LOXLI* is a cross-linking enzyme involved in elastogenesis and ECM maintenance. It catalyzes the deamination of lysine residues in tropoelastin monomers and polymerizes the monomers to elastin polymers in the ECM in the presence of other proteins such as fibulins, fibrillin, and integrins. *LOXLI* also aids in the cross-linking of elastin and collagen fibrils in

the ECM and maintains its integrity. LOXL1 deposits have been found in the XFM, suggesting an aberrant deposition of LOXL1 in PEX fibrils. An increased expression of LOXL1 in the lens capsule and ciliary body in the early stage of PEXS and a subsequent decrease in its expression in the advanced glaucomatous stage of PEXG has been recorded, implying a destabilization of ECM in the severe form of the condition. However, a couple of other studies have shown a decreased expression of LOXL1 in even the PEXS stage of the disease in lamina cribrosa and peripapillary sclera, including lens capsules.<sup>68-70</sup> Although LOXL1 is the major genetic risk factor for PEX, allele reversals in different ethnicities and incomplete penetrance of alleles prompted researchers to look for other risk factors for PEX.

### **CACNA1A**

In 2016, another GWAS conducted in a Japanese population and subsequently followed up in individuals from 17 countries across six continents identified a novel locus, rs4926244, in *CACNA1A*, as a risk factor for PEXS.<sup>63,67</sup> This variant was, however, not found to be associated with PEX in the Uighur population. Immunostaining for CACNA1A showed localisation of the protein in various ocular structures such as the ciliary body, iris, anterior lens epithelium, retina, and optic nerve glia. However, no difference in the distribution or expression of CACNA1A was observed in the PEXS eyes compared to non-PEXS eyes.<sup>67</sup> The PEX-associated risk loci in *CACNA1A* might not affect the expression or localisation of the protein and might be involved in PEX pathology through some other unknown mechanism. We also observed a significant association of rs4926244 with PEX in the Indian population. rs4926246 in linkage disequilibrium (LD) with rs4926244 was also found to be associated with PEXS and PEXG in our study population (Hayat *et al.*, PhD Thesis, Unpublished data).

*CACNA1A* codes for the alpha 1A subunit of the P/Q voltage-gated calcium ion channel. Calcium channels maintain the influx and efflux of calcium in the cell and are involved in the neurotransmission of electric signals, vesicle trafficking, muscle contraction, and gene regulation.<sup>71</sup> Electron microscopic images have shown deposits of calcium in PEX aggregates, and an altered calcium ion channel functioning might lead to an imbalance in calcium concentrations.<sup>72</sup> Calcium is essential for stable aggregate formation by fibrillin, and altered calcium levels might lead to the generation of PEX aggregates.

## **CLU**

*CLU* encodes for a ubiquitously expressed multifunctional protein called clusterin or Apolipoprotein-J. Although GWAS did not identify clusterin as a risk locus for PEX, independent case-control studies have identified risk loci in clusterin for PEX susceptibility. The variants rs2279590 and rs3087554 were found to be significantly associated with pseudoexfoliation in various ethnic groups such as German, Australian, and Indian populations.<sup>73-75</sup> We further found that the intronic SNP rs2279590 is a functional variant, presence of 'G' allele at the variant results in an increase in *CLU* expression.<sup>75,76</sup> We and others have observed increased levels of clusterin in aqueous humor, tears, and lens capsule of PEX patients compared to controls.<sup>75,77,78</sup> Clusterin is an extracellular molecular chaperone that aids in proper protein folding, maintenance of misfolded proteins, cell-cell, and cell-matrix adhesions. Immunohistochemical analysis has shown strong positivity of *CLU* in PEX fibrils. A dysregulated *CLU* expression and its impaired chaperoning effect might lead to the excess generation of PEX fibrils.

## **CNTNAP2**

*CNTNAP2* encodes for the Contactin Associated protein-like 2. Krumbiegel *et al.* identified two SNPs associated with PEX in a German population through GWAS.<sup>74</sup> rs2107856 and

rs2141388 are intronic variants that were further associated with PEX in a replication cohort of Germans but not Italians.<sup>79</sup> These SNPs were later not found to be associated with PEX in Polish and Turkish populations as well.<sup>80,81</sup> rs2107856 did not correlate with retinal nerve fibre layer thickness, cup/disk ratio, intraocular pressure, or central corneal thickness in the Turkish study.<sup>80</sup> CNTNAP2 is a membrane protein involved in potassium channel trafficking, and required for neuron-glia interactions.

### **MMPs and TIMPs**

The ECM turnover is maintained by the matrix metalloproteinases (MMPs) and their inhibitors, the tissue inhibitors of matrix metalloproteinases (TIMPs). The MMPs belong to a group of zinc and calcium-dependent endopeptidases that maintain the ECM homeostasis. The functionality of the MMPs is kept under check by the TIMPs. Any imbalance in the ratio of MMPs to TIMPs may result in excessive or insufficient matrix degradation and accumulation. MMPs also regulate the outflow of AH, and any alteration in the levels of MMPs could affect the intraocular pressure due to a disturbed outflow of AH. The levels of MMP-2 and -3 and TIMP-1 and -2 were found to be elevated in the aqueous humor of PEX patients compared to controls.<sup>49</sup> Also, the ratio of MMP-2 and its principal inhibitor TIMP-2 was found to be decreased in patients with PEXG suggesting inappropriate matrix degradation and progressive matrix accumulation.<sup>49</sup> In a separate study, a significant increase in aqueous humor TIMP4 was observed in PEXG patients compared to controls.<sup>82</sup> Increased levels of TIMP4 could affect the activity of MMPs resulting in disrupted ECM homeostasis. Though some researchers have tried to study the association of *MMP* polymorphisms with PEX, the reports are limited. From two independent studies, no significant association of variants of *MMP1*, *MMP2*, *MMP3*, and *MMP9* was found with PEX in Greek and Austrian populations.<sup>83,84</sup> However, a meta-analysis by He *et al.* reported an association of rs1799750 of *MMP1* with PEXG.<sup>85</sup> Recently, Starikova *et al.* studied the association of six

polymorphisms in *MMP9* (rs3918242, rs3918249, rs17576, rs3787268, rs2250889, rs17577), rs679620 of *MMP3* and rs1799750 of *MMP1* with PEXG in the Caucasian population of Central Russia.<sup>86</sup> Significant association of two SNPs, rs3918249 and rs2250889, were found to be associated with PEXG. The ‘C’ at rs3918249 decreased the risk for PEXG, and the allele ‘G’ at rs2250889 increased the risk for PEXG. rs2250889 is a missense variant, and rs3918249 is in strong LD with another missense variant, rs17576. HaploReg analysis had shown both variants to have a potential regulatory effect.<sup>86</sup> The contradictory results of the association of *MMP* polymorphisms with PEX could be ethnicity-dependent.

### **Other genetic factors**

The homocysteine metabolism genes, cytokines, adenosine receptor A3, and lysosomal trafficking regulator (*LYST*) have been reported to be associated with PEX. Increased plasma homocysteine (Hcy) levels were found in PEXS and PEXG patients compared to the control.<sup>87,88</sup> Plasma Hcy can be altered due to various factors, such as genetic, folic acid deficiency, and vitamin deficiency, among others. The methylenetetrahydrofolate reductase (*MTHFR*) regulates the Hcy concentration. Therefore, researchers looked for variants in *MTHFR* that could be responsible for homocysteinemia in PEX. However, none of the genetic association studies reported any association of *MTHFR* polymorphisms with PEX.<sup>89,90</sup>  $\text{TNF-}\alpha$  is a proinflammatory cytokine that can be either neuroprotective or contribute to neurodegeneration depending on the receptor it binds to. The  $\text{TNF-}\alpha$  polymorphism rs1800629 was found to be strongly associated with PEXG in the Pakistani cohort. The ‘GG’ and ‘AG’ genotypes were found to be associated with the PEXG in Pakistani and Iranian cohorts. However, this variant did not show an association with the disease in Caucasian and Turkish populations.<sup>91</sup> Fakhraie *et al.* studied the association of three polymorphisms, rs1800872, rs1800871, and rs1800896, in the promoter of IL-10 (anti-inflammatory cytokine) with PEXS, PEXG, and POAG.<sup>92</sup> While the genotypes at both

rs1800871 ('TT') and rs1800896 ('AA') showed association with all three groups, the 'AA' genotype of rs1800872 was found to be significantly associated with only PEXS. These polymorphisms had previously been associated with aging, various cancers, Alzheimer's disease, schizophrenia and acute myocardial infarction.<sup>92</sup> Animal studies have shown that the lysosomal transport regulator (LYST) gene may be significant in PEXS pathology. LYST is crucial for the synthesis of the proteins needed for lysosomal function. Chediak-Higashi syndrome, a lysosomal storage disorder in humans, is caused by mutations in the LYST gene.<sup>93</sup> B6-Lyst<sup>bg-J</sup> mice that are homozygous for the beige-J (bg-J) allele exhibit a variety of ocular PEXS-like characteristics. The pattern of iris transillumination defects, aggregation of XFM-like material on the iris and elsewhere in the anterior chamber, and the iris pigment dispersion were the three main similarities observed between the LYST mutant mice and PEXS.<sup>94</sup> A 3-bp deletion in the LYST protein's WD40 domain resulting in the deletion of one isoleucine amino acid, leads to the beige mutation. This suggests that protein-protein interactions have been hampered. Although the LYST mutant mice do not recapitulate PEXS entirely, they have the potential to be used as an animal model for the condition and may provide insight into the disease's complex genetic and molecular risk factors.

### **c. Epigenetic factors**

Epigenetic regulation of gene expression through environmental factors such as dietary intake, latitude effect, smoking, and UV exposure may lead to disease susceptibility and progression, and phenotype variation in many common diseases such as pseudoexfoliation, age-related macular degeneration (ARMD), glaucoma, Alzheimer's disease, and cancers.<sup>63,95–98</sup> The retinal cell death seen in many ocular disorders involves oxidative stress, activation of apoptotic signals, mitochondrial dysfunction, loss of synaptic connectivity, and excitotoxic damage. Many of these signaling pathways are regulated by epigenetic modifications.<sup>99,100</sup>

Epigenetics refers to the heritable changes to the chromatin and gene function without affecting the DNA sequence. These changes can alter the gene expression and cellular signaling pathways, which predispose an individual to various diseases. Epigenetic mechanisms comprise of DNA methylation, histone modifications and chromatin remodelling, and non-coding RNA regulations. A single epigenetic mechanism or all the mechanisms synergistically can cause aberrant gene expressions leading to a variety of disease phenotypes, many of which are detrimental. Two independent studies found that *LOXL1* is downregulated in the lens capsule of PEXS patients and in the human tenon fibroblasts (HTFs) of PEXG patients. The downregulation of *LOXL1* in these patients correlated with significant hypermethylation of its promoter.<sup>69,70</sup> The methyl groups hinder the access of the transcription factors to the promoter for transcription resulting in decreased gene expression. We reported downregulation of *HSP70* in PEX patients which correlated with exon hypermethylation compared to controls.<sup>101</sup> *HSP70* deficiency contributes to the accumulation of misfolded protein aggregates that lead to PEX phenotype. A possible model showing the effect of epigenetic regulation of *LOXL1* and *HSP70* on PEX pathology is shown in **Figure 5**.

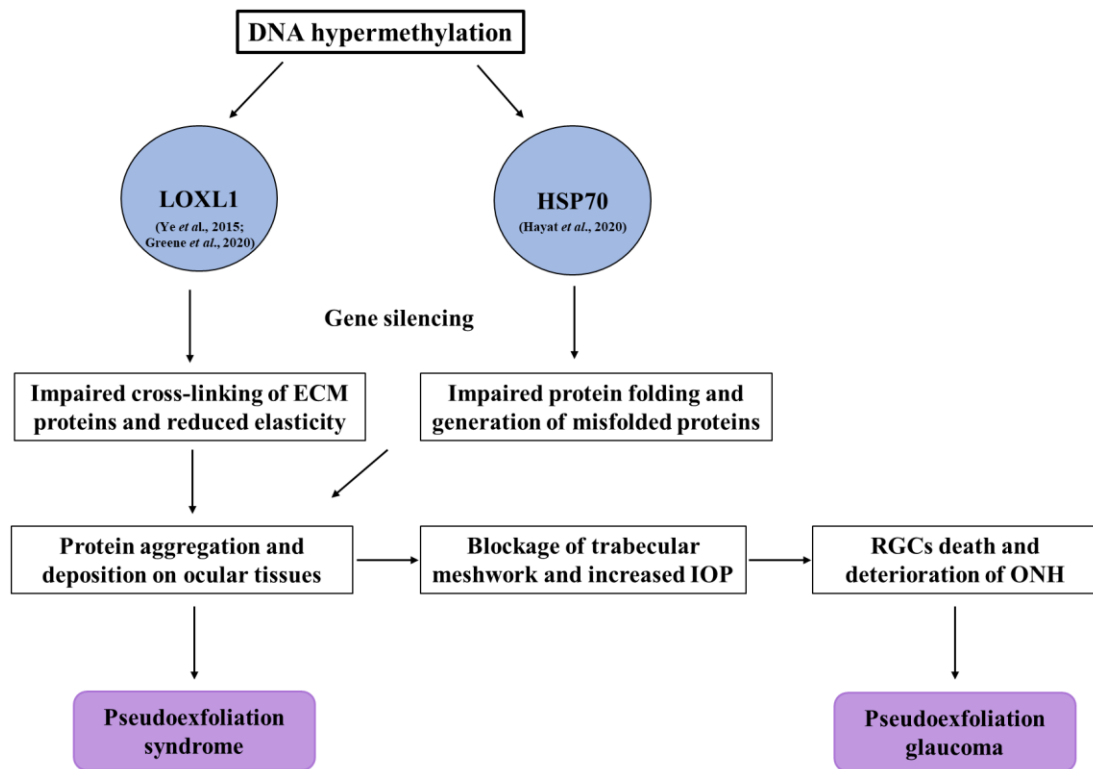


**Figure 1.5. Role of epigenetic silencing of LOXL1 and HSP70 in PEX pathogenesis.** A proposed hypothetical model showing that promoter hypermethylation of LOXL1 and HSP70 results in their reduced expression. Decreased LOXL1 results in an impaired ECM metabolism and elasticity that results in the aggregation of ECM proteins as the exfoliative material.<sup>69,70</sup> Reduced HSP70 leads to impaired protein folding and the generation of misfolded proteins.<sup>101</sup> Deposition of the protein aggregates on the ocular tissues such as trabecular meshwork impedes the aqueous humor outflow pathway resulting in increased intraocular pressure and eventual retinal ganglion cell death.

Although they do not code for a protein, non-coding RNAs (ncRNAs) play immense roles in post-transcriptional gene regulation and disease pathogenesis. ncRNAs participate in determining DNA methylation patterns and chromatin remodelling. Based on the size, ncRNAs are classified as micro RNAs (miRNAs), small interfering RNAs (siRNAs), and Piwi-interacting RNAs (piRNAs) if less than 200 nucleotides and long non-coding RNAs (lncRNAs) if more than 200 nucleotides. Micro RNAs are generally 18-21 nucleotides long and exhibit complementarity to regions of mRNA to which they bind and recruit proteins and complexes (RNA-induced silencing complex-RISC) that prevent the translation of the said mRNA to proteins, thereby silencing the gene. Recently, analysis of the miRNA profiles in

aqueous humor samples of PEXG versus controls by Drewry and co-workers resulted in 5 differentially expressed (DE) microRNAs, miR-122-5P, miR-3144-3p, miR-320a, miR-320e, and miR630 in PEXG compared to control. These DE miRNAs were found to target many genes involved in pathways associated with PEXG pathogenesis, such as TGF $\beta$  signaling and pathways related to neuroprotection or programmed death of RGCs through AKT signaling, and Bcl-2-regulated apoptosis pathways. Also, these DE miRNAs targeted glaucoma-associated proteins that are expressed in the anterior segment of the eye.<sup>102</sup> These differentially expressed miRNAs, in turn, affect the regulation of essential genes involved in PEXG. Cho *et al.* profiled the microRNAs in aqueous humor in the Korean population through RNA sequencing. They observed two significantly upregulated miRNAs (hsa-miR-30d-5p, hsa-miR-320a) and ten significantly downregulated miRNAs (hsa-miR-3156-5p, hsa-miR-4458, hsa-miR-6717-5p, hsa-miR-6728-5p, hsa-miR-6834-5p, hsa-miR-6864-5p, hsa-miR-6879-5p, hsa-miR-877-3p, hsa-miR-548e-3p, and hsa-miR-6777-5p) in the PEXG group compared to controls. Only one miRNA was found to be common between the study done by Drewry *et al.* and Cho *et al.* Drewry and their group found that hsa-miR-320a was found to be significantly downregulated in PEXG while it was found to be upregulated in the Korean PEXG patients.<sup>103</sup> This shows that although the same molecule is involved in the risk of the disease, a different mechanism of action occurs in the different ethnicities. Kyoto Encyclopaedia of Genes and Genomes (KEGG) pathway analysis showed that the top three enriched pathways were ‘the proteoglycans in cancer’, ‘glioma’, and ‘TGF $\beta$  signaling pathways. The exfoliative material is enriched with glycoprotein and proteoglycan aggregates, so the top KEGG pathway may contribute to PEX pathogenesis. Enrichment of the TGF $\beta$  signaling pathway emphasizes the role of TGF $\beta$  regulation in PEX aetiology in the majority of ethnicities. Another study involving Polish subjects reported an abundance of seven microRNAs in the aqueous humor of various glaucoma groups- primary open-angle

glaucoma (POAG), primary angle-closure glaucoma (PACG), and PEXG. However, these microRNAs were not differentially expressed between glaucoma and control groups or within the glaucoma subgroups. In this study, however, a strong positive correlation was observed between hs-miR-1260b and mean defect in visual field examination, wherein the miRNA expression decreased with increased severity of PEXG.<sup>104</sup>

Tomczyk-Socha and group were the first to study the differential levels of microRNAs in the lens capsule of PEX patients. They observed increased expression of miR-125b in PEXS individuals compared to control through the qRT-PCR technique. However, this microRNA was not found to be differentially expressed in the PEXG group.<sup>105</sup> miR-125b is a negative regulator of p53, and excessive oxidative stress increases its expression. Its expression is known to increase even under hypoxic conditions. Chronic inflammatory changes clubbed with increased oxidative stress, and ROS might affect the p53 activity through dysregulation of miR-125b and alter the transcription of genes involved in apoptosis. The same group recently reported microRNA expression in the lens capsule of PEXS patients determined using Next-Generation Sequencing. Ten microRNAs (miR-184, let-7a-5p, let-7c-5p, let7f-5p, let-7b-5p, miR-204-5p, miR-486-5p, miR-181a-5p, miR-30a-5p, miR-26a-5p) were found to be abundantly present in the lens capsule of both PEXS and control groups. Only miR-671-3p was found to be significantly decreased in the PEXS group.<sup>106</sup> miR-671-3p was reported to regulate the proliferation, apoptosis, migration, and invasion of lung cancer cells by targeting the FoXP2 protein. The miR-671-3p is also known to affect the Wnt/ $\beta$ -catenin signaling cascade.

Long non-coding RNAs (LncRNAs) are transcripts that are longer than 200 nucleotides. They are transcribed just as the mRNA and undergo all post-transcriptional processing such as capping, tailing, and alternative splicing; contain single nucleotide polymorphisms but they lack protein-coding capacity. LncRNAs recruit complexes, including transcription

factors, to activate or silence gene expression in response to various stimuli. They are also involved in alternate splicing, post-translational modifications, and protein trafficking. Wiggs *et al.* showed an association of variants in the lncRNA, *CDKN2BAS*, to be associated with PEXG as well as with POAG.<sup>107</sup> Also, variants in the promoter of lncRNA of *LOXLI-AS1* were seen to increase susceptibility to PEXS. Moreover, *LOXLI-AS1* was found to be modulated by stressors already implicated in PEX pathologies, such as oxidative stress and cyclic mechanical stress.<sup>108</sup> Knockdown of *LOXLI-AS1* altered the expression of genes involved in ECM homeostasis (MMP9, FBLN1, COL6A6, LAMA5), TGF $\beta$  signaling (TGF $\beta$ -2) and actin cytoskeleton assembly. *LOXLI-AS1* localizes to the nucleus and selectively binds to heterogeneous nuclear Ribonucleoprotein-L (hnRNPL), a protein involved in mRNA processing, and regulates downstream gene expression.<sup>109</sup> In a rat model of glaucoma, the lncRNA MALAT1 was found to prevent RGC apoptosis by activating the Akt pathway.<sup>110</sup> In contrast, the knockdown of lncRNA-Gas5 increased the survival rate of RGCs in glaucoma.<sup>111</sup>

## **1.8. Molecular and cellular pathways implicated in pseudoexfoliation pathology**

Numerous molecular and cellular pathways are disrupted in PEX, contributing to the XFM formation and other pathological features associated with PEX.

### **TGF $\beta$ signaling**

Transforming growth factor beta (TGF $\beta$ ) belongs to the superfamily of secreted polypeptides that are essential ECM modulators. Dysregulation of TGF $\beta$  has been linked to various diseases involving ECM abnormalities such as fibrotic diseases. Overexpression of TGF $\beta$  affects the ECM metabolism leading to excessive fibrosis,<sup>112</sup> and TGF $\beta$  is seen to be elevated in pseudoexfoliation individuals. Elevated TGF $\beta$ 1 and TGF $\beta$ 2 in the aqueous humor of PEXS

and PEXG patients have been reported.<sup>113</sup> An increase in TGFβ1 also induces the expression of fibrillin-1, an ECM scaffold protein, through JNK (c-Jun N-terminal 20 kinase) and MAPK (Mitogen-activated protein kinase) pathways.<sup>114</sup> TGFβ1 also stabilizes PEX fibrillar aggregates.<sup>115</sup> Further, studies have shown an increase in latent TGFβ1 binding protein (LTBP) levels in the aqueous humor, ciliary processes, iris tissues, and lens epithelial cells of PEX patients.<sup>116</sup> LTBPs are a group of glycoproteins that regulate the metabolism of TGFβs. Thus, increased LTBPs further contribute to ECM remodelling in PEX pathology. Recently, genome-wide RNA sequencing analysis of human trabecular meshwork cells stimulated with TGFβ1 showed dysregulation of many genes present in the exfoliative material such as elastin, fibrillins, *LTBP2*, and apolipoprotein E. TGFβ1 also increases the expression of *LOXLI*, the major genetic locus associated with PEX. Further, TGFβ1 stimulation of human trabecular meshwork cells led to modulation of oxidative stress and anti-oxidant system and upregulation of the unfolded protein response, which have been previously implicated in PEX pathology.<sup>117</sup> Thus, altered TGFβ signaling plays an important role in ECM protein regulation and metabolism in PEX.

### **Oxidative Stress**

PEX has also been associated with oxidative stress, a consequence of an imbalance between oxidants and antioxidants in the body. Oxidative stress plays an important role in the pathology of various other ocular diseases such as age-related cataract (ARC), ARMD, diabetic retinopathy; neurodegenerative diseases such as AD, PD, glaucoma; systemic diseases such as diabetes, rheumatoid arthritis, and various cancers.<sup>118–120</sup> Increased oxidative stress and an impaired anti-oxidant system in PEX eyes have been widely established. Enzymatic as well as non-enzymatic antioxidants such as superoxide dismutase (SOD), glutathione-S-transferases (mGST1 and GSTT1), ascorbic acid, oxidative selenium, and glutathione are significantly decreased in aqueous humor, serum and anterior segment tissues

in PEX eyes.<sup>11,121–123</sup> Concomitantly, the oxidative stress markers and oxidants such as malondialdehyde (lipid peroxidation marker), protein carbonyl (protein oxidation marker), hydrogen peroxide, nitric oxide, 8-hydroxydeoxyguanosine (8-OHdG) and homocysteine were found to be significantly increased in aqueous humor, serum and ocular tissues of pseudoexfoliation affected individuals.<sup>124–127</sup> Also, levels of antioxidant enzymes like Paraoxonase (PON) and Arylesterase (ARE) were found to be significantly reduced in AH and serum of PEXG individuals compared to controls in a Turkish population. Furthermore, the total antioxidant status (TAS), a measure of antioxidative defense capacity in the cell, was found to be decreased in the plasma of PEXG individuals.<sup>128</sup>

The generated free radicals and oxidation products cause changes in signaling pathways, gene transcription, mitochondrial functioning, chromatin architecture, and DNA damage leading to cell death. Risk loci in *GSTT1* and *GSTMI* have been identified in Pakistani female patients with PEXG but the results could not be replicated in other populations.<sup>129–131</sup> Further, SNPs, rs10432782 and rs2070424, in the *SOD* gene were not found to be associated with PEXS.<sup>132</sup> The lack of causal variants in anti-oxidant defense genes implies an epigenetic trigger responsible for their aberrant downregulation in PEXS and PEXG.

### **ER-UPR pathway**

Many pathological conditions can lead to endoplasmic reticulum (ER) stress, such as hypoxia, oxidative stress, aging, or metabolic disorders. The unfolded protein response (UPR) and the ER-associated degradation (ERAD) pathway kickstart to combat the ER stress and maintain cellular homeostasis. Hayat *et al.* reported a reduced proteasome activity and impaired ubiquitin-proteasome system in PEX eyes, suggesting an accumulation of misfolded proteins in the cell resulting in an increased ER stress. In concordance with these observations, the authors further noted increased expression of ER-UPR genes and ERAD

pathway components, such as DnaJ homolog subfamily B member 11 (*DNAJB11*), heat shock protein 60 member 1 (*HSPD1*), DnaJ homolog subfamily B member 1 (*DNAJB1*), heat shock protein 70 member 5 (*HSPA5*), synoviolin (*SYVN*) and calnexin (*CANX*).<sup>133</sup>

Recently, Roodnat *et al.* developed a potential cellular model for PEXG by stimulating human trabecular meshwork cells with TGF- $\beta$ 1, which resulted in changes in the transcriptome of the cell that mapped to crucial pathways and genes dysregulated in PEXG. The authors observed activation of the UPR with upregulation of UPR-associated genes, such as *HSPA5*, heat shock protein 90 beta family member 1 (*HSP90B1*), eukaryotic translation initiation factor 2 alpha kinase 3 (*EIF2AK3*), and X-box binding protein 1 (*XBPI*).<sup>117</sup> These findings suggest impairment of the ubiquitin-proteasome system coupled with ER-UPR contributes to PEX pathology.

### **Autophagy**

Autophagy is a cellular process for the elimination of proteins marked for degradation, such as the ubiquitinated misfolded proteins. It has been observed that the autophagic processes are compromised in PEX, which could result in the excess generation of misfolded proteins and their aggregation, as seen in PEX pathology. Two research groups independently studied autophagy dysfunction in cultured Tenon's fibroblasts (TFs) from PEXS patients. Want *et al.* reported the presence of larger vacuoles filled with cellular waste in TFs from PEXS patients. Also, on induction of autophagy, a reduced autophagosome clearance along with the failure of relocation of lysosomes to the perinuclear region was observed. Starvation-induced autophagy increased the ratio of autophagosome-bound LC3 (LC3-II) and LC3-II/LC3-I and congestion of the LAMP-1 positive vesicles, indicating a reduced level of autophagosome clearance from the cell. Similarly, Bernstein *et al.* reported the dysfunction of lysosomal and autophagosome positioning in PEXS TFs. The patient TFs further exhibited an irregular

autophagic flux seen through the accumulation of the autophagosome marker, LC3-II, and the process of clearance of autophagosomes from PEXS cells was slowed. Similar observations were reported in the neurons cultured from advanced stage Alzheimer's patients in which autolysosomes were dispersed widely throughout the cell, LC3-II positive enlarged autophagosomes accumulated and autophagic flux, and clearance of autophagosomes was slowed, demonstrating a clear parallel between neurodegenerative pathological markers and PEXS. Thus, a self-reinforcing loop of dysfunctional autophagy impacting autophagic flux may be an important contributor to a sudden onset of cellular pathology.

### **1.9. Lacunae and unanswered questions in the field**

Although extensive research in the past two decades in the field of pseudoexfoliation has identified numerous risk factors associated with the disease, the aetiology of PEX is partially understood. Major discoveries in this field are concentrated on the genetic basis of the disease. However, the genetic studies have been inconsistent due to allele reversals in populations of different ethnicities, the absence of association of reported variants in replicate studies, and incomplete penetrance with the presence of risk alleles in the normal population at higher frequencies. Thus, novel factors and variants need to be identified that could be major genetic contributors to the disease pathology, factors that are unaffected by and are independent of race and ethnicity in the context of the disease.

Further, a few aspects of PEX pathogenesis, such as the progressive nature of the disease, age-related onset, and only a subset of PEXS individuals developing the glaucomatous neuropathy and unilateral or asymmetric ocular manifestation of PEX, cannot be explained by accumulating mutations alone. Also, we and others have reported differential gene expression in the different stages of the disease, i.e., PEXS and PEXG. While some genes or proteins were seen to be dysregulated in PEXS and not PEXG, a few others have been

reported to be dysregulated in PEXG but not in PEXS.<sup>76,101,115,123,133,134</sup> This difference in the risk factors and molecular pathways involved in PEXS and PEXG pathology implies that the underlying aetiology is different for the early and the severe advanced stages of pseudoexfoliation. The missing link of information could be epigenetic factors which are just starting to be appreciated in understanding PEX pathogenesis. Reports have suggested that differences in monozygotic twins over non-Mendelian and complex diseases could be due to a combination of genetic and epigenetic factors.<sup>135</sup>

With this background, my thesis aims at exploring the association of four candidate genes- fibulin-5, clusterin, glutathione-S-transferase and vimentin with PEX with the following objectives:

1. To study the association of common variants in fibulin-5 with PEX.
2. To identify risk variants in clusterin and study its promoter methylation status in PEX.
3. To understand the candidature of vimentin in PEX pathology
4. To study the epigenetic regulation of glutathione-S-transferases in PEX
5. To identify potential biomarkers and novel genetic variants for PEX

\*\*\*\*\*

## *Chapter 2*

# **Association of genetic variants within fibulin-5 with PEX**

## 2. Association of genetic variants within fibulin-5 with PEX

### 2.1. Introduction

In this chapter, we report the genetic association of variants in fibulin-5 (*FBLN5*) with PEX.

*FBLN5* (MIM: 604580) is a 66 kDa secreted extracellular calcium-binding scaffold protein highly crucial for assembling elastic fibers. *FBLN5* protein contains six calcium-binding epidermal growth factor-like (cbEGF) domains. Within the first cbEGF domain at the N-terminal resides the evolutionarily conserved RGD (Arginine-Glycine-Aspartate) motif, which facilitates the binding of *FBLN5* to integrins on the surface of cells.<sup>136</sup> *FBLN5* interacts with various ECM proteins and cell surface molecules through its cbEGF domains, essential for elastogenesis. Elastogenesis is the process of assembly of elastic fibers formed of elastin polymers from tropoelastin monomers (**Figure 2.1**). Numerous extracellular proteins are involved in this sequential process. During elastogenesis, coacervation of tropoelastin occurs, and the fibrillins form microfibrils, a scaffold for the deposition of tropoelastin monomers. The N-terminus of fibulin-5 binds to fibrillins and deposits the cross-linking enzyme LOXL1 in the ECM via the C-terminus, where LOXL1 crosslinks tropoelastin monomers to elastic fibers.<sup>137</sup> Fibulin-5 (*Fbln5*<sup>-/-</sup>) null mice show progressively worsening elastic fiber defects in all elastogenic tissues such as skin, lungs, genitalia, and aorta.<sup>136</sup>

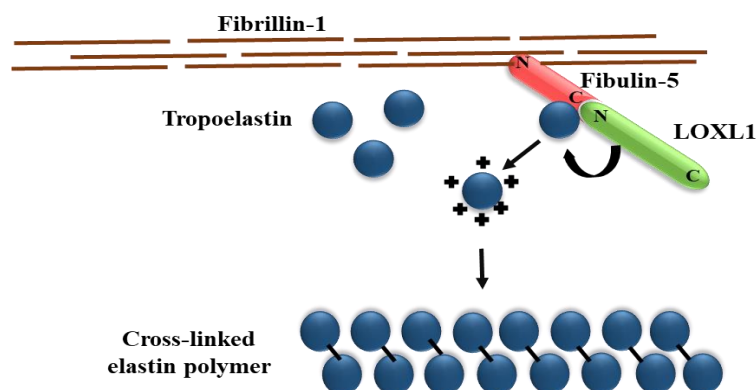


**Figure 2.1. Role of fibulin-5 in elastogenesis.** Schematic diagram showing the interaction of fibulin-5 with the fibrillin scaffold and LOXL1. LOXL1 catalyzes the deamination of tropoelastin monomers and their subsequent polymerization to elastin polymers.

Also, fibulin-5 is involved in other essential cellular functions such as cell-matrix adhesion, integrin-dependent regulation of reactive oxygen species (ROS) in the ECM, regulation of cell receptor signaling, endothelial to mesenchymal transition, modulation of matrix proteases, and vascular injury.<sup>138–140</sup>

Fibulin-5 has been associated as a risk factor with for various diseases involving ECM anomalies. Aberrant expression or deposition of fibulin-5 has been observed in age-related macular degeneration (ARMD), cutis laxa (CL), Charcot-Marie-Tooth syndrome, abdominal aortic aneurysms and pelvic organ prolapse (POP).<sup>141–144</sup> Further, mutations in *FBLN5* have been related to complications such as ARMD, CL, and POP.<sup>145–147</sup> Missense variations in *FBLN5* associated with ARMD and CL were reported to lead to structural defects and decreased protein secretion. Downregulation of fibulin-5 could lead to decreased availability of the protein for interaction with elastin, fibrillins, and LOXL1 affecting the elastic fibre assembly, which has been attributed as a major cause of these elastinopathies. Dysregulation of fibulin-5 and its altered function contribute to various cancers. *FBLN5* was found to be downregulated in epithelial ovarian cancer, urothelial carcinoma of the bladder, and prostate cancers.<sup>148–150</sup> Yue *et al.* observed that fibulin-5 suppresses the lung cancer invasion by inhibiting the MMP-7.<sup>151</sup> On the contrary, Schiemann *et al.* have reported that overexpression of *FBLN5* leads to fibrosarcoma cell migration.<sup>152</sup>

The exfoliative material (XFM) observed in PEX showed the presence of other fibulins and LOXL1 in the aggregates. PEX being an ECM disorder, we hypothesized the involvement of *FBLN5* in PEX pathology.<sup>134</sup> Also, it had been reported that LOXL1 fails to colocalize with *FBLN5* in PEX eyes compared to controls.<sup>153</sup> This implied a loss of interaction which could be due to impaired or reduced protein production of the complete fibulin-5 protein in PEX patients. Further, Want *et al.* observed aggregation of fibulin-5 in a 3D culture of tenon fibroblasts from PEXS patients.<sup>154</sup> Additionally, biochemical and pathological analysis has

shown an association between PEX and other diseases such as ARMD, abdominal aortic aneurysms and, POP.<sup>51,155,156</sup> In 2019, we reported a novel genetic association of two variants, rs7149187 and rs929608, residing in the 5'-UTR and 10<sup>th</sup> intron, respectively, of *FBLN5* as a risk for pseudoexfoliation. We further reported the downregulation of *FBLN5* in PEXS individuals. However, the associated variants did not show a functional regulatory role *in vitro*.<sup>134</sup>

Therefore, in search of putative regulatory variants in *FBLN5*, which could be causal variants playing pivotal roles in PEX pathogenesis, through the Tag SNP genotyping approach, we looked for the association of variants in *FBLN5* with PEX.

## **2.2. Materials and methods**

### **2.2.1. Study subjects' recruitment and sample collection**

This study was approved by the Institutional Biosafety and Human Ethics committee of the National Institute of Science Education and Research and adhered to the tenets of the Declaration of Helsinki. All study participants underwent a detailed ocular examination, including slit lamp microscopy, ocular biometry, Goldman applanation tonometry, +90D biomicroscopic fundus evaluation, and four-mirror gonioscopy. Cataract patients aged above 40 years with clinically evident PEX-like material over lens capsule (LC) and pupillary ruff having untreated IOP < 21 mmHg without any visual field defects were included under the PEXS group and those with untreated IOP > 21mmHg, glaucomatous nerve head damage with repeatable field defects corresponding to disc damage were included under the PEXG group. Patients with corneal or retinal pathology precluding reliable visual field were excluded from the PEXG group. Cataract patients above 40 years without PEXS or PEXG, with untreated IOP < 21 mmHg having normal discs and visual field, were included as

controls. Patients with systemic diseases such as diabetes were not included in the study. Informed written consent was obtained from all participants for this study. Due to the higher disease presentation of PEXS patients visiting the hospital, the number of PEXS subjects is higher than that of PEXG. Peripheral blood was collected in EDTA vacutainers from the participants and stored at  $-80^{\circ}\text{C}$  until further experimentation.

### **2.2.2. DNA isolation from blood**

The phenol-chloroform RBC lysis method was used to isolate DNA from peripheral blood. 4 ml of peripheral blood was collected in EDTA-vacutainer tubes and stored at  $-80^{\circ}\text{C}$  until further use. 500  $\mu\text{l}$  of blood was centrifuged at 11000 rpm for 10 minutes. To the pellet, 1.0 ml of RBC lysis buffer [0.32 M sucrose, 1.0 mM  $\text{MgCl}_2$ , 1.0% Triton X-100, 12 mM Tris-HCl, pH 7.6] was added, and the pellet suspended uniformly in the buffer. The suspension was centrifuged at 11000 rpm for 5 minutes. The pellet was again suspended in 200  $\mu\text{l}$  of RBC lysis buffer and centrifuged at 13000 rpm for 10 minutes. The pellet was then suspended in 200  $\mu\text{l}$  milliQ water and centrifuged at 13000 rpm for 10 minutes. The supernatant was discarded, and the pellet was suspended in 10% SDS, 5M NaCl, and milliQ. 400  $\mu\text{l}$  of PCI (phenol: chloroform: isoamyl alcohol) was added to the suspension and mixed thoroughly by inverting. The mixture was centrifuged at 12000 rpm for 10 minutes. The upper layer was carefully transferred to a fresh centrifuge tube. To this, 1.0 ml of absolute ethanol was added and mixed by inverting slowly. The mixture was centrifuged at 12000 rpm for 10 minutes. The pellet was washed with 70% ethanol at 13000 rpm for 5.0 minutes. All the reactions were carried out at room temperature. The supernatant was discarded, and the pellet dried overnight. The pellet was suspended in Tris-EDTA buffer and dissolved properly at  $56^{\circ}\text{C}$  for 1.0 hour.

### 2.2.3. Taqman SNP genotyping assay

The tag SNP genotyping approach was chosen for higher genetic coverage of the *FBLN5* gene. Thirteen tag SNPs within *FBLN5* were chosen based on 1000 genomes HapMap South Asian GIH dataset with a pair-wise tagging of  $r^2 > 0.9$  and minor allele frequency (MAF)  $> 0.1$  (**Table 2.1**). Peripheral blood was collected from the study subjects, and genomic DNA was extracted using the phenol-chloroform method. The SNPs were genotyped using TaqMan SNP genotyping assays (Applied Biosystems, Carlsbad) on Quantstudio 7 (ThermoFisher Scientific). Each 5  $\mu$ l PCR reaction mix consisted of a 20 ng DNA sample, 2.5  $\mu$ l of 2X Taqman master mix, and 1.25  $\mu$ l of Taqman SNP assay, and the volume was made up using nuclease-free water. The PCR conditions were: initial denaturation at 95<sup>0</sup>C followed by 40 cycles of denaturation at 95<sup>0</sup>C for 15 seconds and annealing and extension at 60<sup>0</sup>C for 1.0 min. The data was analyzed using the instrument software and Taqman Genotyper software.

**Table 2.1.** Tag SNPs in *FBLN5* (Chr 14, hg38 build) chosen for this study

Variant	dbSNP ID	Location on gene	Taqman Assay ID
NC_000014.9:g.91943755T>C	rs12432450:T>C	Intron 1	C__2485312_10
NC_000014.9:g.91926682C>T	rs8012648:C>T	Intron 4	C_189552237_10
NC_000014.9:g.91913280G>A	rs17732466:G>A	Intron 4	C__34507447_10
NC_000014.9:g.91911458G>A	rs12589592:G>A	Intron 4	C__11473329_10
NC_000014.9:g.91904479G>T	rs2498835:G>T	Intron 4	C__16028647_10
NC_000014.9:g.91902891C>G	rs2267997:C>G	Intron 4	C__2674168_10
NC_000014.9:g.91897442T>C	rs917908:T>C	Intron 4	C___325514_20
NC_000014.9:g.91896083T>C	rs2244158:T>C	Intron 4	C__16028658_10
NC_000014.9:g.91892576C>T	rs2243400:C>T	Intron 5	C__15799126_10
NC_000014.9:g.91891905G>C	rs2267995:G>C	Intron 5	C__2674154_1_
NC_000014.9:g.91890855C>T	rs72705342:C>T	Intron 6	C__99168492_10
NC_000014.9:g.91885243A>C	rs2498841:A>C	Intron 7	C__16028659_10

NC_000014.9:g.91874378G>A	rs2284337:G>A	Intron 10	C__15960961_10
---------------------------	---------------	-----------	----------------

#### **2.2.4. Cloning techniques**

##### ***Competent cell preparation***

Inoculum from stock culture was added to 5.0 ml LB broth and incubated at 37<sup>0</sup>C overnight, with a shaking at 220 rpm. The next day, 1.0% from the previous night culture was added to 250 ml LB broth and incubated at 37<sup>0</sup>C at 220 rpm. Intermittently, the culture's optical density (OD) was measured spectrophotometrically at 600 nm against LB broth as blank. Once the OD reached 0.4-0.6, the growth was arrested by incubating the culture on ice for 15 minutes. Further steps were carried out at 4<sup>0</sup>C. The culture was centrifuged at 4000 rpm for 10 minutes. The supernatant was discarded, and a pellet from every 50 ml of culture was suspended in 25 ml of TFBI [30 mM potassium acetate, 100 mM rubidium chloride, 10 mM calcium chloride, 80 mM manganese chloride, and 15% glycerol; pH 5.8] buffer. The suspension was incubated on ice for 15 minutes and centrifuged at 4000 rpm for 10 minutes. The supernatant was discarded, and the total pellet was suspended in 2.0 ml of TFBII [10 mM MOPS, 10 mM calcium chloride, 10 mM rubidium chloride, and 15% glycerol; pH 6.5] buffer. The suspension was incubated on ice for 30 minutes. The suspension/ competent cells were then aliquoted, snap-frozen on liquid nitrogen, and stored at -80<sup>0</sup>C until further use.

##### ***Restriction digestion***

Restriction enzyme digestion was carried out at 37<sup>0</sup>C for three hours. Double digestion for cloning was done by digesting the vector and inserting it with the target enzymes in a 30 µl reaction containing 500-1000 ng of target DNA, 1X cut smart buffer, and 0.5 µl each of the enzymes. For cloning of the oligo-annealed inserts, the oligos were synthesised such that they carried digested sticky overhangs specific for the enzyme, and only the vector was digested

with the specific enzyme pair. The digested products were then resolved and purified on 1.2% agarose gel.

### ***Ligation***

Ligation of the inserts and vectors carrying compatible sticky overhangs was carried out by T4 DNA ligase or Quick ligase enzymes. Ligation with T4 DNA ligase was carried out at 16<sup>0</sup>C overnight, and ligation with Quick ligase was carried out at 25<sup>0</sup>C for 10 minutes. The 20 µl reaction mix contained insert: vector in the ratio of 3:1, 1X ligase buffer, and 1.0 µl of ligase enzyme. The ligated product was immediately transfected into competent cells.

### ***Transformation***

5.0 µl of the ligated product was mixed with 50 µl of competent cells and incubated on ice for 30 minutes. Heat shock was given to the cells at 42<sup>0</sup>C for 45 seconds, and immediately the cells were placed on ice for another 15 minutes. The cells were then incubated at 37<sup>0</sup>C with 1.0 ml LB broth for 1.0 hour at 220 rpm. The cells were centrifuged at 13000 rpm for 3.0 minutes. Excess LB broth was removed, and the pellet was suspended in 100 µl of LB broth. The bacterial cell suspension was then plated on LB agar with a selective antibiotic. The plates were incubated at 37<sup>0</sup>C overnight. Positive colonies were screened by Sanger sequencing.

### **2.2.5. Plasmid isolation**

Plasmid from the bacteria was isolated using the QiaPrep spin miniprep kit (Qiagen, Cat. No. 27104). The bacterial culture was centrifuged at 13000 rpm for 5.0 minutes. The pellet was suspended in 250 µl ice-cold P1 buffer. 250 µl P2 buffer was added to the suspension and mixed thoroughly until the solution turned blue. 350 µl of N3 buffer was added to the solution and mixed immediately by inverting until the solution turned colorless. The solution was then centrifuged at 13000 rpm for 10 minutes. The supernatant was carefully applied to

the column and centrifuged at 13000 rpm for 1.0 minute. The flow through was discarded, and the column was washed twice with 750 µl PE wash buffer at 13000 rpm for 1.0 minute. The flow-through was discarded, and the column was given a dry spin and air-dried. The plasmid was eluted from the column in 50 µl EB buffer by centrifuging at 13000 rpm for 1.0 minute.

### **2.2.6. Cell culture**

Human lens epithelial B3 cells (HLE B-3), an immortalized cell line that was derived from the human lens infant tissue and transformed with an adenovirus 12-Simian Virus 40 hybrid (Ad12SV40),<sup>157</sup> were purchased from ATCC (B-3 CRL11421, VA, USA). They were grown in DMEM/F12 medium (11330057, Invitrogen GIBCO) supplemented with 10% inactivated fetal bovine serum (16000044, Invitrogen), 1.0% penicillin (100U/ml) and streptomycin (0.1 mg/ml) (A001, HiMedia) at 37<sup>0</sup>C and 5.0% CO<sub>2</sub>.

### **2.2.7. Luciferase assay**

To test the functional effect of the SNPs, two reporter vectors, pGL4.23 with the minimal promoter of the reporter and pGL3 containing the fibulin-5 core promoter region, were used. The region from -675 bp to ATG start codon of the *FBLN5* gene was amplified using Phusion High Fidelity DNA polymerase (NEB) and cloned into pGL3 basic luciferase reporter vector using BglII and NcoI (NEB). Twenty-nine base pairs long DNA fragments surrounding the SNPs (**Table 2.2**) with either allele at the center were cloned into the reporter vectors using KpnI HF and XhoI (NEB). HLE B-3 cells were seeded in a 24-well plate, and at 80% confluency, the cells were transiently transfected with 500 ng of the constructs along with 5.0 ng of *Renilla* vector (pGL4.74) using lipofectamine (Thermo Scientific, USA). After 24 hours post-transfection, the cells were harvested, and luciferase activity was assayed using the Dual-Luciferase Reporter assay system (Promega). The Firefly luciferase activity from each construct was normalized to Renilla luciferase activity, and the ratio has been plotted as percent luciferase activity relative to that of empty vector (taken as 100 per cent).

### 2.2.8. Electrophoretic mobility shift assay (EMSA)

Twenty-nine base pairs sense (S) and antisense (A) oligonucleotides encompassing the rs72705342:C>T (NC\_000014.9:g.91890855C>T) were synthesized for performing the EMSAs (Table 2.2). The oligos were synthesized with their 5' end labelled with biotin, and unlabelled oligos were procured as well. The oligos were annealed by incubating the mix of complementary strands at 95<sup>0</sup>C for 5 minutes, then gradually cooling down the mix to room temperature. Nuclear extract from HLE B-3 cells was prepared using the NE-PER Nuclear and Cytoplasmic Extraction Reagents kit (Thermo Scientific, USA). The binding reaction included poly (dI.dC) as non-specific competitor DNA. For competition experiments, a 200-fold excess of unlabelled oligonucleotides was included in the pre-incubation mixture. For supershift assays, EMSA-specific antibodies for TFII I (sc-46670X, Santa Cruz) and GR- $\alpha$  (PA1516, Invitrogen) were pre-incubated with the nuclear extract for one hour before adding the final reaction mixture. The complexes, after incubation, were resolved on 6.0% native polyacrylamide gels, transferred to nylon membranes, and developed. EMSA was performed with the Lightshift Chemiluminescent EMSA kit (Thermo Scientific, USA). Detection was done using Fusion Solo S Chemi-Doc (Vilber Lourmat), and gel shifts were quantified with the Evolution Capt software (Vilber Lourmat Fusion Solo S).

**Table 2.2.** List of oligos used in the study

S. No	ID	Purpose	Sequence (5'→3')
1	rs72705342 'C'	Luciferase assay	Top: CTTCCTGAGGCCTGAGGAGGGTTGGTCAGGC Bot: TCGAGCCTGACCAACCCTCCTCAGGCCTCAGGAAG GTAC
2	rs72705342 'T'	Luciferase assay	Top: CTTCCTGAGGCCTGAAGAGGGTTGGTCAGGC Bot: TCGAGCCTGACCAACCCTCTTCAGGCCTCAGGAAG GTAC

3	rs17732466 'G'	Luciferase assay	Top: CATCCTCCAAAATATTCAGGCATGATATTCC Bot: TCGAGGAATATCATGCCTGAATATTTTGGAGGATG GTAC
4	rs17732466 'A'	Luciferase assay	Top: CATCCTCCAAAATATTTAGGCATGATATTCC Bot: TCGAGGAATATCATGCCTAAATATTTTGGAGGATG GTAC
5	<i>FBLN5</i> promoter	Luciferase assay	FP: CACGAAGCTTTTTCTAGTCCCTGGAGCTGCG RP: CACTCCATGGGTCCAAGACGCGCGAGGA
7	rs72705342 'C' labelled	EMSA	S: TTCCTGAGGCCTGAGGAGGGTTGGTCAGG A: CCTGACCAACCCTCCTCAGGCCTCAGGAA
8	rs72705342 'T' labelled	EMSA	S: TTCCTGAGGCCTGAAGAGGGTTGGTCAGG A: CCTGACCAACCCTCTTCAGGCCTCAGGAA

### 2.2.9. *In silico* analysis

The PROMO software ([http://alggen.lsi.upc.es/cgi-bin/promo\\_v3/promo/promoinit.cgi?dirDB=TF\\_8.3](http://alggen.lsi.upc.es/cgi-bin/promo_v3/promo/promoinit.cgi?dirDB=TF_8.3)) was used to identify transcription factor binding sites to the region surrounding rs72705342C>T. The sequences of the genomic region flanking the 'T' allele or 'C' allele of the SNP rs72705342 ( $\pm 15$  bp) were used as input.

### 2.2.10. Genetic and statistical analysis

Age and sex-matched samples were taken for the experiments. The matching was done by performing the Student's t-test between the groups. No data were missing for the participants. The allelic association tests, Hardy-Weinberg equilibrium (HWE), and logistic regression analysis for covariates were done using PLINK. Haplotype analysis and linkage disequilibrium (LD) analysis were done using Haploview V4.2. The statistical significance of group-wise results was analyzed using Student's t-test, and  $p < 0.05$  was considered as statistically significant. The Bonferroni and Holm correction was applied for multiple pairwise comparisons. All experiments were done at least three times independently. Data are presented as mean  $\pm$  SEM.

## 2.3. Results

### 2.3.1. Demographics of the study subjects

A total of 273 PEX (169 PEXS and 104 PEXG) and 200 age-and-sex-matched control subjects participated in this study. The demographics of the study subjects are shown in **Table 2.3**. The mean age in years  $\pm$  SD of controls, PEXS, and PEXG were  $70.17 \pm 7.17$ ,  $71.09 \pm 7.29$ , and  $70.21 \pm 7.39$ , respectively. The age range of controls, PEXS, and PEXG was 60-90 years, 50-90 years, and 60-92 years, respectively. Of the study participants, 36.1% were females. One hundred and seventy-one females (80 control, 64 PEXS, and 27 PEXG) and 302 males (120 control, 105 PEXS, and 77 PEXG) participated in the study.

**Table 2.3.** Demographic details of the study subjects

Subjects	Sample Size (N)	Age (in years)		p-value	Sex		p-value
		Mean $\pm$ SD	Range		Male	Female	
Control	200	$70.17 \pm 7.17$	60-90		120	80	
PEXS	169	$71.09 \pm 7.29$	50-90	0.10	105	64	0.41
PEXG	104	$70.21 \pm 7.39$	60-92	0.50	77	27	0.12

### 2.3.2. Intronic variants, rs72705342 and rs17732466, within *FBLN5* are genetically associated with PEXG

Thirteen tag SNPs (**Figure 2.2**) within *FBLN5* were genotyped in 169 PEXS, 104 PEXG, and 200 age and sex-matched control subjects. The thirteen SNPs chosen for the study are rs12432450 located in the intron 1, rs8012648, rs17732466, rs12589592, rs2498835, rs2267997, rs917908 and rs2244158 located in the intron 4, rs2243400 and rs2267995 located in the intron 5, rs72705342 located in the intron 6, rs2498841 located in the intron 7 and rs2284337 located in the intron 10.

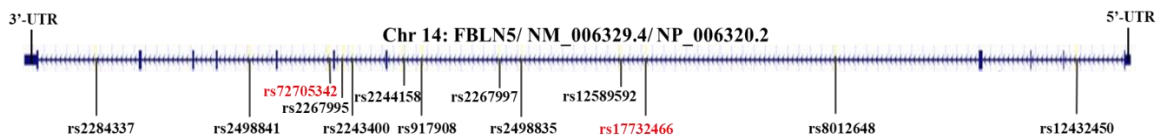


**Figure 2.2. Position of Tag SNPs.** Gene structure of *FBLN5* showing the position of the thirteen tag SNPs (obtained from UCSC genome browser 05 June 2022).

All the studied SNPs passed the HWE test set at a default significance threshold of  $p \leq 0.001$ . Allele frequencies, odds ratio, and statistical significance of the genotyped *FBLN5* variants are presented in Table 2.4. Two variants, NC 000014.9:g.91913280G>A (rs17732466:G>A) and NC 000014.9:g.91890855C>T (rs72705342:C>T), located in the 4<sup>th</sup> and the 6<sup>th</sup> introns of *FBLN5*, respectively, were found to be significantly associated with PEXG with the risk alleles being ‘G’ ( $p=0.04$ ) and ‘C’ ( $p=0.02$ ), respectively. Risk analysis showed that the minor alleles ‘A’ at rs17732466 and ‘T’ at rs72705342 confer a protective effect with an odds ratio (OR) of 0.66 (95% CI 0.43-0.99) and 0.60 (95% CI 0.39-0.93), respectively. However, none of the studied variants showed a significant association with PEXS.

Genotypic distribution of the variants in controls, PEXS, and PEXG is presented in Table 2.5. None of the SNPs showed any genotypic association with PEXS. However, individuals with the risk genotype ‘CC’ at rs72705342 showed higher susceptibility to PEXG than individuals carrying the ‘TT’ genotype ( $p=0.04$ ).

**Table 2.4.** Distribution of *FBLN5* variants in PEXS and PEXG compared to the controls

SNP ID	Major allele	Minor allele	MAF			Control versus PEXS		Control versus PEXG	
			Control (N=200)	PEXS (N=169)	PEXG (N=104)	OR (95% CI)	p-value	OR (95% CI)	p-value
rs12432450	C	T	0.37	0.39	0.39	1.14 (0.84-1.55)	0.37	1.07 (0.75-1.53)	0.68
rs8012648	C	T	0.35	0.36	0.30	1.04 (0.76-1.41)	0.80	0.77 (0.53-1.12)	0.17
<b>rs17732466</b>	G	A	0.28	0.26	0.21	0.87 (0.62-1.22)	0.44	0.66 (0.43-0.99)	<b>0.04</b>
rs12589592	G	A	0.25	0.20	0.22	0.78 (0.55-1.12)	0.18	1.03 (0.69-1.53)	0.86
rs2498835	G	T	0.36	0.37	0.30	1.03 (0.75-1.41)	0.74	0.72 (0.50-1.05)	0.08
rs2267997	G	C	0.32	0.32	0.33	1.18 (0.76-1.85)	0.85	1.08 (0.75-1.56)	0.65
rs917908	T	C	0.11	0.13	0.11	0.87 (0.37-2.04)	0.44	0.95 (0.55-1.64)	0.86
rs2244158	C	T	0.31	0.30	0.33	0.94 (0.68-1.30)	0.74	0.98 (0.68-1.43)	0.95
rs2243400	C	T	0.14	0.17	0.15	1.18 (0.78-1.79)	0.40	1.02 (0.62-1.66)	0.93
rs2267995	G	C	0.31	0.31	0.37	1.02 (0.73-1.39)	0.94	1.32 (0.92-1.90)	0.12
<b>rs72705342</b>	C	T	0.25	0.24	0.17	0.96 (0.68-1.35)	0.81	0.60 (0.39-0.93)	<b>0.02</b>
rs2498841	C	A	0.24	0.26	0.18	1.12 (0.80-1.57)	0.49	0.67 (0.44-1.04)	0.07
rs2284337	G	A	0.29	0.25	0.22	0.84 (0.63-1.17)	0.31	0.71 (0.47-1.07)	0.1

CI: confidence interval, OR: odds ratio, PEXS: pseudoexfoliation syndrome, PEXG: pseudoexfoliation glaucoma

**Table 2.5.** Genotypic distribution of *FBLN5* variants in control, PEXS and PEXG

SNP ID	Genotype	Freq. in Control (n=200)	Freq. in PEXS (n=169)	Freq. in PEXG (n=104)	Genetic Model	Control versus PEXS		Control versus PEXG	
						OR (95% CI)	p-value	OR (95% CI)	p-value
rs12432450	TT	0.12	0.12	0.05	Additive	1.09 (0.77-1.54)	0.59	1.16 (0.79-1.70)	0.43
	CT	0.51	0.54	0.34	Dominant	1.17 (0.76-1.81)	0.45	1.06 (0.64-1.75)	0.79
	CC	0.37	0.34	0.60	Recessive	1.09 (0.58-2.05)	0.78	1.35 (0.67-2.73)	0.39
rs8012648	TT	0.13	0.15	0.01	Additive	1.05 (0.76-1.44)	0.75	0.81 (0.54-1.21)	0.31
	CT	0.43	0.42	0.34	Dominant	1.02 (0.67-1.55)	0.91	0.79 (0.48-1.29)	0.35
	CC	0.44	0.43	0.65	Recessive	1.11 (0.61-2.02)	0.73	0.71 (0.33-1.55)	0.39
rs17732466	AA	0.10	0.08	0.01	Additive	0.87 (0.59-1.27)	0.47	0.65 (0.39-1.10)	0.11
	AG	0.37	0.35	0.33	Dominant	0.86 (0.56-1.31)	0.49	0.63 (0.38-1.04)	0.07
	GG	0.53	0.56	0.66	Recessive	0.79 (0.37-1.66)	0.53	0.49 (0.18-1.37)	0.17
rs12589592	GG	0.07	0.04	0.13	Additive	0.70 (0.44-1.12)	0.14	0.97 (0.60-1.56)	0.90
	AG	0.35	0.35	0.46	Dominant	0.76 (0.50-1.16)	0.21	1.11 (0.69-1.79)	0.65
	AA	0.58	0.56	0.40	Recessive	0.53 (0.21-1.33)	0.18	0.89 (0.35-2.25)	0.80
rs2498835	TT	0.14	0.15	0.03	Additive	1.05 (0.76-1.44)	0.75	0.657(0.41-1.03)	0.06
	GT	0.43	0.44	0.23	Dominant	1.08 (0.71-1.65)	0.71	0.81 (0.49-1.31)	0.39
	GG	0.43	0.41	0.74	Recessive	1.06 (0.59-1.91)	0.82	0.44 (0.18-1.06)	0.06
rs2267997	CC	0.08	0.13	0.08	Additive	1.22 (0.85-1.76)	0.27	1.10 (0.70-1.73)	0.67
	CG	0.48	0.39	0.45	Dominant	0.86 (0.56-1.31)	0.48	1.10 (0.67-1.80)	0.68
	GG	0.44	0.48	0.46	Recessive	1.72 (0.85-3.46)	0.12	1.16 (0.48-2.75)	0.73
rs917908	CC	0.01	0.04	0.02	Additive	2.66 (0.92-7.74)	0.07	1.94 (0.58-6.52)	0.27

	CT	0.22	0.19	0.18	Dominant	1.04 (0.63-1.72)	0.84	0.88 (0.48-1.60)	0.68
	TT	0.77	0.77	0.80	Recessive	7.27 (0.86-61.0)	0.06	3.95 (0.35-44.20)	0.26
rs2244158	TT	0.07	0.09	0.09	Additive	1.10 (0.74-1.65)	0.61	1.06 (0.66-1.71)	0.79
	CT	0.49	0.41	0.49	Dominant	0.82 (0.54-1.25)	0.36	0.92 (0.56-1.50)	0.75
	CC	0.44	0.49	0.42	Recessive	1.39 (0.64-3.03)	0.39	1.20 (0.48-3.00)	0.69
rs2243400	TT	0.01	0.03	0.07	Additive	1.76 (0.77-4.05)	0.17	1.69 (0.68-4.11)	0.25
	CT	0.27	0.27	0.45	Dominant	1.13 (0.71-1.80)	0.59	0.93 (0.53-1.61)	0.80
	CC	0.72	0.69	0.48	Recessive	3.08 (0.59-16.12)	0.18	2.96 (0.48-18.0)	0.23
rs2267995	CC	0.09	0.09	0.06	Additive	0.98 (0.67-1.43)	0.92	1.29 (0.86-1.93)	0.20
	CG	0.42	0.44	0.38	Dominant	1.05 (0.69-1.60)	0.80	1.37 (0.83-2.24)	0.20
	GG	0.48	0.47	0.55	Recessive	0.93 (0.44-1.93)	0.85	1.47 (0.68-3.13)	0.31
<b>rs72705342</b>	TT	0.07	0.06	0.05	<b>Additive</b>	0.93 (0.60-1.45)	0.77	<b>0.35 (0.12-0.98)</b>	<b>0.04</b>
	CT	0.37	0.36	0.31	Dominant	0.93 (0.61-1.41)	0.74	0.64 (0.39-1.06)	0.08
	CC	0.56	0.58	0.64	Recessive	0.90 (0.38-2.11)	0.81	0.14 (0.01-1.08)	0.05
rs2498841	AA	0.04	0.05	0.10	Additive	1.18 (0.69-2.00)	0.53	0.48 (0.16-1.40)	0.18
	AC	0.40	0.42	0.40	Dominant	1.12 (0.74-1.69)	0.58	0.68 (0.41-1.12)	0.13
	CC	0.56	0.53	0.49	Recessive	1.34 (0.47-3.78)	0.57	0.26 (0.03-2.21)	0.22
rs2284337	AA	0.09	0.04	0.15	Additive	0.67 (0.42-1.07)	0.09	0.69 (0.41-1.17)	0.17
	AG	0.39	0.42	0.49	Dominant	0.93 (0.61-1.41)	0.73	0.69 (0.42-1.14)	0.15
	GG	0.52	0.54	0.36	Recessive	0.45 (0.18-1.11)	0.08	0.54 (0.19-1.52)	0.24

CI: confidence interval, OR: odds ratio, PEXS: pseudoexfoliation syndrome, PEXG: pseudoexfoliation glaucoma

### 2.3.3. Haplotypes in the Tag SNPs of *FBLN5* are associated with PEXG

The linkage disequilibrium (LD) pattern across the thirteen studied *FBLN5* SNPs is shown in **Figure 2.3A**. The confidence interval algorithm (Gabriel *et al.*)<sup>26</sup> defined two LD blocks.

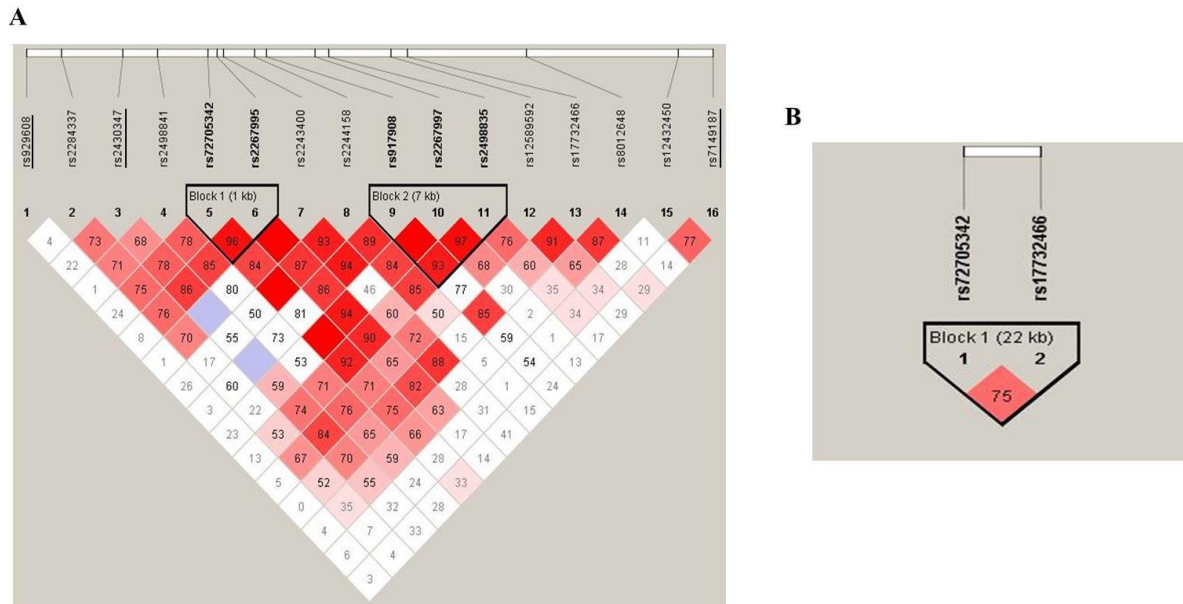


**Figure 2.3. Linkage disequilibrium pattern and haplotype association analysis.** **A.** LD pattern across all the SNPs. The LD blocks are defined using the confidence interval algorithm. **B.** LD block pattern with rs72705342-rs17732466.

The frequency of haplotype ‘T-G’ in Block 1 (rs72705342-rs2267995) was found to be significantly lower in PEXG (0.17,  $p=0.03$ ) but not in PEXS (0.23,  $p=0.70$ ) compared to control (0.24) (**Table 2.6**). Also, the haplotype analysis was done for the SNPs significantly associated with PEXG (**Figure 2.3B**). The frequency of the risk haplotype ‘C-G’ at ‘rs72705342-rs17732466’ was significantly higher in PEXG (0.76,  $p=0.03$ ) compared to controls (0.67) but was not associated with PEXS (0.69,  $p=0.6$ ) (**Table 2.6**).

**Table 2.6.** Haplotype association of Tag SNPs of *FBLN5* with PEXS and PEXG

Haplotype 'T-G' (rs72705342-rs2267995)	Freq.	OR (95%CI)	p-value
Control	0.24	1.06 (0.75-1.50)	0.70
PEXS	0.23		
PEXG	0.17	0.63 (0.41-0.98)	<b>0.03</b>
Haplotype 'G-C' (rs17732466-rs72705342)	Freq.	OR (95%CI)	p-value
Control	0.67	0.93 (0.68-1.28)	0.69
PEXS	0.69		
PEXG	0.76	1.51 (1.02-2.22)	<b>0.03</b>

CI: confidence interval, OR: odds ratio, PEXS: pseudoexfoliation syndrome, PEXG: pseudoexfoliation glaucoma

None of the haplotypes in Block 2 (rs917908-rs2267997-rs2498835) showed an association with either PEXS or PEXG (**Table 2.7**).

**Table 2.7.** Haplotype distribution of *FBLN5* variants in block 2 of controls, PEXS and PEXG

Haplotype (rs917908- rs2267997- rs2498835)	Freq. in control	Freq. in PEXS	Freq. in PEXG	Control versus PEXS		Control versus PEXG	
				OR (95% CI)	p-value	OR (95% CI)	p-value
T-G-G	0.32	0.30	0.36	1.11 (0.81-1.53)	0.50	0.83 (0.58-1.19)	0.32
T-C-G	0.31	0.32	0.33	0.97 (0.71-1.33)	0.87	0.93 (0.64-1.34)	0.69
T-G-T	0.24	0.24	0.18	1.02 (0.72-1.44)	0.89	1.40 (0.91-2.14)	0.11
C-G-T	0.11	0.12	0.10	0.90 (0.56-1.43)	0.65	1.06 (0.61-1.85)	0.80

CI: confidence interval, OR: odds ratio, PEXS: pseudoexfoliation syndrome, PEXG: pseudoexfoliation glaucoma

#### **2.3.4. Haplotypes of Tag SNPs and previously reported SNPs in *FBLN5* gene are associated with PEXS and PEXG**

We further performed haplotype analysis by including the already reported fibulin-5 SNPs (rs7149187, rs2430347 and rs929608) by our group.<sup>134</sup> The haplotype association analysis of all the sixteen SNPs- the thirteen Tag SNPs and three previously reported SNPs is shown in **Table 2.8**. None of the haplotypes were found to be associated with either PEXS or PEXG.

However, as only rs12432450 and rs7149187 showed a  $D'$  of 0.75, we analyzed the association of haplotype at these two loci with PEXS and PEXG. We observed a significant association of the protective haplotype 'C-A' at 'rs12432450-rs7149187' with both PEXS ( $p=0.01$ ) and PEXG ( $p=0.03$ ) (**Table 2.9**).

**Table 2.8.** Haplotype distribution of all *FBLN5* variants studied in controls, PEXS and PEXG

Haplotypes	Haplotype frequency			Control versus PEXS		Control versus PEXG	
	Control	PEXS	PEXG	OR (95% CI)	p-value	OR (95% CI)	p-value
CGGCCCCCTGGAGCTG	0.04	0.034	0.08	0.72 (0.36-1.76)	0.53	1.80 (0.94-3.78)	0.10
TGGCCCCCTGGAGCCA	0.04	0.024	0.03	0.45 (0.19-1.05)	0.05	0.67 (0.26-1.73)	0.39
TGGCCGCTTCGGGCCG	0.03	0.020	0.04	1.01 (0.33-3.05)	0.82	1.38 (0.58-3.28)	0.51
CAAATGCCTGTGATCA	0.05	0.056	0.01	0.92 (0.48-1.73)	0.80	0.36 (0.11-1.12)	0.06
CGGCCGCTTCGGGCTG	0.04	0.027	0.03	0.78 (0.31-1.93)	0.73	0.76 (0.29-2.01)	0.67
TAAATGCCTGTGATTG	0.02	0.033	0.04	2.20 (0.80-6.03)	0.13	1.57 (0.60-4.04)	0.35
TGGCCGCTTCGGGCCA	0.02	0.025	0.03	0.94 (0.36-2.42)	0.97	1.24 (0.47-3.25)	0.53
TGGCCGTCCGTGGCCG	0.02	0.03	0.02	2.40 (0.81-7.11)	0.09	0.96 (0.32-2.87)	0.86
CGGCCGTCCGTGGCCG	0.02	0.03	0.02	0.98 (0.41-2.30)	0.91	1.21 (0.39-3.77)	0.66
CAGCCGCTTCGGGCTG	0.02	0.01	0.02	0.36 (0.08-1.52)	0.16	0.85 (0.26-2.82)	0.85
TGGCCCCCTGGGGCCG	0.01	0.02	0.02	1.78 (0.50-6.39)	0.36	1.39 (0.43-4.44)	0.47
CGGCCCCCTGGAGCCG	0.02	-	0.01	-	-	0.56 (0.14-2.15)	0.39

TGGCCCCCTGGAGCTG	0.02	0.05	0.02	1.52 (0.76-3.04)	0.27	1.00 (0.29-3.44)	0.99
TGGCCCCCTGGAGCCG	0.01	-	0.02	-	-	1.77 (0.50-5.74)	0.33
TGGCCCCCTGGGGCCA	0.01	0.01	0.01	0.82 (0.25-2.64)	0.79	0.90 (0.22-3.61)	0.86
CGGCCGCTTCGGGCCA	0.01	-	0.01	-	-	0.70 (0.16-3.04)	0.64
CGGCCCCCTGGAGTTG	0.01	-	0.02	-	-	1.66 (0.44-6.29)	0.45
TGGCCCCCTGGGGCTG	0.01	0.03	0.02	2.43 (0.79-7.42)	0.11	2.05 (0.52-8.03)	0.28
CGGCCGTCCTGGGCCA	0.01	0.01	0.01	0.90 (0.27-3.05)	0.86	0.59 (0.11-3.02)	0.52
CGGCCGCTTCGGATCA	0.01	-	0.01	-	-	0.70 (0.13-3.56)	0.67
CGGCCGTCCTGGCTG	0.01	0.01	0.01	0.91 (0.21-3.78)	0.92	0.79 (0.11-3.59)	0.54
CAGCCGCTTCGGGCCG	0.01	-	0.01	-	-	1.45 (0.32-6.55)	0.87
CGAATGCCTGTGATCA	0.01	-	0.00	-	-	0.02 (0.00-14.00)	0.07
CGGCCCCCTGGGGCCG	0.01	0.01	0.01	0.93 (0.25-3.42)	0.92	2.07 (0.44-9.64)	0.33
CGGCCGCTTCGGATTG	0.01	0.01	0.01	0.80 (0.22-2.85)	0.75	0.35 (0.04-3.02)	0.33
CGGCCCCCTGGGGCCA	0.01	0.01	0.01	0.67 (0.74-0.52)	0.53	0.38 (0.04-3.31)	0.42
TAAATGCCTGTGATCA	0.01	0.01	0.01	0.98 (0.29-3.25)	0.94	0.96 (0.17-5.30)	0.81

CGGCCGCTTCGGGCCG	0.02	0.03	-	1.07 (0.45-2.56)	0.87	-	-
TAACTGCCTGTGATCA	0.01	0.01	-	1.18 (0.33-4.12)	0.88	-	-
CGGCCGCTTCGGGTCA	0.01	0.01	-	0.94 (0.25-3.55)	0.99	-	-
TGGCCGTCCGTGGCCA	0.02	0.00	-	0.16 (0.02-1.35)	0.07	-	-
CGGCCGTCTCGGGTCG	0.01	0.01	-	1.64 (0.42-6.44)	0.52	-	-
CGGCCCCCTGGGGCTA	0.01	0.01	-	0.80 (0.19-3.35)	0.78	-	-
CAAATGCCTGTGGCCG	0.01	0.01	-	1.64 (0.37-7.14)	0.50	-	-

CI: confidence interval, OR: odds ratio, PEXS: pseudoexfoliation syndrome, PEXG: pseudoexfoliation glaucoma

**Table 2.9.** Haplotype distribution at rs12432450-rs7149187 in controls, PEXS and PEXG

Haplotype 'C-A' (rs12432450-rs7149187)	Freq.	OR (95%CI)	p-value
Control	0.38	0.67 (0.49-0.92)	<b>0.01</b>
PEXS	0.29		
PEXG	0.29	0.68 (0.47-0.99)	<b>0.03</b>

CI: confidence interval, OR: odds ratio, PEXS: pseudoexfoliation syndrome, PEXG: pseudoexfoliation glaucoma

We also performed a haplotype analysis with only the four loci that were associated with the disease in this study (rs72705342 and rs17732466) and the previous study (rs7149187 and rs929608) (**Table 2.10**). The risk haplotype 'T-G-C-G' at 'rs929608-rs72705342-rs17732466-rs7149187' was found to be significantly associated with both PEXS ( $p=0.008$ ) and PEXG ( $p=0.007$ ). However, the haplotype 'C-G-C-A' at 'rs929608-rs72705342-rs17732466-rs7149187' was found to be significantly associated with only PEXS ( $p=0.03$ ) conferring a protective effect of 0.62 but it was not found to be associated with PEXG ( $p=0.31$ ).

**Table 2.10.** Haplotype distribution at rs929608-rs72705342-rs17732466-rs7149187 in controls, PEXS and PEXG

Haplotype 'T-G-C-G' 'rs929608-rs72705342-rs17732466- rs7149187	Freq.	OR (95%CI)	p-value
Control	0.20	1.49 (1.10-2.00)	<b>0.008</b>
PEXS	0.28		
PEXG	0.30	1.63 (1.13-2.35)	<b>0.007</b>

Haplotype 'C-G-C-A' 'rs929608-rs72705342-rs17732466- rs7149187	Freq.	OR (95%CI)	p-value
Control	0.11	0.62 (0.40-0.98)	<b>0.03</b>
PEXS	0.07		
PEXG	0.09	0.75 (0.44-1.30)	0.31

CI: confidence interval, OR: odds ratio, PEXS: pseudoexfoliation syndrome, PEXG: pseudoexfoliation glaucoma

### 2.3.5. rs72705342 shows an allele-specific regulatory effect

Luciferase reporter assays were performed to evaluate the putative regulatory effect of the regions containing these SNPs. Twenty-nine base pair region flanking the SNPs were cloned upstream of the minimal promoter in pGL4.23 and transiently transfected into HLE B-3 cells. The cells containing constructs with either the 'G' (p=0.1) or 'A' (p=0.5) allele at rs17732466 did not show any differential luciferase activity compared to the empty vector. Also, no significant changes in luciferase activity were observed between the alleles (p=0.4) (**Figure 2.4A**). On the other hand, the alleles at rs72705342 element showed significant allele-specific changes in the luciferase activity. The presence of the protective allele 'T' at rs72705342 significantly increased the expression of luciferase compared to the construct with the risk allele 'C' (p=0.03) or the empty vector (p=0.001). No significant difference was observed between the empty vector and the construct with the 'C' allele. (**Figure 2.4B**). Further, to assess the direct effect of rs72705342 element on fibulin-5 promoter, the core promoter of *FBLN5*<sup>158</sup> was cloned into pGL3 basic vector, and the twenty-nine base pair rs72705342 loci with either allele 'T' or allele 'C' was cloned upstream of the *FBLN5* promoter. These constructs were transiently transfected into HLE B-3 cells. The reporter activity showed that the alleles at rs72705342 showed an allele-specific effect on the *FBLN5*

promoter (Figure 2.4C). Change in allele ‘C’ to ‘T’ at rs72705342 showed an increased luciferase activity (p=0.02), implying an allele-specific regulatory effect of the rs72705342 element on the *FBLN5* promoter.

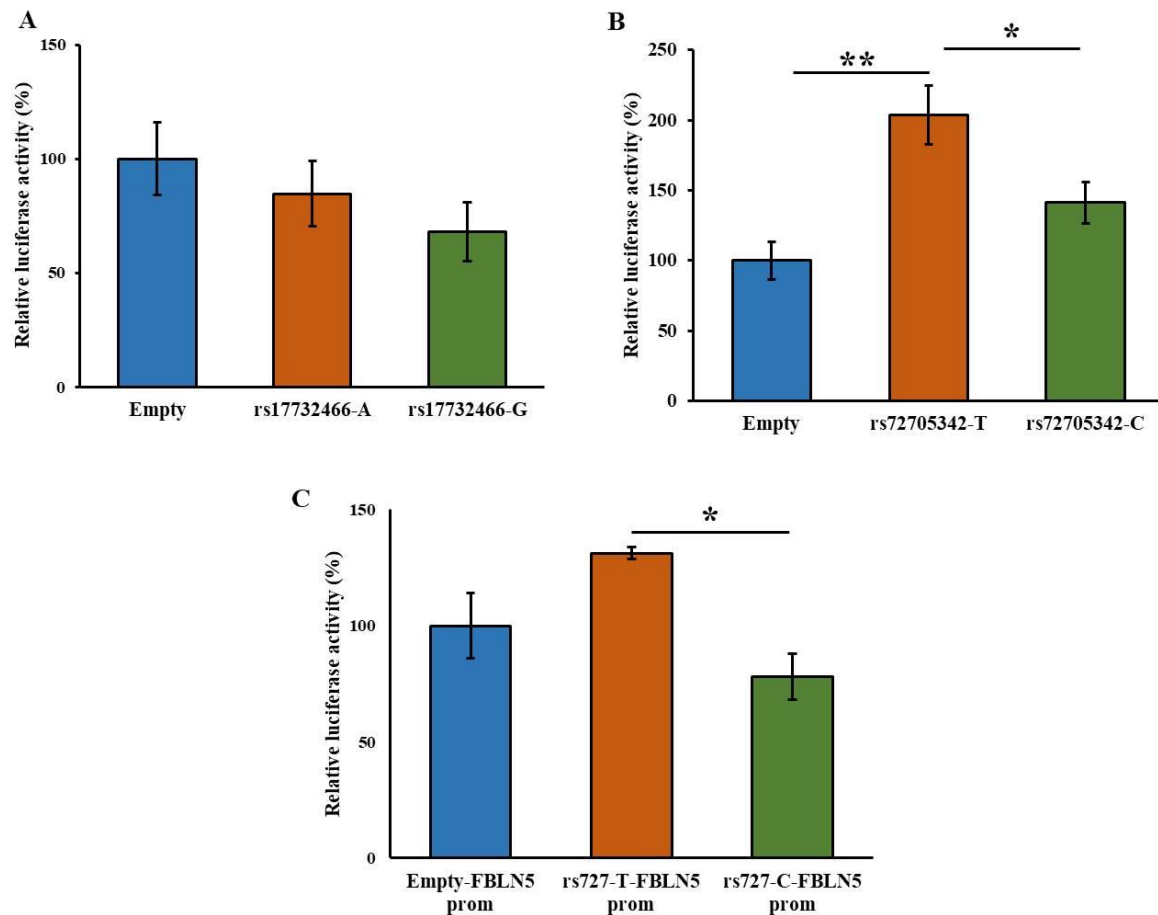


**Figure 2.4. Putative regulatory effect of *FBLN5* variants.** **A.** Relative luciferase activity of constructs containing rs17732466 with either ‘A’ or ‘G’ alleles cloned upstream of the minimal promoter. No difference in reporter activities was observed with either ‘A’ (84.8±14.3) or ‘G’ (68.2±12.9) alleles compared to empty vector (100.0±15.8) with p-values 0.50 and 0.17, respectively. Also, no difference in activity with a change in alleles was observed (p=0.42). Data represent mean ± SEM of four independent experiments. **B.** Relative luciferase activity of constructs containing rs72705342 with either allele ‘T’ or allele ‘C’ cloned upstream of the minimal promoter. Significant differences in reporter activities between the rs72705342 element with the ‘T’ allele (203.8±20.8) and ‘C’ allele (141.3±14.8) or empty vector (100.0±13.5) were observed with p-values of 0.03 and 0.001, respectively. No significant difference was observed between the empty vector and the construct with the ‘C’ allele (p=0.06). Data represent mean ± SEM of four independent experiments. **C.** Relative luciferase activity of constructs containing rs72705342 with either allele ‘C’ or ‘T’ allele upstream of *FBLN5* core promoter. Change from allele ‘C’ to ‘T’ showed a significant increase (p=0.02) in luciferase activity. No significant difference was observed between the empty vector and the construct with allele ‘T’ (p=0.15) or allele ‘C’ (p=0.27). Data represent mean ± SEM of three independent experiments. \*\*p<0.01 \*p<0.05.

### 2.3.6. Risk allele ‘C’ at rs72705342 showed greater protein binding affinity compared to the ‘T’ allele

Electrophoretic mobility shift assays (EMSA) were performed to study specific DNA-protein interactions at rs72705342. EMSA yielded specific shifted bands. Shifts could be competitively inhibited by an excess of unlabelled oligonucleotides (**Figure 2.5A**). Quantitative analysis of the shifted bands showed greater protein binding to the sequence containing the risk allele ‘C’ compared to that containing allele ‘T’ ( $p=0.04$ ), implying a differential transcription factor binding at rs72705342 (**Figure 2.5B**).

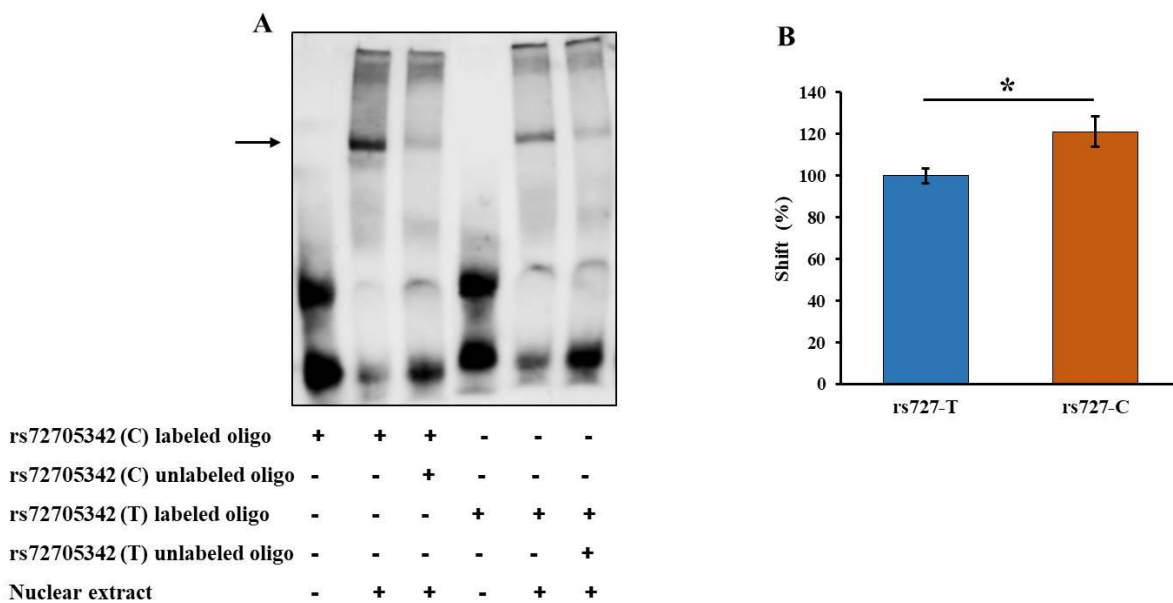


**Figure 2.5. Binding of nuclear proteins to rs72705342.** **A.** EMSA using 29bp biotinylated DNA probes with rs72705342 ‘C’ or ‘T’ allele and nuclear extract from HLE B-3 cells showed specific DNA-protein complexes which vanished on competitive inhibition with respective unlabelled excess probes. **B.** Quantitative analysis of the shifted bands relative to the unshifted bands showed allele-specific differences with significantly stronger binding of the ‘C’ allele with the nuclear protein compared to the ‘T’ allele set at 100%. Data represent mean  $\pm$  SEM of at least three independent experiments. \* $p<0.05$ .

Competitive EMSA on the labelled rs72705342 ‘C’ probe with increasing concentration of unlabelled rs72705342 ‘C’ oligo (50-, 100-, 200- and 400-fold excess) showed progressive reduction of the shifted band (**Figure 2.6**).

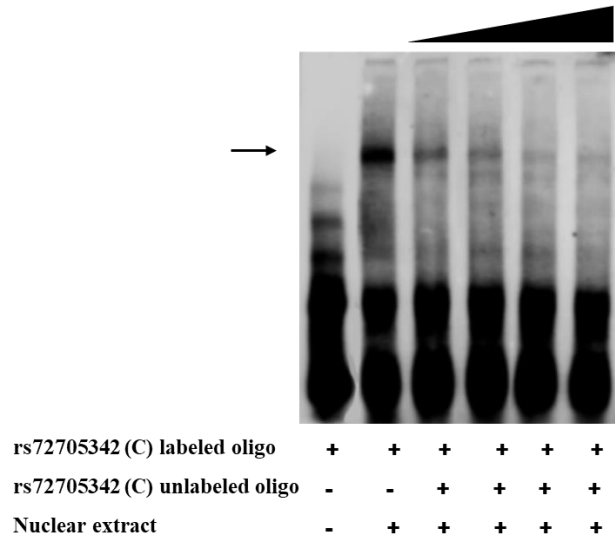


**Figure 2.6. Competitive EMSA on rs72705342.** ‘C’ probe with increasing concentrations of unlabelled excess (50-, 100-, 200-, 400-fold) showed a gradual decrease in the intensity of the shift.

*In silico* analysis using PROMO software predicted the binding of ten transcription factors to the region flanking rs72705342 ( $\pm 14$ bp), i.e., glucocorticoid receptor  $\alpha$  (GR- $\alpha$ ), Activating enhancer binding Protein 2 alpha (AP-2 $\alpha$ A), CCAAT/enhancer-binding protein beta (C/EBP $\beta$ ), c-Jun, Nuclear factor I (NF-1), estrogen receptor alpha (ER- $\alpha$ ), forkhead box P3 (FOXP3), Retinoid X receptor alpha (RXR- $\alpha$ ), Retinoic acid receptor alpha (RAR- $\alpha$ ), CAAT box transcription factor (CTF) and c-ETS-2. The binding of only one transcription factor, TFII I, was predicted to be affected by variation at rs72705342. **A change in allele from ‘C’ to ‘T’ at rs72705342 predicted a loss of the binding site for the TFII I transcription factor. Also, although GR- $\alpha$  had binding sites in the 29 bp sequence, an additional binding site for GR- $\alpha$  was created in the presence of the ‘C’ allele (Figure 2.7).**

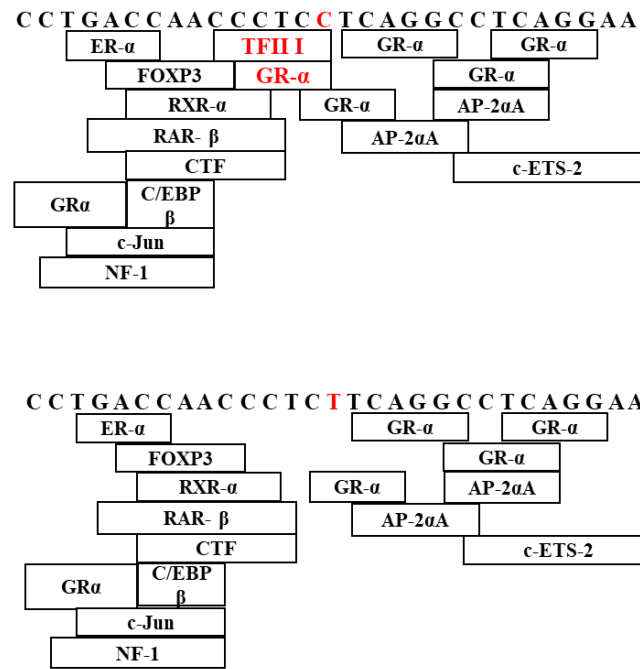


**Figure 2.7. In-silico prediction of transcription factors binding to rs72705342 element.** Allele (encircled) specific transcription factor binding at rs72705342 as predicted on PROMO software. The 'C' allele at rs72705342 is predicted to bind to GR- $\alpha$  and TFII I transcription factors, the binding of which is lost on change in allele from 'C' to 'T'.

To check the binding of TFII I and GR- $\alpha$  to rs72705342 'C', EMSA was performed using antibodies specific to either of the transcription factors. On pre-incubating the nuclear extract with TFII I antibody, a decreased intensity of the shift was noted, which did not happen in the presence of a non-specific HSF1 antibody (**Figure 2.8A**). Further, as shown in **Figure 2.8B**, a reduced intensity in the shift was observed in the presence of the GR- $\alpha$  antibody as well but not in the presence of the non-specific HSF1 antibody.

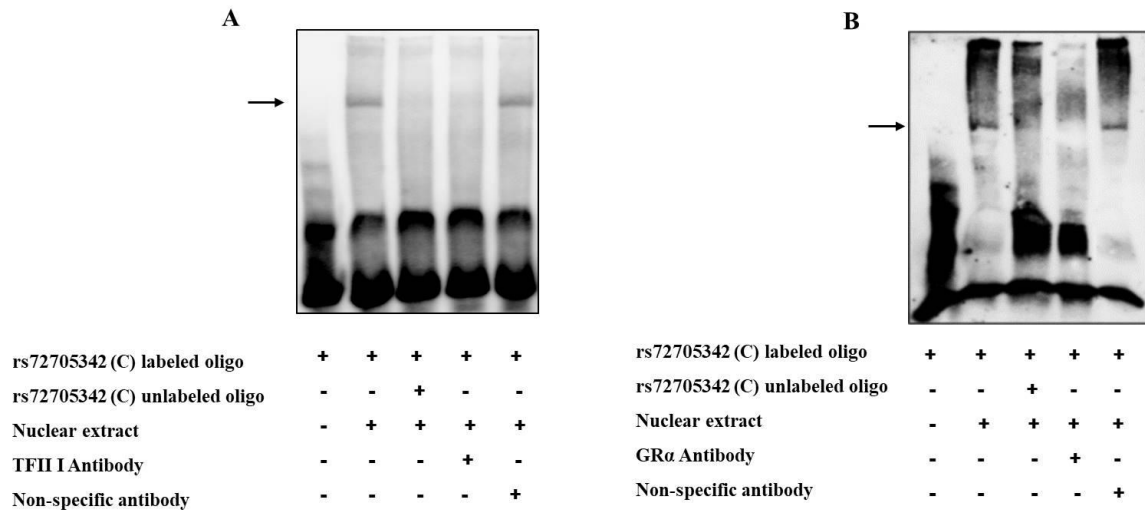


**Figure 2.8. Binding of specific transcription factors to rs72705342.** **A.** EMSA shows that in the presence of TFII I specific antibody, the intensity of the shift reduced, which did not happen in the presence of non-specific antibody (HSF1) taken as control. **B.** EMSA shows that in the presence of GR- $\alpha$  specific antibody, the intensity of the shift reduced, which did not happen in the presence of non-specific antibody taken as control.

## 2.4. Discussion

In this study, we investigated the association of *FBLN5* variants with pseudoexfoliation (PEX) by Tag-SNP genotyping approach. PEX is a complex progressive multifactorial disorder of the extracellular matrix (ECM) that manifests primarily in the ocular tissues. Impaired cross-linking of the ECM proteins and their subsequent aggregation is a hallmark of PEX. Association of numerous ECM proteins, such as elastin, tropoelastin, fibrillin-1, matrix metalloproteinase and their inhibitors, LOXL1, and fibulin-5, with the disease pathology, substantiates the debilitating effect of impaired ECM production and maintenance in development of PEX fibrils and subsequent PEX pathogenesis. Fibulin-5 (FBLN5) is a matricellular scaffold protein with a crucial role in elastogenesis. Fibulin-5 interacts with integrins on the cell surface through its N-terminal domain and with LOXL1 through its C-terminal domain and brings the other ECM proteins into proximity to facilitate elastogenesis.<sup>159</sup> Genetic variants in fibulin-5 and its deregulation leads to various elastinopathies such as CL, POP, CMT disease, and ARMD.<sup>142,145,146,160</sup> Missense substitutions leading to improper secretion of fibulin-5 and reduced interaction with elastin and fibrillin-1 have been reported in recessive cutis laxa.<sup>161</sup> Khadzhievaa *et al.* reported association of several tag SNPs with the advanced POP.<sup>147</sup>

We and others have reported dysregulation of *FBLN5* in PEX patients, which may result in impaired elastic fiber formation, degenerative tissue alterations, and subsequent ECM protein deposition.<sup>77,134</sup> We also identified novel genetic associations of two variants, rs7149187 in the 5'-UTR and rs929608 in the 10<sup>th</sup> intron within *FBLN5* with PEX which were, however, not found to be causal variants.<sup>134</sup> In this study, we identified two intronic variants, NC\_000014.9:g.91913280G>A (rs17732466:G>A) and NC\_000014.9:g.91890855C>T (rs72705342:C>T) to be associated with pseudoexfoliation glaucoma (PEXG) as risk factors. However, these SNPs were not found to be associated with the early stage of PEX, pseudoexfoliation syndrome (PEXS). The minor alleles 'A' and 'T' at rs17732466 and rs72705342 were present in higher frequency in the controls and conferred a protective effect. The frequency of risk alleles at rs17732466 and rs72705342 was 78.0% and 82.0%, respectively, in PEXG. The 1000 Genomes Project data on the Ensembl database recorded that the frequency of the risk allele 'G' at rs17732466 is the highest in the African population (88.0%), followed by American (87.0%), East Asian (84.0%), European (75.0%) and South Asian (73.0%) populations. The frequency of the risk allele 'C' at rs72705342 is the highest in the African population (96.0%), followed by American (88.0%), East Asian (85.0%), European (77.0%) and South Asian (74.0%) populations. We found that the risk genotype 'CC' frequency at rs72705342 was the highest in PEXG (64.0%) compared to 56.0% in control and 58.0% in PEXS. Further, the haplotypes among the Tag-SNPs across the gene showed a significant association with PEXG but not with PEXS. This suggests that the underlying mechanism of pathogenesis of PEXS and PEXG could be different, with novel risk factors contributing to the severity of PEX in its advanced stage. Many diseases show an association of genetic variants with the severe forms of the disease compared to their early stages. Variants in *CFH* and *ARMS2* were found to be more common with increasing severity of ARMD.<sup>162</sup> Tang *et al.* show that an intronic variant in the *PAX6* gene is associated with extreme but not mild myopia.<sup>163</sup> Our findings suggest that these variants in fibulin-5 might contribute to the development and/or progression of pseudoexfoliation to a severe form rather than to the onset of the disease. However, haplotype analysis of the previously associated *FBLN5* SNPs and the Tag SNPs from this study showed significant association of the haplotype 'C-T' at 'rs12432450-rs7149187' with both PEXS and PEXG and it conferred a protective effect of 0.67 and 0.68, respectively. Further, analysis of a

haplotype block with only the SNPs associated with the disease showed that the risk haplotype ‘T-G-C-G’ at ‘rs929608-rs72705342-rs17732466-rs7149187’ was significantly associated with both PEXS and PEXG conferring a risk effect of 1.42 and 1.67, respectively. However, the haplotype ‘C-G-C-A’ conferred a protective effect of 0.62 in only PEXS but was not associated with PEXG. Thus, although the thirteen common variants did not show allelic or genotypic association with PEXS, as a haplotype with other risk variants, they might contribute to risk of PEXS as well.

As causal variants for complex disorders are also found in regions outside the coding areas of protein-coding genes, the functional effect of rs17732466 and rs72705342 was assessed.<sup>66,76</sup> Reporter assays showed that rs72705342 has an allele-specific regulatory effect on the fibulin-5 promoter. The risk allele ‘C’ at rs72705342 significantly reduced the reporter gene expression compared to allele ‘T’. This finding is supported by the eQTL data from the GTeX database, which shows a significant increase in fibulin-5 expression in tissues from individuals with the ‘TT’ genotype compared to those with the ‘CC’ genotype (**Figure 2.9**).

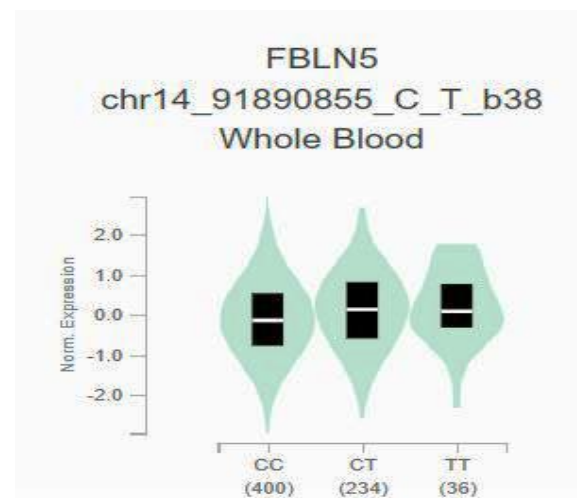


**Figure 2.9. rs72705342 is an eQTL for FBLN5 expression.** The eQTL violin plot obtained from the GTex portal shows that tissue with homozygous alternate genotype ‘TT’ shows increased *FBLN5* expression ( $p < 0.001$ ) compared to the homozygous reference genotype ‘CC’.

Further, DNA- protein binding assay showed that the sequence with the ‘C’ allele has more affinity to protein binding compared to that with the ‘T’ allele implying that the allele-specific differential regulation by rs72705342 could be due to differential transcription factor binding at the alleles. The *in-silico* analysis supported this finding, which showed differential binding of two transcription

factors, GR- $\alpha$  and TFII I, with the 'C' allele at rs72705342. Electrophoretic mobility shift assays, including the antibodies against TFII I and GR- $\alpha$ , showed that these proteins might bind to rs72705342. However, the extent of binding affinity of these proteins to the alleles at rs72705342 needs to be verified further using CRISPR-edited cell lines followed by chromatin immunoprecipitation experiments.

This study might have a limitation in terms of the sample size included, and replication of this genetic association study at a larger scale and in different cohorts is needed to gain confidence in the association of these intronic variants with PEXG and their non-association with PEXS. Also, though rs72705342 showed a regulatory effect on gene expression, we observed that *FBLN5* is downregulated in PEXS individuals but not PEXG. However, the association of rs72705342 with only PEXG but not PEXS suggests that this SNP might have an unknown effect on PEXG progression. It is possible that this variant could influence the expression of distal genes contributing to PEXG pathology, which needs to be studied further.

In conclusion, this study elucidated the genetic association of thirteen tag SNPs in *FBLN5* with pseudoexfoliation. We identified several SNPs and haplotypes of *FBLN5* associated with the advanced stage of PEX, pseudoexfoliation glaucoma (PEXG) but not with the early stage of PEXS. The intronic SNP rs72705342 showed a plausible regulatory effect on *FBLN5* expression. Further *in vivo* studies can help understand the exact effect of these deep intronic variants and haplotypes on the progression of the disorder.

\*\*\*\*\*

## *Chapter 3*

# **Mechanism of regulation of clusterin in the pathogenesis of PEX**

### 3. Mechanism of regulation of clusterin in the pathogenesis of PEX

#### 3.1. Introduction

In this chapter, we report the genetic association of 3'-UTR variants in clusterin (*CLU*) with PEX and explore the epigenetic regulation of the *CLU* gene in PEX pathology.

Clusterin is a multifunctional secreted glycoprotein encoded by the *CLU* gene that resides in the short arm of chromosome 8 in humans, which is ubiquitously expressed in tissues and is present in many body fluids. *CLU* gene is approximately 18 kb and has nine exons and eight introns. Upon maturation, *CLU* protein consists of two 40 kDa chains, alpha and beta, covalently joined by disulfide bonds.<sup>164</sup> *CLU* is an extracellular molecular chaperone involved in various cellular mechanisms, such as stabilization of cell-cell adhesions, cell-matrix adhesions, apoptosis, and preventing misfolded proteins. Dysregulation of *CLU* has been associated with various neurodegenerative disorders such as Alzheimer's disease, multiple sclerosis, age-related macular degeneration, and pseudoexfoliation.<sup>75,165-167</sup>

The *CLU* gene encodes two discrete isoforms with distinct functions: secretory clusterin (*sCLU*) and nuclear clusterin (*nCLU*), depending on the physiologic state of the cell. The *sCLU* (80 kDa), consisting of the  $\alpha$  and  $\beta$  peptides, is the predominant isoform expressed under normal physiologic conditions that prevents protein aggregation in the extracellular space and hence is cytoprotective.<sup>168</sup> The *nCLU* (55 kDa), on the other hand, is synthesized under chronic stress from a second in-frame AUG codon. The *nCLU* consists of a nuclear localization signal and localizes to the nucleus, where it is pro-apoptotic and acts as a pro-death protein in cells under chronic stress.<sup>169</sup> Depending on the substrate concentration in the ECM, the *sCLU* can also stop being cytoprotective and becomes detrimental. *In vivo* studies have shown that in the initial stages, *sCLU* binds to and prevents the aggregation of A $\beta$  peptides and the subsequent formation of senile plaques.<sup>170</sup> However, at a later stage when

the ratio of sCLU protein to its substrate decreases, clusterin is pro-amyloidogenic. In a failed attempt, it deposits with its substrate and becomes cytotoxic by increasing oxidative stress.<sup>171</sup>

CLU has been identified as a component of the XFM, and Creasey *et al.* observed increased large deposits of CLU on the surface of LC of PEX patients compared to controls.<sup>172</sup> Zenkel *et al.* observed decreased *CLU* expression in the anterior eye tissues such as the cornea, trabecular meshwork, iris, lens and ciliary processes. However, increased levels of clusterin were observed in the AH of PEXG patients compared to controls.<sup>75,78,173</sup> Recently, Rebecca *et al.* noted increased CLU expression in the LC of PEX patients compared to controls.<sup>77</sup> CLU has several single nucleotide polymorphisms (SNPs) that might affect the mRNA stability.<sup>76,174,175</sup> Two of its SNPs, rs2279590 and rs3087554, were found to be significantly associated with pseudoexfoliation in various ethnic groups such as German, Australian, and Indian populations.<sup>73-75</sup> We have also previously found that the intronic SNP rs2279590 is a functional variant, wherein the presence of the 'G' allele at the variant results in an increase in *CLU* expression.<sup>75,76</sup>

Apart from genetic variants in *CLU* contributing to a disease predisposition, the epigenetic modifications of clusterin are also known to contribute towards disease causation and progression. The clusterin promoter has a mini-island rich in CpG dinucleotides that have shown susceptibility to DNA methylation. Promoter methylation of clusterin has resulted in its reduced expression in ovarian, and breast cancer tissues, tumour endothelial cells, and hormone-refractory prostate carcinoma.<sup>176-179</sup> Induced demethylation has resulted in a repressed expression of clusterin in tumour cell lines and retinal pigment epithelial cells.<sup>167,176</sup> Studies show that the promoter is hypomethylated in tissues showing constitutive clusterin expression but not in other tissues with lower expression levels. We hypothesised that dysregulation of clusterin expression in PEX could be driven by more than one regulatory

mechanism and that along with functional genetic variants; epigenetic factors could also contribute to its dysregulation.

In this study, we scanned the region of *CLU* surrounding rs2279590 and rs3087554 in search of other variants associated with PEX that could be in linkage with the previously identified risk variants. We found three variants in the 3'-UTR of *CLU* in our study subjects, of which two SNPs showed novel genetic association with PEX. Reporter assays showed that these variants influence the binding of microRNAs to *CLU*. We further studied the methylation status of clusterin promoter in PEX patients compared to controls and noted that the clusterin promoter is hypomethylated in PEX patients contributing to its increased expression.

## **3.2. Materials and methods**

### **3.2.1. Study subjects' selection, recruitment, and sample collection**

This study was approved by the Institutional Biosafety and Human Ethics committee of the National Institute of Science Education and Research and adhered to the tenets of the Declaration of Helsinki. Participants were recruited at Sri Sri Borda Hospital, Bhubaneswar, and All India Institute of Medical Sciences, Bhubaneswar. Inclusion-exclusion criteria as mentioned in Chapter 2, page no. 41 was followed. Informed consent was obtained from all participants. Peripheral blood was collected in EDTA vacutainers from the participants. The lens capsules were collected during cataract surgery from consented participants in RNAlater and stored at -80°C until further use.

### **3.2.2. DNA isolation from blood**

Peripheral blood (4 ml) was collected from study subjects for genomic DNA extraction through the Phenol-Chloroform method as described in Chapter 2, page no. 42.

DNA was isolated from human cells using the Qiagen Blood DNA kit as per the manufacturer's protocol. The cell pellet was suspended in 200  $\mu$ l 1X PBS and 20  $\mu$ l Protease. 200  $\mu$ l of AL lysis buffer was added to the suspension, vortexed, and incubated at 56<sup>0</sup>C for 10 minutes. 200  $\mu$ l of absolute ethanol was added to the mixture, vortexed, transferred to the provided column, and centrifuged at 8000 rpm for a minute. The flow-through was discarded, and the column was washed with 500  $\mu$ l of AW1 buffer at 8000 rpm for 1.0 minute. The column was washed again with 500  $\mu$ l of AW2 buffer at 8000 rpm for 1.0 minute. Post dry spin for 1.0 minute at 13000 rpm, the column was air-dried for a minute. DNA was eluted in 50  $\mu$ l of AE buffer, quantitated, and stored at -20<sup>0</sup>C until further use.

DNA from lens capsules was isolated using the QiaAmp micro kit as per the manufacturer's protocol. 180  $\mu$ l of lysis buffer- ATL was added to the tissue in a 1.5 ml centrifuge tube. 20  $\mu$ l Proteinase K was added to the tube and pulse-vortexed for 15 seconds. The tube was then placed at 56<sup>0</sup>C on a thermomixer for 4-6 hours for complete lysis of the tissue. Post-lysis, 200  $\mu$ l of AL buffer containing carrier RNA was added to the tube and mixed by pulse-vortexing. The sample was then mixed with 200  $\mu$ l of absolute alcohol, pulse-vortexed, and incubated for 5.0 minutes at room temperature. The mixture was then transferred to the columns provided in the kit and centrifuged at 8000 rpm for a minute. The flow-through was discarded, and the column was washed with 500  $\mu$ l of AW1 buffer at 8000 rpm for 1.0 minute. The column was washed again with 500  $\mu$ l of AW2 buffer at 8000 rpm for 1.0 minute. Post dry spin for 1.0 minute at 13000 rpm, the column was air dried for a minute. DNA was eluted in 20  $\mu$ l of AE buffer, quantitated, and stored at -20<sup>0</sup>C until further use.

### **3.2.3. Polymerase Chain Reaction**

The region (~2.9 kb) of the *CLU* gene encompassing the previously studied SNPs, rs2279590 and rs3087554, was amplified by polymerase chain reaction (PCR) using four sets of primers. Primers were designed by Primer-BLAST, and their detailed information is presented in

**Table 3.1.** PCR reactions were performed in 25 µl volumes containing Taq Buffer with 1.5 mM MgCl<sub>2</sub> (GenetBio, India), 100 mM dNTP mixture (GenetBio, India) 0.5 µM of each primer (GCC, India), 100 ng of genomic DNA, and 0.5 unit of Taq DNA polymerase (GenetBio, India). These reactions were incubated at 95<sup>0</sup>C for 5 minutes, followed by 35 cycles of 30 seconds of denaturation at 95<sup>0</sup>C, 35 seconds at annealing temperatures, and extension for 45 seconds at 72<sup>0</sup>C, and finally incubated at 72<sup>0</sup>C for 10 minutes for the final extension. The amplicons were stored at -20<sup>0</sup>C until further use.

#### **3.2.4. Gel elution**

PCR products or DNA was resolved on agarose gel in 1X TAE buffer [Tris, acetate, 0.5 M EDTA]. For eluting DNA resolved on agarose gels, QIAquick Gel Extraction Kit, QIAGEN, Hilden was used as per the manufacturer's protocol. The DNA band was excised from the gel and placed in a 1.5 ml tube. The gel was solubilized in 650 µl of QG buffer at 56<sup>0</sup>C for 25 minutes in shaking conditions. The solubilized solution was mixed well and transferred to the column provided with the kit. The column was centrifuged at 8000 rpm for 1.0 minute. The flowthrough was discarded, and the column was incubated with 650 µl of wash buffer PE for 5.0 minutes. The column was centrifuged at 13000 rpm for 1.0 minute. The column was washed again with 250 µl of PEX buffer as done in the previous step. The flow-through was discarded, the column was given a dry spin at 13000 rpm for 1.0 minute, and air-dried for a minute. The DNA was eluted in 15 µl of EB buffer, quantified, and stored at -20<sup>0</sup>C until further use.

#### **3.2.5. Bisulfite conversion**

500 ng of genomic DNA was converted using the Epiect Bisulfite kit (Qiagen, Hilden, Germany). The DNA sample was mixed with 85 µl of bisulfite mix that converts unmethylated cytosines to uracil and 15 µl DNA protect buffer in a reaction volume of 140

µl. The samples were placed in a thermal cycler with repeated cycles of denaturation at 95<sup>0</sup>C and incubation at 60<sup>0</sup>C. After the bisulfite treatment was done, the samples were cleaned. The treated samples were transferred to 1.5 ml tubes and mixed with 560 µl of freshly prepared BL buffer containing the carrier RNA (1µg/ml). The entire mixture was transferred to the column provided with the kit and centrifuged at 13000 rpm for 1.0 minute. The flow-through was discarded, and the column was washed with 500 µl of BW buffer at 13000 rpm for a minute. The column was then incubated with the BD (desulfonation) buffer for 15 minutes at room temperature. The column was centrifuged at 13000 rpm for a minute and washed with 500 µl of BW buffer twice as done previously. The column was given a dry spin and air-dried for a minute. The converted DNA was eluted in 20 µl of EB buffer, quantified, and used for bisulfite-specific PCR.

The bisulfite-converted template-specific PCR primers (**Table 3.1**) were designed using MethPrimer and BiSearch software packages, encompassing the CpG islands in *CLU*. Bisulfite-specific PCR was carried out using EpiTaq HS methylation-specific polymerase. Each PCR reaction included 100 ng of bisulfite-converted DNA template, 10X buffer, 10 mM dNTPs, 25 mM MgCl<sub>2</sub>, 10 µM each of forward and reverse primers and 1.0 unit of EpiTaq polymerase. The template was amplified in a thermal cycler with an initial denaturation at 95<sup>0</sup>C for 5.0 minutes followed by 40 cycles of denaturation at 95<sup>0</sup>C for 30 seconds, incubation at annealing temperatures for 40 seconds, extension at 72<sup>0</sup>C for 45 seconds and a final extension at 72<sup>0</sup>C for 10 minutes. The amplified products were resolved on 1.2% agarose gel, eluted, and sequenced using the Sanger sequencing technique.

### **3.2.6. Sequencing PCR, Clean up, and Sequencing**

For Sanger sequencing of amplified PCR products or plasmids, sequencing PCR was carried out with BigDye Terminator v.3.1 cycle sequencing kit (Applied Biosystems, Austin, TX78744, USA). Each reaction mix of 10 µl contained 50 ng of template DNA, 1X dilution

buffer, 0.25X of the ready reaction mix, and 0.4  $\mu\text{M}$  of a primer specific to the template. A unidirectional sequencing reaction was carried out in the thermal cycler with 25 cycles of denaturation at 96<sup>0</sup>C for 10 seconds, annealing at 50<sup>0</sup>C for 5.0 seconds, and extension at 60<sup>0</sup>C for 4.0 minutes.

The PCR products were cleaned using Master Mix I [2  $\mu\text{l}$  of 125mM EDTA and 10  $\mu\text{l}$  of NFW] and Master Mix II [2  $\mu\text{l}$  of 3 M sodium acetate and 50  $\mu\text{l}$  of absolute ethanol]. The PCR products were mixed well with both the master mixes and incubated at room temperature for 20 minutes. The samples were then centrifuged at 12000 g for 20 minutes. Without disturbing the pellet, the supernatant was discarded, and the pellet was washed with 70% ethanol at 12000 g for 10 minutes. Without disturbing the pellet, again the supernatant was discarded, and the pellet was air-dried until the complete removal of ethanol.

The dried pellet was suspended in 10  $\mu\text{l}$  of HiDi formamide and loaded onto the 96-well sequencing plate for Sanger sequencing in 3130xl Genetic Analyzer. The sequencing output files were generated in .abi format that was analyzed using BioEdit v7.1. For plasmid sequence confirmation and SNP genotyping of PCR amplified products, the sequences were aligned with target sequences, and complete alignment or any variations were noted for further analysis.

For bisulfite sequencing, the presence of methylated CpGs was analyzed using BiQ analyzer software. The .abi files were converted to .fasta and submitted as input to the software. The methylated cytosines are resistant to the conversion by bisulfite and remain as cytosines post bisulfite conversion. However, the unmethylated cytosines are converted to uracil on bisulfite treatment and are read as thymine on sequencing. The BiQ Analyzer software converts the target sequence such that all non-CpG cytosine is converted to thymine and performs a Needleman-Wunsch alignment of our samples' sequences with the target. The output is

generated in machine-readable format as well as lollipop plots where closed circles represent methylated CpGs, and open circles represent unmethylated CpGs.

### **3.2.7. RNA extraction, cDNA conversion, and quantitative real-time PCR**

Total RNA was isolated from the cells and tissues using the Qiagen RNeasy kit. The sample was incubated in 350  $\mu$ l RLT buffer at room temperature for 10 minutes. Post incubation, the sample was placed in ice and ruptured. 350  $\mu$ l of 70% ethanol was added to the sample and mixed well. The sample was then loaded into the column and centrifuged at 9000 g for 30 seconds at 4<sup>0</sup>C. The flow-through was discarded, and the column was washed with 500  $\mu$ l of RW1 buffer at 9000 g for 30 seconds at 4<sup>0</sup>C. The column was incubated with 500  $\mu$ l RPE wash buffer for 5.0 minutes and then centrifuged at 9000 g for 30 seconds at 4<sup>0</sup>C. The column was given a dry spin at 13000 rpm for 1.0 minute, transferred to a fresh 1.5 ml vial, and air dried for a minute. The column was incubated with 15  $\mu$ l NFW for 5.0 minutes and centrifuged at 13000 rpm for 1.0 minute at 4<sup>0</sup>C. RNA was eluted by centrifugation at 13000 rpm for 1.0 minute at 4<sup>0</sup>C. The isolated RNA was quantified and converted to cDNA immediately.

Total RNA was extracted from blood cells using the MN Nucleospin kit as per the manufacturer's instructions. 200  $\mu$ l of whole blood was transferred to a 1.5 ml RNase-free tube. The blood was mixed with 200  $\mu$ l of DL buffer and 5.0  $\mu$ l of proteinase K and incubated on a thermomixer for 15 minutes at room temperature. 200  $\mu$ l of 70% ethanol was added to the sample, mixed well, and transferred to the column provided with the kit. The sample was centrifuged at 11000 g for 1.0 minute. The flow-through was discarded, and 350  $\mu$ l of MDB buffer was added to the column and centrifuged at 11000 g for 1.0 minute. 95  $\mu$ l of rDNase was added to the column and incubated at room temperature for 15 minutes. rDNase was inactivated with 200  $\mu$ l of RB2 and centrifuged at 11000 g for 1.0 minute. The column was washed with 600  $\mu$ l of RB3 at 13000 rpm for 1.0 minute. After another wash

with 250  $\mu$ l of RB3, the column was given a dry spin at 13000 rpm for 1.0 minute and air dried. The RNA was eluted in 15  $\mu$ l of RNase-free water by centrifugation at 13000 rpm for 1.0 minute. The isolated RNA was quantified and converted to cDNA immediately.

The verso cDNA conversion kit was used for converting the RNA to cDNA. A total 1.0  $\mu$ g of RNA was converted per reaction. The reaction mix included 1 $\mu$ l of random hexamers, 1.0  $\mu$ l of RT enhancer, 50  $\mu$ M of dNTPs, 1X reaction buffer, and 1.0  $\mu$ l of enzyme mix in a 20  $\mu$ l reaction volume. The conversion was carried out at 45<sup>0</sup>C for 30 minutes in a Thermal Cycler, followed by heating at 95<sup>0</sup>C for 2 minutes. The converted cDNA was diluted to 2.5 ng/ $\mu$ l concentration and stored at -20<sup>0</sup>C until further analysis.

### **3.2.8. Protein isolation**

Protein from the tissues and cells was isolated using the nuclear protein extraction NEPER kit as per the manufacturer's instructions. The sample was washed with 1X PBS at 1100 g for 5.0 minutes. All the steps were performed at 4<sup>0</sup>C. The sample was lysed or homogenised in 100  $\mu$ l of CERI and 1X Protease Inhibitor Cocktail. The sample was pulse vortexed vigorously for 15 seconds and incubated on ice for 10 minutes until complete disruption of tissues by repeating the disruption procedure. 5.5  $\mu$ l of ice-cold CREII was added to the sample, vortexed vigorously for 5.0 seconds, and incubated on ice for a minute. The sample was then centrifuged at 16000 g for 5 minutes. The supernatant containing the cytosolic fraction was immediately transferred to a clean pre-chilled tube. The pellet from the previous step was processed further for the isolation of the nuclear extract. The pellet was suspended in 50  $\mu$ l of NER, vortexed vigorously for 15 seconds, and incubated on ice for 10 minutes. The sample was thus vortexed for 15 seconds every 10 minutes for 40 minutes and centrifuged at 16000 g for 10 minutes. The supernatant was transferred to a pre-chilled tube and quantitated. Quantitated protein was aliquoted and stored at -80<sup>0</sup>C.

The total protein in the sample was estimated using the Bradford reagent. Bovine serum albumin was used to generate the standard curve. Four BSA standard concentrations were used to determine the unknown protein concentration in the sample. The photometric estimation was done at 595 nm using a Varioskan plate reader.

### **3.2.9. Western blotting**

The protein sample was denatured by heating at 95<sup>0</sup>C with 1X Laemlli buffer [Tris, SDS, Glycerol,  $\beta$ -mercaptoethanol, bromophenol blue] for 5 minutes. The denatured extracted of specific concentration was resolved on 8-12% SDS polyacrylamide gel [Acrylamide: bisacrylamide, Tris buffer, 10% SDS, 10% APS, TEMED] and transferred onto a 0.45  $\mu$ m PVDF membrane. Depending on the molecular size of the target protein, either semi-dry transfer (35 kDa-100 kDa) or wet transfer (MW>100 kDa) was done. The semi-dry transfer was carried out at 15V for 35 minutes in 1X transfer buffer [25 mM Tris, 190 mM Glycine, 20% methanol]. The wet transfer was carried out overnight at 30V at 4°C. After completion of the transfer, the blot was blocked with 5.0% skimmed milk for one hour and incubated with primary antibody overnight. The blot was washed with 1X TBST [20 mM Tris, 160 mM NaCl, 0.1% Tween 20] thrice for 15 minutes each. The blot was then incubated with the specific secondary antibody for one hour at room temperature and then washed with 1X TBST thrice for 10 minutes each wash. Primary antibodies for clusterin (sc-5289, Santa Cruz Biotechnology, USA) and GAPDH (ABM22C5, Abgenex, India) were used at a dilution of 1:250. Goat anti-mouse IgG-HRP (621140680011730, Bangalore GeNei, India) at 1:5000 dilutions was used as the secondary antibody. The blot was developed with the Supersignal West Femto kit and detected in Fusion Solo S Chemi-Doc. Image acquisition and densitometric analysis were carried out using the EvolutionCapt software. The antibodies used and their dilutions are mentioned in **Table 3**.

### 3.2.10. Cell culture

The human embryonic kidney cells, HEK293 (NCCS, Pune), and human lens epithelial cells, HLE B-3 (ATCC, Virginia, USA), were cultured in Dulbecco's Modified Eagle Medium (AL007G, HiMedia) supplemented with 10% inactivated fetal bovine serum (GIBCO, Invitrogen) and 1.0% penicillin and streptomycin (A001, Himedia) and maintained at 37<sup>0</sup>C and 5.0% CO<sub>2</sub>. For demethylation studies, HLE B-3 cells were treated with 1.0 μM 5-aza-deoxycytidine (5-aza-dC) for 72 hours.

### 3.2.11. Plasmid construction and luciferase assay

To test the functional effect of the SNPs, the pMIR-report vector (Invitrogen, USA) with a promoter of the luciferase reporter gene was used. The wild-type 3'UTR of *CLU* was cloned into the vector at the 3'-end of the luciferase gene using MluI and NotI enzymes by the PCR-based restriction digestion cloning method. The constructs with the variants at rs9331942 and rs9331949 were generated from the wild-type 3'-UTR-pMIR construct using site-directed mutagenesis (NEB enzymes, USA) (**Table 3.1**). HEK293 cells were seeded in a 24-well plate. At 80% confluency, the cells were transiently transfected with 500 ng of constructs along with 5 ng of *Renilla* vector (pGL4.74), and either the miR-223, miR-1283, or negative miR control (Applied Biological Materials Inc., abm goods, Canada) using lipofectamine (ThermoFisher Scientific, USA). After 24 hours post-transfection, the cells were harvested, and luciferase activity was assayed using the Dual-Luciferase Reporter assay system (Promega, USA).

For DNMT1 overexpression studies in HLE B-3 cells, the pcDNA3/Myc-DNMT1 plasmid was procured from Addgene, USA. At 80% confluency, HLE-B-3 cells seeded in a 24-well plate were transfected with 1.0 μg of either DNMT1 or the empty pcDNA3 vector using lipofectamine. Post-24 hours of transfection, cells were harvested, and the expression of clusterin was checked.

### **3.2.12. *In silico* analysis**

To determine any potential effect on microRNA binding to *CLU* due to the studied SNPs, *in silico* analysis was carried out using two databases- miRdB and SNPinfo. These programs predicted microRNA binding sites within the 3'-UTR of *CLU*. miRNAs assigned a cut-off above 70 by miRdB, and  $\pm 30$  nucleotides of the variant were considered. SNPinfo analyzed the input SNPs for miRNA binding sites using the miRanda software.<sup>180</sup> JASPAR was used to predict the binding of Sp-1 to clusterin promoter.

### **3.2.13. Chromatin immunoprecipitation**

The effect of 5-aza-dC on the binding of Sp1 to *CLU* promoter was checked by chromatin immunoprecipitation (ChIP) followed by semi-quantitative PCR. The ChIP experiment was carried out using the Chromaflash High-Sensitivity ChIP kit (Epigentek) as per the manufacturer's instructions. Briefly, HLE B-3 cells were grown on a 6-well plate and treated with either 5-aza-dC or the DMSO vehicle for 72 hours. At 90% confluency, the cells were cross-linked with 1.0% formaldehyde for 15 minutes and quenched with 125 mM glycine solution for 10 minutes. The nuclei were isolated, and chromatin was fragmented (200-700 bp average) using a probe sonicator. The sonication efficiency was checked through agarose gel electrophoresis. The sheared chromatin was centrifuged for 10 minutes and the chromatin solution was diluted in ChIP buffer and used for the ChIP reaction. The wells were incubated with the Sp1 and IgG (negative control) antibodies overnight. After washing the unbound antibody, the antibody-coated wells were incubated with chromatin solution for 2.0 hours. The antibody-chromatin complexes were collected, reverse cross-linked, and the DNA was eluted using the spin columns provided with the kit. The enrichment of the target region in the *CLU* promoter was quantified by the semi-quantitative PCR method. The PCR products were resolved on 5.0% agarose gel, and the intensities of the bands were quantified using

Evolution Capt software (Vilber Lourmat fusion solo S). The primer details are mentioned in

**Table 3.1.**

**Table 3.1.** List of oligos used in the study

S. No.	ID	Purpose	Sequence (5'→3')
1	Reg I	Sequencing	F: CGCAAGGCGAAGACCAGTA R: GCAGCCCTTGGTCAGAGTAG
2	Reg II	Sequencing	F: GCCCTCTGGATTCCTTTTCTA R: GCTGGGGCCTGGTTACTT
3	Reg III (rs9331942)	Sequencing	F: CAAGAACAAAGCCAGGAAGTTA R: TGGTCCAGGGAAAGGTATGA
4	Reg IV (rs9331949, rs9331950)	Sequencing	F: TGCCCAGAAGTCCAAATTATC R: GAGTCTAGCAACATAACAGTGGA
5	BSP Region I	Bisulfite sequencing	F: TTTATTTAATGGGTAAAGAGAAGTG R: CCCCTTTAAACTAACTACAAACC
6	BSP Region II	Bisulfite sequencing	F: TAGTTAGTTTTAAAGGGGGTGTGTG R: TCTCTACCTAACTACCATCCCCTAC
7	<i>CLU</i> qRT	qRT-PCR	F: TTCATACGAGAAGGCGACGAT R: CTGGTCAACCTCTCAGCGAC
8	<i>DNMT1</i> qRT	qRT-PCR	F: CTACTACTCAGCCACCAAGAAC R: GGACTGGACAGCTTGATGTT
9	<i>ACTB</i> qRT	qRT-PCR	F: GCACAGAGCCTCGCCTT R: GTTGTCGACGACGAGCG
9	<i>CLU</i> 3'-UTR WT	Luciferase assay	F: CACCACGCGTGATGTGGATGTTGCTTTTGC R: CACGGCGGCCGCTAACTTTTGAAACAGTGTGA
10	rs9331942 SDM	Luciferase assay	F: TATAATGCATAACTGATGTTTTTCGT R: ATACCAAGTACACCTTACACTTACTG
11	rs9331949 SDM	Luciferase assay	F: CACATGTAAATTTGTAGCTTAGAATAT R: GACTTTGCTACACACCTGGGATGCA
12	<i>CLU</i> for ChIP	ChIP	F: CGGTGCTGCACCGGCC R: CTGGGAGGCGCCGTATTTATAGC

### 3.2.14. Genetic and Statistical analysis

The allelic association tests, Hardy-Weinberg equilibrium (HWE), and logistic regression model were done using PLINK. Haplotype analysis and linkage disequilibrium (LD) analysis were done using Haploview V4.2. Age and sex-matched samples were taken for the experiments. Matching was done by performing Student's t-test between the groups. The statistical significance of group-wise results was analyzed through Student's t-test, and  $p \leq 0.05$  was considered as statistically significant. All experiments were done at least three times independently. Data are presented as mean  $\pm$  SEM.

### 3.3. Results

#### 3.3.1. Demographics of the study subjects

313 PEX (207 PEXS and 106 PEXG) and 250 age and sex-matched control subjects were selected for this study. The demographics of the study subjects included in the genetic association study are shown in **Table 3.2**. The mean age in years  $\pm$  SD of controls, PEXS, and PEXG were  $69.24 \pm 7.78$ ,  $70.34 \pm 6.86$ , and  $68.80 \pm 7.78$ , respectively. The age range of controls, PEXS, and PEXG was 51-90 years, 50-84 years, and 51-88 years, respectively. The number of females visiting the hospital was relatively very low, as women are less likely to receive cataract surgery compared to men in low-resource countries/localities.<sup>32</sup> Of the study participants (in both control and PEX groups), 23.75% were females. A total of 133 females (57 control, 57 PEXS, and 19 PEXG) and 430 males (193 control, 150 PEXS, and 87 PEXG) were selected for this study.

**Table 3.2.** Demographics of the study subjects

Group	Sample size (N)	Age (in years)		p-value	Sex		p-value
		Mean $\pm$ SD	Range		Male	Female	
Control	250	$69.24 \pm 7.78$	51-90		193	57	
PEX	313	$69.82 \pm 7.34$	50-88	0.36	240	73	0.88
PEXS	207	$70.34 \pm 6.86$	50-84	0.10	150	57	0.24
PEXG	106	$68.80 \pm 8.12$	51-88	0.63	87	19	0.28

#### 3.3.2. 3'-UTR variants of *CLU*, rs9331942 and rs9331949 are genetically associated with PEX

The region of the *CLU* gene surrounding the SNPs rs2279590 and rs3087554 was sequenced in a discovery set of randomly chosen 30 PEX-affected individuals and 30 age-sex matched controls using four sets of primers. We found three novel single nucleotide polymorphisms, rs9331942, rs9331949, and rs9331950, in the 3'-UTR of clusterin gene that had previously not been studied in association with PEX (**Figure 3.1**).

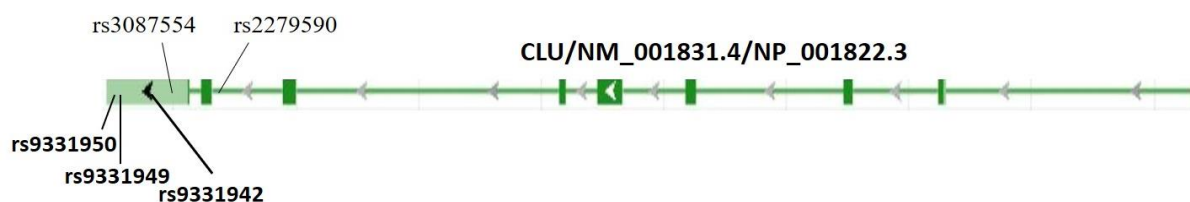


**Figure 3.1. Gene structure of clusterin with SNPs.** Shows the position of the three SNPs rs9331942, rs9331949, and rs9331950 in the 3'-UTR of the *CLU* gene. Also marked are previously studied SNPs, rs2279590, and rs3087554.

In the replicative set, the three SNPs were genotyped in 313 PEX (207 PEXS and 106 PEXG) and, 250 age-sex matched control subjects. All three SNPs passed the Hardy-Weinberg Equilibrium (HWE) test set at a default significance threshold of  $p \leq 0.001$ . The HWE  $p$ -values for rs9331942, rs9331949, and rs9331950 were 0.35, 1.00, and 0.41, respectively. The allele frequencies, odds ratios, and statistical significance of the three variants are presented in **Table 3.3. The variant rs9331942 was significantly associated with PEX ( $p=0.003$ ), with the minor allele 'C' being the risk allele. The variant rs9331949 also showed a significant association with PEX ( $p=0.007$ ), with the minor allele 'G' being the risk allele.** However, rs9331950 was not found to be genetically associated with PEX ( $p=0.88$ ). The genetic analysis of the SNPs after segregating the PEX group into PEXS and PEXG is shown in **Table 3.3.** Like the PEX group, both rs9331942 and rs9331949 showed association with both PEXS ( $p=0.005$  and  $p=0.03$ , respectively) and PEXG ( $p=0.03$  and  $p=0.01$ , respectively) groups. However, rs9331950 did not show any significant association with either PEXS ( $p=0.72$ ) or PEXG ( $p=0.36$ ). The risk analysis showed that the minor allele 'C' at rs9331942 confers a risk of 1.68 (odds ratio) in PEX, 1.71 in PEXS, and 1.64 in PEXG. Further, the minor allele 'G' at rs9331949 confers a risk for PEX, PEXS, and PEXG with an odds ratio of 1.57, 1.49, and 1.74, respectively.

### 3.3.3. Genotypic association of 3'-UTR SNPs in *CLU* with PEX

The genotypic distribution of the variants is shown in **Table 3.4**. The frequencies of the genotypes TT, CT, and CC of rs9331942 were 66.0%, 28.0%, and 6.0%, respectively, in PEX compared to 77.0%, 22.0%, and 1.0%, respectively, in controls. The genotypic association with PEX at rs9331942 was seen with the additive [TT versus CT versus CC:  $p=0.01$ ], the dominant [TT versus CT+CC:  $p=0.01$ ], and the recessive [TT+CT versus CC:  $p=0.02$ ] models. The frequencies of the genotypes AA, AG, and GG at rs9331949 were 66.0%, 30.0%, and 4.0%, respectively, in PEX compared to 74.0%, 24.0%, and 2.0%, respectively, in controls. The dominant model [AA versus AG+GG:  $p=0.01$ ] showed a significant association of rs9331949 with PEX susceptibility. The genotypic distribution and genotypic association of the variants with PEX after segregating them into PEXS and PEXG are shown in **Table 3.4**. The genotypic association of the additive ( $p=0.02$ ), the dominant ( $p=0.02$ ), and the recessive ( $p=0.03$ ) models at rs9331942 was observed with PEXS. The dominant model ( $p=0.04$ ) at rs9331949 showed a significant association with PEXS. The additive model ( $p=0.05$ ) at rs9331942 and the dominant model ( $p=0.01$ ) at rs9331949 retained significance with PEXG.

### 3.3.4. Haplotypes at 'rs9331942-rs9331949-rs9331950' are associated with PEX

Linkage Disequilibrium (LD) block pattern across the three SNPs is shown in **Figure 3.2**. Haplotype analysis identified five haplotype associations in the study subjects, and the haplotype distribution in the cases and controls are shown in **Table 3.5**. The haplotype 'C-G-C' of 'rs9331942-rs9331949-rs9331950' is significantly higher in PEX (0.17,  $p=0.02$ ) as compared to controls (0.11). The odds of having PEX increased by 1.54-fold in individuals with the 'C-G-C' haplotype. The risk haplotype is also significantly associated with PEXS (0.17,  $p=0.02$ ) but not with PEXG (0.16,  $p=0.11$ ) compared to controls. The haplotype 'C-G-C' increased the odds of having PEXS and PEXG by 1.58-fold and 1.45-fold, respectively.

On the other hand, the protective haplotype ‘T-A-C’ at ‘rs9331942-rs9331949-rs9331950’ was found to be significantly associated with PEX ( $p=0.01$ ). On segregation, this haplotype was found to be associated with both PEXS ( $p=0.02$ ) and PEXG ( $p=0.05$ ) as well. However, the haplotype ‘T-G-C’ at ‘rs9331942-rs9331949-rs9331950’ was found to be significantly more in PEXG ( $p=0.008$ ) but not in PEXS ( $p=0.62$ ). We further analyzed the haplotype association of the previously reported rs2279590 and the 3’-UTR SNPs from the current study with PEX. **The risk haplotype ‘C-C-G-C’ at ‘rs2279590-rs9331942-rs9331949-rs9331950’ was significantly associated with PEX ( $p=0.01$ ). On segregation of the PEX group, the risk haplotype was found to be significantly associated with only PEXS ( $p=0.01$ ) but not PEXG ( $p=0.10$ ).**

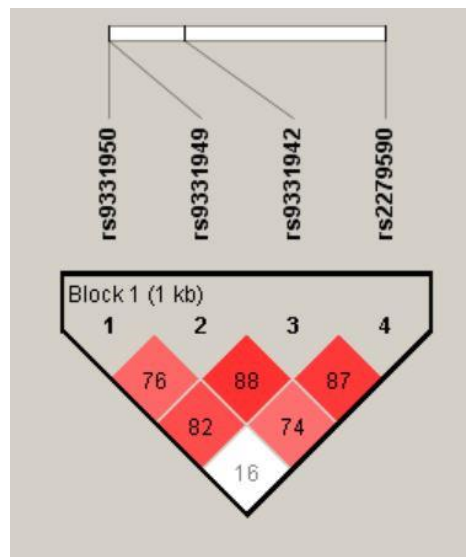


**Figure 3.2. LD block pattern generated by Haploview.** The block consisted of the three 3’-UTR SNPs- rs9331942, rs9331949 and rs9331950 and the previously associated intronic variant rs2279590 of *CLU* gene. The color scale ranges from red to white (color intensity decreases with decreasing  $D'$  value).

**Table 3.3.** Genetic association of 3'-UTR variants in PEX versus control

SNP ID	Major allele	Minor allele	MAF				Control versus PEX		Control versus PEXS		Control versus PEXG	
			Control (N=250)	PEX (N=313)	PEXS (N=207)	PEXG (N=106)	OR (95% CI)	p-value	OR (95% CI)	p-value	OR (95% CI)	p-value
rs9331942	T	C	0.12	0.19	0.19	0.18	1.68 (0.18-2.37)	<b>0.003</b>	1.70 (1.16-2.50)	<b>0.005</b>	1.63 (1.05-2.55)	<b>0.03</b>
rs9331949	A	G	0.13	0.19	0.18	0.20	1.57 (1.12-2.19)	<b>0.007</b>	1.49 (1.03-2.14)	<b>0.03</b>	1.73 (1.12-2.67)	<b>0.01</b>
rs9331950	C	T	0.11	0.11	0.12	0.08	0.97 (0.66-1.42)	0.88	1.07 (0.71-1.62)	0.72	0.77 (0.44-1.35)	0.36

CI: confidence interval, OR: odds ratio, MAF: minor allele frequency, PEXS: pseudoexfoliation syndrome, PEXG: pseudoexfoliation glaucoma

**Table 3.4.** Genetic Models and genotypic distribution of CLU 3'-UTR variants in PEX

SNP ID	Genotype	Freq. in Control (n=250)	Freq. in PEX (n=313)	Freq. in PEXS (n=207)	Freq. in PEXG (n=106)	Genetic Model	Control versus PEX		Control versus PEXS		Control versus PEXG	
							OR (95% CI)	p-value	OR (95% CI)	p-value	OR (95% CI)	p-value
rs9331942	TT	0.77	0.66	0.72	0.72	Additive	2.13 (1.13-4.00)	<b>0.01</b>	2.16 (1.11-4.20)	<b>0.02</b>	2.07 (0.99-4.29)	<b>0.05</b>
	CT	0.22	0.28	0.25	0.25	Dominant	1.62 (1.10-2.40)	<b>0.01</b>	1.65 (1.06-2.55)	<b>0.02</b>	1.59 (0.95-2.64)	0.07
	CC	0.01	0.06	0.03	0.03	Recessive	4.11 (1.16-14.5)	<b>0.02</b>	4.24 (1.13-15.9)	<b>0.03</b>	3.90 (0.91-16.6)	0.06
rs9331949	AA	0.74	0.66	0.68	0.68	Additive	1.58 (0.88-2.82)	0.12	1.52 (0.81-2.84)	0.18	1.69 (0.5)	0.14
	AG	0.24	0.30	0.28	0.28	Dominant	1.63 (1.12-2.38)	<b>0.01</b>	1.53 (1.01-2.32)	<b>0.04</b>	1.85 (1.12-3.04)	<b>0.01</b>
	GG	0.02	0.04	0.04	0.04	Recessive	2.20 (0.69-7.02)	0.17	2.09 (0.60-7.26)	0.24	2.43 (0.59-9.92)	0.21
rs9331950	TT	0.81	0.77	0.83	0.83	Additive	0.79 (0.40-1.54)	0.49	0.98 (0.50-1.90)	0.95	0.00 (0.00-inf)	0.99
	CT	0.17	0.21	0.17	0.17	Dominant	1.01 (0.66-1.54)	0.94	1.10 (0.69-1.74)	0.67	0.84 (0.46-1.53)	0.58
	CC	0.02	0.02	0.00	0.00	Recessive	0.62 (0.16-2.35)	0.48	0.94 (0.24-3.54)	0.92	0.00 (0.00-inf)	0.99

CI: confidence interval, OR: odds ratio, MAF: minor allele frequency, PEXS: pseudoexfoliation syndrome, PEXG: pseudoexfoliation glaucoma

**Table 3.5.** Haplotype distribution of the 3'UTR variants

Haplotype (rs9331942- rs9331949-rs9331950)	Freq. in control	Freq. in PEX	Freq. in PEXS	Freq. in PEXG	Control versus PEX		Control versus PEXS		Control versus PEXG	
					OR (95% CI)	p-value	OR (95% CI)	p-value	OR (95% CI)	p-value
T-A-C	0.76	0.68	0.69	0.68	0.70 (0.54-0.92)	<b>0.01</b>	0.71 (0.52-0.95)	<b>0.02</b>	0.70 (0.49-1.09)	<b>0.05</b>
C-G-C	0.11	0.17	0.17	0.16	1.54 (1.07-2.19)	<b>0.01</b>	1.58 (1.07-2.31)	<b>0.01</b>	1.45 (0.91-2.32)	0.11
T-A-T	0.11	0.11	0.11	0.08	0.96 (0.65-1.42)	0.86	1.06 (0.75-1.62)	0.76	0.76 (0.43-1.35)	0.36
T-G-C	0.01	0.02	0.01	0.04	1.63 (0.64-4.17)	0.29	0.73 (0.20-2.57)	0.62	3.79 (1.30-11.01)	<b>0.008</b>
C-A-C	0.01	0.02	0.02	0.02	2.77 (0.84-9.17)	0.08	2.37 (0.64-8.71)	0.18	3.52 (0.89-13.88)	<b>0.05</b>
Haplotype (rs2279590- rs9331942-rs9331949- rs9331950)	Freq. in control	Freq. in PEX	Freq. in PEXS	Freq. in PEXG	Control versus PEX		Control versus PEXS		Control versus PEXG	
					OR (95% CI)	p-value	OR (95% CI)	p-value	OR (95% CI)	p-value
C-T-A-C	0.44	0.41	0.40	0.43	1.09 (0.86-1.39)	0.44	1.14 (0.87-1.49)	0.31	0.99 (0.71-1.37)	0.95
T-T-A-C	0.30	0.27	0.29	0.25	1.19 (0.92-1.55)	0.17	1.13 (0.85-1.51)	0.36	0.76 (0.52-1.09)	0.14
C-C-G-C	0.11	0.16	0.16	0.15	1.55 (1.09-2.21)	<b>0.01</b>	1.60 (1.09-2.35)	<b>0.01</b>	1.47 (0.92-2.34)	0.10
C-T-A-T	0.09	0.08	0.10	0.06	1.16 (0.76-1.76)	0.46	0.99 (0.64-1.53)	0.97	1.09 (0.86-1.39)	0.14
T-T-A-T	0.02	0.02	0.01	0.02	0.76 (0.33-1.75)	0.52	1.37 (0.44-4.21)	0.58	0.62 (0.33-1.18)	0.69
C-C-A-C	0.01	0.02	-	0.02	0.52 (0.18-1.52)	0.19	-	-	2.22 (0.58-8.49)	0.22
C-T-G-C	0.01	0.01	0.01	0.02	0.88 (0.27-2.84)	0.83	1.68 (0.52-5.43)	0.38	2.12 (0.56-8.03)	0.23

CI: confidence interval, OR: odds ratio, MAF: minor allele frequency, PEXS: pseudoexfoliation syndrome, PEXG: pseudoexfoliation glaucoma

### 3.3.5. Bioinformatic analysis- binding sites of miRNAs are predicted to be affected by the 3'-UTR variants

As 3'-UTR is susceptible to the binding of micro RNAs, the effect of rs9331942, rs9331949, and rs9331950 on putative miRNA binding sites was assessed *in silico*. miRdB reported 73 miRNAs targeting the 3'-UTR of *CLU*. However, only 29 miRNAs crossed the target score cut-off of 70 (assigned by the database). miRdB predicted the seed location for hsa-miR-586 just one base upstream of rs9331942 with a high score of 88 (**Figure 3.3A**). Though the binding of this miRNA could plausibly be affected by rs9331942, there was no prediction of allele-specific differential binding of hsa-miR-586 to rs9331942. SNPinfo using data integrated from miRanda showed a differential binding of hsa-miR-223 to the rs9331942 element with the 'C' allele but not with the 'T' allele (**Figure 3.3B**). Also, SNPinfo predicted a binding site for hsa-miR-1283 to the rs9331949 element with the 'G' allele but not with the 'A' allele (**Figure 3.3C**).

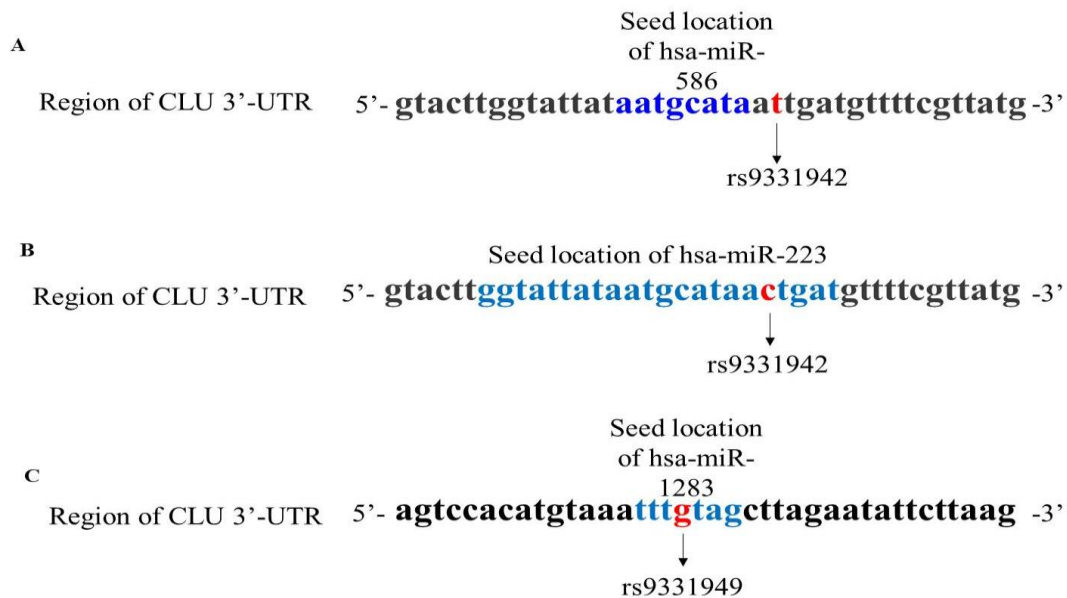


**Figure 3.3. Location of binding of microRNAs to 3'-UTR of *CLU* at rs9331942 and rs9331949. A.** miRdB software predicted the binding hsa-miR-586 near rs9331942. **B.** SNPinfo (miRanda) software predicted binding of hsa-miR-223 to the risk allele 'C' at rs9331942 but not to the 'T' allele. **C.** SNPinfo (miRanda) software predicted the binding of hsa-miR-1283 to the risk allele 'G' at rs9331949 but not to the 'A' allele.

### 3.3.6. Risk variants at rs9331942 and rs9331949 have a functional significance

To assess the functional effect of rs9331942 and rs9331949 on gene expression and to check if the change in alleles at these SNPs affects the binding of the *in silico* predicted microRNAs, luciferase reporter assays along with the predicted miRNA mimics were performed. HEK293 cells were transfected with either the empty pMIR vector, wild-type construct (rs9331942 ‘T’ – rs9331949 ‘A’) or the mutant constructs with rs9331942 ‘C’ or rs9331949 ‘G’. The constructs were co-transfected with 50 nmoles of either the miR-223 mimic for rs9331942 and miR-1283 for rs9331949 or the negative miR. As shown in **Figure 3.4A**, cells transfected with rs9331942 ‘C’ allele and the miR-223 showed decreased luciferase activity ( $p=0.04$ ) compared to the cells transfected with negative miR. However, no difference in luciferase activity was observed between cells transfected with either wild-type 3’-UTR of CLU and miR-223 or negative miR ( $p=0.17$ ). Similarly, no difference was observed in luciferase activity from cells transfected with empty vector and miR-223 or negative miR ( $p=0.19$ ). These results imply that the ‘C’ allele at rs9331942 binds to miR-223, and the change from allele ‘C’ to ‘T’ at rs9331942 affects this binding. Further, after normalizing the luciferase values of miR-223 to those of negative miR, rs9331942 ‘C’ allele showed a significantly decreased luciferase activity ( $p=0.03$ ) compared to the wild type (rs9331942 ‘T’ allele) (**Figure 3.4B**). As shown in **Figure 3.4C**, cells transfected with rs9331949 ‘G’ allele and miR-1283 showed decreased luciferase activity ( $p=0.02$ ) compared to the cells transfected with the negative miR. However, no difference in luciferase activity was observed between cells transfected with either wild type 3’-UTR of CLU and miR-1283 or negative miR ( $p=0.21$ ). Similarly, no difference was observed in luciferase activity from cells transfected with empty vector and miR-223 or negative miR ( $p=0.41$ ). These results imply that the ‘G’ allele at rs9331949 binds to miR-1283, and the change from allele ‘G’ to ‘A’ at

rs9331949 affects this binding. Further, after normalizing the luciferase values of miR-1283 to those of negative miR, rs9331949 ‘G’ allele showed a significantly decreased luciferase activity ( $p=0.02$ ) compared to the wild type (rs9331942 ‘A’ allele) (**Figure 3.4D**). These findings suggest that the presence of the risk variants ‘C’ at rs9331942 and ‘G’ at rs9331949 propagate the binding of microRNAs to the 3’-UTR of *CLU*, which might lead to differential gene regulation.

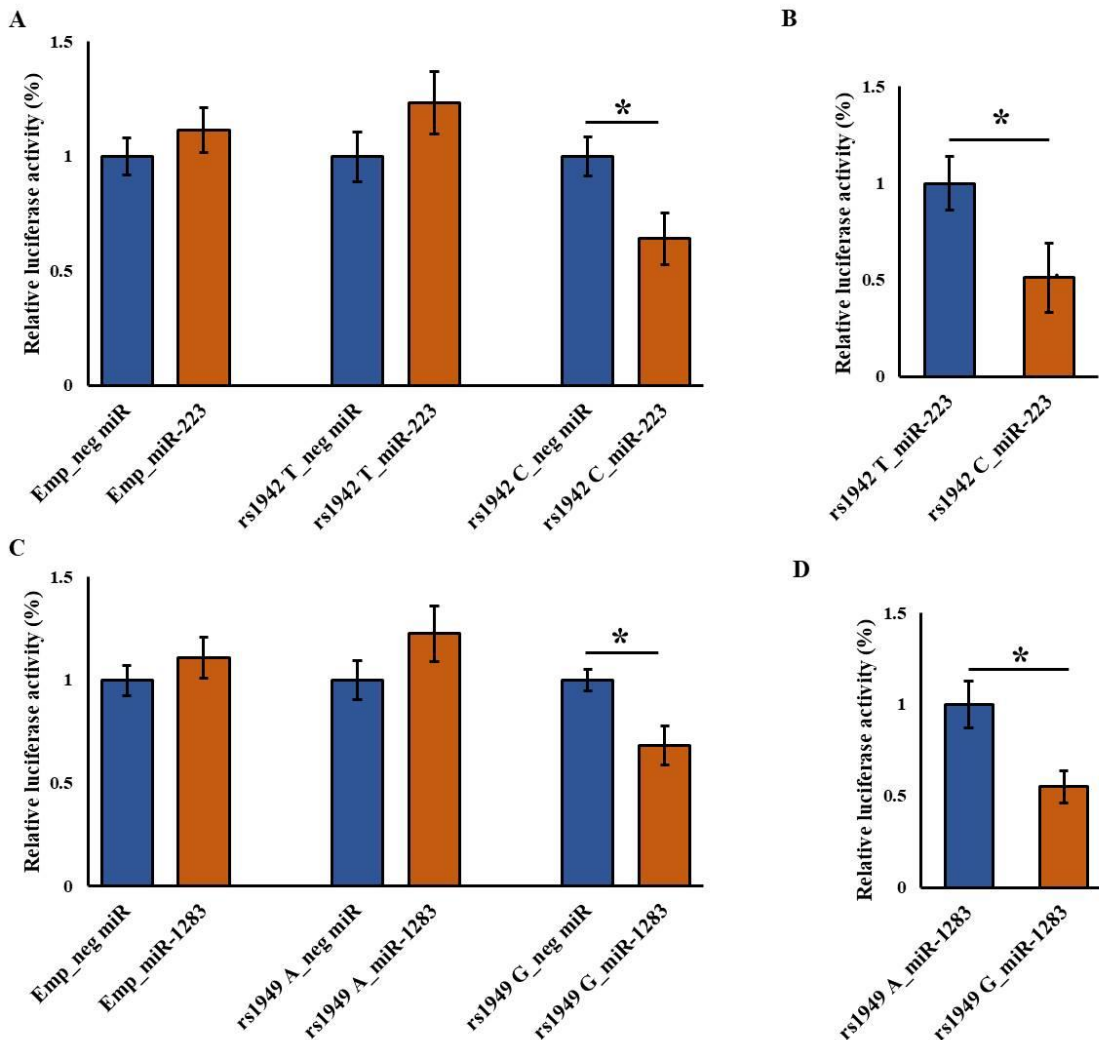


**Figure 3.4. rs9331942 and rs9331949 showed differential luciferase activity.** A. Relative luciferase activity of empty vector, wild type *CLU* 3’-UTR (rs9331942 ‘T’ allele) and rs9331942 ‘C’ allele. The cells were co-transfected with either the miR-223 mimic or the negative miR control. There is a significant decrease in luciferase activity in cells transfected with the ‘C’ allele and miR-223 mimic compared to the negative control ( $p=0.04$ ). No difference was observed between cells transfected with

wild-type construct and miR-223 or negative miR ( $p=0.17$ ); and with just empty vector and miR-223 or negative miR ( $p=0.19$ ) **B.** Relative luciferase activity between wild-type and rs9331942 ‘C’ allele after normalizing the values from miR-223 to the negative miR. There is a significant decrease in luciferase activity on change from the ‘T’ to ‘C’ allele at rs9331942 ( $p=0.03$ ). **C.** Relative luciferase activity of empty vector, wild type *CLU* 3’-UTR (rs9331949 ‘A’ allele) and rs9331949 ‘G’ allele. The cells were co-transfected with either the miR-1283 mimic or the negative miR control. There is a significant decrease in luciferase activity in cells transfected with the ‘G’ allele and miR-1283 mimic compared to negative control ( $p=0.02$ ). No difference was observed between cells transfected with wild-type construct and miR-1283 or negative miR ( $p=0.21$ ); and with just empty vector and miR-1283 or negative miR ( $p=0.41$ ) **D.** Relative luciferase activity between wild-type and rs9331949 ‘G’ allele after normalizing the values from miR-223 to the negative miR. There is a significant decrease in luciferase activity on change from the ‘A’ to ‘G’ allele at rs9331949 ( $p=0.02$ ). Each experiment is repeated at least three times. Data represented as mean  $\pm$  SEM, \*  $p<0.05$ .

### 3.3.7. *CLU* promoter is hypomethylated in pseudoexfoliation patients

As clusterin promoter is also susceptible to aberrant CpG methylation changes, we checked the methylation status of *CLU*  $\pm 1$  kb from the transcription start site. ENCODE data from the UCSC genome browser showed that the clusterin promoter region has 46 CpG sites. MethPrimer software identified two CpG islands within this region, Region I (-113 bp to -321 bp) containing 19 CpG sites and Region II (-97 bp to +67 bp) containing 17 CpG sites (**Figure 3.5A**). Direct bisulfite sequencing of blood DNA showed that region I is significantly hypomethylated in both PEXS ( $p=0.006$ ) and PEXG ( $p=0.001$ ) compared to the control (**Figures 3.5B and 3.5C**). However, there was no significant change observed in the methylation pattern in region II of PEXS ( $p=0.52$ ) or PEXG ( $p=0.45$ ) compared to controls (**Figures 3.5D and 3.5E**). Hypomethylation in the region I corroborated with an increased expression of *CLU* in blood cells of both PEXS ( $p=0.04$ ) and PEXG ( $p=0.02$ ) compared to controls (**Figure 3.5F**).

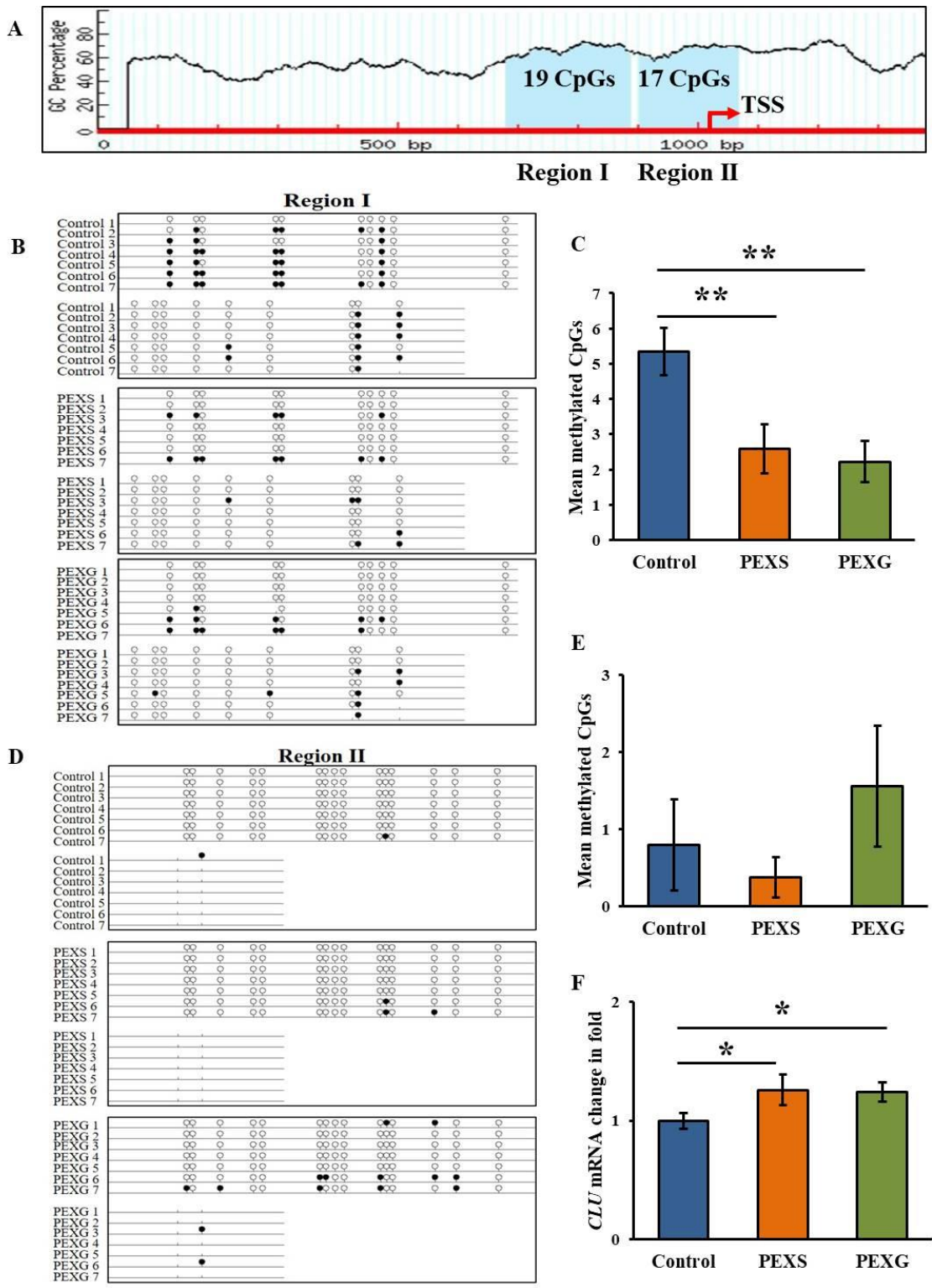


**Figure 3.5. Promoter methylation pattern of clusterin in blood cells of PEX versus controls. A.** MethPrimer software delineating the two CpG islands present in clusterin promoter **B.** Representative lollipop plot of methylated and unmethylated CpGs in the region I of clusterin promoter of controls, PEXS, and PEXG. **C.** Bar graph representation of methylation pattern in region I of control, PEXS, and

PEXG. Significant hypomethylation was observed in both PEXS (n=19, p=0.006) and PEXG (n=18, p=0.001) compared to controls (n=20). **D.** Representative lollipop plot of methylated and unmethylated CpGs in region II of clusterin of controls, PEXS, and PEXG. **E.** Bar graph representation of methylation pattern in region II of control, PEXS, and PEXG. No difference in methylation pattern was observed in either PEXS (n=19, p=0.52) or PEXG (n=18, p=0.45) compared to controls (n=20). **F.** *CLU* mRNA was significantly upregulated in blood cells of PEXS (n=9, p=0.04) and PEXG (n=9, p=0.02) compared to the control (n=12). Closed circle in the lollipop plot represents a methylated CpG and an open circle represents an unmethylated CpG. Data represented as mean  $\pm$  SEM, \*\* p<0.01, \*p $\leq$ 0.05.

We had previously observed increased *CLU* in the LC and aqueous humor of PEXG through immunostaining and western blotting analysis, respectively.<sup>75</sup> Recently, Rebecca *et al.* observed increased mRNA expression of *CLU* in LC of PEXS and increased protein levels of *CLU* in AH of both PEXS and PEXG. In this study, we observed significantly increased clusterin in the LC of both PEXS (p=0.03) and PEXG (p=0.03) compared to controls through western blotting (**Figure 3.6A and 3.6B**). Therefore, we checked the promoter methylation pattern of *CLU* in lens capsule tissue of PEX patients and controls to understand if an aberrant methylation change could be responsible for the increased clusterin in LC of PEX patients. Like the blood DNA, the region I showed significant hypomethylation in PEXS (p=0.02) and PEXG (p=0.02) compared to controls (n=6) (**Figures 3.6C and 3.6D**). Region II in LC tissue did not show any significant differential methylation pattern in either PEXS (p=0.84) or PEXG (p=0.08) compared to controls (**Figures 3.6E and 3.6F**). **Thus, we observed that the region I of clusterin promoter is hypomethylated in PEX patients in both blood and lens capsule.**

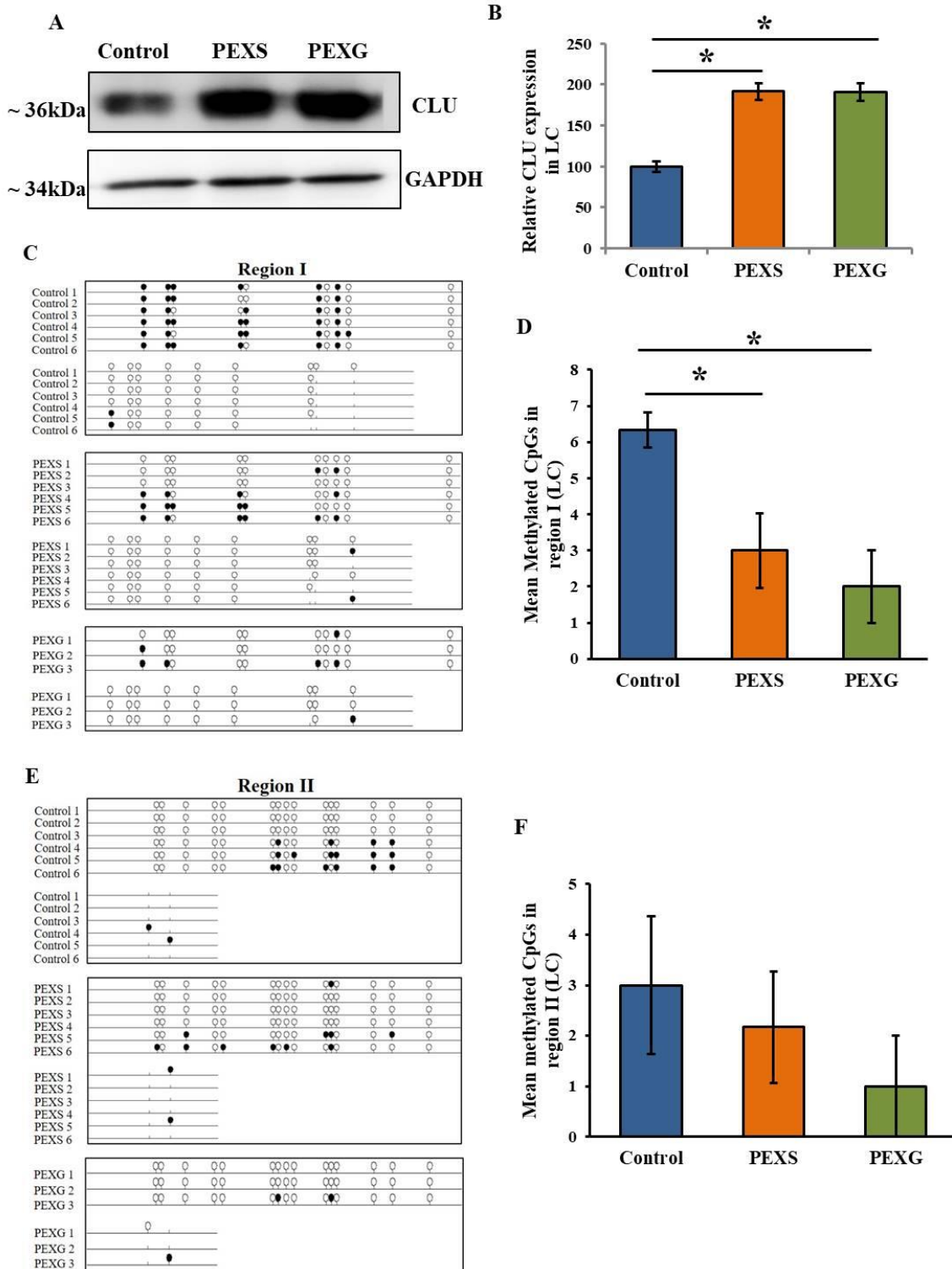


**Figure 3.6. Promoter methylation pattern of clusterin in the lens capsule of PEX versus controls. A.** Representative western blot showing increased expression of clusterin in the lens capsule of PEXS and PEXG compared to controls. **B.** Densitometry analysis shows significantly increased expression of CLU in the LC of PEXS ( $p=0.03$ ) and PEXG ( $p=0.03$ ) patients compared to controls. **C.** Representative

lollipop plot of methylated and unmethylated CpGs in the region I of clusterin promoter in the lens capsule of controls, PEXS and PEXG. **D.** Bar graph representation of methylation pattern in the region I of control, PEXS, and PEXG. Significant hypomethylation was observed in both PEXS (n=6, p=0.02) and PEXG (n=3, p=0.02) compared to controls (n=6). **E.** Representative lollipop plot of methylated and unmethylated CpGs in region II of clusterin of controls, PEXS, and PEXG. **F.** Bar graph representation of methylation pattern in the region II of control, PEXS, and PEXG. No difference in methylation pattern was observed in either PEXS (n=6, p=0.64) or PEXG (n=3, p=0.27) compared to controls (n=6). Closed circle in the lollipop plot represents a methylated CpG and an open circle represents an unmethylated CpG. Data represented as mean  $\pm$  SEM, \*p $\leq$ 0.05.

### 3.3.8. Clusterin promoter hypomethylation corroborates with decreased *DNMT1*

CpG methylation is catalyzed by the DNA methyltransferases (DNMTs), mainly DNMT1, DNMT3A, and DNMT3B. DNMT1 is the maintenance methyltransferase that catalyzes the binding of methyl groups to CpGs in the presence of methyl donors such as S-adenosyl methionine. DNMT3A and DNMT3B are *de novo* methyltransferases. We had previously reported an upregulation of DNMT3A in LC of PEXS patients but not PEXG.<sup>101</sup> In this study, we checked the expression of DNMT1 in blood cells and lens capsule tissue of PEX patients to check if clusterin promoter hypomethylation could be due to any changes in DNMT1 expression. qRT-PCR analysis showed that the expression of *DNMT1* in blood cells is significantly decreased in both PEXS (p=0.04) and PEXG (p=0.008) compared to controls (**Figure 3.7A**). Similarly, *DNMT1* is significantly decreased in the lens capsule of both PEXS (p=0.04) and PEXG (p=0.04) compared to controls (**Figure 3.7B**). To further validate if DNMT1 affects the methylation pattern and subsequent expression of clusterin, DNMT1 was overexpressed in HLE B-3 cells. Increased hypermethylation of CpGs in the region I of *CLU* was observed in cells overexpressed with DNMT1 (p=0.009) compared to cells transfected with just the empty vector (**Figure 3.7C**). **This hypermethylation correlated with a decreased expression of clusterin in cells transfected with the DNMT1 overexpression vector compared to the empty vector at**

**both mRNA (p=0.02) and protein (p=0.02) levels (Figure 3.7D-3.7F). These findings suggest that DNMT1 regulates the expression of clusterin.**

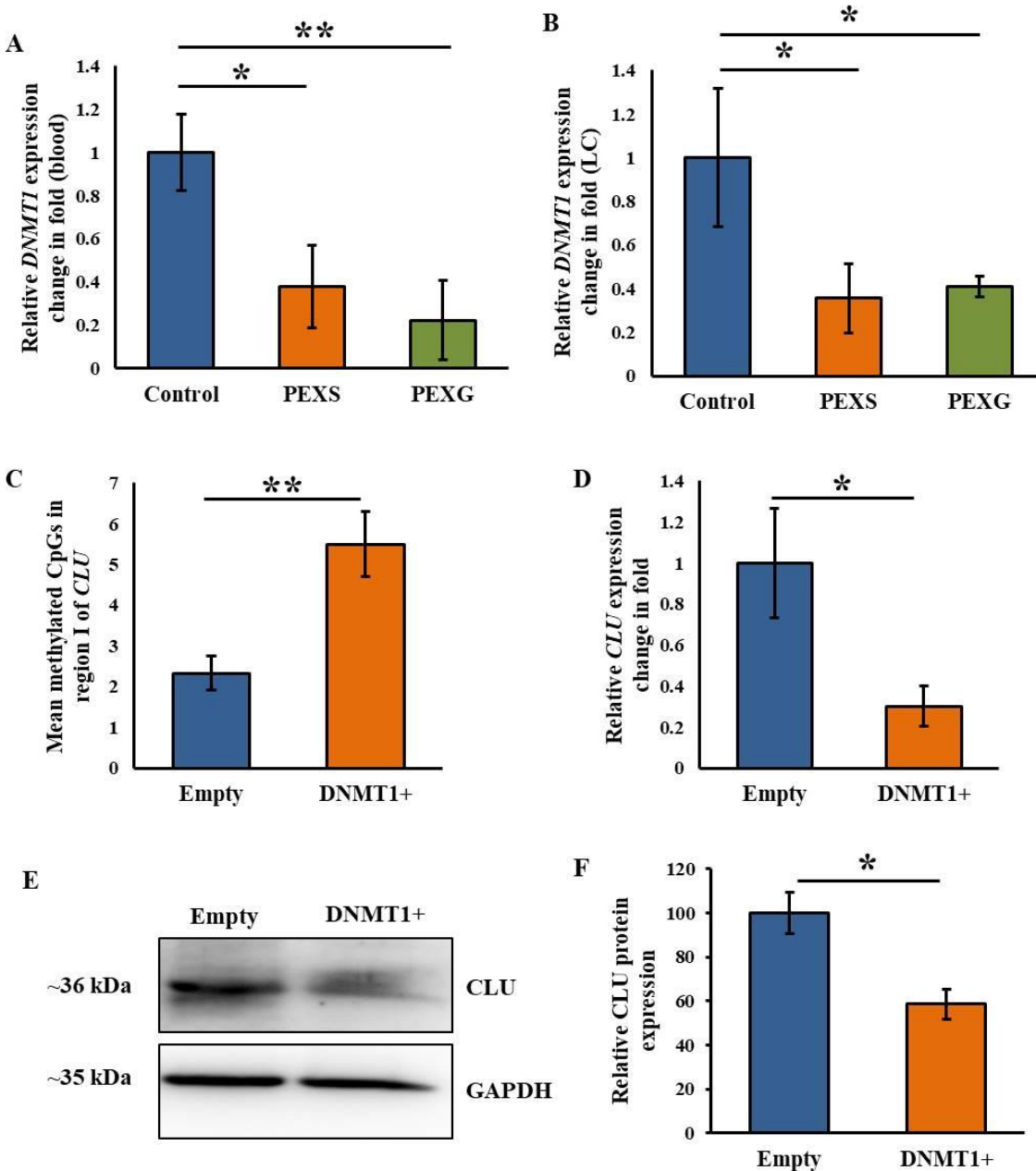


**Figure 3.7. Effect of DNMT1 overexpression on clusterin in HLE B-3 cells. A.** *DNMT1* is significantly decreased in blood cells of PEXS (n=7, p=0.04) and PEXG (n=6, p=0.008) compared to control (n=5) **B.** *DNMT1* is significantly decreased in the lens capsule of PEXS (n=6, p=0.04) and PEXG (n=6, p=0.04) compared to control (n=9). **C.** Overexpression of DNMT1 in HLE B-3 cells significantly increased mean methylated CpGs (p=0.009) in the region I of *CLU* promoter compared to cells

transfected with empty vector. **D.** Overexpression of DNMT1 decreased the expression of *CLU* ( $p=0.02$ ) in HLE B-3 cells compared to cells transfected with just the empty vector. **E.** Representative blot showing decreased expression of CLU in HLE B-3 cells overexpressed with DNMT1 compared to empty vector **F.** Densitometry analysis showed significantly decreased expression ( $p=0.02$ ) of CLU in HLE B-3 cells overexpressed with DNMT1 vector compared to cells treated with the empty vector. Data represented as mean  $\pm$  SEM of at least three independent experiments. \*\* $p<0.01$ , \* $p\leq 0.05$ .

### **3.3.9. DNA methylation inhibitor, 5-aza-dC induced increased Sp-1 binding to hypomethylated region in the promoter and higher expression of CLU**

We induced DNA hypomethylation in Human lens epithelial cells (HLE B-3) using 5-aza-deoxycytidine (5-aza-dC). HLE B-3 cells treated with 1.0  $\mu\text{M}$  5-aza-dC for 72 hours showed hypomethylated region I ( $p=0.02$ ) in *CLU* promoter compared to cells treated with DMSO control (**Figure 3.8A**). 5-aza-dC treated cells showed increased clusterin expression at both mRNA ( $p=0.02$ ) and protein ( $p=0.02$ ) levels compared to the cells treated with DMSO control (**Figure 3.8B-3.8D**).

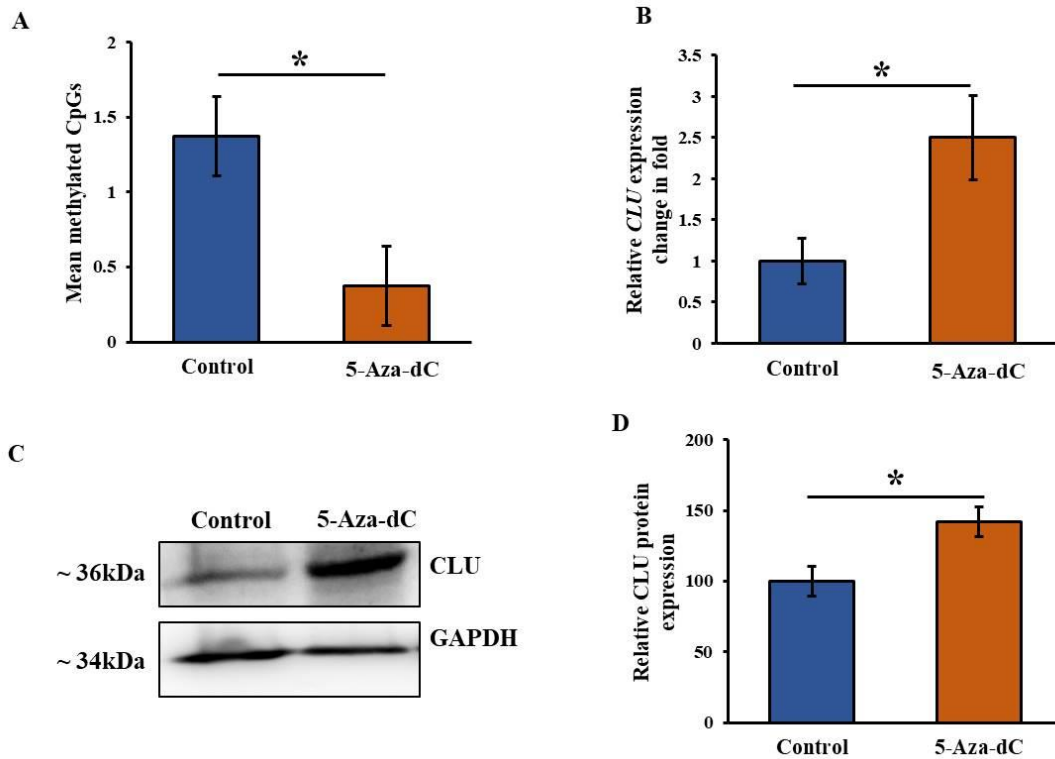


**Figure 3.8. Effect of 5-Aza-dC on clusterin expression in HLE B-3 cells.** **A.** Region I in clusterin is significantly hypomethylated ( $p=0.02$ ) in 5-aza-dC treated HLE B-3 cells compared to cells treated with DMSO. **B.** *CLU* mRNA was significantly increased ( $p=0.02$ ) in 5-aza-dC treated cells compared to the control. **C.** Representative immunoblot showing increased clusterin expression in 5-aza-dC treated cells compared to control **D.** Bar graph shows significantly increased clusterin protein expression in 5-aza-dC treated cells ( $p=0.02$ ).

To check if promoter hypomethylation of clusterin influences the binding of any transcription factor to this region, we identified the transcription factors predicted to bind to the region I on the JASPAR database. Twenty transcription factors were predicted to bind in the region I of the clusterin promoter (**Table 3.6**).

**Table 3.6.** Predicted transcription factor binding sites to CpGs in *CLU* region I

Transcription Factor	Start	End	Strand	Predicted site sequence
ETS1	260	265	+	TTTCCG
TFAP2A	192	200	-	GCCGGGGC
VDR	101	108	+	GCCGGGAG
NFE2	280	290	-	CGAGTTCA
FOS:JUN	279	289	+	CATGACTCACG
BNC2	279	290	+	CATGACTCACG
TCFL5	94	103	-	TCGCGTGCCC
SP5	229	238	+	CACCTCCCGG
HES1	95	104	+	CTCGCGTGCC
SP1	225	235	+	CCCACCTCCCG
	190	196	+	CCGGCGC
NFATC3	258	266	-	GCGGAAAG
KLF	276	284	+	TGGGCGTG
MGA	277	284	+	GGGCGTGA
BATF	280	290	+	CATGACTCACG
ARNT:HIF1A	277	284	+	GGGCGTGA
TBX3	137	146	-	GAGGTGCGGC
INSM1	200	211	-	GGGCTGGGGGCG
ZNF610	128	141	-	GCGGCCGCTCGGCG
NRC2	189	196	-	GGGGGCGC
SOX18	176	183	-	CACCACGA

Predictions are based on results generated from the JASPAR database (<http://jaspar.genereg.net/>; [14]). The “Start” and “End” indicate the respective base pair in the investigated CpG island-region I (-113 bp to -321 bp). The “Strand” labels orientation on the forward strand or the reverse strand.

Of these transcription factors, Sp1 (specificity protein 1) was predicted to bind to two regions spanning the CpG sites within the region I. Since Sp1 is an important regulator of clusterin gene expression, we performed chromatin immunoprecipitation (ChIP) assays to check if hypomethylation induced by 5-aza-dC influences the binding of Sp-1 with *CLU* promoter (region I).<sup>181,182</sup> **ChIP assays showed that treatment of 5-aza-dC induced significantly increased binding (p=0.01) of Sp-1 with *CLU* promoter in HLE B-3 cells (Figure 3.9A and 3.9B). These results demonstrated that the binding of Sp-1 to hypomethylated region I in the *CLU* promoter regulates its expression.**

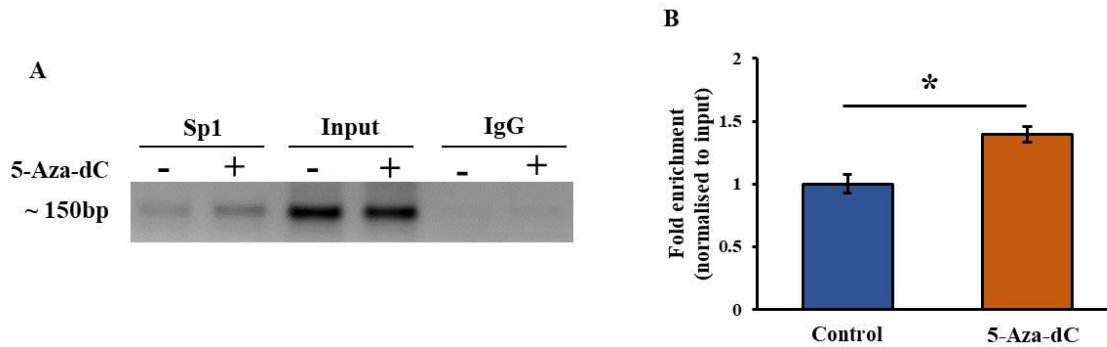


**Figure 3.9. Effect of clusterin promoter demethylation on Sp-1 binding.** **A.** Gel image shows PCR amplified products representing the pull down of region I of *CLU* by Sp1 and IgG. **B.** Bar graph showing fold enrichment of *CLU* region I by Sp1 in cells treated with 5-aza-dC and DMSO control after normalizing the densitometric values of the bands to those of the input. There is a significantly increased enrichment of DNA pull down by Sp1 in cells treated with 5-aza-dC compared to control cells. Data represented as mean  $\pm$  SEM of at least three independent experiments, \* $p \leq 0.05$ .

### 3.4. Discussion

Pseudoexfoliation is an elastotic fibrilopathy and a disorder of protein aggregation. Ubiquitin-proteasome system and the molecular chaperones work in a coordinated fashion to maintain protein homeostasis inside the cell. However, these systems, along with other cytoprotective mechanisms, are highly dysregulated in pseudoexfoliation.<sup>75,77,123,133</sup> *CLU* is a molecular chaperone involved in a number of functions inside a cell. Numerous reports have shown increased levels of *CLU* in various tissues, such as lens capsules and circulating fluids in PEXS and/or PEXG.<sup>75,77,78,173</sup> Also, *CLU* was found to be a constituent of the XFM by three different groups.<sup>42,172,183</sup> Considering the essential roles that *CLU* plays in the cell, dysregulation of *CLU* in PEX implies that it is a very important risk factor for PEX. In this study, we have shown that both genetic risk variants and epigenetic modifications of clusterin contribute to PEX pathophysiology.

The association of several genetic variants of clusterin with PEX has been studied in various populations. Genotyping of nine tagged SNPs of *CLU* showed a nominal association ( $p=0.04$ ) of rs3087554 haplotype with PEX in an Australian cohort, but on restricting the age of controls, the significance was lost ( $p=0.07$ ).<sup>73</sup> Krumbiegel *et al.* studied the genetic association of five SNPs in *CLU* with PEX, of which only rs2279590 showed a strong association with PEX in two German cohorts, with A' being the risk allele but it was not associated with PEX in the Italian cohort. They did not find an association of rs3087554 with PEX in their study cohorts.<sup>74</sup> However, we observed a significant association of both rs2279590 (residing in the 7<sup>th</sup> intron) and rs3087554 (residing in the 3'-UTR) with the Indian population. We further showed that rs2279590 is a functional variant, and the genotype 'GG' increased *CLU* mRNA expression by 2-fold compared to the 'AA' genotype.<sup>75</sup> Contradicting previous findings, Dubey *et al.* did not find any association of either rs2279590 or rs3087554 with PEX in the South Indian population.<sup>184</sup> Incomplete penetrance and allele reversals in different populations imply the presence of other genetic variants in *CLU* that could be responsible for the association of *CLU* with PEX susceptibility.

This study was undertaken to identify variants in linkage disequilibrium with rs2279590 in its vicinity. We observed a strong association of rs9331942 and rs9331949, residing in the 3'-UTR with PEX compared to controls. Both these SNPs were found to be strongly associated with another neurodegenerative disorder, Alzheimer's disease (late-onset), in Han Chinese population.<sup>185-187</sup> Similar to our findings, in these studies, the minor alleles at the SNPs increased the risk of the disease. In our study, the minor allele 'C' at rs9331942 increased the risk of PEX by 1.6-fold, and the minor allele 'G' at rs9331949 increased the risk of PEX by 1.5-fold. However, rs9331950, also residing in the 3'UTR, was not found to be associated with PEX. The

risk haplotype, 'C-G-C' at 'rs9331942-rs9331949-rs9331950' and the risk haplotype 'C-C-G-C' at 'rs2279590-rs9331942-rs9331949-rs9331950' were found to be significantly associated with PEX, and the effect of these SNPs could be synergistic on *CLU* regulation.

3'UTRs of genes are targets of several microRNAs that might affect the translation of a gene and, thereby, might affect the protein levels. Change in alleles at an SNP in the 3'-UTR can affect the binding sites for miRNAs and lead to differential protein expression. Bioinformatic analysis revealed the binding sites for has-miR-223 and hsa-miR-1283 with minor allele or the risk allele at rs9331942 and rs9331949, respectively. Luciferase reporter assays in HEK293 cells from this study showed that the presence of the risk allele 'C' at rs9331942 and 'G' allele at rs9331949 facilitate the binding of miR-223 and miR-1283, respectively, to the 3'-UTR of *CLU* and decreased luciferase reporter activity implies that binding of these miRNAs to *CLU* could regulate its expression. Also, both rs9331942 and rs9331949 were found to be functional variants displaying allele-specific regulatory effects. However, the *in silico* predictions and subsequent molecular studies showed that the presence of risk alleles at both these SNPs decreases the expression of *CLU*, which is contrary to the observed upregulation of *CLU* in PEX. One plausible explanation for this could be decreased presence of these regulatory microRNAs in PEX, resulting in an uninhibited expression of *CLU*. We have observed decreased expression of miR-223 in the plasma of PEX patients compared to the controls (Lipsa Sahoo *et al.*, Ph.D. thesis, unpublished data).

Apart from genetic variants, DNA methylation can also affect gene expression; therefore, we hypothesised that other than genetic variants, epigenetic factors could also be responsible for aberrant *CLU* expression in PEX. To address the same, we studied the methylation status of two CpG islands in *CLU* promoter by bisulfite sequencing. Decreased methylation in the region I of

*CLU*, upstream (-113 bp to -321 bp) to the transcription start site corroborated with an increased expression of clusterin in both blood cells as well as the lens capsule tissue of PEX patients compared to controls. Promoter hypomethylation results in active chromatin that facilitates increased access of the transcription factors to the regulatory elements present in the promoter leading to enhanced gene expression.

Further, treatment of HLE B-3 cells with the DNMT inhibitor, 5-aza-deoxycytidine (5-aza-dC), resulted in promoter hypomethylation and increased expression of clusterin, implying that CpG methylation changes in clusterin promoter regulate its expression. Similar to our findings, Suuronen *et al.* observed that treatment of retinal pigment epithelial cells with 5-aza-dC resulted in an upregulation of clusterin and implied a similar regulatory mechanism of clusterin in the pathology of age-related macular degeneration.<sup>167</sup> As promoter hypomethylation results in open chromatin giving access to transcription factors, we checked if DNA hypomethylation influenced the binding of any transcription factor to clusterin promoter using the demethylating agent, 5-aza-dC. Of the twenty transcription factors predicted to bind to the region I in clusterin promoter, we chose to study the interaction of Sp1 with clusterin promoter under the effect of 5-aza-dC. Sp1 is an important transcription factor with cis-regulatory binding motifs present in the promoters of many genes. Clusterin promoter has seven Sp1 binding sites, of which two reside in the region I of CpG island I of the promoter. ChIP assays showed increased binding of Sp1 to clusterin promoter on hypomethylation. This increased access of Sp1 to *CLU* promoter could lead to its enhanced expression on promoter hypomethylation of *CLU*.

DNA methylation is governed by the DNA methyltransferases (DNMTs) that catalyze the transfer of methyl residues to cytosines from methyl group donors. DNMT3A and DNMT3B are de novo methyltransferases, and DNMT1 is an important maintenance methyltransferase that

copies the methylation signature from the parent DNA strand to the daughter strand. We have previously reported decreased expression of another chaperone, HSP70, in the lens capsule of PEXS patients owing to its promoter hypermethylation that correlated with an increased expression of DNMT3A. We, however, did not observe any differential expression of DNMT3B in PEX patients compared to the controls.<sup>101</sup> In this study, we observed a decreased expression of the maintenance methyl transferase, DNMT1, in PEX patients in both blood cells and lens capsule tissue that corroborated with promoter hypomethylation of clusterin and its increased expression. Overexpression of DNMT1 in human lens epithelial cells (HLE B-3) resulted in increased expression of clusterin validating the finding from PEX patients. The opposite alteration in the expression of two DNA methyltransferase genes, DNMT1 and DNMT3A, suggests the involvement of specific methyltransferase genes in regulating the expression of different proteins. A recent report on RNA sequencing of the human lens epithelium from PEX patients showed a decreased expression of DNMT1 in line with our findings.<sup>188</sup> However, Greene *et al.* reported an increased expression of DNMT1 in the human tenon fibroblasts of PEXG patients<sup>69</sup> suggesting that tissue-specific expression of these epigenetic ‘writers’ might lead to tissue-specific expression changes in target genes and pathway modulations.

A replicative study in a larger cohort including different ethnicities can substantiate the findings reported in this study here that 3’UTR variants of *CLU* are a risk for pseudoexfoliation. In conclusion, the 3’UTR variants of *CLU*, rs9331942 and rs9331949, are significantly associated with pseudoexfoliation as a risk factor. The haplotype ‘C-G-C’ at rs9331942-rs9331949-rs9331950 increases the risk of PEX by 1.5-fold. Both rs9331942 and rs9331949 are functional variants, and differential miRNA binding at these SNPs could affect the clusterin gene expression. Further, the promoter region proximal to the transcription start site of clusterin is

hypomethylated in PEX patients resulting in its increased expression. Also, functional molecular assays in HLE B-3 cells showed that this hypomethylation results in enhanced binding of Sp1 to clusterin promoter leading to its enhanced expression. A concluding remark from our findings is that a combination of genetic and epigenetic factors contributes to the regulation of clusterin in PEX pathology and that PEX causation and progression is a complex interplay of genetic and epigenetic modulators.

\*\*\*\*\*

## *Chapter 4*

# **Protein aggregation and vimentin in PEX**

## **pathology**

## 4. Protein aggregation and vimentin in PEX pathology

### 4.1. Introduction

In this chapter, we report the dysregulation of vimentin in PEX and the contribution of DKK1 to protein aggregation and vimentin regulation.

Increasing evidence suggests that PEX pathology involves impaired proteostasis and dysregulated chaperone system.<sup>75,76,101,123,133</sup> Proteasome impairment and proteotoxic stress are known to cause protein aggregates and aggresome formation, the latter being a fail-safe mechanism adapted by a cell to combat proteotoxic stress. Aggresomes are structures formed by the trafficking of misfolded proteins to centrosomes, encaged by vimentin (VIM) filaments, and subsequently degraded by autophagy. VIM is a 57kDa type III intermediate filament protein that regulates cellular and tissue functions, such as cell proliferation, apoptosis, and differentiation.<sup>189</sup> Along with other cytoskeletal proteins such as actin, glial fibrillary acidic protein, tubulin, vinculin, etc., vimentin maintains cellular integrity and provides a cytoskeletal framework.

Vimentin is predominantly expressed in cells of mesenchymal origin, in undifferentiated and cultured cells.<sup>190</sup> Although once thought to be dispensable, the versatile roles of intracellular and soluble forms of VIM are being recognised now. Aberrant upregulation of vimentin is noted in various cancers, including pancreatic cancer, oral cell carcinomas, prostate cancers, gastrointestinal tumours, and lung cancer.<sup>191–195</sup> Vimentin marks the epithelial-to-mesenchymal transitions in tumorigenic tissues and aids cellular migration. Kalyansundaram *et al.* suggest that post-translational modifications (PTMs) on VIM affect the vimentin intermediate filament network, affecting the cytoskeletal integrity and ECM remodelling.<sup>196</sup> Vimentin also interacts with various cell signalling molecules, and these PTMs might affect this interaction disturbing the signalling. Vimentin plays a role in cellular homeostasis and stress response through its interactions with

RNA-binding proteins, misfolded aggregates, stress granules, and processing bodies.<sup>197</sup> Further, recent evidence suggests that VIM is crucial for protein turnover at the aggresome.<sup>198</sup> Enhanced expression and genetic variants of VIM have been associated with pulverized cataracts, microphthalmia, and retinal stress.<sup>199–201</sup> As VIM is involved in crucial cellular functions such as proteostasis, apoptosis, inflammation, and signalling pathways induced by oxidative stress and hypoxia, all of which are seen to be dysregulated in PEX, we hypothesized the involvement of VIM in PEX pathology.<sup>202,203</sup>

Although numerous researchers have studied the composition of exfoliative material, the actual cause of protein aggregation in PEX is yet to be elucidated. Studies have reported the involvement of the Wnt signalling antagonist, Dickkopf-1 (DKK1) in the formation of A $\beta$  aggregates in AD brain and the inhibition of the Rho kinase- ROCK2 leads to decreased A $\beta$  aggregates.<sup>204–206</sup> We had previously observed upregulation of DKK1 in the lens capsule of PEX patients that corroborated with upregulation of ROCK2 in the LC of PEXS individuals (Dr. Bushra Hayat, Ph.D. thesis, unpublished data). DKK1 is a potent inhibitor of the  $\beta$ -catenin-driven Wnt signalling pathway. It is upregulated in various cancers and neurological diseases such as AD and PD.<sup>207–209</sup> ROCK2 is a downstream effector of DKK1 and a non-canonical Wnt target implicated in neurological aggregopathies such as Huntington's disease and AD.<sup>205,210</sup> Reports have suggested DKK1 and ROCK2 as upstream regulators of vimentin expression. In this objective, we studied the presence of protein aggregates in the lens capsule of PEX patients. We further explored the involvement of DKK1 and ROCK2 in protein aggregate formation and vimentin regulation using the human lens epithelial cells.

## 4.2. Materials and Methods

### 4.2.1. Study subjects' selection, recruitment, and sample collection

This study was approved by the Institutional Biosafety and Human Ethics committee of the National Institute of Science Education and Research and adhered to the tenets of the Declaration of Helsinki. Participants were recruited at Sri Sri Borda Hospital, Bhubaneswar. Inclusion-exclusion criteria, as mentioned in Chapter 2, page no. 41 were followed. Informed consent was obtained from all participants. The lens capsules and aqueous humor were collected during cataract surgery from consented participants and stored at  $-80^{\circ}\text{C}$  until further use.

### 4.2.2. Quantitative Real time-PCR (qRT-PCR) for mRNA expression studies

Lens capsules were collected from study participants at the time of cataract surgery and immediately frozen in liquid nitrogen and stored at  $-80^{\circ}\text{C}$  until further use. Total RNA was extracted from lens capsules of age and sex-matched study subjects using a commercial kit (RNeasy Mini Kit, QIAGEN GmbH, Hilden) as per the manufacturer's protocol. The detailed protocol is mentioned in Chapter 3, page no. 78. Gene-specific primers were designed using PrimerQuest Tool (IDT). The primers used for *VIM* (NM\_003380.5) were: forward primer 5'-AATGGCTCGTCACCTTCGTGAAT-3' and reverse primer 5'-CAGATTAGTTTCCCTCAGGTTTCAG-3' and for *GAPDH* (NM\_003380.5) taken as an endogenous control were: forward primer 5'-GGTGTGAACCATGAGAAGTATGA-3' and reverse primer 5'-GAGTCCTTCCACGATACCAAAG-3'. The housekeeping gene, *GAPDH*, was used as an endogenous control. The comparative threshold cycle ( $\Delta\Delta\text{Ct}$ ) method was used to get the expression fold change for a target gene and represented as fold difference compared to the control.

### **4.2.3. Western blotting**

Western blot analysis was performed with protein extracts of lens capsules and aqueous humor from study subjects and HLE-B3 cell lysates. Proteins from tissues and cells were extracted using the NE-PER Nuclear and Cytoplasmic Extraction Reagents (#78835) as mentioned in Chapter 3, page no. 79. Detailed protocol for western blotting is mentioned in Chapter 3, page no. 80. Antibodies for Dickkopf-1 (sc-374574, Santa Cruz Biotechnology; 1:500), ROCK2 (sc-398519, Santa Cruz Biotechnology; 1:200), and vimentin (ab45939 Abcam; 1:500) were used as primary antibody, and HRP conjugated Goat anti-rabbit IgG (621140380011730, GeNei, India), Goat anti-mouse IgG-HRP (621140680011730, GeNei, India) each at 1:5000 dilutions were used as the secondary antibody. GAPDH (ABM22C5, Abgenex, India; 1:250) was used for verifying equal loading and for normalisation. Detection was performed in a Fusion Solo S Chemi-Doc (Vilber Lourmat) using the chemiluminescence kit (Super Signal Femto Maximum Sensitivity Substrate, PI34094, Thermo Fisher Scientific). Evolution Capt software (Vilber Lourmat fusion solo S) was used for image acquisition, and signal intensity ratios relative to GAPDH were calculated for the normalization of protein expression level.

### **4.2.4. Immunostaining**

The tissue or cell samples (grown on coverslips) were washed thrice with 1X PBS. The samples were then fixed with 4.0% paraformaldehyde at room temperature for 20 minutes. The samples were washed thrice with 1X PBS for 5.0 minutes each time. The samples were permeabilized with 0.5% PBST for 10 minutes and blocked with 10% NHS (Normal horse serum prepared in 0.5% PBST) for 45 minutes. The blocking solution was then replaced with a primary antibody, and the samples were incubated at 4<sup>0</sup>C overnight. The human vimentin (ab45939, Abcam, UK) or human DKK1 (sc- 374574, Santa Cruz Biotechnology, USA) at 1:500 or 1:250 dilutions,

respectively, in blocking solution, was used as the primary antibody. After staining with primary antibody, the samples were washed thrice with 0.5% PBST for 5.0 minutes each time. The samples were incubated with specific secondary antibodies in the dark at room temperature for 2.0 hours. Alexa-Fluor 488 Chicken anti-mouse IgG (A21200, Invitrogen, USA) or Alexa-Fluor 594 goat anti-rabbit IgG (A21210, Invitrogen, USA) was used as the secondary antibody at 1:500 dilutions. The samples were washed thrice with 0.5% PBST for 5 minutes and with 1X PBS four times for 5.0 minutes each time. The samples were incubated with 2.5 µg/ml DAPI for 20 minutes, washed with 1X PBS once for 5.0 minutes, and mounted on a coverslip using ProLong Gold antifade reagent (P36934, Invitrogen, USA). The mounted cells/ tissues were imaged on Leica confocal microscope, and analysis was done using Image J software.

#### **4.2.5. Cell culture**

The human lens epithelial cells, HLE B-3 (ATCC, CRL-11421, Virginia, USA) was cultured in Dulbecco's Modified Eagle Medium, F12 (16000044, Invitrogen, USA) with 10% inactivated fetal bovine serum (16000044, Invitrogen, USA) as described in our previous study. The media was supplemented with 1.0% penicillin (100 U/ml) and streptomycin (0.1 mg/ml) (A001, HiMedia, India) and maintained at 37<sup>0</sup>C and 5.0% CO<sub>2</sub>. The cells were treated with either water vehicle or 10 µM Y-27632 ROCK inhibitor (SCM075, Sigma Aldrich, Germany) wherever mentioned for 24 hours as done in previous reports<sup>211–213</sup>, and then the cells were harvested for further experiments.

#### **4.2.6. Plasmid construction and transfection for DKK1 overexpression and knockdown experiments**

Plasmid containing the human full-length cDNA fragment of DKK1 (GenBank accession number NM\_012242) was purchased from Origene (Rockville, MD). This clone (pCMV6-

DKK1) expresses the complete DKK1 open reading frame with a Tag (MYC/DDK) at the C terminal. For the DKK1 overexpression study, HLE B-3 cells were transiently transfected with 1.0 µg of either pCMV6-DKK1 or pCMV6-empty plasmid. Briefly, cells were seeded into 12-well plates and grown for 24 hours until they reached 50–60% confluence, followed by transfection as per the manufacturer's instructions using the lipofectamine 3000 transfection reagent (Life Technologies, Inc., Basel, Switzerland). The cells were incubated with the plasmid/lipofectamine 3000/ medium mixture for 24 hours. In parallel with corresponding experimental samples, control transfection was performed with the empty plasmid, lipofectamine, and Opti-MEM. DKK1 overexpression was confirmed using ELISA (R&D Systems, Minneapolis, MN, USA). For DKK1 knockdown, HLE B-3 cells were seeded at  $2 \times 10^5$  cells/ well in 6-well plates the day before transfection. To prepare lipid siRNA complexes, 40 pmol of the indicated siRNA duplex in 100 µl of transfection medium and 4.0 µl of siRNA Transfection Reagent/Lipo3000 in 100 µl of transfection medium were combined, incubated for 30 minutes at 25<sup>0</sup>C, and then diluted with 800 µl of pre-warmed transfection medium (Opti MEM). The cells were rinsed once with serum-free DMEM, and 1000 µl of lipid-siRNA mixture described above was applied per well. After incubation for 6.0 hours at 37<sup>0</sup>C in a humidified 5.0% CO<sub>2</sub> cell culture chamber, transfection media was removed, and fresh media was added. Cells were harvested after 48 hours of transfection.

#### **4.2.7. Aggresome detection and double labelling**

Aggresomes and protein aggregates in lens capsule tissue and HLE-B3 cells were detected using the Proteostat Aggresome Detection kit (#ENZ-51035, Enzo Life Sciences, Germany) as per the manufacturer's instructions. In brief, the LC tissues or cells were washed twice with 1X PBS and cross-linked with 4.0% paraformaldehyde for 30 minutes. Following cross-linking, the

specimens were washed with 1X PBS and permeabilized at 4<sup>0</sup>C with Triton X-100 for 30 minutes. Subsequently, the samples were washed with 1X PBS and incubated with the dual detection reagent (Proteostat dye and Hoechst 33342 nuclear stain) for 30 minutes. For co-staining with DKK1, or ROCK2 or VIM antibody, after staining with Proteostat, the specimens were blocked with 3.0% BSA for 30 minutes. The samples were incubated with primary antibodies at RT for one hour and with secondary antibody Alexa Fluor 488 for 30 minutes. Subsequently, the samples were mounted, imaging was done using Leica SP8 DLS confocal microscope, and images were analysed using ImageJ software.

#### **4.2.8. Statistical analysis**

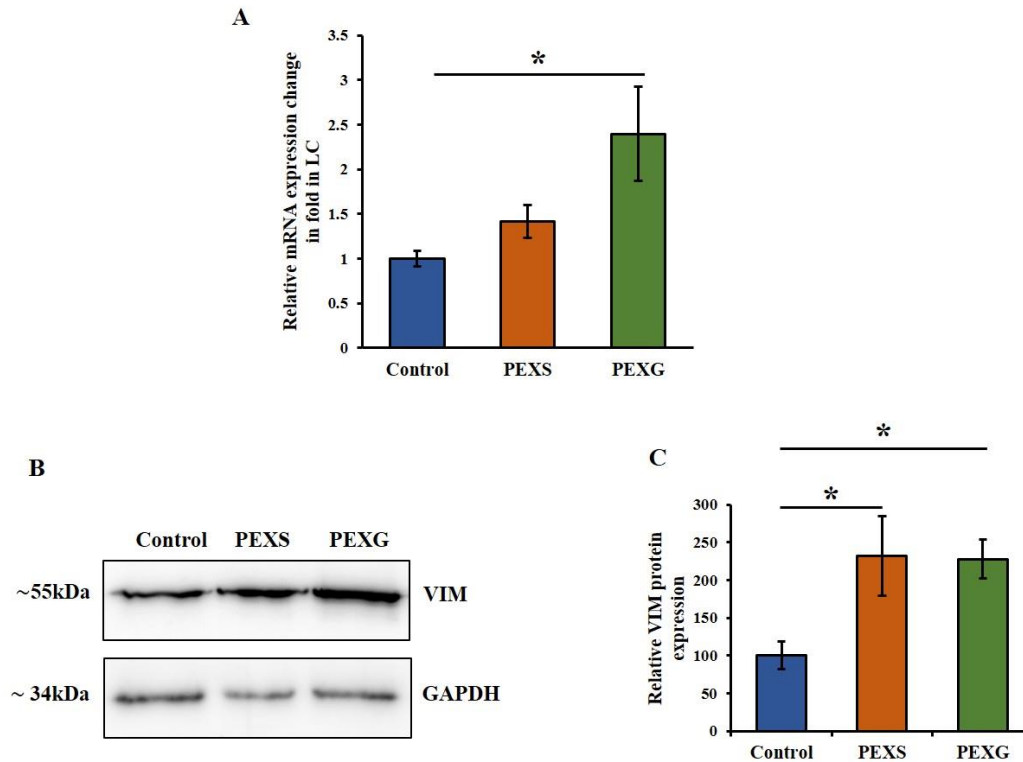
All experiments were carried out independently at least three times and in triplicate each time. Age and sex-matched individuals were chosen for all experiments. A p-value of <0.05 was considered statistically significant for all tests and indicated by asterisks in the figures.

### **4.3. Results**

#### **4.3.1. Vimentin is upregulated in the lens capsule and the aqueous humor of pseudoexfoliation**

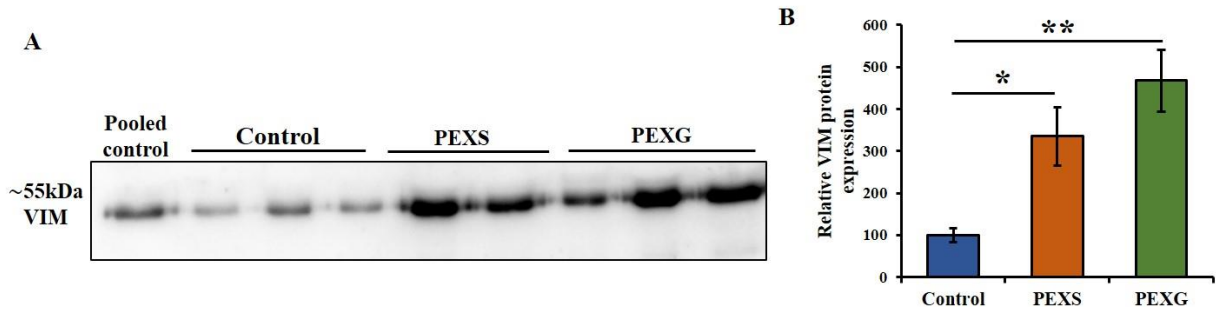
To check the dysregulation of VIM expression and its localization in the lens capsule of patients and controls, qRT-PCR, immunoblotting, and immunostaining assays were performed in a subset of study subjects. A significant increase in *VIM* mRNA was observed in the LC of PEXG individuals (2.4-fold; p=0.03, n=6), whereas, though PEXS individuals showed increased *VIM* expression in LC, it failed to reach significance (1.5-fold; p=0.06, n=8) when compared to the controls (n=14) (**Figure 4.1A**). At the protein level, immunoblotting showed significantly higher

VIM in both PEXS ( $p=0.04$ ,  $n=8$ ) and PEXG ( $p=0.006$ ,  $n=4$ ) LC compared to the controls ( $n=8$ ) (Figures 4.1B and 4.1C).



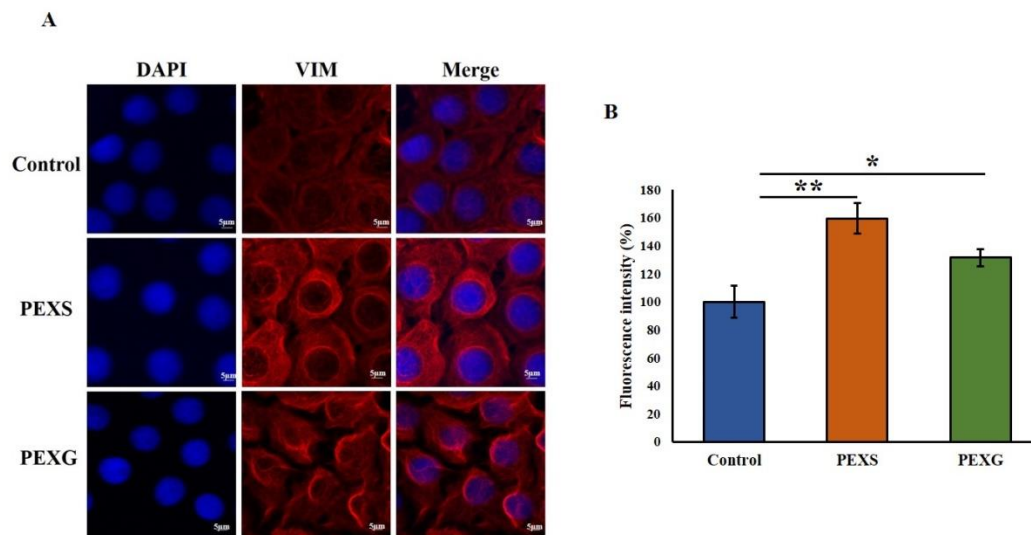
**Figure 4.1. Vimentin is upregulated in the lens capsule of PEX-affected individuals.** **A.** *VIM* mRNA was significantly upregulated in PEXG LC ( $p=0.03$ ,  $n=6$ ) compared to control ( $n=14$ ). Though an increase was seen in *VIM* mRNA expression in PEXS ( $p=0.06$ ,  $n=8$ ) compared to the controls ( $n=14$ ), it failed to reach statistical significance. **B.** Immunoblot of VIM from LC showing increased levels in PEXS and PEXG. **C.** Densitometry analysis showed significantly higher VIM protein levels in LC of PEXS ( $p=0.04$ ,  $n=8$ ) and PEXG ( $p=0.006$ ,  $n=4$ ) compared to the controls ( $n=8$ ). Results are presented as mean  $\pm$  SEM. \* $P<0.05$ .

Also, VIM levels were checked through immunoblotting in the ocular fluid, aqueous humor (AH) (Figure 4.2A). Levels of VIM were significantly higher in AH of PEXS ( $p=0.01$ ,  $n=8$ ) and PEXG ( $p=0.001$ ,  $n=8$ ) compared to the controls ( $n=8$ ) (Figure 4.2B).



**Figure 4.2. Increased vimentin levels in aqueous humor of PEX patients.** **A.** Representative immunoblot of VIM from AH of control, PEXS, and PEXG with pooled control for normalization. **B.** VIM levels in AH were significantly higher in PEXS ( $p=0.01$ ,  $n=8$ ) and PEXG ( $p=0.001$ ,  $n=8$ ) compared to the controls ( $n=8$ ).

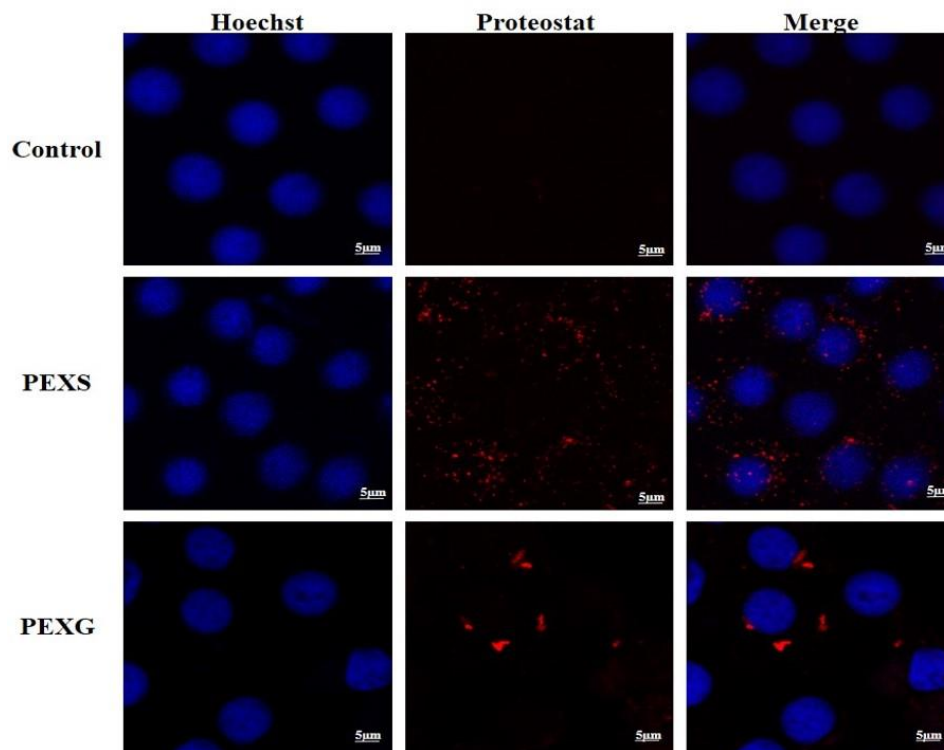
Moreover, analysis of the relative fluorescence intensities of immunostaining of LC showed a significant increase of VIM in PEXS ( $p=0.009$ ,  $n=3$ ) and PEXG ( $p=0.04$ ,  $n=3$ ) compared to control ( $n=6$ ) (**Figures 4.3A and 4.3B**). **Together, these findings hint towards the upregulation of vimentin in LC and AH of pseudoexfoliation patients.**



**Figure 4.3. Increased vimentin expression in lens capsule in PEX patients through immunostaining.** **A.** Confocal image of LC of control, PEXS, and PEXG shows cytoplasmic localization of VIM in the cell and an increased VIM signal in PEXS and PEXG. **B.** Relative mean fluorescence intensities of VIM showed that it was significantly higher in PEXS ( $p=0.009$ ,  $n=3$ ), and PEXG ( $p=0.04$ ,  $n=3$ ) compared to control ( $n=6$ ). Magnification- 63X, Scale- 5µm.

### 4.3.2. Increased formation of protein aggregates in the lens capsule of pseudoexfoliation and DKK1 overexpressed human lens epithelial cells

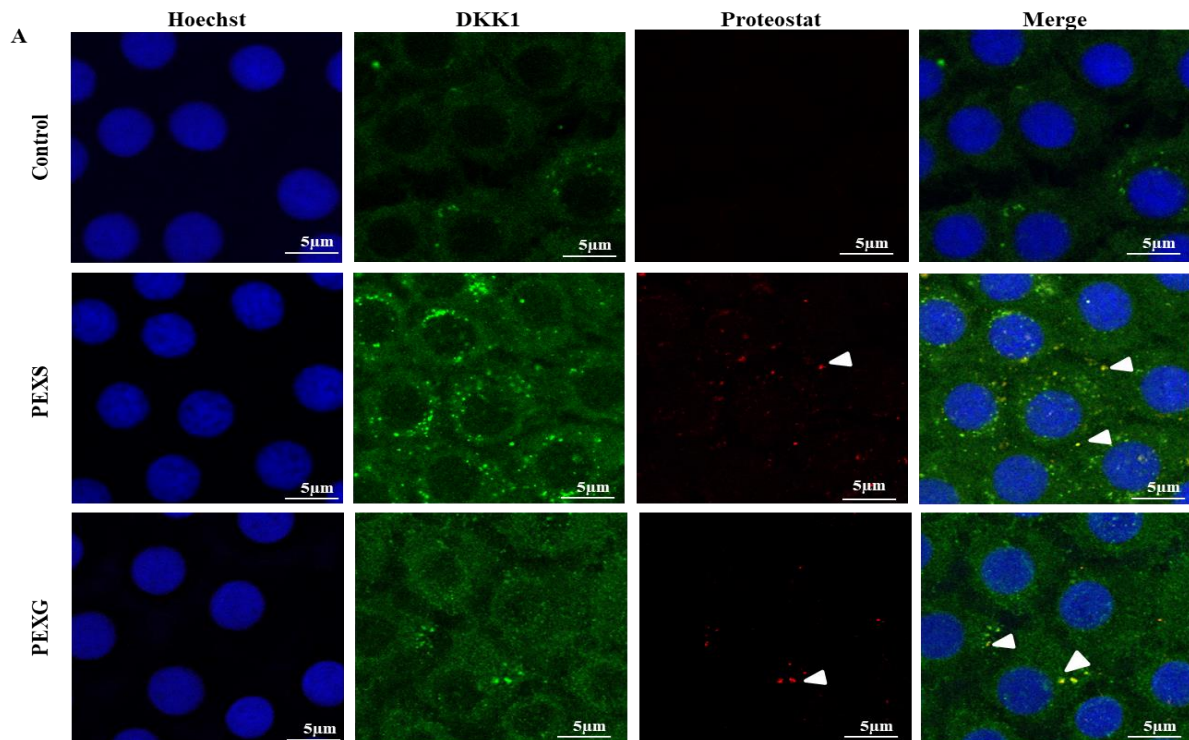
The presence of protein aggregates, a hallmark feature of PEX, was checked in the LC of PEXS, PEXG, and control subjects. Proteostat dye, a rotor fluorescent dye that detects misfolded proteins and protein aggregates in aggresomes and inclusion bodies, was used to detect the protein aggregates. Staining the lens capsules of control, PEXS, and PEXG with Proteostat dye showed an increased Proteostat signal in PEXS and PEXG, prominent around the nucleus, compared to the controls (**Figure 4.4**).



**Figure 4.4. Presence of aggresomes in the lens capsule of PEXS and PEXG.** Confocal images of lens capsule after Proteostat dye staining. Intense Proteostat signal is observed in PEXS individuals (n=3) compared to the controls (n=3) prominent around the nucleus. Also, more aggresomes are observed in PEXG (n=3) LC compared to the controls (n=3). Scale bar- 5µm.

We had previously observed increased expression of DKK1 in LC, conjunctiva, and AH of PEX patients compared to controls (Dr. Bushra Hayat's Ph.D. Thesis). Various reports also suggest

role of DKK1 in A $\beta$  protein aggregation.<sup>214,215</sup> Therefore, we explored the role of DKK1 in the formation of protein aggregates. Staining of LC with DKK1 and Proteostat showed co-localization of DKK1 with the Proteostat around the nucleus (**Figure 4.5A**). To further validate our hypothesis that DKK1 upregulation leads to increased protein aggregate formation, we overexpressed DKK1 in HLE B-3 cells and stained the cells with Proteostat dye. We found increased Proteostat signal in cells transfected with the DKK1 vector compared to cells transfected with an empty vector (**Figure 4.5B**).



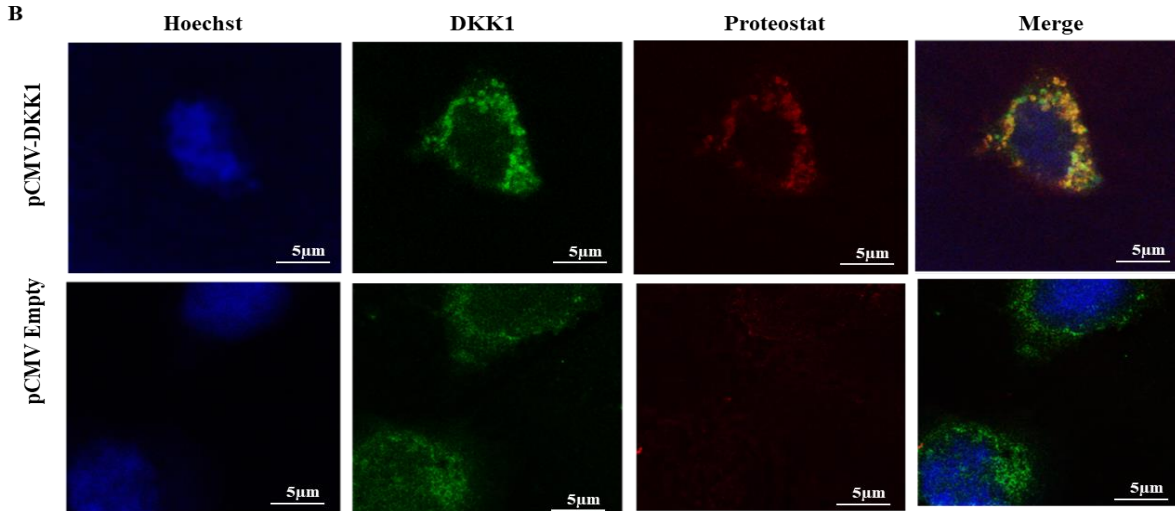


**Figure 4.5. Presence of aggresomes in LC and HLE B-3 cells overexpressed with pCMV-DKK1. A.** Proteostat signal is observed in LC of PEXS and PEXG that co-localized with DKK1 around the nucleus. **B.** Intense Proteostat signal observed in DKK1 overexpressed cells compared to an empty control that co-localized with the Proteostat signal. All the experiments have been conducted a minimum of three times Scale bar- 5 $\mu$ m.

The cells were transfected with GFP as a control gene to confirm that the aggregates formed are due to overexpression of DKK1 and not because of stress arising from protein overexpression. Overexpression of GFP in HLE B-3 cells did not lead to the formation of protein aggregates, as seen with overexpression of DKK1 (**Figure 4.6**). **This implies that an increase in DKK1 levels promotes the formation of misfolded proteins and the accumulation of protein aggregates.**

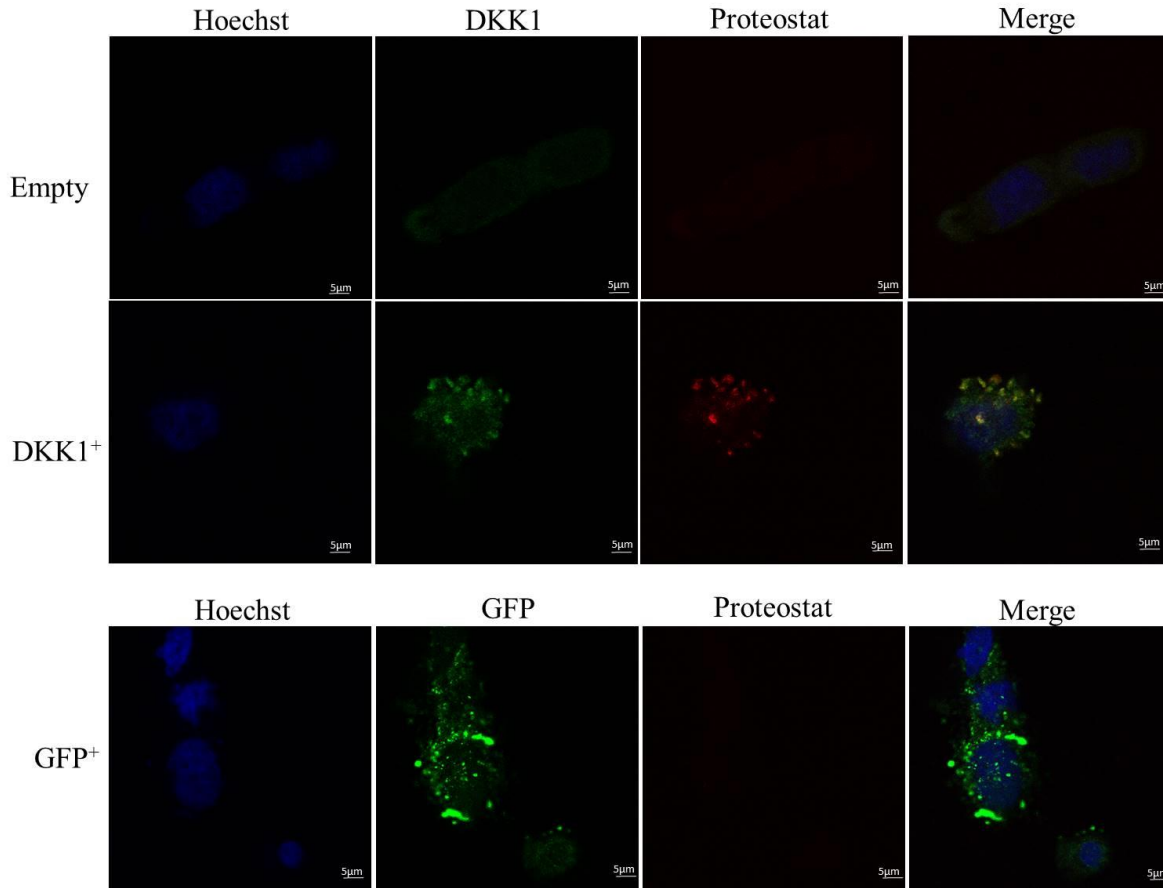


**Figure 4.6. Presence of protein aggregates in HLE B-3 cells overexpressed with pCMV-DKK1.** Intense Proteostat signal is observed prominently around the nucleus in DKK1 overexpressed cells compared to empty control and GFP vector. All the experiments have been conducted a minimum of three times. Scale bar- 5µm.

#### **4.3.3. DKK1 regulates the Wnt pathway gene, ROCK2 and vimentin in HLE B-3 cells**

To validate our hypothesis that DKK1 plays a role in the regulation of ROCK2 and VIM, DKK1 was knocked down (KD) in HLE B-3 cells using DKK1-siRNA, and the protein levels of ROCK2 and VIM were assayed through western blotting. ROCK2 showed a significant downregulation (0.50-fold;  $p=0.02$ ) in DKK1 KD cells compared to cells transfected with control siRNA. Significant downregulation of vimentin was observed in HLE B-3 cells

transfected with DKK1-siRNA (0.45-fold,  $p=0.01$ ) compared to cells treated with control-siRNA (Figures 4.7A and 4.7B).

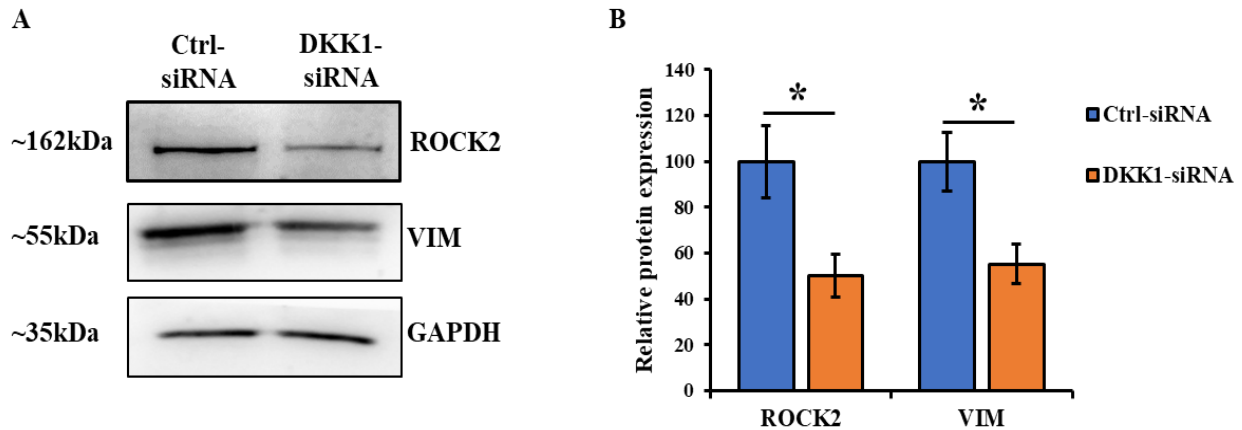


**Figure 4.7. Dysregulation ROCK2 and VIM in cells transfected with DKK1-siRNA.** **A.** Immunoblots show the protein levels of ROCK2 and VIM in protein extracts from HLE B-3 cells transfected with DKK1-siRNA and control-siRNA. **B.** Densitometry quantification of the immunoblots shows significantly decreased levels of both ROCK2 ( $p=0.02$ ) and VIM ( $p=0.01$ ) in DKK1 knockdown cells compared to cells treated with control-siRNA. All the experiments have been conducted a minimum of three times. The data were normalized to GAPDH and are expressed as the mean  $\pm$  SEM,  $*p<0.05$ .

#### 4.3.4. DKK1 regulates vimentin expression and protein aggregation via ROCK2 in HLE B-3 cells

Vimentin has been reported to be a downstream target of ROCK2, and few studies have shown a strong co-localization of both these proteins.<sup>210,216</sup> Therefore, to further check if DKK1 and ROCK2 are regulating vimentin, the changes in vimentin expression were checked in DKK1 overexpressed HLE B-3 cells treated with the ROCK inhibitor, Y-27632. Cells treated with 10  $\mu$ M Y-27632 for 24 hours showed a decreased expression of ROCK2 (Figures 4.8A and 4.8B). Therefore, HLE B-3 cells transfected with an empty vector or DKK1 vector were treated with either the vehicle or 10 $\mu$ M of Y-27632, and the expression of vimentin was checked by western blotting. The cells transfected with empty vector showed a decrease in vimentin expression on treatment with Y-27632, which showed ROCK2 dependent regulation of vimentin ( $p=0.04$ ).

Further, overexpression of DKK1 showed an increase in vimentin ( $p=0.04$ ) which significantly decreased on treatment with the ROCK inhibitor ( $p=0.02$ ) (Figures 4.8C and 4.8D). These findings indicate that vimentin is regulated via ROCK2 in DKK1 overexpressed cells.

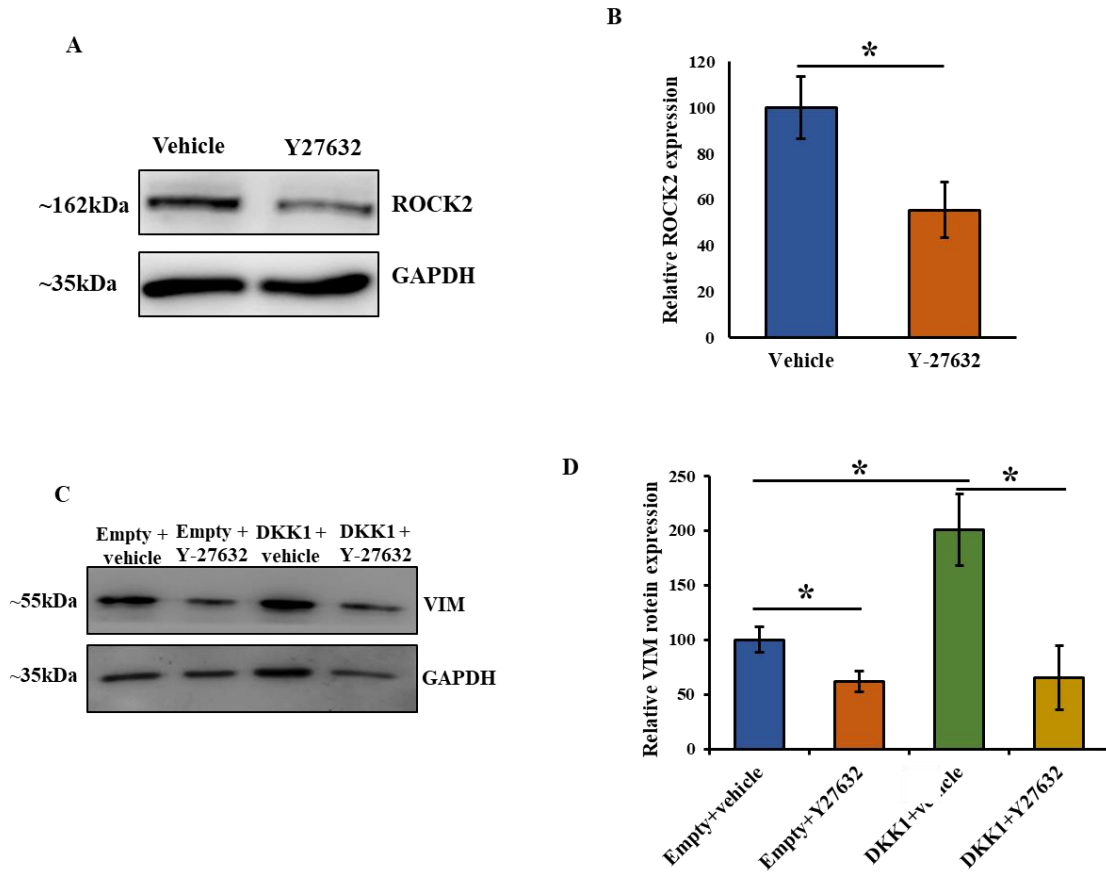


**Figure 4.8. Effect of ROCK inhibitor Y-27632 on ROCK2 and VIM expression in HLE B-3 cells.** **A.** Immunoblot shows the levels of ROCK2 protein in HLE B-3 cells treated with Y-27632. **B.** The cells show a decrease in ROCK2 protein levels on treatment with Y-27632 compared to the water vehicle. **C.** Immunoblot shows VIM level in cells transfected with empty vector and DKK1 overexpression vector and treated with water vehicle or the ROCK inhibitor drug, Y-27632. **D.** DKK1 overexpressed cells show significantly decreased vimentin expression on treatment with Y-27632 compared to DKK1 overexpressed cells treated with a water vehicle. The experiments have been conducted at least three times. The data are normalized to GAPDH and expressed as the mean  $\pm$  SEM, \* $P < 0.05$ .

Further, to check if the inhibition of ROCK2 affects the protein aggregate formation and VIM expression in DKK1 overexpressed cells, we treated the DKK1<sup>+</sup> cells with either 10  $\mu$ M of Y-27632 or the water vehicle and stained with Proteostat and vimentin antibody. We observed that

DKK1<sup>+</sup> cells treated with Y-27632 show a decreased Proteostat signal and vimentin expression compared to DKK1<sup>+</sup> cells treated with just the water vehicle instead of the ROCK inhibitor (Figures 4.9A & B). These findings show that ROCK2 mediates VIM upregulation and formation of protein aggregates in DKK1 overexpressed cells.

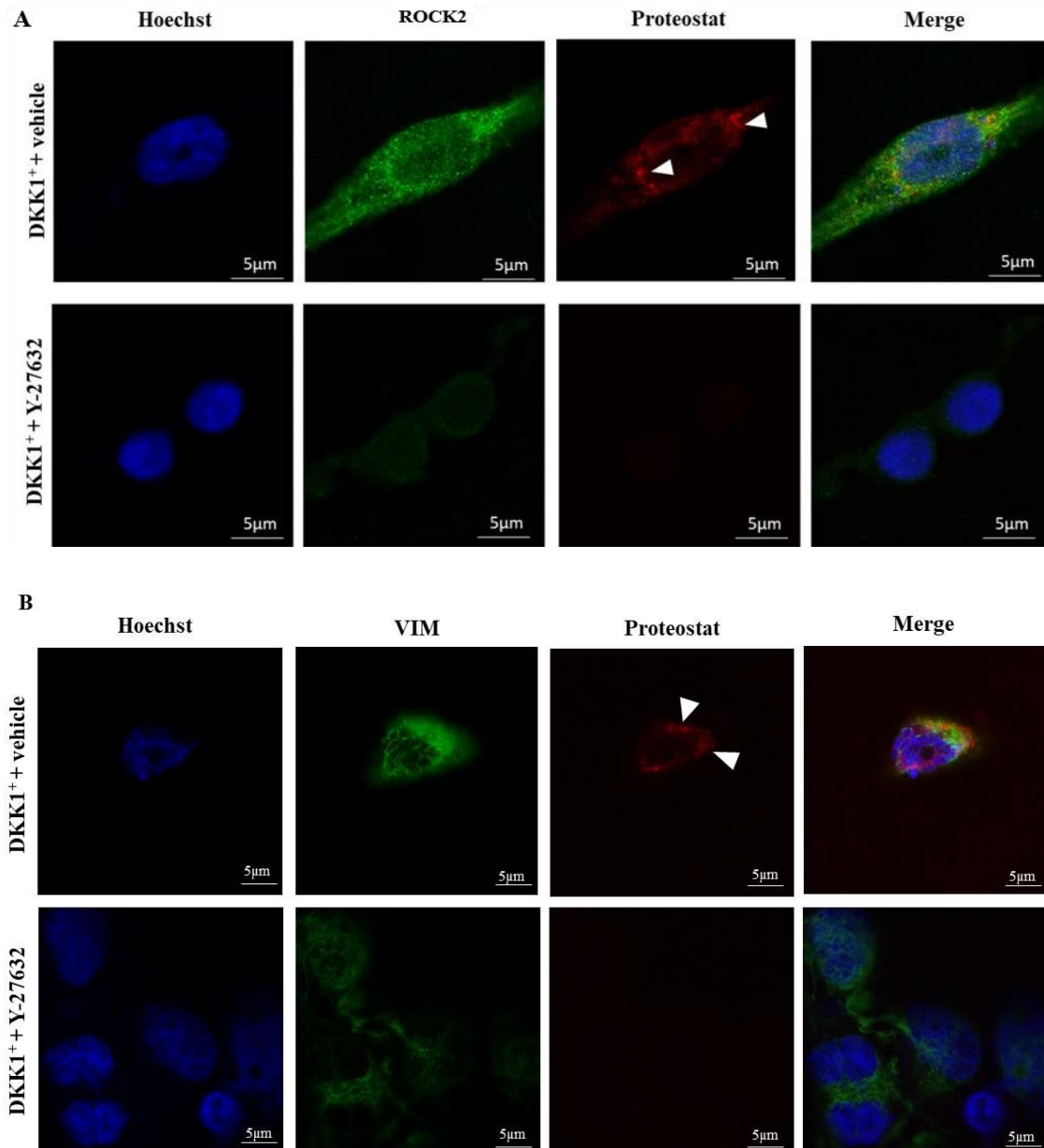


**Figure 4.9. DKK1 regulates protein aggregation via ROCK2 in HLE B-3 cells. A.** DKK1 overexpressed cells were treated with either the water vehicle or the ROCK inhibitor, Y-27632. Immunostaining shows decreased ROCK2 and Proteostat signal (marked with arrowhead) in cells treated with Y-27632 compared to cells treated with just the water vehicle. **B.** Immunostaining shows decreased

VIM and Proteostat signal (marked with arrowhead) in cells treated with Y-27632 compared to cells treated with just the water vehicle. All the experiments have been conducted at least three times. Scale bar- 5 $\mu$ m.

#### 4.4. Discussion

Pseudoexfoliation (PEX) is a disease characterized by aberrant deposition of extracellular fibrillar material. Impaired cytoprotective mechanisms, including protein homeostasis, contribute significantly to PEX pathology. Impediment of the aqueous humor outflow pathway by the accumulated protein aggregates results in increased IOP and subsequent optic nerve head (ONH) damage that are hallmarks of PEXG. Identification of novel risk factors that can help understand the disease's aetiology is needed. Vimentin (VIM) is a multifunctional cytoskeletal intermediate filament that showed a transient increase in glial cells of ONH after the elevation of IOP in Sprague Dawley rats.<sup>217</sup> Besides maintaining the cellular integrity, VIM plays an active role during inflammation, apoptosis, hypoxic insult, and oxidative stress.<sup>203,218,219</sup> As PEX pathology involves increased cell death due to apoptosis, raised inflammatory markers, and oxidative stress; we anticipated active participation of VIM in PEX pathology.<sup>133,220–222</sup>

We observed a significant upregulation of VIM in the lens capsules of PEX eyes, which could be a coping mechanism by the cell to compensate for the impaired proteostasis due to cellular stress, as seen previously in U-937 human promonocytic cells under heat stress and cadmium chloride treatment.<sup>223</sup> Also, VIM upregulation has been documented in ocular diseases such as diabetic cataracts and proliferative vitreoretinopathy.<sup>201,224</sup> Levin and group reported upregulation of VIM during disease progression in the neurons of a mouse model of Alzheimer's disease.<sup>225</sup> During proteotoxic stress, VIM forms a cage around aggresomes containing protein aggregates and misfolded proteins. A recent study showed that VIM at the aggresomes recruits proteasomal

degradation machinery for efficient protein turnover.<sup>198</sup> Further molecular studies will elucidate whether the increase in VIM levels in PEX individuals is a coping mechanism by the stressed cells or is further adding to the toxic load.

Inhibition of the Wnt pathway causes the formation of A $\beta$  aggregates in AD, and activation of the Wnt/PCP pathway increases A $\beta$  synaptotoxicity.<sup>205,226</sup> A recent report by Menet and the group showed that inhibition of DKK1 with the pharmacological drug WAY262611 attenuates the A $\beta$  aggregation seen in AD.<sup>204</sup> In our study, an increase in DKK1 in LC of patients corroborated with an increase in protein aggregates. Aggresomes form due to the accumulation of ubiquitinated misfolded proteins and proteasome dysfunction. Chakraborty *et al.* have observed the formation of oligomer11 aggregates near the nucleus and extensive amyloid fibrils throughout the cell on continued stimulation of human trabecular meshwork cells (hTMs) with TGF $\beta$ 1 and suggested that hTMs can be a plausible cellular model for PEX.<sup>227</sup> We observed that overexpression of DKK1 in HLE B-3 cells resulted in increased protein aggregate formation. These findings show that many risk factors contribute to the formation and accumulation of protein aggregates in PEX and we believe that these intracellular protein aggregates are released freely into the extracellular space and an apparent protein aggregate flux might help in propagation of the disorder as is the case with other protein aggregopathies such as Alzheimer's and Parkinson's diseases.<sup>228</sup>

ROCK2 is a key molecule in the Rho/Rock signalling pathway, which regulates cell contraction, adhesion, migration, proliferation, and apoptosis.<sup>229,230</sup> The role of ROCK2 protein has also been documented in regulating IOP and ciliary muscle contractility, where treatment with ROCK2 inhibitors reduced the IOP in rabbits.<sup>231</sup> Apart from being an essential regulator at the aggresome, vimentin has been reported to be a downstream target of ROCK2. Few studies have

shown a strong co-localization of both these proteins.<sup>210,216</sup> ROCK2 is known to regulate the expression of VIM through  $\beta$ -catenin. Increased expression of ROCK2 stabilizes the expression of  $\beta$ -catenin, which further binds to the promoter of *VIM* and enhances its transcription.<sup>232</sup> On the contrary, DKK1 stimulation upregulates vimentin independent of the Wnt signalling pathway in HUVECs, and activation of the non-canonical Wnt/PCP pathway increased the levels of vimentin without altering  $\beta$ -catenin expression.<sup>233,234</sup> In our study, *in vitro* knockdown assays in HLE B-3 cells, showed that DKK1 knockdown led to decreased expression of ROCK2. Also, in line with previous findings, a significant downregulation of VIM was observed in DKK1 KD HLE B-3 cells. Thus, our studies show that DKK1 regulates the non-canonical Wnt/PCP pathway component ROCK2 and the downstream target, vimentin, in human lens epithelial cells. Inhibition of ROCK2 by the ROCK inhibitor, Y-27632, in DKK1 overexpressed cells further decreased vimentin and protein aggregates. These findings show that DKK1 overexpression increases protein aggregate formation via ROCK2 in HLE B-3 cells.

Further studies need to be done by developing cellular or animal models of PEX to understand how DKK1, ROCK2, and VIM interact in the cellular milieu of PEX and whether the increased expression of these proteins is a mechanism to combat the cellular stress or it is adding to the proteotoxic load of the cell.

\*\*\*\*\*

## *Chapter 5*

# **Regulation of glutathione-S-transferases in PEX**

## 5. Regulation of glutathione-S-transferases in PEX

### 5.1. Introduction

In this chapter, we have reported the dysregulation of glutathione-S-transferases in PEXS and the promoter methylation status of *GSTP1* in PEXS patients versus controls.

PEX has also been associated with oxidative stress, a consequence of an imbalance between oxidants and antioxidants in the body. Oxidative stress plays an important role in the pathology of other ocular diseases such as ARC, ARMD, and diabetic retinopathy; neurodegenerative diseases such as AD, PD, and glaucoma; systemic diseases such as diabetes, rheumatoid arthritis, and various cancers.<sup>118–120</sup> Increased oxidative stress and an impaired anti-oxidant system in PEX eyes have been widely established. Enzymatic as well as non-enzymatic antioxidants such as superoxide dismutase (SOD), glutathione-S-transferases (mGST1 and GSTT1), ascorbic acid and glutathione are significantly decreased in aqueous humor, serum and anterior segment tissues in PEX eyes.<sup>121–124,220</sup> Concomitantly, the oxidative stress markers and oxidants such as malondialdehyde (lipid peroxidation marker), protein carbonyl (protein oxidation marker), nitric oxide, 8-hydroxydeoxyguanosine (8-OHdG) and homocysteine were found to be significantly increased in aqueous humor, serum and ocular tissues of pseudoexfoliation affected individuals.<sup>124–127</sup> The generated free radicals and oxidation products cause changes in signaling pathways, gene transcription, mitochondrial functioning, and chromatin architecture and bring about DNA damage leading to cell death.

Glutathione-S-transferases (GSTs) are multifunctional enzymes that detoxify xenobiotics, such as electrophilic toxins, peroxidized lipids, epoxides, polyaromatic hydrocarbons, and carcinogens.<sup>12</sup> Apart from detoxifying toxins, GSTs bind to and aid in transporting hormones, endogenous metabolites, and drugs.<sup>13</sup> Further, GSTs play a role in signal transduction pathways that control

cell proliferation and cell death. They modulate cellular signaling by sequestering important signaling kinases involved in controlling stress response, apoptosis, and proliferation through protein-protein interactions.<sup>14</sup>

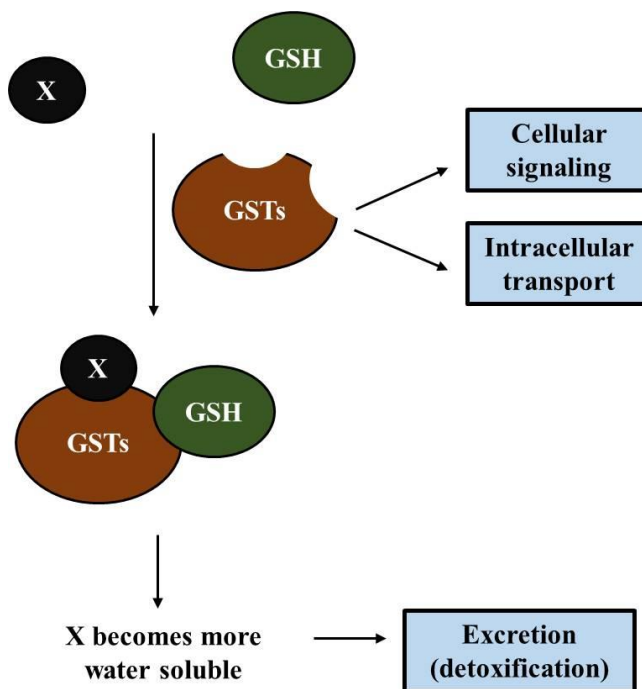


**Figure 5.1. Role of glutathione-S-transferases inside the cell.** A schematic showing the different functions of GSTs in the cell. GSTs are mainly involved in conjugating reduced glutathione to xenobiotics such as lipid peroxides, epoxides, and polyhydrocarbons for their detoxification. GSTs are also involved in a wide array of signal transduction pathways.

The GST proteins have three major families - cytosolic, mitochondrial, and microsomal. The majority of GSTs are cytosolic. However, some are membrane-associated, which constitute the microsomal GSTs. In mammals, there are seven isoenzymes of cytosolic GSTs designated by the Greek letters:  $\alpha$  (alpha),  $\mu$  (mu),  $\pi$  (pi),  $\theta$  (theta),  $\sigma$  (sigma),  $\omega$  (omega), and  $\zeta$  (zeta), and abbreviated in Roman letters as A, M, P, T, S, O and Z, respectively.

Risk loci in *GSTT1* and *GSTM1* have been identified in Pakistani female patients with PEXG, however, the results could not be replicated in other populations.<sup>129–131</sup> The lack of causal variants in glutathione-S-transferase genes implies an epigenetic trigger responsible for their aberrant

downregulation in PEXS and PEXG. Li *et al.* have reported that hypermethylation in the GSTM3 promoter and altered histone modifications might be involved in ARC development.<sup>235</sup> Similarly, they showed that aberrant promoter hypermethylation of GSTP1 is associated with its downregulation in lens epithelial tissues of ARC patients.<sup>236</sup> Epigenetic control on gene regulation of differentially expressed oxidative stress-related genes in PEX needs to be explored to pave the way for targeted therapeutics. Oxidative stress has a significant impact on the DNA methylation process as such. ROS affects the global metabolism and production of epigenetic metabolites, such as S-adenosyl methionine required by DNMTs as a methyl donor group for catalyzing DNA methylation. Also, oxidative stress modulates TGF $\beta$  signaling pathway, which further regulates the production of DNMTs.<sup>237</sup> Further, 8-OHdG prevents the binding of DNMT1 or MeCp2 (methyl CpG binding protein 2) to neighbouring cytosines or hemi-methylated cytosines, thereby affecting the epigenetic regulation of gene expression.<sup>238,239</sup> Under this objective, we checked if any GST isoenzymes- GSTM1, GSTM3, GSTT1, GSTP1, and mGST1 are dysregulated in PEXS, and whether the dysregulation, if any, could be under epigenetic control.

## **5.2. Materials and Methods**

### **5.2.1. Study subjects' selection, recruitment, and sample collection**

Study subject selection and recruitment were done as mentioned in Chapter 2, page no. 41. Peripheral blood and lens capsules were collected from the participants during cataract surgery and stored at -80<sup>0</sup>C.

### 5.2.2. Quantitative Real time-PCR (qRT- PCR) for mRNA expression studies

The total RNA was extracted from lens capsules using a commercial kit (RNeasy Mini Kit, QIAGEN GmbH, Hilden, Germany) according to the manufacturer's protocol and is described in Chapter 3, page no. 78. PrimerQuest Tool (IDT) was used to design gene-specific primers (**Table 5.1**) overlapping exon-exon junctions for the mRNA transcript of *GSTM1*, *GSTM3*, *mGST1*, *GSTP1*, and *GSTT1* respectively. qRT-PCR was performed using 7500 Real-time PCR Systems (Applied Biosystems, USA). The amplification specificity of the PCR product was checked via melt curve analysis. For normalization of gene expression levels, mRNA ratios relative to the *GAPDH* were calculated. The comparative threshold cycle ( $\Delta\Delta C_t$ ) method was used to derive the expression fold change for the target gene and represented as fold difference compared to the controls.

**Table 5.1.** Oligos used in the study

S. No.	ID	Sequence (5'→3')
1	GSTM1 qRT	F: TCTGAGCCCTGCTCGGTTT R: ATAATCAGGAGCGTCCCCCAT
2	GSTM3 qRT	F: TTCCTAATCTGCCCTACCTCCT R: TTCTTCTTCAGTCTCACCACACA
3	GSTP1 qRT	F: ACACCAACTATGAGGCGGG R: ACAGCAGGGTCTCAAAGGC
4	GSTT1 qRT	F: CAGGAATGGCTTGCCTAAGA R: GCATCATTCTCATTGTGGCTTT
5	mGST1 qRT	F: GCAAAGGAGAAAATGCCAAGAAG R: GGGACCACTCAAGGAATACAGG
6	GAPDH qRT	F: GGTGTGAACCATGAGAAGTATGA R: GAGTCCTTCCACGATACCAAAG
7	BSP Region I	F: TTTAGAATTTTAAATAAAAGTTGGA R: TATAACCCAAACTAAAATACAATAAC
8	BSP Region II	F: GGTTTTTATTTTTTTTTTTGTTTTG R: CCCATACTAAAACCTCTAAACCCCA

### **5.2.3. Protein isolation and western blotting**

Western blot analysis was performed with protein extracts of lens capsules, and a detailed protocol is described in Chapter 3 page nos. 79-80. Proteins from tissues were extracted using the RIPA buffer. The proteins were separated by 12% SDS-PAGE and transferred to 0.22 µm PVDF membranes (IPVH00010, Millipore-Merck, Germany). GSTP1 antibody (#ab153949, Abcam, India) was used as the primary antibody at 1:250 dilutions. The GAPDH antibody (ABM22C5, Abgenex, India; 1:250) verified equal loading. HRP conjugated Goat anti-rabbit IgG (621140380011730, GeNei, India) or Goat anti-mouse IgG-HRP (621140680011730, GeNei, India) each at 1:5000 dilutions was used as the secondary antibody. Detection was done in Fusion Solo S Chemi-Doc (Vilber Lourmat) using the chemiluminescence kit (Super Signal Femto Maximum Sensitivity Substrate, PI34094, Thermo Fisher Scientific, USA). Evolution Capt software (Vilber Lourmat fusion solo S) was used for image acquisition, and signal intensity ratios relative to GAPDH were calculated for the normalization of protein expression level.

### **5.2.4. Immunostaining**

Immunostaining was carried out as mentioned in Chapter 4, page no. 113. Lens capsule tissues were stained with GSTP1 antibody (#ab153949, Abcam, India) at 1:500 dilution. Alexa-Fluor 594 goat anti-rabbit IgG (A21210, Invitrogen, USA) was used as the secondary antibody at 1:500 dilution. Nuclear staining was done with DAPI (4,6-diamino-2-phenylindole; 32670-5 MG-F, Sigma-Aldrich, Germany) lens capsule was mounted on the slide along with ProLong Gold antifade reagent (P36934, Invitrogen, USA). Imaging was done in Leica confocal microscopy, and the images were analyzed using ImageJ software (NIH, USA).

### **5.2.5. DNA extraction and bisulfite sequencing**

DNA was extracted from blood using the phenol-chloroform extraction technique, as mentioned in Chapter 3, page no. 42. DNA from the lens capsule was extracted using the Qiagen kit as mentioned on Chapter 3, page no. 73. The extracted DNA was bisulfite converted as mentioned in Chapter 3, page nos. 75. The converted DNA was used as template for bisulfite-specific PCR. The oligos used are mentioned in Table 5.1.

### **5.2.6. Statistical analysis**

All experiments were carried out independently at least three times and in triplicate each time. Age-sex matched samples were taken for the experiments. All data were presented as mean  $\pm$  standard error of mean (SEM). All data obtained from the quantitative measurements were analyzed using Student's *t*-test. For all tests, a p-value of  $<0.05$  was considered statistically significant and indicated by asterisks in the figures.

## **5.3. Results**

### **5.3.1. Differential expression of *GST* genes in PEXS compared to controls**

To identify if the regulation of any specific GSTs is affected in PEX individuals, the mRNA expression of *GSTM1*, *GSTM3*, *GSTP1*, *GSTT1*, and *mGST1* was checked in the lens capsule of PEXS individuals in comparison to controls. *GSTM1* and *mGST1* did not show any significant expression in the capsule of either control (n=6) or PEXS (n=6) individuals, the Ct value for these genes in majority of samples was  $\geq 35$  or undetermined which did not allow for proper analysis and hence, not included for further studies. *GSTM3* showed no significant differential expression in PEXS (p=0.93, n=8) compared to the control (n=11). Likewise, no significant change in expression

was observed for *GSTT1* in PEXS ( $p=0.24$ ,  $n=8$ ) compared to controls ( $n=11$ ). However, *GSTP1* showed a significant decrease in PEXS ( $p=0.008$ ,  $n=8$ ) LC compared to the controls ( $n=11$ ).

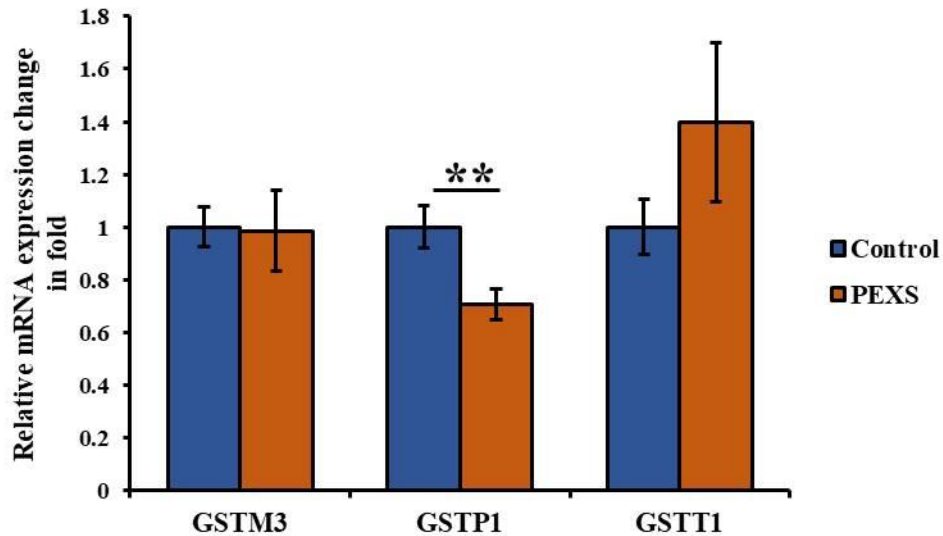


**Figure 5.2. *GSTP1* mRNA is downregulated in the lens capsule of PEXS-affected individuals.** There was no significant difference in the expression of *GSTM3* mRNA in PEXS ( $p=0.93$ ,  $n=8$ ) compared to the controls ( $n=11$ ). *GSTP1* mRNA was significantly downregulated in PEXS LC ( $p=0.008$ ,  $n=8$ ) compared to the controls ( $n=11$ ). No significant differential expression of *GSTT1* was observed in PEXS ( $p=0.27$ ,  $n=8$ ) compared to the controls ( $n=11$ ). Data were normalized to *GAPDH* and presented as mean  $\pm$  SEM. \*\* $p<0.01$ .

### 5.3.2. *GSTP1* is downregulation in PEXS patients

As *GSTP1* mRNA was found to be downregulated in the LC of PEXS compared to controls, we checked the protein expression of *GSTP1* in the LC of control and PEXS by western blotting. We observed that *GSTP1* protein expression in PEXS is decreased compared to controls (**Figure 5.3A**). Further, immunostaining of the LC showed the cytoplasmic distribution of *GSTP1* in PEXS and control (**Figure 5.3B**). Quantification of the fluorescence intensity showed significantly decreased expression of *GSTP1* ( $p=0.005$ ) in the LC of PEXS compared to the controls (**Figure 5.3C**). Together, these findings show that the pi isoenzyme of GSTs is downregulated in the lens capsule of PEXS patients compared to the controls.

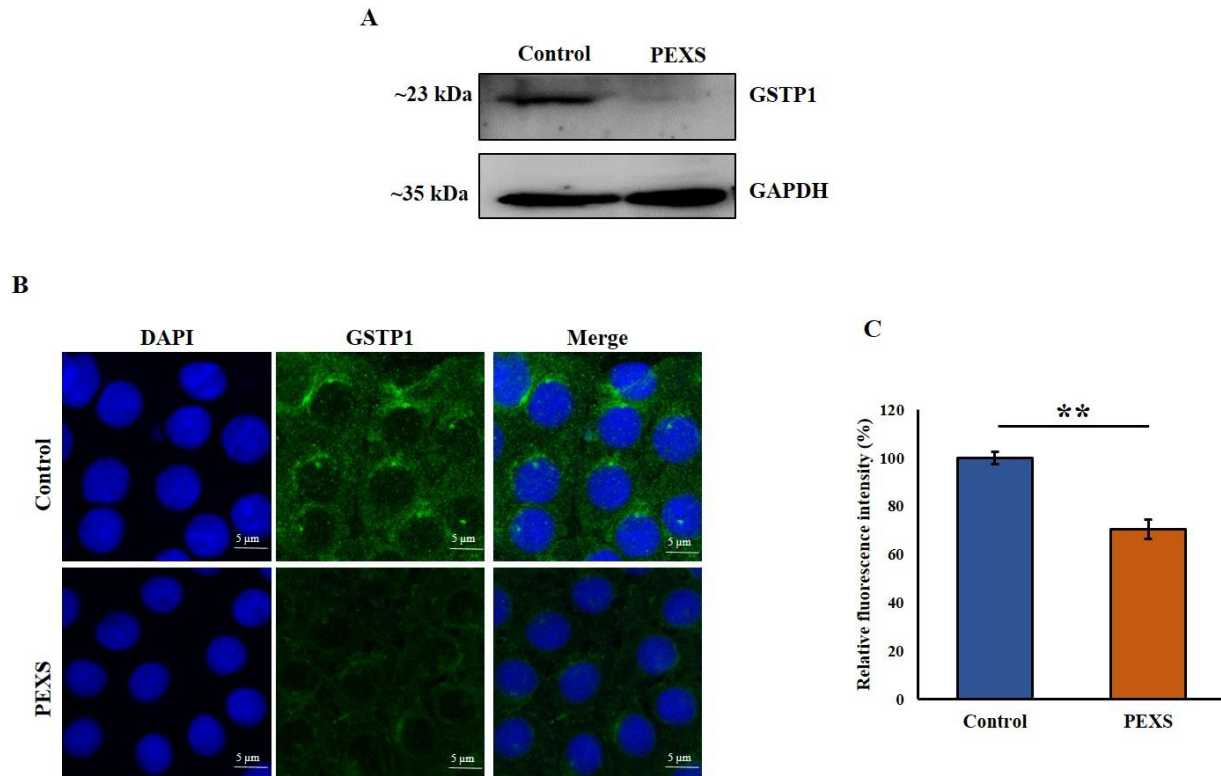
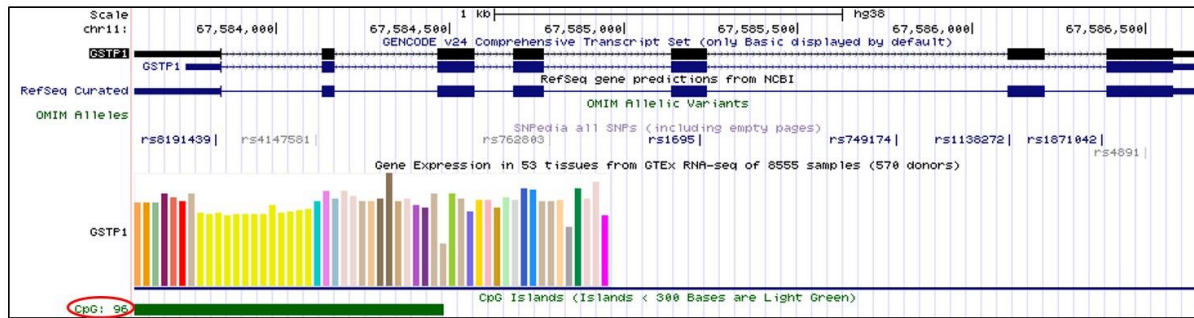


**Figure 5.3. GSTP1 is downregulated in the lens capsule of PEXS-affected individuals. A.** Representative immunoblot shows a decreased expression of GSTP1 protein in LC of PEXS (n=3) compared to the controls (n=3). **B.** Immunostaining of the PEXS and control LC shows the cytoplasmic distribution of GSTP1. **C.** Quantification of the fluorescence intensity shows significantly decreased expression of GSTP1 in LC of PEXS (n=3) compared to controls (n=3). Results are presented as mean  $\pm$  SEM. \*\*p<0.01.

### 5.3.3. *In silico* identification of CpG islands in *GSTP1*

To understand if the decrease in *GSTP1* could be due to DNA hypermethylation in or near its promoter, we studied the methylation pattern of the *GSTP1* promoter region. The encyclopedia of DNA elements (ENCODE) data on the UCSC (University of California, Sanata Cruz) genome browser showed that *GSTP1* has 96 CpG sites. Inputting transcription start site (TSS)  $\pm$  1kb region of *GSTP1* on MethPrimer identified 2 CpG islands near the TSS (**Figures 4.2A and 4.2B**). The first island, referred to as region I, consists of 16 CpGs spanning -600 to -313 bp, and the second CpG island, referred to as region II, contains 52 CpGs spanning from -168 to +305 bp of *GSTP1*.

A



B

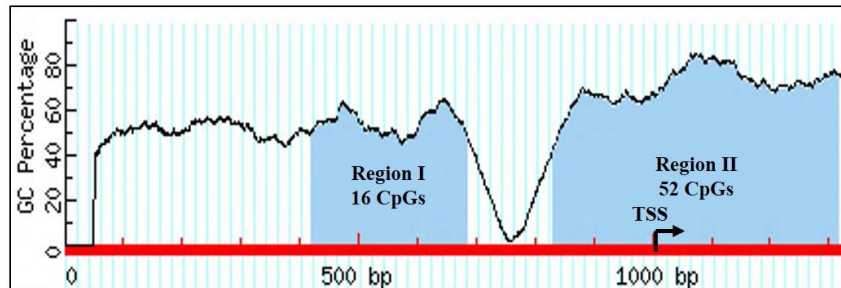
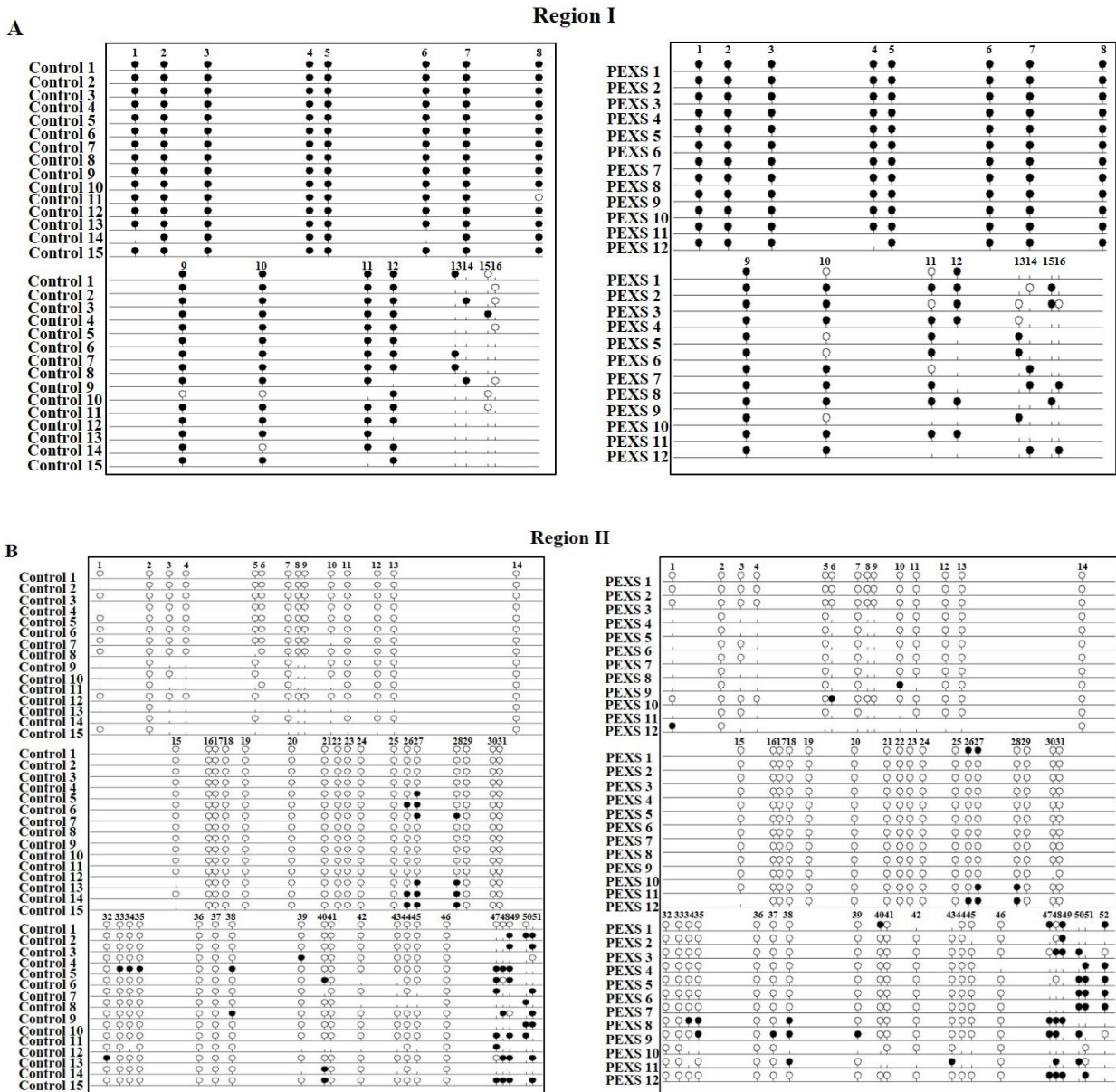


**Figure 5.4. In-silico identification of CpG islands in the promoter of *GSTP1*.** A. ENCODE data on the UCSC genome browser showed the presence of 96 CpGs in the *GSTP1* gene. B. Methprimer software identified 2 CpG islands- the region I comprising 16 CpGs and region II comprising 52 CpGs- near the TSS in *GSTP1* gene.

### 5.3.4. DNA methylation status of *GSTP1* in PEXS individuals

We studied the DNA methylation status of the two regions in the promoter of *GSTP1* (as mentioned in 5.3.3.) through bisulfite sequencing using genomic DNA extracted from the blood. The region I exhibited higher methylation of CpGs in the study subjects compared to region II (**Figures 5.5A & 5.5B**). However, no significant difference was observed in the methylation status in either region I ( $p=0.75$ ) or region II ( $p=0.79$ ) between the PEXS and the controls in blood DNA (**Figures 5.5C**). We further compared the methylation status at each CpG loci between the controls and PEXS. We did not observe any significant difference in methylation status at each CpG site between the groups in neither region I nor region II. **These findings**

imply that the promoter of the *GSTP1* gene in blood cells is not differentially methylated in PEXS compared to controls.



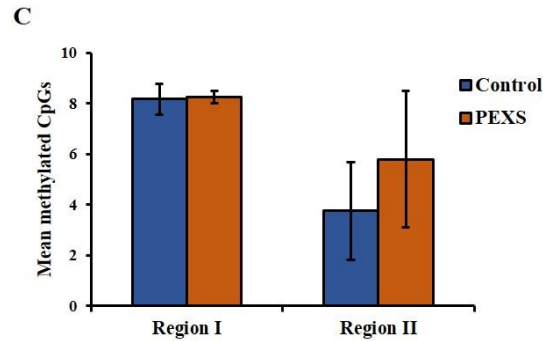


**Figure 5.5. Promoter methylation pattern of GSTP1 in blood cells of PEXS versus controls.** **A.** Representative lollipop plot of methylated and unmethylated CpGs in the region I of *GSTP1* of controls and PEXS. **B.** Representative lollipop plot of methylated and unmethylated CpGs in region II of *GSTP1* of the controls and the PEXS. **C.** Bar graph representation of methylation pattern in regions I and II of the control and PEXS. No difference was observed in the methylation pattern of genomic DNA extracted from the blood samples in the PEXS (n=12) compared to the controls (n=15) in either region I (p=0.75) or region II (p=0.79). Closed circle in the lollipop plot represents a methylated CpG and an open circle represents an unmethylated CpG. Data are represented as mean  $\pm$  SEM.

Further, to check if there could be any tissue-specific DNA methylation marks in the *GSTP1* promoter region, the methylation status of CpGs in *GSTP1* from LC DNA was assessed. Similar to the results of DNA from blood, although region I exhibited higher methylation compared to region II, no significant differential methylation was observed in either region I (p=0.90) or region II (p=0.55) of PEXS LC compared to controls (**Figures 5.5A-5.5C**). Further analysis of the methylation pattern at each CpG site did not show a significant change between controls and PEXS at either of the regions with the current sample size. However, we observed a trend of hypermethylation at CpG23, CpG25, CpG33 and CpG40 in region II of *GSTP1* gene in PEXS compared to controls, but it did not reach statistical significance (p=0.17). As the sample size in the groups is relatively less, including more LC samples from the study subjects for the analysis is needed to better understand if individual CpGs in *GSTP1* might have a functional role in the disease pathology.

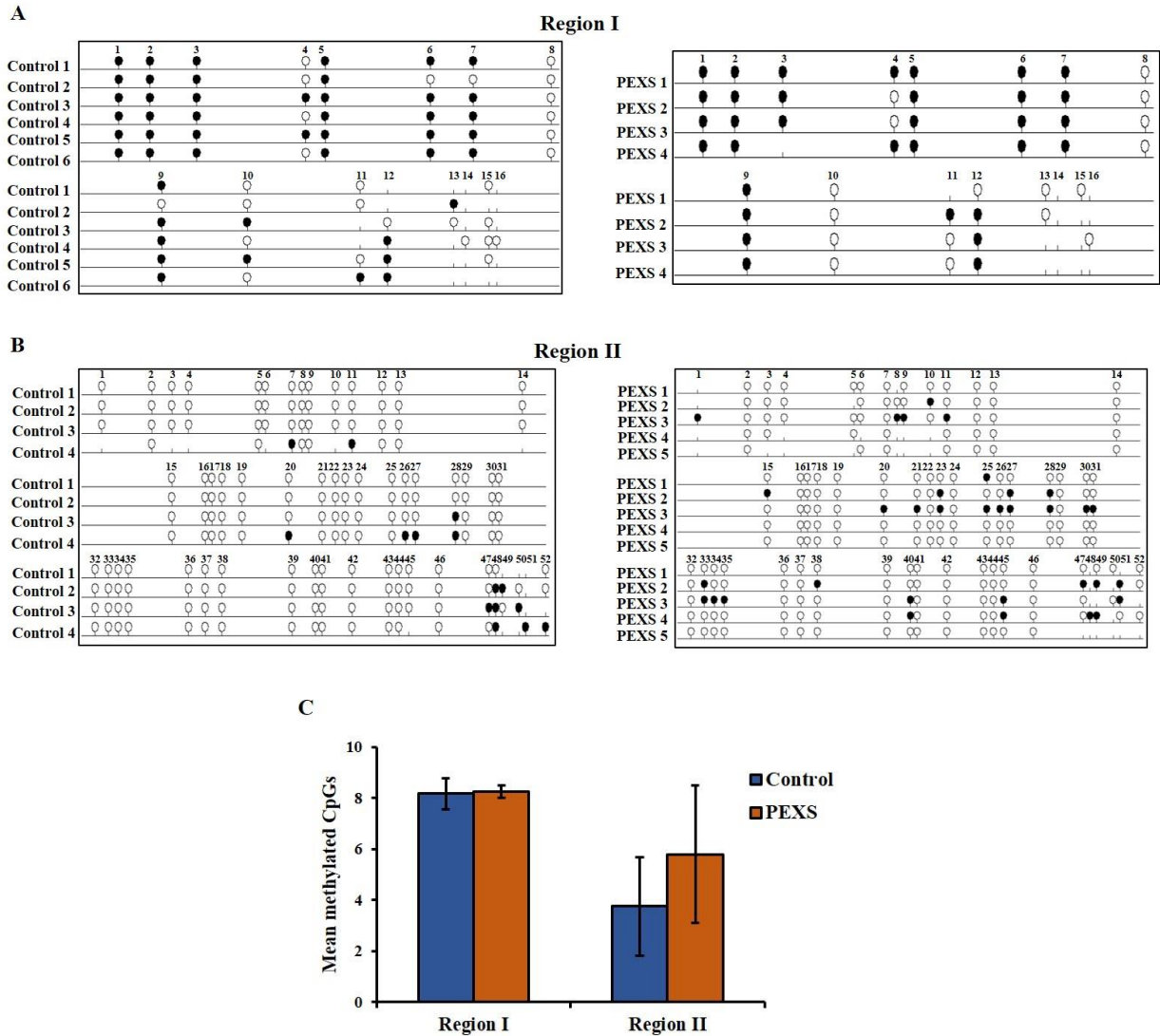


**Figure 5.6. Promoter methylation pattern of GSTP1 in the lens capsule of PEXS versus controls. A.** Representative lollipop plot of methylated and unmethylated CpGs in the region I of *GSTP1* of controls (n=6) and PEXS (n=4). **B.** Representative lollipop plot of methylated and unmethylated CpGs in region II of *GSTP1* of controls (n=4) and PEXS (n=5). **C.** Bar graph representation of methylation pattern in regions I and II of control and PEXS. No difference was observed in the methylation pattern in LC of PEXS compared to controls in either region I (p=0.90) or region II (p=0.55). Closed circle in the lollipop plot represents a methylated CpG and an open circle represents an unmethylated CpG. Data are represented as mean ± SEM.

## 5.4. Discussion

Oxidative stress and dysregulation of antioxidant defense genes in PEX have been widely reported.

We checked the mRNA expression of the cytosolic GSTs- *GSTM1*, *GSTM3*, *GSTP1*, *GSTT1*, and

the membrane-bound *mGSTI*. We did not observe a quantifiable mRNA expression of *GSTM1* and *mGSTI* in the LC of the study subjects. However, this is contrary to the findings by Zenkel *et al.*, which showed significant downregulation of *mGSTI* in the lens epithelium in PEX patients compared to controls.<sup>122</sup> Both the studies were carried out with a limited sample size. Population-specific effect if any cannot be ruled out and should be further explored in a larger sample size. In our study, *GSTM3* and *GSTT1* showed no significant differential expression in PEXS compared to the controls. Similar to our findings, Zenkel *et al.* had previously reported that *GSTT1* is equally expressed in the lens epithelium of controls and PEX patients. However, they observed decreased expression of *GSTT1* in the iris and ciliary processes of PEX patients compared to controls.<sup>122,123</sup> We observed a significant downregulation of *GSTP1* in LC of PEXS patients compared to controls. Recently, a decreased expression of *GSTP1* in the AH of POAG was reported.<sup>240</sup> Also, the downregulation of *GSTP1* in the lens epithelium and cortex of ARC patients and the retina of ARMD patients shows the importance of this enzyme in the pathogenesis of ocular diseases.<sup>241–243</sup> *GSTP1* is widely distributed in the epithelial tissues and plays critical roles in maintaining cell integrity and protecting DNA from genotoxic and cell-damaging molecules. It inactivates various electrophilic carcinogens or stress-induced toxic intermediates by catalyzing their conjugation with reduced glutathione and making them easy for secretion.<sup>244</sup> Through redox regulation by S-glutathionylation of c-Jun terminal kinase, *GSTP1* regulates the apoptosis signaling pathway.<sup>245,246</sup> In response to oxidative stress, increased levels of *GSTP1* are observed in many tumors, such as esophageal, colorectal, renal, lung, and breast cancer.<sup>247</sup> On the other hand, several studies found lower *GSTP1* expression in prostate, endometrial, hepatocellular, and ovarian cancer.<sup>247–249</sup> The decreased levels of *GSTP1* hint at the compromised antioxidant defense system in PEXS patients contributing to increased oxidative stress.

On finding a downregulation of GSTP1 in PEXS patients, we checked if the regulation of the gene expression was under epigenetic control. DNA methylation is the most widely studied epigenetic regulation. Promoter hypermethylation of *GSTP1* resulting in decreased gene expression is frequently observed in different tumor types, such as breast, prostate, and endometrial cancers and hepatocellular carcinoma.<sup>250–253</sup> Zhang *et al.* reported that the piwi-interacting RNA piR-31470 epigenetically suppresses the expression of GSTP1 in prostate cancer by recruiting the DNA methyl transferases 1 and 3a and the methyl-CpG binding domain protein 2 to maintain the GSTP1 promoter in a hypermethylated state.<sup>254</sup> However, we did not observe any significant differential methylation of the studied CpG islands in *GSTP1* promoter in PEXS patients compared to controls in neither blood nor the lens capsule tissue. However, extending the study in the LC of a larger sample set is needed to understand if the differential methylation at individual CpGs might contribute to *GSTP1* downregulation in PEXS.

Mechanisms other than DNA methylation, such as histone modifications and miRNA-dependent gene silencing may also affect the *GSTP1* transcription. Transcription factors such as SP1, AP-1, NF- $\kappa$ B, and GATA1 were reported to play an important role in regulating GSTP1 expression.<sup>255</sup> Similarly, Lo *et al.* showed the ability of wild-type p53 to transcriptionally activate the *GSTP1* gene, wherein low GSTP1 protein level was associated with mutant p53.<sup>256</sup> Other than regulation by TFs, histone modifications were discovered to play a role in regulating *GSTP1* expression.<sup>257</sup> Furthermore, interplay between histone modifications and DNA methylation was observed in prostate cancer. Okino *et al.* noted that treating the prostate cancer cell line LNCaP with the DNMT inhibitor, 5-aza-dC led to the loss of activating histone modifications on *GSTP1*, and the DNA becomes methylated becoming inaccessible to the transcription factors resulting in its silencing.<sup>258</sup> Similarly, Uchida *et al.* demonstrated that GSTP1 expression might be repressed

epigenetically by several miRNAs, notably the miR-133a.<sup>259</sup> Moreover, it has been noted that there is an individual variation of GST-Pi expression related to dietary and lifestyle factors.<sup>260</sup>

Thus, although we did not find that DNA methylation of *GSTPI* in PEXS patients could regulate its expression, there are other layers of epigenetic control, such as histone remodeling and microRNA-dependent gene silencing, that need to be probed further to understand the actual cause of *GSTPI* dysregulation in PEXS patients.

\*\*\*\*\*

## *Chapter 6*

# **Potential biomarkers and novel genetic variants for PEX**

## 6. Potential biomarkers and novel genetic variants for PEX

### 6.1. Introduction

PEX is managed to an extent through medical treatments and/ or surgical interventions. However, many patients are resistant to medical treatments and zonular weakness and poor pupillary dilation arising from PEXS lead to numerous intra-operative and post-operative complications such as lens dislocation, vitreous loss, corneal decompensation, posterior capsular opacification and irreversible glaucomatous damage.<sup>261</sup>

Although numerous genetic risk factors have been associated with PEX, the exact pathogenesis of the disease remains elusive. Only 50% of PEXS individuals develop the glaucomatous condition of PEXG.<sup>15</sup> This implies the involvement of different factors in the etiology of different stages of the disease. Therefore, it is essential to understand the underlying pathophysiology of PEX and identify robust biomarkers for its detection and diagnosis at various stages of disease pathogenesis that can complement the available clinical diagnosis. In this study, we assessed the levels of FBLN5, VIM, and CLU in the plasma of the study subjects to identify if any of these proteins could be a putative biomarker for PEX for early detection of the disease without any surgical intervention. We further initiated the screening of the entire gene sequences of fibulin-5 (FBLN5), clusterin (CLU) and vimentin (VIM), instead of hypothesis-driven targeted genotyping of selected single nucleotide polymorphisms, for identification of novel variants that could be associated with PEX as risk factors in an unbiased way.

Increasing evidence suggests that PEX pathophysiology involves impaired proteostasis, dysregulated chaperone system, and an imbalance in extracellular matrix (ECM) maintenance.<sup>75,76,101,123,133</sup> FBLN5 is an ECM scaffolding protein that plays important roles in elastogenesis and cell-matrix adhesion. Dysregulation in FBLN5 has been associated with various

elastinopathies such as cutis laxa, pelvic organ prolapse, Charcot-Marie Tooth disease, and age-related macular degeneration.<sup>145,146,262,263</sup> We have previously reported a significantly decreased expression of *FBLN5* in PEXS individuals and association of genetic variants in *FBLN5* as risk factors with PEX.<sup>134</sup> Decreased *FBLN5* could be responsible for destabilized ECM.

CLU, or apolipoprotein J, is a multifunctional glycoprotein that acts as an extracellular molecular chaperone. Any dysregulation in clusterin expression leads to impaired proteostasis. Besides aiding in proper folding of proteins, and stabilizing cell-cell and cell-matrix interactions, CLU also stabilizes ECM proteins by chaperoning elastin in the ECM.<sup>264</sup> CLU is induced during stressful conditions such as, oxidative stress. It is a ubiquitously expressed protein in almost all tissues and is constitutively found in most biological fluids. CLU is expressed in the lens, cornea, ciliary body and is also found in the aqueous humor (AH) and vitreous humor. Elevated levels of CLU have been reported in the degenerative disorders, Alzheimer's disease, and retinitis pigmentosa.<sup>165,265,266</sup> We and others have reported increased levels of CLU in the aqueous humor of PEXG patients.<sup>75,173,267</sup>

VIM is an intermediate filament and a proteotoxic stress marker that can increase in response to various stresses, injuries and pathologic processes. Being an epithelial to mesenchymal transition marker, elevated levels of vimentin have been observed in multiple cancers such as colorectal, breast, ovarian and pancreatic cancers. Vimentin is very important for lens development in the eye. Increased levels of vimentin in the vitreous humor have been observed in proliferative vitreoretinopathy.<sup>201</sup>

As we observed dysregulated expression of fibulin-5, clusterin, and vimentin in the eyes of PEX patients compared to controls, we aimed to assess if any of these proteins can be used as a biomarker for distinguishing PEX from controls.

We and other researchers have reported genetic and/or functional association of polymorphisms in *FBLN5* and *CLU* genes with PEX but all these variants are intronic.<sup>73–75,134</sup> So far, there have been no reports showing association of genetic variants in *VIM* gene associated with PEX. As fibulin-5, clusterin and vimentin were found to be dysregulated in PEX, though some intronic SNPs are regulatory, identification of functional exonic variants would be ideal as these variants can result in multiple transcripts arising due to splicing defects, contribute to altered mRNA stability, lead to secretion defects, etc. Also, linkage disequilibrium and minor effects from yet unknown variants could add to the genetic load of a disease. Therefore, we also sequenced the complete *FBLN5*, *CLU*, and *VIM* genes to identify novel variants that could be associated with PEX as risk factors.

## **6.2. Materials and Methods**

### **6.2.1. Study subjects' selection, recruitment, and sample collection**

This study was approved by the Institutional Biosafety and Human Ethics Committee of the National Institute of Science Education and Research. It adhered to the tenets of Declaration of Helsinki. The inclusion-exclusion criteria followed for sample collection is as mentioned in Chapter 2, page no. 51. Peripheral blood (4 ml) was collected in EDTA vacutainers from the participants. After centrifugation of freshly collected blood samples at 3000 rpm for 10 minutes at 4°C, the plasma was separated. Aliquots of plasma and blood samples were stored at –80°C until further use. Age and sex-matched samples were used for all experiments.

### **6.2.2. Enzyme-linked immunosorbent assay (ELISA)**

#### **6.2.2.1. ELISA of fibulin-5 and vimentin**

Plasma and AH VIM levels were measured using a commercial ELISA kit (Human Vimentin (VIM) ELISA kit, CSB-E08982h: CUSABIO). The plasma levels of FBLN5 were assayed using Human Fibulin-5 (FBLN5) ELISA kit, CSB-EL008454HU: CUSABIO. The procedures were performed according to the supplier's instructions. Plasma and AH samples were diluted 200-fold and 7.5-fold with sample dilution buffer, respectively, for assaying VIM levels. Due to the low concentration in plasma, fibulin-5 levels were assayed in undiluted plasma samples. The samples were added to the 96-well plates coated with capture antibody and incubated for 2.0 hours. After removing any unbound protein, the plates were incubated with a biotin-conjugated detection antibody for 1.0 hour. The plates were then washed and incubated with horseradish peroxidase (HRP) conjugated avidin antibody for 1.0 hour. The plates were given another wash and incubated with the substrate for 20 minutes for color development. The reaction was stopped with 2N sulphuric acid. The optical density of each well was measured immediately using Varioskan Flash Multimode Reader (Thermo Scientific, USA) set to 450 nm with a reference wavelength of 540 nm. All incubations were done at 37<sup>0</sup>C.

#### ***6.2.2.2. ELISA of clusterin***

The plasma CLU levels were assayed as per the manufacturer's protocol using the Quantikine ELISA Human Clusterin Immunoassay kit, DCLU00: R&D Systems. The plasma samples were diluted 2000-fold for assaying the CLU levels. In brief, the samples were added to the wells and incubated for 2.0 hours at room temperature. After a wash, the plates were further incubated for 2.0 hours at room temperature with human clusterin conjugate. The wells were washed and incubated with the substrate solution until color development and then the reaction was stopped with the stop solution. The optical density of the wells was measured immediately using

Varioskan Flash Multimode Reader (Thermo Scientific, USA) set to 450 nm with a reference wavelength of 540 nm. All the incubations were done at room temperature.

### **6.2.3. Full gene sequencing of *FBLN5*, *CLU* and *VIM* genes**

DNA was isolated from the blood of the study subjects using the Phenol-Chloroform precipitation method, and the protocol has been mentioned in detail in Chapter 2, page no. 52. The complete genes of fibulin-5, clusterin, and vimentin of 50 PEXS, 44 PEXG, and 50 age-sex matched controls were sequenced using the minion Nanopore sequencing technique. The entire ~72 kb *FBLN5* gene was PCR amplified using nine overlapping primers. Three overlapping primers were used to amplify the entire ~18 kb *CLU* gene. One primer set was used to amplify the ~9.3 kb of the *VIM* gene. The primers were designed using the Primer Blast (NCBI). The primer sequences are shown in **Table 6.1**. The genes were amplified using the LongAmp Taq polymerase. The PCR conditions followed were initial denaturation at 95<sup>0</sup>C for 5 minutes, 32 cycles of denaturation at 95<sup>0</sup>C for 30 seconds, annealing for 35 seconds and extension at 65<sup>0</sup>C for 5.30 minutes, and a final extension at 65<sup>0</sup>C for 10 minutes. The amplified products were resolved on 0.7% agarose gel; the bands were excised and eluted using the QiaQuick gel extraction kit. The amplified products for all three genes from each subject were pooled into a single tube in equimolar concentrations. The PCR Barcoding Expansion 1-96 was used for the library preparation. The ends of the purified PCR products were repaired, and dA-tailing was done. Using Blunt/TA ligase Mix (NEB), specific barcodes were added to the end-repaired DNA. Each individual was given a unique barcode sequence. The barcoded DNA was purified using AMPure XP beads and pooled. Adaptors were added to the pooled library using T4 DNA ligase, purified, and sequenced on the minion sequencer. The data was generated in fastq files on MinKNOW software. The data was basecalled, debarcoded, and variant call format (vcf) files were generated

on NGS Commander software. The variants were called using the hg38 human genome assembly. The variants were annotated using ANNOVAR (Annotate Variation) and VEP (Variant Effect Predictor) tools. The analysis was performed using the bcftools. The variants from all the vcf files were merged (merge command) and then the annotate command was applied.

**Table 6.1.** List of oligos used in the study

S. No.	ID	Sequence (5'→3')
1	FBLN5 I	F: AATCACTTTCGAGCCAGGG R: TGCCAGCCAACAATTTCTAGC
2	FBLN5 II	F: CTTCCAGACATAACAAGCAGAG R: TGTTGCCTACAATGGACAGTAATG
3	FBLN5 III	F: TACTAAGGGTCGTAATCTGGG R: CAGTAGGCTGTGCTGGAATG
4	FBLN5 IV	F: AAGACAACAGGAGATAGTGC R: CAGCCCACATCTCTTCTGTAAC
5	FBLN5 V	F: CCTGATTCCGTGATGCTTG R: CCTCTTCCCATGCCTTCTT
6	FBLN5 VI	F: ATCCAAAAAAGGAAGAGTGG R: CAGGAACAAGAGCCAGTTAG
7	FBLN5 VII	F: CAGTGCCCTCATGTTACTGG R: GAGGCTGAGAATGGGTCAG
8	FBLN5 VIII	F: TTCTCCTGTTTGCCTGCTTAG R: CTCAAGTACCTGCCACAAGAG
9	FBLN5 IX	F: AAAAGCCGAATGTGGAGGTG R: CTAACACCACTTGACCCTG
10	CLU I	F: CTTGGACTGGGACAGACAGC R: CATCTGAAGTAGGGCGACCG
11	CLU II	F: AGAGCCTGGTTCCTCCGAT R: GCAGTCCTCTTCAGTGTAGAC
12	CLU III	F: CCTTAACTGTCCCCCTCCG R: CCTTGACAGCCATGCTAAAATAC
13	VIM	F: CACCCAGAATTTTCAGATC R: TAAATCTTGTAGGAGTGTCGG

#### 6.2.4. Statistical analysis

All experiments were carried out independently at least three times and in triplicate each time. Age and sex-matched samples were taken for the experiments. The groups were matched by performing Student's t-test ( $p > 0.05$  was considered an insignificant difference). No data were missing for the

participants. Three groups were compared using the Kruskal-Wallis H (one-way ANOVA) test. Logistic regression analysis was conducted with the SPSS software package (version 23.0; SPSS, Chicago, IL). Hosmer-Lemeshow goodness-of-fit test was done to check for the calibration of the logistic regression models. GPower 3.1 was used to calculate the power of the study, which was found to be > 80% for both AH and plasma groups keeping an effect size  $d$  of 1.1 and  $\alpha$  error probability of 0.05. All data were presented as mean  $\pm$  standard error of the mean (SEM). Graphical representations for ELISA were generated with GraphPad Prism 7 software. Receiver operating characteristic (ROC) analysis was performed, and the area under the curve (AUC) were generated using the statistical software program XLSTAT. The area under the curve results were considered excellent at 0.9-1.0, good at 0.8-0.9, fair at 0.7-0.8, poor at 0.6-0.7, and failed at 0.5-0.6.<sup>268,269</sup> ROC curves with AUC below 0.5 have not been shown. All data obtained from the quantitative measurements were analyzed using Student's  $t$ -test. The allelic and genotypic association tests and Hardy-Weinberg equilibrium (HWE) analysis were done using Haploview V4.2 and PLINK softwares. A  $p$ -value of <0.05 was considered statistically significant for all tests and indicated by asterisks in the figures.

## 6.3. Results

### 6.3.1. Demographics of the study subjects

The demographics of the eighty-seven subjects (35 control, 35 PEXS, and 17 PEXG) chosen for the study are shown in **Table 6.2**. Age and sex were matched among the groups. The mean age in years  $\pm$  SD of controls, PEXS, and PEXG were  $69.5 \pm 7.1$ ,  $73.6 \pm 6.3$  and  $71.3 \pm 7.6$ , respectively. The age-range of controls, PEXS, and PEXG was 50-78 years, 50-84 years and 57-84 years, respectively. The number of females visiting the hospital was relatively very low as women are

less likely to receive cataract surgery compared to men in low-resource countries/ localities.<sup>35</sup> Twenty-two females (8 control, 12 PEXS, and 2 PEXG) and sixty-five males (27 control, 23 PEXS, and 15 PEXG) participated in the study.

**Table 6.2.** Demographics of study subjects included for ELISA in aqueous humor and plasma samples of control, PEXS and PEXG

	<b>Control (n=35)</b>	<b>PEXS (n=35)</b>	<b>PEXG (n=17)</b>	<b>p-value</b>
<b>Age in years (Mean ± SD)</b>	69.5 ± 7.1	73.6 ± 6.3	71.3 ± 7.6	0.23
<b>Sex (F/M)</b>	8/27	12/23	2/15	0.20

n= sample size, p-value calculated using ANOVA for the average between the three groups, F: female, M: male, PEXS: pseudoexfoliation syndrome, PEXG: pseudoexfoliation glaucoma

### 6.3.2. Plasma fibulin-5 levels did not show differences between controls and patients

Previously, we had reported a significant decrease in fibulin-5 in PEXS LC compared to control through immunoblotting.<sup>134</sup> Recently, Rebecca and her group reported increased levels of fibulin-5 in the aqueous humor of PEX patients compared to control through immunoblotting.<sup>77</sup> To observe whether plasma fibulin-5 shows any disease-specific changes and can be used as a potential minimally invasive biomarker, its levels were assessed in controls and PEX patients using ELISA, a more specific assay. The samples included for fibulin-5 analysis were considerably less as the protein levels in some samples went undetected by the kit, and these samples had to be excluded from the analysis. The mean ± SEM plasma fibulin-5 levels in control, PEXS, and PEXG were found to be 149±32.2 pg/ml, 187.6±32.3 pg/ml, and 203.8±27.3 pg/ml, respectively. There was no significant difference in plasma FBLN5 levels in either PEXS (p=0.4, n=11) or PEXG (p=0.2, n=8) compared to the controls (n=8). Moreover, no difference was observed between the plasma FBLN5 levels of PEXS and PEXG (p=0.7) (**Figure 6.1**).

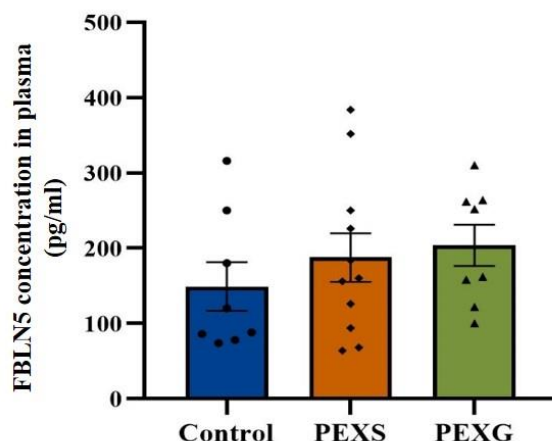


**Figure 6.1. Levels of plasma fibulin-5 in controls, PEXS and PEXG.** Column scatter and bar graph representing fibulin-5 levels in the plasma of controls, PEXS, and PEXG. There was no significant difference in FBLN5 levels in either PEXS ( $187.6 \pm 32.3$  pg/ml,  $p=0.4$ ,  $n=11$ ) or PEXG ( $203.8 \pm 27.3$  pg/ml,  $p=0.2$ ,  $n=08$ ) compared to control ( $149 \pm 32.2$  pg/ml,  $n=08$ ). The results are presented as mean  $\pm$  SEM.

### 6.3.3. Increased plasma levels of clusterin in PEXS

We have previously reported increased levels of CLU in aqueous humor and lens capsule of PEXG patients compared to control.<sup>75</sup> In this study, we checked the plasma levels of CLU in controls and patients to explore the possibility of using plasma CLU levels as a minimally invasive biomarker for PEX diagnosis. The mean  $\pm$  SEM plasma CLU levels in control, PEXS and PEXG were found to be  $298.9 \pm 19.0$   $\mu$ g/ml,  $367.8 \pm 25.6$   $\mu$ g/ml and  $272.9 \pm 16.8$   $\mu$ g/ml, respectively. The plasma clusterin levels were significantly higher in PEXS ( $p=0.03$ ,  $n=35$ ) compared to the controls ( $n=35$ ), but there was no significant difference in CLU levels in PEXG ( $p=0.3$ ,  $n=17$ ). Surprisingly, the plasma CLU was significantly higher in PEXS than in PEXG ( $p=0.003$ ) (**Figure 6.2A**). To check for any correlation between the CLU plasma levels and age, the plasma CLU levels were compared between the age groups of 50-59 years, 60-69 years, and  $\geq 70$  years. There was no significant difference between the plasma CLU levels between the control and PEXS or control and PEXG

across any of the age groups. Further, age did not affect plasma CLU levels within the controls or the PEXS or PEXG groups (**Figure 6.2B**).

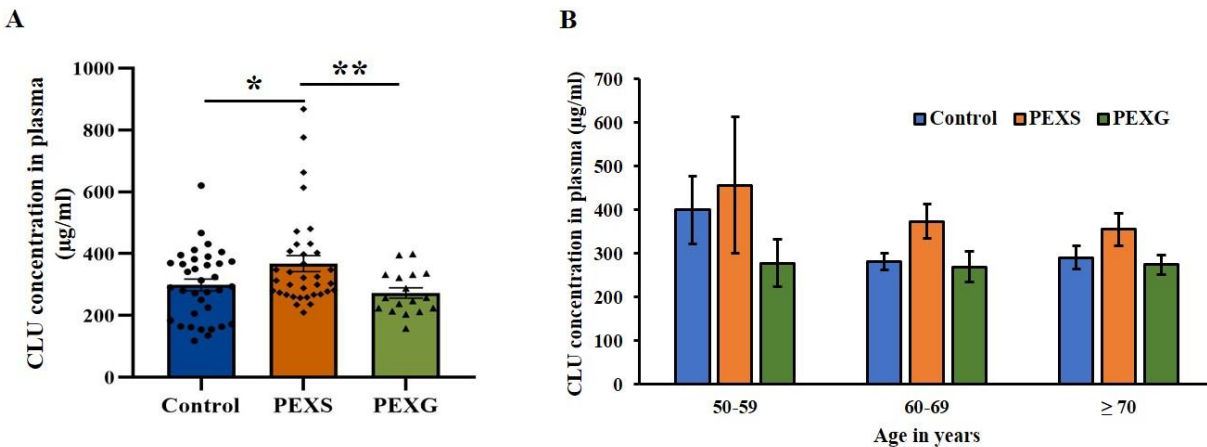


**Figure 6.2. Levels of plasma clusterin in controls, PEXS and PEXG and receiver operating characteristic curves. A.** Column scatter and bar graph representing CLU levels in the plasma of controls, PEXS, and PEXG. A significant increase in circulating CLU in PEXS ( $367.8 \pm 25.6 \mu\text{g/ml}$ ,  $p=0.03$ ,  $n=35$ ) compared to the controls ( $298.9 \pm 19.0 \mu\text{g/ml}$ ,  $n=35$ ) was noted. There was no significant difference in plasma CLU of PEXG ( $272.9 \pm 16.8 \mu\text{g/ml}$ ,  $p=0.3$ ,  $n=17$ ) compared to the controls. PEXG showed a significant decrease in plasma CLU levels compared to PEXS ( $p=0.003$ ). **B.** Plasma CLU levels compared between control, PEXS, and PEXG across three age groups, 50-59 years, 60-69 years and  $\geq 70$  years showed no significant differences. The results are presented as mean  $\pm$  SEM.  $**P < 0.01$ ,  $*P < 0.05$ .

The ROC curve was plotted from the ELISA values for clinical and diagnostic relevance, Receiver operating characteristics (ROC) curves were generated to assess if CLU levels in plasma could be used as a biomarker to differentiate PEXS from controls. Total accuracy was measured by area under the curve (AUC), and Youden index J was used to determine the optimal cut-off value for CLU. The AUC results were considered excellent at 0.9-1, good at 0.8-0.9, fair at 0.7-0.8, poor at 0.6-0.7, and 0.5-0.6 failed.<sup>268,269</sup> ROC analysis showed that the AUC estimate for distinguishing PEXS from controls was 0.602, which was a poor estimate (**Figure 6.3A**). Further, the ROC analysis showed a fair AUC estimate of 0.734 for distinguishing PEXS from PEXG for plasma CLU with an optimum diagnostic cut-off of 288.2 ng/ml (64.7% sensitivity and 62.9% specificity) (**Figure 6.3B**).

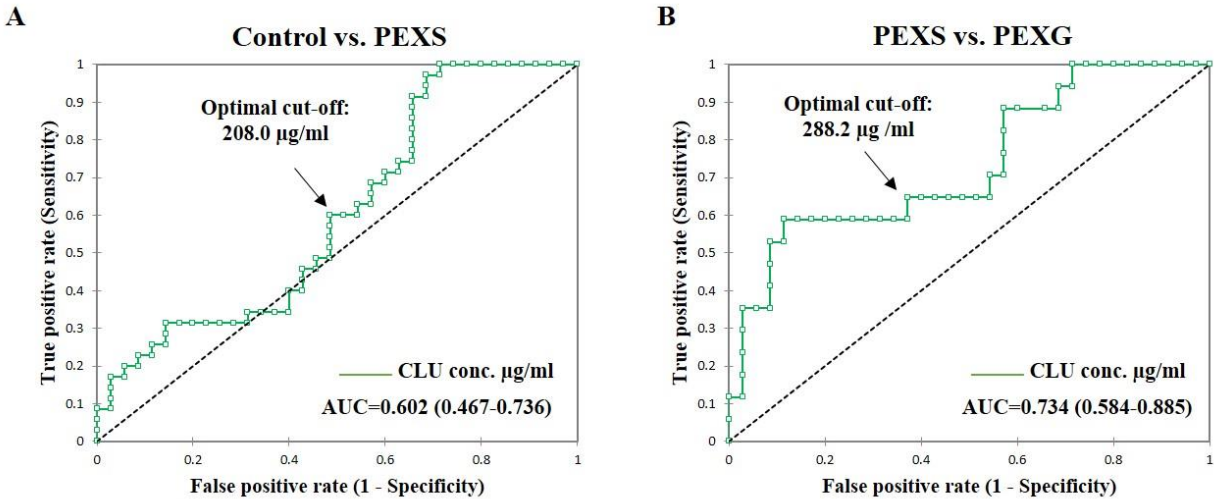


**Figure 6.3. Receiver operating characteristic curves of plasma clusterin. A-B.** ROC analysis of plasma CLU showed that the assay has a 60.2% probability of distinguishing between PEXS and controls (A) and a 73.4% probability of distinguishing between PEXG and PEXS (B).

The ROC curve report of plasma clusterin of PEXS, PEXG and control is shown in **Table 6.3**.

**Table 6.3.** ROC curve report for plasma clusterin

Clusterin						
ROC analysis	AUC (95% CI)	SE	Sensitivity	Specificity	Classifier	p-value
Control versus PEXS	0.60 (0.47-0.74)	0.07	60.0%	51.4%	Poor	0.07
PEXS versus PEXG	0.73 (0.58-0.89)	0.07	64.7%	62.9%	Fair	0.001

AUC: area under the curve, PEXS: pseudoexfoliation syndrome, PEXG: pseudoexfoliation glaucoma, ROC: receiver operating characteristics, SE: standard error

Further, controlling for age and sex, for every 10 units increase in plasma CLU levels, the odds of having PEXS increased by 5.3% (OR=1.053, 95% CI= 1.006-1.102, p=0.02). On comparing PEXS and PEXG, controlling for age and sex, for every 10 units decrease in plasma CLU levels, the odds for having PEXG increased by 11% (OR=0.890, 95% CI= 0.805-0.983, p=0.02). The plasma model for PEXS analysis predicted 65.7% of cases, and calibration of the model was

satisfactory as shown by the Hosmer-Lemeshow goodness-of-fit test (chi-sq.=9.1, 8 degrees of freedom, p=0.33).

#### 6.3.4. Increased levels of vimentin in aqueous humor of PEX affected individuals

As reported in the previous chapter, we observed increased vimentin levels in the aqueous humor through western blotting. To determine if the levels of VIM in the body fluids could be used as a putative biomarker for PEX, its levels in AH were assayed for precise quantitative determination through ELISA. The mean ( $\pm$  SEM) AH VIM concentrations in control, PEXS, and PEXG were  $11.5 \pm 1.4$  ng/ml,  $16.4 \pm 1.8$  ng/ml, and  $20.1 \pm 2.5$  ng/ml, respectively. VIM levels were significantly higher in both PEXS ( $p=0.04$ ,  $n=20$ ) and PEXG ( $p=0.007$ ,  $n=16$ ) compared to the controls ( $n=20$ ) (**Figure 6.4**). No significant difference was observed in VIM levels between PEXS and PEXG groups ( $p=0.2$ ).

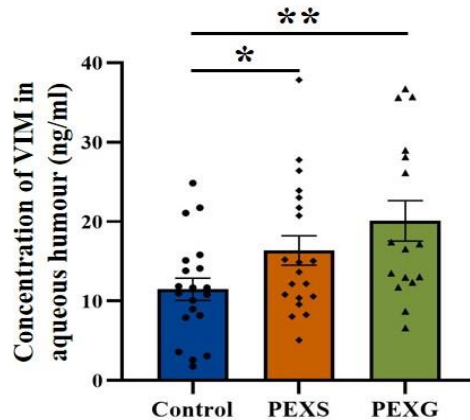


**Figure 6.4. Levels of aqueous humor vimentin in controls, PEXS, and PEXG.** Column scatter and bar graph representing VIM levels in AH of control, PEXS and PEXG. Significant increase in VIM in PEXS ( $16.4 \pm 1.8$  ng/ml,  $p=0.04$ ,  $n=20$ ) and PEXG ( $20.1 \pm 2.5$  ng/ml,  $p=0.007$ ,  $n=16$ ) compared to control ( $11.5 \pm 1.4$  ng/ml,  $n=20$ ) was noted.

Using the highest sensitivity and specificity combination, the optimal cut-off point was derived from ROC analysis. The optimum diagnostic cut-off of AH VIM levels was 12.2 ng/ml (65.0%

sensitivity and 65.0% specificity) for PEXS (**Figure 6.5A**) and 12.4 ng/ml (81.3% sensitivity and 65.0% specificity) for PEXG (**Figure 6.5B**).

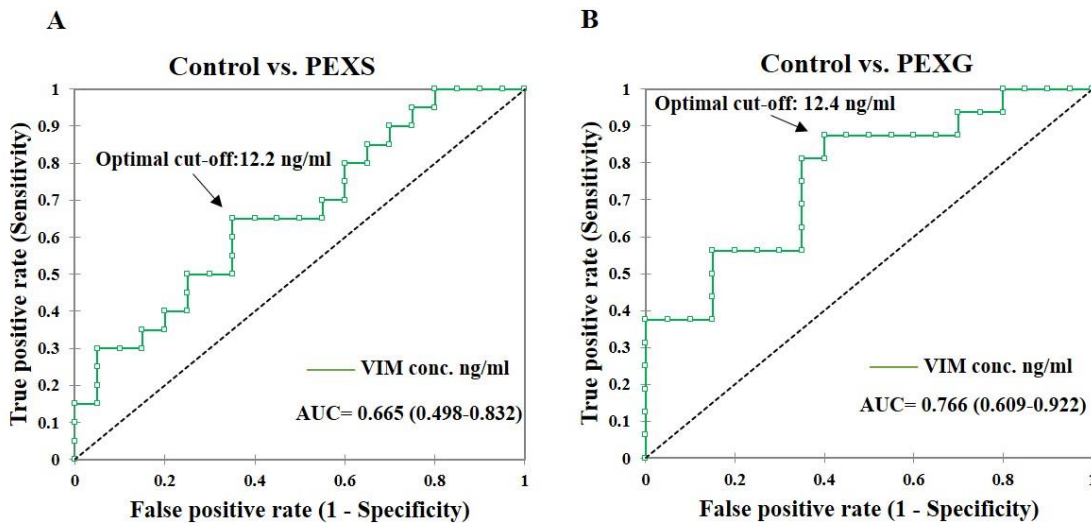


**Figure 6.5. Receiver operating characteristic curves of vimentin levels. A.** ROC analysis of AH VIM showed that the assay has a 66.5% probability of distinguishing between PEXS and controls **B.** ROC curve of AH VIM showed that the assay has a 76.6% probability of distinguishing between PEXG and controls.

The AUC estimates showed that the AH VIM levels are a fair classifier for distinguishing PEXG from controls (**Table 6.4**).

**Table 6.4.** ROC curve report for aqueous humor vimentin

ROC analysis	AUC (95% CI)	SE	Sensitivity	Specificity	Classifier	p-value
Control versus PEXS	0.66 (0.49-0.83)	0.03	65.0%	65.0%	Poor	0.03
Control versus PEXG	0.76 (0.60-0.92)	0.08	81.3%	81.3%	Fair	<0.001

AUC: area under the curve, PEXS: pseudoexfoliation syndrome, PEXG: pseudoexfoliation glaucoma, ROC: receiver operating characteristics, SE: standard error

Binary logistic regression analysis was carried out to investigate the relationship between VIM concentration and PEX groups corrected for age and sex. Controlling for age and sex, for every 10 units increase in AH VIM levels, the odds for having PEXS increased by 2.6 times

(OR=2.625, 95% CI= 0.958-7.192, p=0.06), and the odds for having PEXG increased by 3.5 times (OR=3.587, 95% CI= 1.240-10.370, p=0.01). The AH model for PEXS analysis predicted 62.5% of cases and the calibration of the model was satisfactory as shown by the Hosmer-Lemeshow goodness-of-fit test (chi-sq.= 9.205, 8 degrees of freedom, p=0.32). The model for PEXG analysis predicted 69.4% of cases and the calibration of the model was also satisfactory (chi-sq.=7.080, 7 degrees of freedom, p=0.42).

### **6.3.5. Increased plasma level of vimentin has the potential to be used as a biomarker for PEX**

As aqueous humor can be accessed only during surgery, we also checked the levels of VIM in the plasma of control and patient samples with the idea that if found significantly different, it can be used as a minimally invasive approach for diagnosis. The mean  $\pm$  SEM plasma VIM levels in control, PEXS, and PEXG were found to be 372.2 $\pm$ 15.1 ng/ml, 449.9 $\pm$ 15.7 ng/ml, and 535.5 $\pm$ 25.0 ng/ml, respectively. Plasma VIM was significantly higher in both PEXS (p=0.0006, n=35) and PEXG (p<0.0001, n=17) compared to the controls (n=35). Further, there was a significant increase in plasma VIM levels of PEXG compared to PEXS (p=0.007) (**Figure 6.6A**). To check if there was any correlation between the plasma VIM levels and age, the VIM levels were compared between the control and the patient groups within the three age groups: 50-59 years (5 control, 3 PEXS, 2 PEXG), 60-69 years (15 control, 12 PEXS, 5 PEXG) and  $\geq$  70 years (15 control, 20 PEXS, 10 PEXG). There was a significant increase in the plasma VIM in PEXS compared to the controls in the age group  $\geq$  70 years (p=0.005). Plasma VIM was significantly more in PEXG compared to control in both 60-69 years (p=0.006) and  $\geq$  70 years (p=0.001) age groups. No significant difference in VIM levels was observed between controls, PEXS or PEXG in the age

group of 50-59 years. Also, age did not affect plasma VIM levels within the controls or the PEXS or PEXG groups (**Figure 6.6B**).

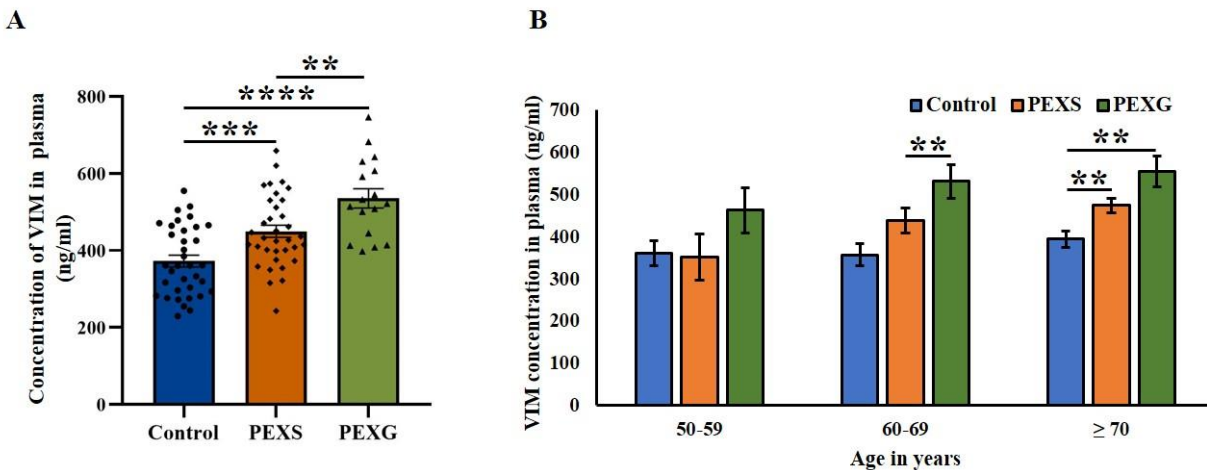


**Figure 6.6. Levels of plasma vimentin in controls, PEXS, and PEXG.** **A.** Column scatter and bar graph representing VIM levels in the plasma of controls, PEXS and PEXG. Significant increase in circulating VIM in PEXS ( $449.9 \pm 15.7$  ng/ml,  $p=0.0006$ ,  $n=35$ ) and PEXG ( $535.5 \pm 25.0$  ng/ml,  $p<0.0001$ ,  $n=17$ ) compared to control ( $372.2 \pm 15.1$  ng/ml,  $n=35$ ) was noted. PEXG showed a significant increase in VIM compared to PEXS ( $p=0.007$ ). **B.** Plasma VIM levels were significantly higher in PEXG ( $p=0.006$ ,  $n=05$ ) compared to control ( $n=15$ ) in the age group of 60-69 years. VIM levels were high in both PEXS ( $p=0.005$ ,  $n=15$ ) and PEXG ( $p=0.001$ ,  $n=20$ ) compared to control ( $n=10$ ) in the age group of  $\geq 70$  years. The results are presented as mean  $\pm$  SEM. \*\*\*\* $P<0.0001$ , \*\*\* $P<0.001$ , \*\* $P<0.01$ .

Further, as shown in **Figure 6.7A**, ROC analysis showed that the optimum diagnostic cut-off of plasma VIM levels was 401.6 ng/ml (71.4% sensitivity and 62.9% specificity) for PEXS. The optimum diagnostic cut-off of plasma VIM was 501.0 ng/ml (70.6% sensitivity and 91.4% specificity) for PEXG (**Figure 6.7B**). The AUC estimates indicate that the levels of circulating VIM in the blood can be a fair (AUC=0.713) classifier for distinguishing PEXS and a good (AUC=0.877) classifier for distinguishing PEXG from controls. **Further, the ROC analysis showed a fair AUC estimate of 0.716 for distinguishing PEXG from PEXS for plasma VIM with an optimum diagnostic cut-off of 501.0 ng/ml (70.6% sensitivity and 71.4% specificity) (Figure 6.7C).** The AUC report for plasma VIM is shown in **Table 6.5**.

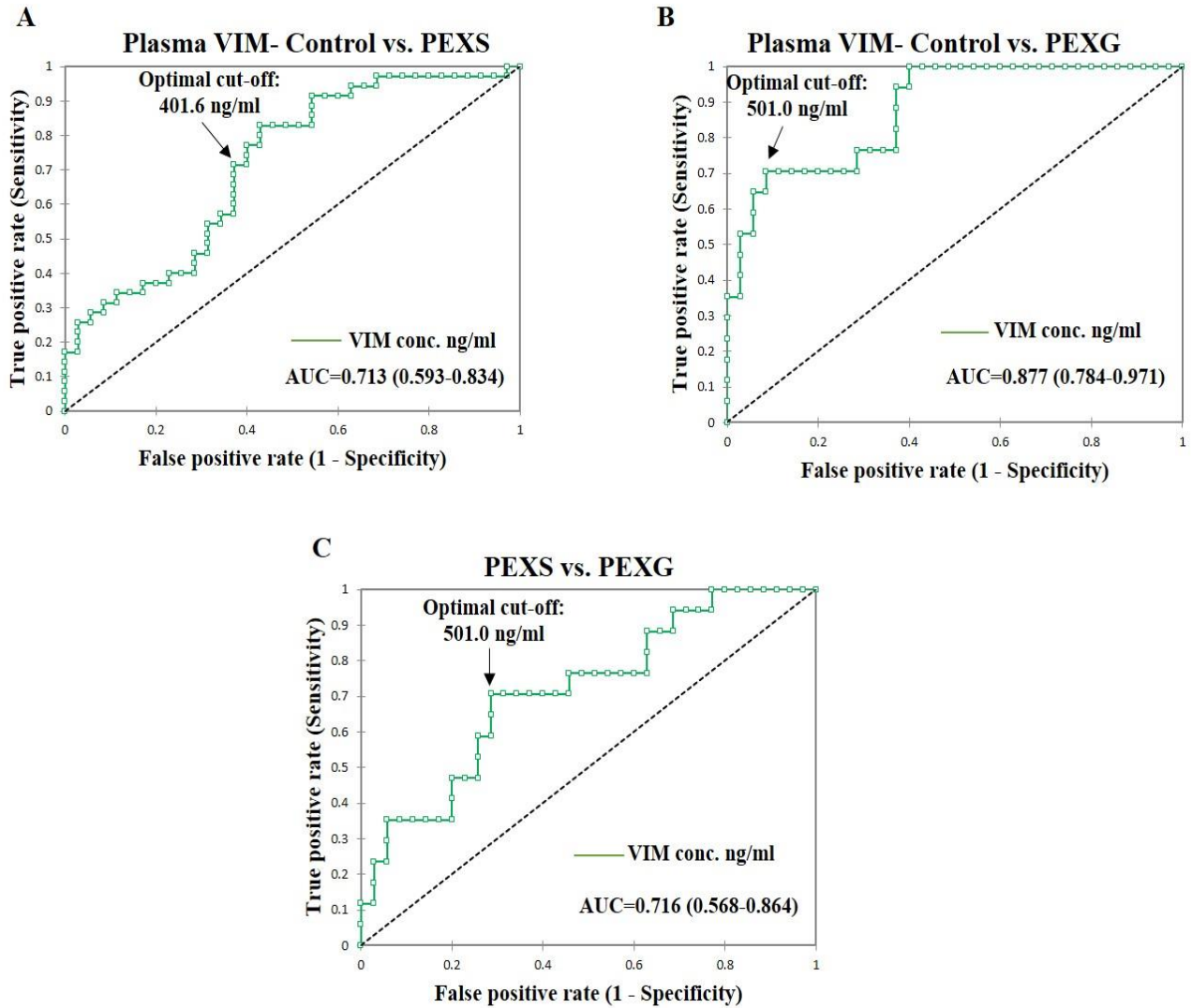


**Figure 6.7.** Levels of plasma clusterin in controls, PEXS and PEXG and receiver operating characteristic curves. A-C. ROC analysis of plasma VIM showed that the assay has a 71.3% probability of distinguishing between PEXS and controls (A), an 87.7% probability of distinguishing between PEXG and controls (B), and a 71.6% probability of distinguishing between PEXG and PEXS (C).

**Table 6.5.** ROC curve report for plasma vimentin

ROC analysis	AUC (95% CI)	SE	Sensitivity	Specificity	Classifier	p-value
Control versus PEXS	0.71 (0.59-0.83)	0.06	71.4%	62.9%	Fair	0.0002
Control versus PEXG	0.87 (0.78-0.97)	0.05	70.6%	91.4%	Good	<0.0001

PEXS versus PEXG	0.71 (0.56-0.86)	0.08	70.6%	71.4	Fair	0.002
------------------------	---------------------	------	-------	------	------	-------

AUC: area under curve, PEXS: pseudoexfoliation syndrome, PEXG: pseudoexfoliation glaucoma, ROC: receiver operating characteristics, SE: standard error

Further, controlling for age and sex, for every 10 units increase in plasma VIM levels, the odds for having PEXS increased by 10.1% (OR=1.101, 95% CI= 1.031-1.173, p=0.004), and the odds for having PEXG increased by 21.8% (OR=1.218, 95% CI= 1.086-1.367, p=0.001). On comparing PEXS and PEXG, after controlling for age and sex, for every 10 units increase in plasma VIM levels, the odds for having PEXG increased by 10.8% (OR=1.108, 95% CI= 1.028-1.196, p=0.008). The plasma model for PEXS analysis predicted 65.7% of cases, and the calibration of the model was satisfactory, as shown by the Hosmer-Lemeshow goodness-of-fit test (chi-sq.=9.1, 8 degrees of freedom, p=0.33). The model for PEXG analysis predicted 86.5% of cases, and the calibration of the model was also found to be adequate (chi-sq.= 11.9, 8 degrees of freedom, p=0.15).

A Pearson correlation analysis was carried out to determine if there was any correlation between the aqueous humor and plasma vimentin levels. We observed a significant positive correlation of 0.314 between plasma and AH VIM levels (p=0.04) (**Figure 6.8**).

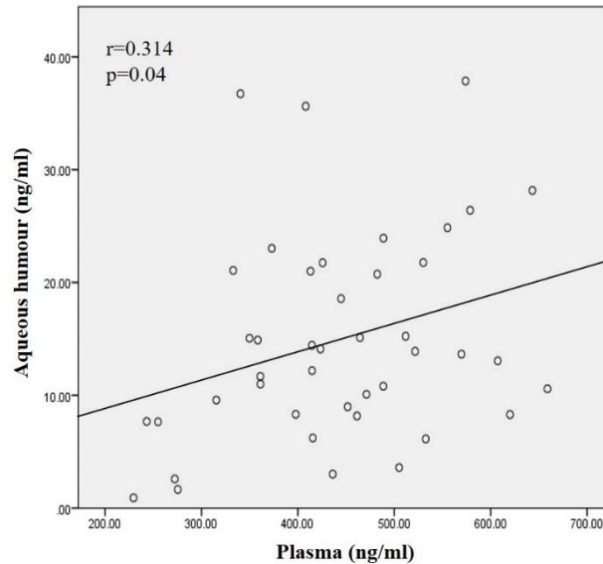


**Figure 6.8. Correlation between plasma and aqueous humor vimentin.** Pearson correlation analysis between plasma and AH VIM levels showed a positive correlation ( $r=0.314$ ,  $p=0.04$ ).

### 6.3.5. Single nucleotide polymorphisms identified in *FBLN5* gene in PEX patients

In search of unknown genetic variants associated with PEX as risk factors, the whole genes of *FBLN5*, *CLU*, and *VIM* were sequenced using the minION sequencer of 50 PEXS, 44 PEXG, and 50 age-sex matched controls. For subsequent analysis of the genetic association of the variants with PEX, the variants in the exons with a MAF > 0.1 in the GIH (Gujarati Indians in Houston) population from the 1000 Genomes Project were chosen so as to have representation of all the genotypes for proper analysis the data. *FBLN5* resides in chromosome 14 and has 11 exons and 10 introns (**Figure 6.9**). A total of 439 annotated variants (**Table 6.6**) were observed in the *FBLN5* gene in the study subjects.



**Figure 6.9. Gene structure of fibulin-5 gene.** Showing the 11 exons and 10 introns (taken from UCSC genome browser 13 April, 2023).

**Table 6.6.** List of annotated variants observed in the *FBLN5* gene

SNP ID	Alleles	Location	MAF on 1000 Genomes project
rs115237925 <sup>a</sup>	A>G	Exon 11	BEB G: 0.076, GIH G: 0.078
rs79375113 <sup>a</sup>	C>T	Exon 11	BEB T: 0.076, GIH T: 0.078
<b>rs929608</b>	<b>T&gt;C</b>	<b>Intron 10</b>	<b>BEB C: 0.506, GIH C: 0.612</b>
rs551213111	C>T	Intron 10	BEB T: 0.006, GIH T: 0.005
<b>rs929609</b>	<b>C&gt;T</b>	<b>Intron 10</b>	<b>BEB T: 0.494, GIH T: 0.602</b>
<b>rs929610</b>	<b>G&gt;C</b>	<b>Intron 10</b>	<b>BEB C: 0.337, GIH C: 0.374</b>
rs929611	G>A	Intron 10	BEB A: 0.076, GIH A: 0.083
rs7142368	T>C	Intron 10	BEB C: 0.006, GIH C: 0.000
rs76347065	C>T	Intron 10	BEB T: 0.006, GIH T: 0.000
<b>rs55903830</b>	<b>TAAAAAAAA&gt; TAAAAAAAAAAAAA,T</b>	<b>Intron 10</b>	<b>BEB AAAAAA...: 0.273, GIH AAAAAA...: 0.214</b>
<b>rs75033136</b>	<b>G&gt;A</b>	<b>Intron 10</b>	<b>BEB A: 0.198, GIH A: 0.223</b>
rs1384883790	AC>A	Intron 10	SAS CCCCC: 0.000
<b>rs2430340</b>	<b>G&gt;A</b>	<b>Intron 10</b>	<b>BEB A: 0.169, GIH A: 0.165</b>
<b>rs7143288</b>	<b>T&gt;C</b>	<b>Intron 10</b>	<b>BEB T: 0.390, GIH T: 0.390</b>
rs1321836175	TG>T	Intron 10	SAS GGGGG: 0.000
<b>rs111668602</b>	<b>TAAAAA&gt; TAAA,TA,TAA,T</b>	<b>Intron 10</b>	<b>BEB AAAAAAAAAA...: 0.320, GIH AAAAAAAAAA...: 0.311</b>
<b>rs2498849</b>	<b>T&gt;G</b>	<b>Intron 10</b>	<b>BEB G: 0.198, GIH G: 0.160</b>
<b>rs12586948</b>	<b>G&gt;A</b>	<b>Intron 10</b>	<b>BEB A: 0.215, GIH A: 0.301</b>
rs1214081173	TGG>T	Intron 10	SAS GGGGGG: 0.000
rs770697680	C>T	Intron 10	SAS T: 0.0002071
<b>rs917907</b>	<b>A&gt;T</b>	<b>Intron 10</b>	<b>BEB T: 0.180, GIH T: 0.155</b>
<b>rs929612</b>	<b>T&gt;A</b>	<b>Intron 10</b>	<b>BEB A: 0.163, GIH A: 0.102</b>
<b>rs2267989</b>	<b>G&gt;A</b>	<b>Intron 10</b>	<b>BEB A: 0.430, GIH A: 0.432</b>
<b>rs2267990</b>	<b>C&gt;T</b>	<b>Intron 10</b>	<b>BEB T: 0.430, GIH T: 0.427</b>
rs142113108	T>C	Intron 10	BEB C: 0.006, GIH C: 0.000
rs888995909	C>T	Intron 10	SAS T: 0.000
<b>rs35341842</b>	<b>A&gt;G</b>	<b>Intron 10</b>	<b>BEB G: 0.215, GIH G: 0.306</b>
<b>rs2284337</b>	<b>G&gt;A</b>	<b>Intron 10</b>	<b>BEB A: 0.203, GIH A: 0.301</b>
<b>rs2284338</b>	<b>G&gt;A</b>	<b>Intron 10</b>	<b>BEB A: 0.209, GIH A: 0.301</b>
<b>rs2284339</b>	<b>A&gt;G</b>	<b>Intron 10</b>	<b>BEB G: 0.430, GIH G: 0.447</b>
<b>rs34762631</b>	<b>G&gt;A</b>	<b>Intron 10</b>	<b>BEB A: 0.203, GIH A: 0.301</b>
<b>rs2267991</b>	<b>T&gt;G</b>	<b>Intron 10</b>	<b>BEB G: 0.227, GIH G: 0.301</b>
rs557483016	C>T	Intron 10	SAS T: 0.000
rs542678477	G>A	Intron 10	BEB A: 0.006, GIH A: 0.005
rs559829032	G>C	Intron 10	BEB C: 0.000, GIH C: 0.000
<b>rs10484030</b>	<b>G&gt;C</b>	<b>Intron 10</b>	<b>BEB C: 0.221, GIH C: 0.286</b>

rs117055435	G>T	Intron 10	BEB T: 0.012, GIH T: 0.000
rs533654273	G>C	Intron 10	BEB C: 0.000, GIH C: 0.000
rs149656123	C>A	Intron 10	BEB A: 0.006, GIH A: 0.034
rs763945183	TT>-,T,TTT	Intron 10	SAS TTTTTTTT: 0.000
rs186669329	A>G	Intron 10	BEB G: 0.006
rs2430341	C>T	Intron 10	BEB C: 0.00, GIH T: 0.000
<b>rs2430342</b>	<b>T&gt;C</b>	<b>Intron 9</b>	<b>BEB C: 0.436, GIH C: 0.354</b>
rs1041359935	G>A	Intron 9	SAS A: 0.000
<b>rs2498847</b>	<b>A&gt;G</b>	<b>Intron 9</b>	<b>BEB G: 0.436, GIH G: 0.354</b>
rs71430741	G>A	Intron 9	BEB A: 0.023, GIH A: 0.073
rs1264847008	CA>C	Intron 9	SAS AAA: 0.000
rs1449122291	ATTT>A,AT	Intron 9	SAS TTTTTT: 0.000
rs17127683	C>T	Intron 9	BEB T: 0.029, GIH T: 0.073
<b>rs2267992</b>	<b>A&gt;T</b>	<b>Intron 9</b>	<b>BEB A: 0.250, GIH A: 0.311</b>
<b>rs2430343</b>	<b>T&gt;C</b>	<b>Intron 9</b>	<b>BEB T: 0.256, GIH T: 0.311</b>
<b>rs5810558</b>	<b>C&gt;CA</b>	<b>Intron 9</b>	<b>BEB -: 0.227, GIH -: 0.238</b>
rs149367738	C>T	Intron 9	BEB T: 0.006
rs17127685	T>C	Intron 9	BEB C: 0.029, GIH C: 0.073
<b>rs2430344</b>	<b>T&gt;C</b>	<b>Intron 9</b>	<b>BEB T: 0.256, GIH T: 0.311</b>
rs35350142	C>G	Intron 9	BEB G: 0.029, GIH G: 0.073
rs34929185	C>G	Intron 9	BEB G: 0.029, GIH G: 0.073
rs1366037108	TGG>T	Intron 9	SAS G: 0.000
rs2498845	G>T	Intron 9	BEB G: 0.227, GIH G: 0.248
rs1034540260	C>T	Intron 9	SAS T: 0.000
rs140201135	C>T	Intron 9	SAS GTGTGTGTGT...: 0.139
rs868696226	CGTGT>C,CGTGTGTGT	Intron 9	Not available
<b>rs2267993</b>	<b>G&gt;A</b>	<b>Intron 9</b>	<b>BEB A: 0.308, GIH A: 0.340</b>
<b>rs2430345</b>	<b>A&gt;G</b>	<b>Intron 9</b>	<b>BEB A: 0.221, GIH A: 0.238</b>
<b>rs2498844</b>	<b>C&gt;A</b>	<b>Intron 9</b>	<b>BEB C: 0.221, GIH C: 0.248</b>
rs71123306	A>ACACC	Intron 9	Not available
rs113395651	A>ACC	Intron 9	BEB C: 0.076, GIH C: 0.083
rs557153944	CACACACACA>CCA,C	Intron 9	Not available
rs2430346	A>C	Intron 9	SAS C: 0.219
rs1555374875	CACACACACA>C	Intron 9	SAS ACATACA: 0.015
rs113102377	C>CATAT	Intron 9	SAS ATA: 0.539
rs10145067	C>T	Intron 9	BEB T: 0.041, GIH T: 0.053
<b>rs2498843</b>	<b>C&gt;T</b>	<b>Intron 9</b>	<b>BEB T: 0.163, GIH T: 0.136</b>
rs539972949	G>A	Intron 9	BEB A: 0.000, GIH A: 0.000
rs74071605	C>T	Intron 9	BEB T: 0.017, GIH T: 0.015
<b>rs2430347<sup>b</sup></b>	<b>A&gt;G</b>	<b>Exon 9</b>	<b>BEB A: 0.221, GIH A: 0.233</b>
<b>rs35187606</b>	<b>TA&gt;T</b>	<b>Intron 8</b>	<b>BEB -: 0.308, GIH -: 0.335</b>

rs1458205353	G>A	Intron 8	SAS A: 0.000
rs967847519	G>A	Intron 8	SAS A: 0.0002078
rs912165357	ATTT>AT,A	Intron 8	SAS TTTTTTTTTT: 0.000
rs1244386789	TAAAA>TA,T	Intron 8	SAS AAAAAA: 0.000
rs148895558	A>G	Intron 8	BEB G: 0.006
rs17127688	C>T	Intron 8	BEB T: 0.023, GIH T: 0.078
<b>rs2430348</b>	<b>A&gt;G</b>	<b>Intron 8</b>	<b>BEB A: 0.250, GIH A: 0.311</b>
<b>rs2430349</b>	<b>A&gt;G</b>	<b>Intron 8</b>	<b>BEB A: 0.262, GIH A: 0.311</b>
rs185053478	G>A	Intron 7	BEB A: 0.006
<b>rs3753161</b>	<b>C&gt;A</b>	<b>Intron 7</b>	<b>BEB C: 0.250 , GIH C: 0.311</b>
rs77700973	C>A	Intron 7	SAS A: 0.001
<b>rs2430350</b>	<b>T&gt;C</b>	<b>Intron 7</b>	<b>BEB T: 0.256, GIH T: 0.306</b>
rs2498842	C>G	Intron 7	BEB C: 0.000, GIH C: 0.000
<b>rs2498841</b>	<b>A&gt;C</b>	<b>Intron 7</b>	<b>BEB A: 0.221, GIH A: 0.252</b>
<b>rs966382</b>	<b>T&gt;A</b>	<b>Intron 7</b>	<b>BEB T: 0.221, GIH T: 0.252</b>
<b>rs2248052</b>	<b>C&gt;T</b>	<b>Intron 7</b>	<b>BEB C: 0.221, GIH C: 0.252</b>
<b>rs2430351</b>	<b>A&gt;G</b>	<b>Intron 7</b>	<b>BEB A: 0.215, GIH A: 0.252</b>
rs113655279	T>A	Intron 7	BEB A: 0.006
rs143399453	A>G	Intron 7	BEB G: 0.006
rs150762179	T>A	Intron 7	BEB A: 0.006
rs139218416	C>T	Intron 7	BEB T: 0.006
rs117702914	T>G	Intron 7	BEB G: 0.000, GIH G: 0.000
rs116467689	G>C	Intron 7	BEB C: 0.006
rs147699855	A>G	Intron 6	BEB G: 0.006
rs78277125	G>A	Intron 6	BEB A: 0.047, GIH A: 0.068
<b>rs1006856</b>	<b>C&gt;G</b>	<b>Intron 6</b>	<b>BEB C: 0.471, GIH C: 0.403</b>
<b>rs1010325</b>	<b>C&gt;T</b>	<b>Intron 6</b>	<b>BEB T: 0.198, GIH T: 0.165</b>
rs535394332	C>G	Intron 6	BEB G: 0.000, GIH G: 0.000
rs530833496	T>C	Intron 6	BEB C: 0.052, GIH C: 0.034
rs531323572	CAAA>CA,C,CAA	Intron 6	GIH AAAAAAAAAA: 0.019
<b>rs34117518</b>	<b>CAAAAAA&gt;</b> <b>CAAA,CAA,C,CA</b>	<b>Intron 6</b>	<b>BEB AAAAAAAAAA...: 0.273,</b> <b>GIH AAAAAAAAAA...: 0.306</b>
rs987651934	TATA> -,TA,TATATA,TATATATA	Intron 6	Not available
rs1380151045	C>T	Intron 6	SAS T: 0.000
rs141620039	C>T	Intron 6	BEB T: 0.012, GIH T: 0.005
rs1430818711	G>C	Intron 6	SAS C: 0.000
<b>rs2430353</b>	<b>C&gt;A</b>	<b>Intron 6</b>	<b>BEB A: 0.186, GIH A: 0.155</b>
rs2430354	T>C	Intron 6	BEB T: 0.000, GIH T: 0.000
rs561028349	C>T	Intron 6	BEB T: 0.006, GIH T: 0.010
rs776567641	G>A	Intron 6	SAS A: 0.000
<b>rs17732060</b>	<b>T&gt;G</b>	<b>Intron 6</b>	<b>BEB G: 0.215, GIH G: 0.248</b>

rs181248842	C>T	Intron 6	BEB T: 0.000, GIH T:0.000
rs148453107	G>A	Intron 6	BEB A: 0.006, GIH A: 0.000
rs150590117	G>A	Intron 6	BEB A: 0.006, GIH A:0.000
<b>rs72705340</b>	<b>T&gt;C</b>	<b>Intron 6</b>	<b>BEB C: 0.215, GIH C: 0.257</b>
rs2430355	A>C	Intron 6	BEB A: 0.000, GIH A: 0.000
rs72705341	G>A	Intron 6	BEB A: 0.023, GIH A: 0.019
rs2430356	A>T	Intron 6	BEB T: 0.203, GIH T: 0.146
rs141896059	GAATCCAGGGTCAA>G	Intron 6	BEB A: 0.000, GIH A: 0.005
<b>rs2267994</b>	<b>A&gt;G</b>	<b>Intron 6</b>	<b>BEB G: 0.273, GIH G: 0.345</b>
rs529834011	G>C	Intron 6	BEB C: 0.012, GIH C: 0.024
<b>rs876043</b>	<b>A&gt;G</b>	<b>Intron 6</b>	<b>BEB A: 0.326, GIH A: 0.277</b>
rs887897	C>T	Intron 6	BEB T: 0.006, GIH T: 0.019
<b>rs72705342</b>	<b>C&gt;T</b>	<b>Intron 6</b>	<b>BEB T: 0.227, GIH T: 0.286</b>
<b>rs17805119</b>	<b>C&gt;G</b>	<b>Intron 6</b>	<b>BEB G: 0.227, GIH G: 0.286</b>
rs572244591	T>C	Intron 5	BEB C: 0.000, GIH C: 0.024
rs2267995	G>C	<b>Intron 5</b>	<b>BEB C: 0.291, GIH C: 0.325</b>
rs545926926	G>A	Intron 5	BEB A: 0.012, GIH A: 0.005
<b>rs2243400</b>	<b>C&gt;T</b>	<b>Intron 5</b>	<b>BEB T: 0.180, GIH T: 0.160</b>
<b>rs1861084</b>	<b>T&gt;C</b>	<b>Intron 5</b>	<b>BEB C: 0.180, GIH C: 0.160</b>
<b>rs2244643</b>	<b>A&gt;C</b>	<b>Intron 5</b>	<b>BEB C: 0.186, GIH C: 0.175</b>
<b>rs2244642</b>	<b>C&gt;G</b>	<b>Intron 5</b>	<b>BEB G: 0.180, G: 0.160</b>
rs555843140	GCCCCCT>G,GCCCCCT	Intron 5	SAS CCCCC: 0.002
rs538294764	C>T	Intron 5	BEB T: 0.023, GIH T: 0.015
<b>rs17805191</b>	<b>T&gt;C</b>	<b>Intron 5</b>	<b>BEB C: 0.227, GIH C: 0.286</b>
<b>rs2430357</b>	<b>C&gt;T</b>	<b>Intron 5</b>	<b>BEB T: 0.105, GIH T: 0.063</b>
<b>rs3831760</b>	<b>GA&gt;G</b>	<b>Intron 5</b>	<b>BEB -: 0.302, GIH -: 0.320</b>
rs2267996	C>T	Intron 5	BEB T: 0.041, GIH T: 0.058
rs2244505	A>G	Intron 5	BEB A: 0.564, GIH A: 0.573
<b>rs2244504</b>	<b>A&gt;C</b>	<b>Intron 5</b>	<b>BEB C: 0.436, GIH C: 0.427</b>
rs539357652	G>T	Intron 5	BEB T: 0.012, GIH T: 0.019
<b>rs2430358</b>	<b>T&gt;C</b>	<b>Intron 5</b>	<b>BEB C: 0.436, GIH C: 0.422</b>
<b>rs2430359</b>	<b>A&gt;T</b>	<b>Intron 5</b>	<b>BEB T: 0.436, GIH T: 0.422</b>
rs112924179	C>T	Intron 5	BEB T: 0.041, GIH T: 0.058
rs58035118	CAAAAAAAAA>C,CA,CAA	Intron 5	Not available
rs1343595874	AAAAAAAC>A	Intron 5	Not available
rs1348901073	AAAAAC>A	Intron 5	Not available
<b>rs2430360</b>	<b>C&gt;A</b>	<b>Intron 5</b>	<b>BEB C: 0.297, GIH C: 0.228</b>
rs974496902	G>A	Intron 5	SAS A: 0.000
rs544473433	ACC>A	Intron 5	SAS CCCCCCCC: 0.003
<b>rs2430361</b>	<b>T&gt;C</b>	<b>Intron 4</b>	<b>BEB T: 0.297, GIH T: 0.228</b>
rs60216411	CAAAAAAAAA>	Intron 4	Not available

rs2430362	CAA,CAAA, C	Intron 4	<b>BEB G: 0477, GIH G: 0.481</b>
rs2244158	T>G	Intron 4	<b>BEB T: 0.297, GIH T: 0.228</b>
rs10538021	T>C	Intron 4	<b>BEB -: 0.442, GIH -: 0.417</b>
rs78122063	GACCA>G	Intron 4	SAS G: 0.000
rs78615151	C>G	Intron 4	SAS A: 0.000
rs185293777	C>G,A	Intron 4	BEB A: 0.000, GIH A: 0.005
rs117184514	G>A	Intron 4	BEB T: 0.023, GIH T: 0.024
rs917908	C>T	Intron 4	<b>BEB C: 0.140, GIH C: 0.097</b>
rs2300136	T>C	Intron 4	<b>BEB T: 0.291, GIH T: 0.228</b>
rs2244017	T>C	Intron 4	<b>BEB T: 0.140, GIH T: 0.097</b>
rs2498838	G>T	Intron 4	<b>BEB T: 0.285, GIH T: 0.223</b>
rs2430363	T>C	Intron 4	<b>BEB G: 0.512, GIH G: 0.515</b>
rs35840279	G>A CTTTTTTTTT> CT,CTT, CTTTT	Intron 4	SAS TTTTTTTTTT...: 0.065
rs11160031	C>T	Intron 4	<b>BEB C: 0.448, GIH C: 0.481</b>
rs2498837	A>C	Intron 4	<b>BEB A: 0.273, GIH A: 0.228</b>
rs146885552	C>T	Intron 4	BEB T: 0.047, GIH T: 0.073
rs561213364	C>T	Intron 4	BEB T: 0.006, GIH T: 0.024
rs59077653	C>CGT	Intron 4	SAS GTGTGTGTGT...: 0.406
rs61988362	C>T	Intron 4	BEB T: 0.023, GIH T: 0.019
rs8013684	G>A	Intron 4	<b>BEB A: 0.302, GIH A: 0.325</b>
rs559833767	A>G	Intron 4	BEB G: 0.012, GIH G: 0.000
rs2017488	T>C	Intron 4	<b>BEB C: 0.140, GIH C: 0.102</b>
rs741198	C>T	Intron 4	<b>BEB T: 0.215, GIH T: 0.126</b>
rs17127722	A>T	Intron 4	BEB T: 0.000, GIH T: 0.000
rs1363997488	TTTTG>T	Intron 4	SAS TTTGTTTGT...: 0.001
rs376843305	GTTTGTT>G	Intron 4	SAS TTTT: 0.005
rs1449735211	GTTTGTTT>GTT,G	Intron 4	Not available
rs1220743148	GTTTGTTT>GTT,G	Intron 4	Not available
rs1274929866	G>GTT	Intron 4	<b>BEB A: 0.233, GIH A: 0.282</b>
rs72705349	G>A	Intron 4	SAS C: 0.0004146
rs749479430	T>C	Intron 4	<b>BEB C: 0.326, GIH C: 0.291</b>
rs2267997	C>G	Intron 4	SAS TTTTTTTTTT: 0.000
rs886606487	ATT,A,AT	Intron 4	BEB TCTCT: 0.012, GIH TCTCT: 0.012
rs537691678	TTCTC>T	Intron 4	BEB TCTCT: 0.012, GIH TCTCT: 0.000
rs17805293	C>T	Intron 4	<b>BEB T: 0.233, GIH T: 0.282</b>
rs2254453	G>A	Intron 4	<b>BEB A: 0.372, GIH A: 0.379</b>
rs2300137	G>A	Intron 4	<b>BEB A: 0.372, GIH A: 0.379</b>
rs2430365	A>G	Intron 4	BEB A: 0.058 GIH A: 0.107
rs553086593		Intron 4	BEB G: 0.017, GIH G: 0.005

rs549324724	T>G	Intron 4	BEB C: 0.000, BEB C:0.000
<b>rs2498835</b>	T>C	<b>Intron 4</b>	<b>BEB T: 0.372, GIH T: 0.374</b>
rs534008387	G>T	Intron 4	BEB C: 0.012, GIH C: 0.019
<b>rs2498834</b>	T>C	<b>Intron 4</b>	<b>BEB A: 0.326, GIH A: 0.291</b>
rs117980027	A>C	Intron 4	BEB A: 0.000, GIH A: 0.000
<b>rs2430366</b>	C>T	<b>Intron 4</b>	<b>BEB T: 0.140, GIH T: 0.097</b>
<b>rs2254320</b>	A>T	<b>Intron 4</b>	<b>BEB A: 0.372, GIH A: 0.374</b>
rs1566813053	G>A	Intron 4	Not available
<b>rs1861085</b>	TGG>TG,T	<b>Intron 4</b>	<b>BEB T: 0.326, GIH T: 0.291</b>
<b>rs1861087</b>	T>C	<b>Intron 4</b>	<b>BEB T: 0.140, GIH T: 0.097</b>
rs117042873	C>T	Intron 4	BEB A: 0.000, GIH A: 0.000
rs34047802	G>A	Intron 4	BEB TTTT...: 0.128, GIH TTTT...: 0.165
<b>rs2498833</b>	CTTTTT> CT,CTT,C,CTTT	<b>Intron 4</b>	<b>BEB T: 0.163, GIH T: 0.097</b>
rs149035995	C>T	Intron 4	BEB TTGTTT...: 0.000, GIH TTGTTT...: 0.000
rs1555376789	GTTGT>G,GTTGTTGT	Intron 4	Not available
<b>rs2254090</b>	GTTTGT>G	<b>Intron 4</b>	<b>BEB T: 0.273, GIH T: 0.233</b>
<b>rs2254085</b>	T>C	<b>Intron 4</b>	<b>BEB C: 0.326, GIH C: 0.291</b>
<b>rs2018736</b>	C>T	<b>Intron 4</b>	<b>BEB A: 0.442, GIH A: 0.427</b>
rs373689829	C>A	Intron 4	BEB C: 0.017, GIH C: 0.015
rs726063	G>C	Intron 4	BEB T: 0.052, GIH T: 0.058
rs1566814226	C>T	Intron 4	SAS GGGGG: 0.000
<b>rs60132655</b>	CGG>C,CG	<b>Intron 4</b>	<b>BEB A: 0.233, GIH A: 0.277</b>
<b>rs2160079</b>	G>A	<b>Intron 4</b>	<b>BEB A: 0.273, GIH A: 0.233</b>
rs2267998	A>C	Intron 4	BEB C: 0.052, GIH C: 0.058
<b>rs2160080</b>	T>C	<b>Intron 4</b>	<b>BEB G: 0.140, GIH G: 0.102</b>
rs76232437	T>G	Intron 4	BEB T: 0.017, GIH T: 0.015
<b>rs72705351</b>	G>T	<b>Intron 4</b>	<b>BEB T: 0.233, GIH T: 0.282</b>
rs182473152	C>T	Intron 4	BEB A: 0.017, GIH A: 0.015
rs17127742	G>A	Intron 4	BEB A: 0.023, GIH A: 0.019
<b>rs7157817</b>	G>A	<b>Intron 4</b>	<b>BEB C: 0.465, GIH C: 0.388</b>
<b>rs2498830</b>	C>T	<b>Intron 4</b>	<b>BEB A: 0.273, GIH A: 0.233</b>
<b>rs2498829</b>	A>G	<b>Intron 4</b>	<b>BEB G: 0.192, GIH G: 0.155</b>
rs72705353	A>G	Intron 4	BEB T: 0.233, GIH T: 0.282
rs370310128	C>T	Intron 4	SAS A: 0.000
<b>rs2498827</b>	C>A	<b>Intron 4</b>	<b>BEB A: 0.424, GIH A: 0.427</b>
<b>rs72705356</b>	G>A	<b>Intron 4</b>	<b>BEB T: 0.233, GIH T: 0.282</b>
<b>rs2498826</b>	A>T	<b>Intron 4</b>	<b>BEB G: 0.273, GIH G: 0.233</b>
rs77784449	G>A	Intron 4	BEB T: 0.047, GIH T: 0.058
rs1169008678	C>T	Intron 4	SAS T: 0.000
<b>rs2498825</b>	C>T	<b>Intron 4</b>	<b>BEB C: 0.273, GIH C: 0.199</b>

<b>rs34810596</b>	A>C	<b>Intron 4</b>	<b>BEB TTTTTTTTTTT...: 0.512, GIH TTTTTTTTTTT...: 0.422</b>
rs112824518	ATTTT>A,ATT,AT	Intron 4	BEB T: 0.035, GIH T: 0.039
rs112739092	C>T	Intron 4	BEB T: 0.035, GIH T: 0.039
<b>rs12589592</b>	C>T	<b>Intron 4</b>	<b>BEB A: 0.250, GIH A: 0.252</b>
<b>rs2300139</b>	G>A	<b>Intron 4</b>	<b>BEB C: 0.250, GIH C: 0.252</b>
rs138226356	G>C	Intron 4	BEB A: 0.035, GIH A: 0.053
rs574674808	G>A	Intron 4	BEB TATTATTA: 0.029, GIH TATTATTA: 0.029
<b>rs8021116</b>	A>ATAT	<b>Intron 4</b>	<b>BEB A: 0.291, GIH A: 0.296</b>
rs561662280	C>A	Intron 4	BEB A: 0.000, GIH A: 0.000
rs200501822	G>A	Intron 4	BEB AAAAAAAAAA...: 0.233, GIH AAAAAAAAAA...: 0.267
rs555211877	CAAAA>CA,C,CAA	Intron 4	BEB A: 0.006, GIH A: 0.015
<b>rs72705359</b>	G>A	<b>Intron 4</b>	<b>BEB A: 0.203, GIH A: 0.286</b>
<b>rs17732466</b>	G>A	<b>Intron 4</b>	<b>BEB A: 0.203, GIH A: 0.286</b>
rs74071614	G>A	Intron 4	BEB A: 0.041, GIH A: 0.039
rs1166920235	C>A	Intron 4	SAS TT: 0.000
<b>rs4904823</b>	AT>A	<b>Intron 4</b>	<b>BEB T: 0.459, GIH T: 0.350</b>
rs146524501	T>A	Intron 4	BEB T: 0.116, GIH T: 0.044
rs57302887	C>T	Intron 4	SAS AAAAAAAAAA...: 0.008
rs964981867	CAAAAAAAAA>CAA,CA,C	Intron 4	SAS AAAAAAAAAA...: 0.001
rs192061814	TAAA>T,TA	Intron 4	BEB G: 0.000, GIH G: 0.005
rs34675184	A>G	Intron 4	SAS AAAAAAAAAA...: 0.290
rs4904824	CAAAAAAAAA>C,CAA, CA	Intron 4	BEB C: 0.093, GIH C: 0.087
<b>rs2498824</b>	C>A	<b>Intron 4</b>	<b>BEB A: 0.209, GIH A: 0.160</b>
rs531133150	C>A	Intron 4	BEB C: 0.012, GIH C: 0.015
<b>rs2430367</b>	T>C	<b>Intron 4</b>	<b>BEB T: 0.203, GIH T: 0.160</b>
rs146215042	C>T	Intron 4	BEB T: 0.070, GIH T: 0.044
<b>rs58690818</b>	A>T	<b>Intron 4</b>	<b>BEB A: 0.203, GIH A: 0.286</b>
rs969504178	G>A	Intron 4	SAS T: 0.000
rs1010874883	C>T	Intron 4	SAS A: 0.000
rs34458933	G>A	Intron 4	SAS AAAAAAAAAA...: 0.006
rs111586099	CAAAAAAAAA>CAA,CA,C	Intron 4	SAS G: 0.004
<b>rs2249954</b>	A>G	<b>Intron 4</b>	<b>BEB C: 0.140, GIH C: 0.141</b>
<b>rs2249946</b>	C>T	<b>Intron 4</b>	<b>BEB A: 0.140, GIH A: 0.141</b>
rs989988440	A>T	Intron 4	SAS T: 0.000
rs147909151	C>T	Intron 4	BEB A: 0.035, GIH A: 0.053
rs79442066	G>A	Intron 4	BEB G: 0.041, GIH G: 0.039
rs141633530	A>G	Intron 4	BEB T: 0.035, GIH T: 0.053
<b>rs111821463</b>	C>T	<b>Intron 4</b>	<b>BEB G: 0.203, GIH G: 0.286</b>
rs1295929135	C>G	Intron 4	SAS A: 0.004

rs143450705	G>A	Intron 4	SAS G: 0.050
rs2498823	A>G	Intron 4	SAS G: 0.000
rs200566752	A>G	Intron 4	SAS A: 0.070
rs1215020904	G>A	Intron 4	SAS AAA: 0.000
rs191214106	CA>C	Intron 4	BEB C: 0.000, GIH C: 0.005
<b>rs116377195</b>	T>C	<b>Intron 4</b>	<b>BEB G: 0.116, GIH G: 0.053</b>
<b>rs17732513</b>	T>G	<b>Intron 4</b>	<b>BEB T: 0.250, GIH T: 0.262</b>
<b>rs7140720</b>	C>T	<b>Intron 4</b>	<b>BEB T: 0.157, GIH T: 0.107</b>
rs869254221	C>T	Intron 4	Not available
<b>rs34873410</b>	TTA>T	<b>Intron 4</b>	<b>BEB -: 0.500, GIH -: 0.466</b>
<b>rs2430368</b>	TA>T	<b>Intron 4</b>	<b>BEB A: 0.140, GIH A: 0.141</b>
<b>rs34828343</b>	A>T	<b>Intron 4</b>	<b>BEB G: 0.203, GIH G: 0.282</b>
<b>rs2430369</b>	A>G	<b>Intron 4</b>	<b>BEB C: 0.343, GIH C: 0.422</b>
<b>rs17732602</b>	C>T	<b>Intron 4</b>	<b>BEB A: 0.203, GIH A: 0.282</b>
rs1461801619	C>A	Intron 4	SAS A: 0.000
rs3031542	G>A	Intron 4	SAS TAAATAAATA...: 0.0004439
<b>rs2402088</b>	GTAAATAAA>GTAAA, G	<b>Intron 4</b>	<b>BEB G: 0.459, GIH G: 0.437</b>
<b>rs2284340</b>	A>G	<b>Intron 4</b>	<b>BEB T: 0.291, GIH T: 0.316</b>
rs1471307213	C>T	Intron 4	SAS A: 0.000
rs1188056371	G>A	Intron 4	SAS A: 0.000
rs2267999	G>A	Intron 4	BEB A: 0.047, GIH A: 0.053
<b>rs2268000</b>	G>A	<b>Intron 4</b>	<b>BEB T: 0.198, GIH T: 0.286</b>
rs566857448	C>T	Intron 4	BEB A: 0.006, GIH A: 0.010
rs979404341	G>A	Intron 4	SAS GGGG: 0.000
<b>rs2246416</b>	AG>A	<b>Intron 4</b>	<b>BEB G: 0.349, GIH G: 0.432</b>
rs11354516	A>G	Intron 4	BEB AAAAAA: 0.680, GIH AAAAAA: 0.762
<b>rs2430370</b>	CAA>CA,C	<b>Intron 4</b>	<b>BEB G: 0.233, GIH G: 0.150</b>
rs7159475	G>C	Intron 4	BEB G: 0.006, GIH G: 0.000
rs7159817	A>G	Intron 4	BEB G: 0.006, GIH G: 0.000
rs2430371	C>G	Intron 4	BEB G: 0.081, GIH G: 0.078
<b>rs11277734</b>	A>G	<b>Intron 4</b>	<b>BEB AA: 0.273, GIH AA: 0.257</b>
rs200334529	TAAATC>T	Intron 4	SAS C: 0.036
<b>rs8023114</b>	A>C	<b>Intron 4</b>	<b>BEB A: 0.267, GIH A: 0.248</b>
rs139737360	G>A	Intron 4	BEB T: 0.035, GIH T: 0.053
rs2430372	C>T	Intron 4	BEB A: 0.081, GIH A: 0.078
rs74071631	T>A	Intron 4	BEB T: 0.093, GIH T: 0.107
rs2474033	C>T	Intron 4	BEB A: 0.988, GIH A: 0.985
rs2498820	C>A	Intron 4	BEB T: 0.081, GIH T: 0.078
<b>rs8012648</b>	C>T	<b>Intron 5</b>	<b>BEB T: 0.273, GIH T: 0.398</b>
rs77197951	C>T	Intron 4	BEB A: 0.140, GIH A: 0.073

rs8014161	G>A	Intron 4	<b>BEB A: 0.267, GIH A: 0.252</b>
rs60014967	T>A	Intron 4	<b>BEB T: 0.140, GIH T: 0.073</b>
rs4904826	C>T	Intron 4	<b>BEB G: 0.273, GIH G: 0.403</b>
rs10149504	T>G	Intron 4	<b>BEB T: 0.273, GIH T: 0.398</b>
rs2430373	C>T	Intron 4	BEB A: 0.081, GIH A: 0.078
rs11628643	G>A	Intron 4	BEB A: 0.029, GIH A: 0.029
rs1239579946	G>A	Intron 4	SAS AAAAAAA: 0.000
rs182213115	CA>C	Intron 4	Not available
rs2430374	G>A	Intron 4	<b>BEB A: 0.500, GIH A: 0.544</b>
rs117095517	G>A	Intron 4	BEB C: 0.017, GIH C: 0.000
rs75230778	T>C	Intron 4	<b>BEB T: 0.140, GIH T: 0.068</b>
rs1266589353	G>T	Intron 4	SAS AAAAAAA: 0.000
rs554185623	CA>C	Intron 4	BEB A: 0.029, GIH A: 0.024
rs11844281	G>A	Intron 4	<b>BEB A: 0.273, GIH A: 0.398</b>
rs1196370267	C>A	Intron 4	SAS AAAAAAAAA: 0.000
rs113397883	CAAAAA> CAAAAAAA,CAAAA AACACACAC>A	Intron 4	<b>BEB ACACACACAC...: 0.302, GIH ACACACACAC...: 0.432</b>
rs773940343		Intron 4	SAS -: 0.000
rs981959344	CACACACACA>C	Intron 4	SAS A: 0.000
rs147219382	C>A	Intron 4	BEB C: 0.006, GIH C: 0.005
rs1204577828	A>C	Intron 4	SAS AAAAAAAAAA: 0.001
rs2430375	TAAA>TA,T	Intron 4	BEB G: 0.081, GIH G: 0.078
rs184234725	T>G	Intron 4	BEB G: 0.035, GIH G: 0.058
rs113857192	C>G	Intron 4	BEB AAAAAAA: 0.052, GIH AAAAAAA: 0.053
rs60975757	GAA>GA,G	Intron 4	BEB T: 0.017, GIH T: 0.005
rs2245701	C>T	Intron 4	<b>BEB A: 0.186, GIH A: 0.126</b>
rs2268001	A>G	Intron 4	<b>BEB A: 0.279, GIH A: 0.388</b>
rs2268002	G>A	Intron 4	<b>BEB G: 0.337, GIH G: 0.233</b>
rs370203497	C>G	Intron 4	SAS T: 0.000
rs2268003	C>T	Intron 4	<b>BEB G: 0.151, GIH G: 0.102</b>
rs530225779	C>G	Intron 4	BEB T: 0.006, GIH T: 0.000
rs112676697	C>T	Intron 4	BEB T: 0.006, GIH T: 0.005
rs17127751	C>T	Intron 4	Not available
rs143502523	G>A	Intron 4	BEB A: 0.000, GIH A: 0.005
rs370738540	C>G	Intron 4	SAS A: 0.003
rs138716231	G>A	Intron 4	BEB G: 0.006, GIH G: 0.000
rs557883806	A>G	Intron 4	BEB T: 0.017, GIH T: 0.024
rs2268005	C>T	Intron 4	<b>BEB T: 0.291, GIH T: 0.374</b>
rs2256768	C>T	Intron 4	<b>BEB T: 0.134, GIH T: 0.068</b>
rs2256767	T>C	Intron 4	<b>BEB T: 0.436, GIH T: 0.490</b>

rs1369103495	C>T	Intron 4	SAS TTTTTT: 0.000
<b>rs2430376</b>	AT>A	<b>Intron 4</b>	<b>BEB A: 0.430, GIH A: 0.490</b>
rs112484868	G>A	Intron 4	BEB A: 0.029, GIH A: 0.029
<b>rs28424272</b>	G>A	<b>Intron 4</b>	<b>BEB G: 0.262, GIH G: 0.330</b>
rs547424703	C>G	Intron 4	BEB A: 0.000, GIH A: 0.005
rs79676376	C>A	Intron 4	BEB A: 0.023, GIH A: 0.024
rs112087397	G>A	Intron 4	BEB A: 0.035, GIH A: 0.044
<b>rs4904827</b>	G>A	<b>Intron 4</b>	<b>BEB C: 0.128, GIH C: 0.102</b>
rs111893360	T>C	Intron 4	BEB T: 0.035, GIH T: 0.029
<b>rs12586793</b>	G>T	<b>Intron 4</b>	<b>BEB G: 0.308, GIH G: 0.364</b>
rs2474026	A>G	Intron 4	BEB G: 0.002, GIH G: 0.005
rs202179114	C>G	Intron 4	BEB AAAAAAAAAA: 0.001
<b>rs78639364</b>	TA>T	<b>Intron 4</b>	<b>BEB C: 0.105, GIH C: 0.087</b>
rs373136895	A>C	Intron 4	BEB C: 0.041, GIH C: 0.010
rs540480523	T>C	Intron 3	BEB A: 0.012, GIH A: 0.000
rs60910640	G>A	Intron 3	BEB G: 0.047, GIH G: 0.034
<b>rs2474028</b>	C>G	<b>Intron 3</b>	<b>BEB C: 0.692, GIH C: 0.617</b>
rs556839719	T>C	Intron 3	Not available
rs58984750	G>C	Intron 3	BEB C: 0.047, GIH C: 0.034
rs58235990	T>C	Intron 3	BEB C: 0.047, GIH C: 0.034
rs560380323	T>C	Intron 3	BEB T: 0.023, GIH T: 0.000
rs755988190	C>T	Intron 3	SAS AAAAAAAAAA: 0.0002097
rs1306195503	CAA>CA,C	Intron 3	SAS A: 0.000
rs60683460	G>A	Intron 3	BEB G: 0.047, GIH G: 0.029
rs74071636	T>G	Intron 3	BEB G: 0.035, GIH G: 0.029
rs5810562	T>G	Intron 3	BEB TTTTTTTTTT...: 0.587, TTTTTTTTTTTT...: 0.524
rs2268006	ATTTTT> ATTTT,A,AT,ATT	Intron 3	BEB T: 0.477, GIH T: 0.437
rs1209342426	C>T	Intron 3	SAS TTTTTT: 0.000
rs145525643	AT>A	Intron 3	BEB A: 0.006, GIH A: 0.010
rs10148084	G>A	Intron 3	BEB T: 0.000, GIH T: 0.010
rs60302087	C>T	Intron 3	BEB T: 0.047, GIH T: 0.029
rs533149489	C>T	Intron 3	BEB G: 0.006, GIH G: 0.000
rs940483333	C>G	Intron 2	SAS AAAAA: 0.000
rs201221729	CAA>C,CA	Intron 2	BEB AAAAAAAAA: 0.122, GIH AAAAAAAAA: 0.073
rs59354603	TAAAAA>TA,TAAAA,T	Intron 2	BEB T: 0.093, GIH T: 0.053
rs6575223	A>T	Intron 2	BEB G: 0.052, GIH G: 0.044
<b>rs3783937</b>	T>G	<b>Intron 2</b>	<b>BEB T: 0.227, GIH T: 0.335</b>
rs13379480	C>T	Intron 2	BEB G: 0.052, GIH G: 0.044
rs3783936	C>G	Intron 2	BEB C: 0.052, GIH C: 0.039
<b>rs75462826</b>	T>C	<b>Intron 2</b>	<b>BEB A: 0.110, GIH A: 0.083</b>

rs72705370	G>A	Intron 2	BEB T: 0.017, GIH T: 0.073
rs74071640	C>T	Intron 2	BEB A: 0.035, GIH A: 0.029
<b>rs13379081</b>	G>A	<b>Intron 2</b>	<b>BEB G: 0.128, GIH G: 0.078</b>
rs74071641	A>G	Intron 2	BEB C: 0.052, GIH C: 0.034
rs572342789	G>C	Intron 2	BEB T: 0.000, GIH T: 0.010
rs186775729	G>T	Intron 2	BEB A: 0.000, GIH A: 0.010
rs60976221	G>A	Intron 2	BEB G: 0.035, GIH G: 0.029
rs8014548	T>G	Intron 2	BEB C: 0.035, GIH C: 0.019
rs113167395	T>C	Intron 2	BEB T: 0.000, GIH T: 0.010
rs17127768	A>T	Intron 1	BEB C: 0.047, GIH C: 0.019
rs561605840	T>C	Intron 1	BEB A: 0.006, GIH A: 0.000
rs17127770	C>A	Intron 1	BEB C: 0.047, GIH C: 0.019
rs117570884	T>C	Intron 1	BEB C: 0.047, GIH C: 0.019
rs78470618	T>C	Intron 1	BEB T: 0.035, GIH T: 0.029
rs977019613	A>T	Intron 1	SAS CCCCC: 0.000
rs572665463	TCC>T,TC	Intron 1	BEB A: 0.000, GIH A: 0.000
rs114159189	C>A	Intron 1	BEB T: 0.035, GIH T: 0.029
<b>rs12432450</b>	C>T	<b>Intron 1</b>	<b>BEB T: 0.448, GIH T: 0.383</b>
rs78823781	T>C	Intron 1	BEB T: 0.047, GIH T: 0.019
rs74071642	C>T	Intron 1	BEB A: 0.035, GIH A: 0.029
<b>rs72705373</b>	G>A	<b>Intron 1</b>	<b>BEB C: 0.320, GIH C: 0.461</b>
<b>rs55895055</b>	G>C	<b>Intron 1</b>	<b>BEB G: 0.366, GIH G: 0.485</b>
<b>rs10133540</b>	A>G	<b>Intron 1</b>	<b>BEB T: 0.448, GIH T: 0.383</b>
rs10144473	T>C	Intron 1	BEB G: 0.000, GIH G: 0.010
<b>rs7148054</b>	A>G	<b>Intron 1</b>	<b>BEB A: 0.105, GIH A: 0.073</b>
rs8010405	G>A	Intron 1	BEB A: 0.047, GIH A: 0.029
rs7152232	C>A	Intron 1	BEB T: 0.035, GIH T: 0.029
rs1423869106	A>T	Intron 1	SAS T: 0.000
rs531351053	C>T	Intron 1	BEB A: 0.017, GIH A: 0.019
<b>rs8015218</b>	C>A	<b>Intron 1</b>	<b>BEB G: 0.448, GIH G: 0.388</b>
rs941447733	A>G	Intron 1	SAS T: 0.000
rs57271358	C>T	Intron 1	BEB C: 0.047, GIH C: 0.019
rs545285563	G>C	Intron 1	BEB AAAAAAAAAA...: 0.006, GIH AAAAAAAAAA...: 0.015
rs72705374	CAAA>C	Intron 1	BEB G: 0.070, GIH G: 0.058
rs567621074	T>G	Intron 1	BEB T: 0.000, GIH T: 0.000
rs74360508	C>T	Intron 1	BEB A: 0.093, GIH A: 0.068
rs11365622	C>A	Intron 1	SAS AAAAAAAAAA...: 0.480
rs776184182	TAAAAAAAA> T,TAATAA,TAATAA	Intron 1	SAS GGGGG: 0.000
rs72705375	TG>T	Intron 1	BEB G: 0.070, GIH G: 0.058
<b>rs34059355</b>	A>G	<b>Intron 1</b>	<b>BEB CACACACACA...: 0.430,</b>

	<b>GCACA&gt; G,GCA,GCACACA</b>		<b>GIH CACACACACA...: 0.364</b>
rs546827390 <sup>c</sup>	C>A,T	Exon 1	BEB T: 0.023, GIH T: 0.000
rs139387007 <sup>c</sup>	G>A,T	Exon 1	BEB A: 0.041, GIH A: 0.035
rs7149187 <sup>c</sup>	G>A	<b>Exon 1</b>	<b>BEB A: 0.273, GIH A: 0.388</b>
rs369441736 <sup>c</sup>	C>T	Exon 1	BEB T: 0.017, GIH T: 0.010

NC\_000014.9 GRCh38 (91869411..91947694, complement), BEB: Bengalis in Bangladesh, GIH: Gujarati Indians in Houston, MAF: Minor allele frequency, SAS: South Asians, <sup>a</sup> 3'-UTR variant, <sup>b</sup> synonymous variant, <sup>c</sup> 5'-UTR variant. The variants with MAF>0.1 are in boldface.

Of these variants, 98.44% were intronic, and 1.56% resided in the exons [0.89% in the 5'-UTR, 0.22% in the CDS, and 0.45% in the 3'-UTR] (**Figure 6.10A**). Majority of variants (83.93%) were substitutions, and 16.07% were INDELS (**Figure 6.10B**). The variants annotated to the 5'-UTR were rs369441736 (MAF=0.01, exon 1), rs7149187 (MAF=0.38, exon 1), rs139387007 (MAF=0.04, exon 1) and rs546827390 (MAF=0.02, exon 1). Only one variant was identified in the CDS, rs2430347 (MAF=0.76, exon 9), a synonymous variant located in the exon 9 of the *FBLN5* gene. We had previously observed that rs2430347 does not show any significant association with PEX.<sup>134</sup> The variants annotated to the 3'-UTR were rs115237925 (MAF=0.07, exon 11) and rs79375113 (MAF=0.07, exon 11).

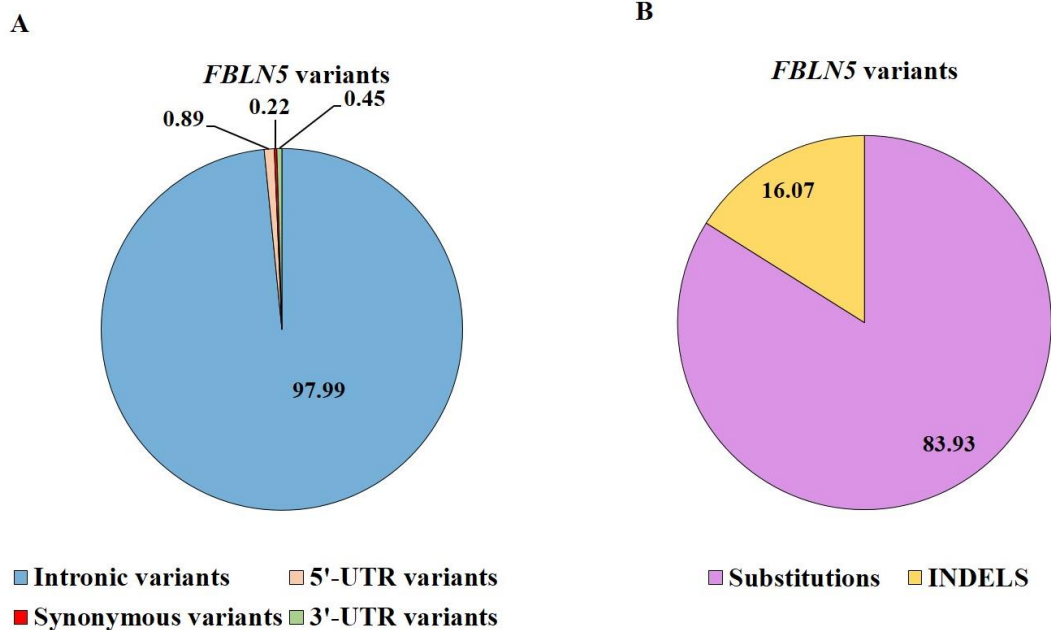


**Figure 6.10. Distribution of variants in *FBLN5* gene in controls, PEXS and PEXG. A.** Graphical representation showing the classification of the annotated variants. **B.** Graphical representation of the type of the variants in *FBLN5* gene.

A total of 91 variants with the alternate allele frequency  $\leq 0.05$  were observed in PEX patients but not in controls. **Of these variants one variant, rs115237925 is located in the 3'-UTR and 2 variants, rs546827390 and rs139387007, are located in the 5'-UTR.** The rest of the variants are intronic. Of these 91 variants, 32 variants were present in only PEXS subjects (24 substitutions- rs551213111, rs186669329, rs1041359935, rs113655279, rs139218416, rs78277125, rs181248842, rs117184514, rs749479430, rs553086593, rs117042873, rs1169008678, rs111586099, rs1188056371, rs182213115, rs370203497, rs145525643, rs10148084, rs533149489, rs572342789, rs186775729, rs113167395, rs10144473, rs57271358; 8 INDELS- rs1264847008, rs71123306, rs557153944, rs1555374875, rs555843140, rs1449735211, rs1220743148, rs773940343). 37 variants were present in only PEXG subjects (32 substitutions- rs7142368, rs76347065, rs770697680, rs559829032, rs185053478, rs77700973, rs535394332, rs776567641, rs185293777, rs182473152, rs561662280, rs555211877, rs531133150, rs969504178, rs989988440, rs547424703, rs373136895, rs556839719, rs1306195503, rs74071636, rs72705370, rs74071640, rs74071641, rs60976221, rs561605840, rs572665463, rs114159189, rs74071642, rs7152232, rs531351053, rs546827390, rs139387007; 5 INDELS- rs1366037108, rs1343595874, rs1274929866, rs537691678, rs1215020904). 22 variants (18 substitutions- rs115237925, rs72705341, rs529834011, rs974496902, rs373689829, rs17127742, rs112739092, rs79442066, rs6575223, rs13379480, rs75462826, rs8014548, rs17127768, rs17127770, rs117570884, rs78470618, rs78823781, rs7148054; 4 INDELS- rs5810562, rs1209342426, rs11365622, rs34059355) were present in both PEXS and PEXG subjects.

### 6.3.6. Single nucleotide polymorphisms identified in *CLU* gene in PEX patients

The *CLU* gene resides in chromosome 8 and has nine exons and eight introns (**Figure 6.11**).

A total of 75 annotated variants (**Table 6.7**) were observed in the *CLU* gene of the study subjects.



**Figure 6.11. Gene structure of clusterin gene.** Showing the 9 exons and 8 introns (taken from UCSC genome browser 13 April, 2023).

**Table 6.7.** List of annotated variants observed in *CLU* gene

SNP ID	Alleles	Location	MAF on 1000 Genomes project
rs9331950 <sup>a</sup>	G>A	Exon 9	<b>BEB A: 0.146, GIH A: 0.140</b>
rs9331949 <sup>a</sup>	T>C	Exon 9	<b>BEB C: 0.131, GIH C: 0.157</b>
rs150082283 <sup>a</sup>	A>G	Exon 9	BEB G: 0.029, GIH G: 0.017
rs531190008 <sup>a</sup>	G>A	Exon 9	BEB A: 0.000, GIH A: 0.000
rs9331942 <sup>a</sup>	A>G	Exon 9	<b>BEB G: 0.146, GIH G: 0.169</b>
rs1173766191 <sup>a</sup>	TC>-	Exon 9	SAS TCTCT: 0.000
rs3087554 <sup>a</sup>	T>C	Exon 9	<b>BEB C: 0.282, GIH C: 0.267</b>
rs2279590	T>C	Intron 7	<b>BEB T:0.301, GIH T:0.297</b>
rs61366982	AA>-	Intron 7	SAS -: 0.153
rs9331931	G>C	Intron 6	<b>BEB C: 0.146, GIH C: 0.140</b>
rs9331930	T>G	Intron 6	<b>BEB G: 0.146, GIH G: 0.140</b>
rs191654282	T>C	Intron 6	BEB C: 0.005, GIH C: 0.000
rs568809975	G>A	Intron 6	BEB A: 0.000, GIH A: 0.006
rs60056423	C>A	Intron 6	<b>BEB A: 0.146, GIH A: 0.140</b>
rs1027893098	CAAAA>CAA,CA,CAAAA,C	Intron 6	SAS AAAAAAAAAA: 0.00021
rs66969288	G>A	Intron 6	<b>BEB A: 0.146, GIH A: 0.140</b>
rs549493501	T>C	Intron 6	BEB C:0.000, GIH C:0.006
rs1324988552	A>-,AA	Intron 6	Not available
rs780867922	AAAAA> -,AAA,A,AA,AAAAAAAAA	Intron 6	SAS AAAAAAAAAAAAAAAAAA: 0.008
rs7812347	G>A	Intron 6	<b>BEB A: 0.146, GIH A: 0.140</b>
rs9331928	G>C	Intron 6	SAS A: 0.0004153
rs564660046	T>C	Intron 6	BEB C: 0.000, GIH C: 0.00
rs9331926	C>G	Intron 6	SAS G: 0.007
rs9331922	G>A	Intron 6	BEB A: 0.000, GIH A: 0.000
rs4732729	C>A	Intron 6	<b>BEB A: 0.563, GIH A: 0.564</b>
rs1477408059	T>-	Intron 6	SAS TTTTT: 0.000
rs1016052216	C>T	Intron 6	SAS T: 0.000

rs200376447	A>G	Intron 6	Not available
rs754448694	G>-	Intron 6	SAS GGGGG: 0.000
rs543116935 <sup>b</sup>	C>T	Exon 6	BEB T: 0.000, GIH T: 0.006
<b>rs28541694</b>	<b>C&gt;G</b>	<b>Intron 5</b>	<b>BEB G: 0.146, GIH G: 0.140</b>
rs555182137	C>T	Intron 5	BEB T: 0.000, GIH T: 0.012
<b>rs9331916</b>	<b>C&gt;T</b>	<b>Intron 5</b>	<b>BEB T: 0.189, GIH T: 0.145</b>
rs9331914	T>A	Intron 5	BEB A: 0.000, GIH A: 0.017
<b>rs7982<sup>b</sup></b>	<b>A&gt;G</b>	<b>Exon 5</b>	<b>BEB A: 0.291, GIH A: 0.297</b>
rs371557794 <sup>c</sup>	G>C	Exon 5	BEB C: 0.000, GIH C: 0.012
rs200681033	AA>-,A,AAA	Intron 4	SAS AAAAAAAAAAAAAAAAAA: 0.001
<b>rs9331908</b>	<b>C&gt;T</b>	<b>Intron 4</b>	<b>BEB T: 0.563, GIH T: 0.564</b>
<b>rs9331905</b>	<b>T&gt;C</b>	<b>Intron 3</b>	<b>BEB C: 0.146, GIH C: 0.128</b>
rs1306854493	CTCT>-	Intron 3	Not available
<b>rs11136000</b>	<b>T&gt;C</b>	Intron 3	<b>BEB T: 0.297, GIH T: 0.291</b>
rs6150518	AAAAAC>A	Intron 3	SAS: 0.000
<b>rs4236673</b>	<b>A&gt;G</b>	Intron 3	<b>BEB A: 0.291, GIH A: 0.297</b>
rs1465044369	A>-	Intron 3	Not available
rs35500730	AA>-,A,AAA,AAAA,AAAAA	Intron 3	SAS AAAAAAAAAAAAAAAAAA: 0.297
<b>rs11787077</b>	<b>T&gt;C</b>	<b>Intron 3</b>	<b>BEB T: 0.291, GIH T: 0.297</b>
rs538267001	C>T	Intron 3	BEB T: 0.000, GIH T: 0.006
rs117620140	G>A	Intron 3	BEB A: 0.000, GIH A: 0.000
<b>rs1532276</b>	<b>T&gt;C</b>	<b>Intron 3</b>	<b>BEB T: 0.291, GIH T: 0.297</b>
<b>rs1532277</b>	<b>T&gt;C</b>	Intron 3	<b>BEB T: 0.291, GIH T: 0.297</b>
<b>rs1532278</b>	<b>T&gt;C</b>	Intron 3	<b>BEB T: 0.291, GIH T: 0.297</b>
rs571779970	A>G	Intron 3	Not available
rs11449170	A>-,AA,AAA	Intron 2	SAS AAAAAAAAAAAAAA: 0.293
<b>rs867232</b>	<b>A&gt;G</b>	<b>Intron 2</b>	<b>BEB G: 0.146, GIH G: 0.134</b>
<b>rs867231</b>	<b>G&gt;C</b>	<b>Intron 2</b>	<b>BEB C: 0.146, GIH C: 0.134</b>
rs1315302089	G>-	Intron 2	Not available
rs9331897	G>T	Intron 2	BEB T: 0.000, GIH T: 0.000
<b>rs9331896</b>	<b>C&gt;T</b>	<b>Intron 2</b>	<b>BEB C: 0.286, GIH C: 0.291</b>
<b>rs2070926</b>	<b>C&gt;G</b>	<b>Intron 2</b>	<b>BEB C: 0.286, GIH C: 0.291</b>
rs553977649	G>A	Intron 2	BEB A: 0.005, GIH A: 0.012
rs1354595955	GGG>-	Intron 1	SAS GGG: 0.000
<b>rs867230</b>	<b>C&gt;A</b>	<b>Intron 1</b>	<b>BEB C: 0.306, GIH C: 0.302</b>
rs137998664	A>T	Intron 1	BEB T: 0.000, GIH T: 0.000
<b>rs9331888</b>	<b>C&gt;G</b>	<b>Intron 1</b>	<b>BEB G: 0.388, GIH G: 0.401</b>
rs528311520	C>G	Intron 1	BEB G: 0.000, GIH G: 0.006
rs551634059	C>A	Intron 1	BEB A: 0.000, GIH A: 0.006
rs9331883	G>C	Intron 1	BEB C: 0.000, GIH C: 0.017
<b>rs17515931</b>	<b>G&gt;T</b>	<b>Intron 1</b>	<b>BEB T: 0.277, GIH T: 0.297</b>
<b>rs34109053</b>	<b>G&gt;A</b>	<b>Intron 1</b>	<b>BEB A: 0.282, GIH A: 0.302</b>
<b>rs73231005</b>	<b>C&gt;G</b>	<b>Intron 1</b>	<b>BEB G: 0.282, GIH G: 0.302</b>
<b>rs11467299</b>	<b>GAAAA&gt;GA,G,GAA</b>	<b>Intron 1</b>	<b>BEB A: 0.291, GIH A: 0.291</b>

rs1455323160	A>G	Intron 1	SAS G: 0.0002136
rs917298922	T>-	Intron 1	SAS TTTTTTTTTT: 0.000

NC\_000008.11 GRCh38 (27596917..27614700, complement), BEB: Bengalis in Bangladesh, GIH: Gujarati Indians in Houston, MAF: Minor allele frequency, SAS: South Asians, <sup>a</sup> 3'-UTR variant, <sup>b</sup> synonymous variant, <sup>c</sup> missense variant. The variants with MAF>0.1 are in boldface.

Of these, 86.67% were intronic, and 13.33% were exonic [4% in the CDS and 9.33% in the 3'-UTR] (**Figure 6.12A**). 76% were substitutions, and 24% were INDELS (**Figure 6.12B**). No SNPs were observed in the 5'-UTR of the *CLU* gene in the study subjects. Three SNPs, rs371557794 (MAF=0.01; exon 5), rs7982 (MAF=0.70, exon 5) and rs543116935 (MAF=0.006, exon 6) were observed in the CDS of *CLU* gene of the study subjects. **The SNP rs371557794 is a missense variant, and the SNPs rs7982 and rs543116935 are synonymous variants.** Seven SNPs located in the exon 9, rs3087554 (MAF=0.26), rs1173766191 (MAF=0.00), rs9331942 (MAF=0.16), rs531190008 (MAF=0.00), rs150082283 (MAF=0.01), rs9331949 (MAF=0.15) and rs9331950 (MAF=0.14) were observed in the *CLU* gene in the study subjects.

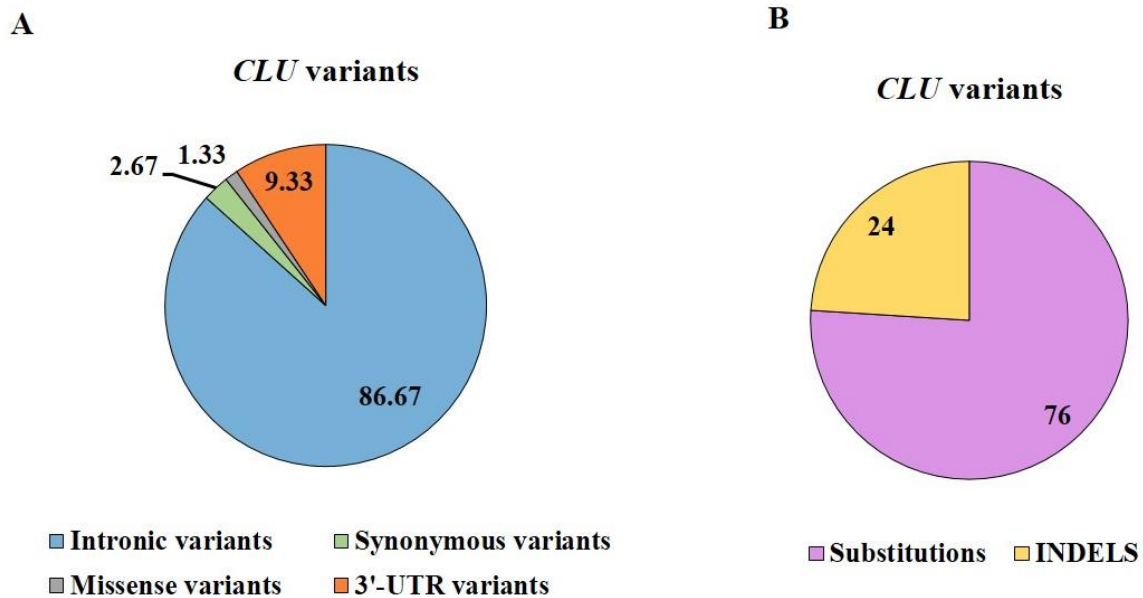


**Figure 6.12. Distribution of variants in *CLU* gene in controls, PEXS and PEXG. A.** Graphical representation showing the classification of the annotated variants. **B.** Graphical representation of the type of the variants in *CLU* gene.

A total of 8 variants with the alternate allele frequency  $\leq 0.02$  were observed in PEX patients but not in controls. One of these variants, rs1173766191, is located in the 3'-UTR and the rest of them are intronic variants. Of these 8 variants, 6 variants (4 substitutions- rs9331922, rs9331897, rs137998664, rs9331883; 2 INDELS- rs1173766191, rs1315302089) were present in only PEXS subjects and 2 variants (substitutions- rs191654282 and rs549493501) were observed in PEXG subjects.

The 3'-UTR SNP, rs3087554 was previously found to be associated with PEX.<sup>73,75</sup> The genetic association of rs9331942, rs9331949 and rs9331950 with PEX has already been detailed in chapter 3. We further analyzed the association of the synonymous variant rs7982 with PEX. The allele frequencies, odds ratio, and statistical significance are presented in **Table 6.8. The SNP rs7982 was found to be significantly associated with PEX (p=0.01).**

Although the GG genotype was more in PEX patients, it did not reach statistical significance (p=0.06). On segregating the PEX group into PEXS and PEXG, rs7982 retained its significant association with PEXS (p=0.04) and PEXG (p=0.03). No significant genotypic association was observed at rs7982 with either PEXS (p=0.12) or PEXG (p=0.17).

**Table 6.8.** Genetic association of rs7982 with PEX, PEXS, and PEXG versus control

rs7982 (A>G)	Allele freq.		OR (95%CI)	p-value	Genotype freq.			p-value
	A	G			AA	AG	GG	
Control (n=50)	0.42	0.58	1.89 (1.13-3.15)	0.01	0.26	0.32	0.42	0.06
PEX (n=94)	0.28	0.72			0.10	0.34	0.55	
PEXS (n=50)	0.28	0.72	1.86 (1.03-3.35)	0.04	0.10	0.36	0.54	0.12
PEXG (n=44)	0.27	0.73	1.93 (1.04-3.57)	0.03	0.11	0.32	0.57	0.17

### 6.3.7. Single nucleotide polymorphisms identified in the *VIM* gene in PEX patients

The human *VIM* gene resides on chromosome 10. It has 10 exons and 9 introns (**Figure 6.13**). A total of 22 annotated variants (**Table 6.9**) were observed in the *VIM* gene in the study subjects.

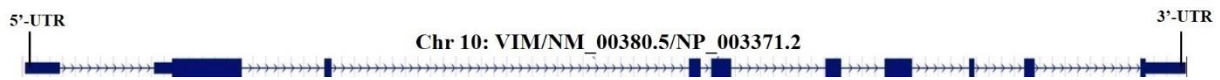


**Figure 6.13. Gene structure of vimentin gene.** Showing the 10 exons and 9 introns (taken from UCSC genome browser 13 April, 2023).

**Table 6.9.** List of annotated variants identified in the *VIM* gene

SNP ID	Alleles	Location	MAF on 1000 Genomes project
rs41289325	T>C	Intron-1	BEB C: 0.029, GIH C: 0.034
<b>rs3758412</b>	<b>A&gt;C,G</b>	<b>Intron-1</b>	<b>BEB G: 0.180, GIH G: 0.184</b>
rs144610656	C>G,T	Intron-1	BEB T: 0.000, GIH T: 0.000
<b>rs3758411</b>	<b>G&gt;C</b>	<b>Intron-1</b>	<b>BEB C: 0.151, GIH C: 0.150</b>
<b>rs3758410<sup>a</sup></b>	<b>G&gt;A,C</b>	<b>Exon-2</b>	<b>BEB C: 0.238, GIH C: 0.282</b>
rs531385322 <sup>b</sup>	G>A,C,T	Exon-2	BEB T: 0.000, GIH T: 0.005
rs371414928	G>A	Intron-2	BEB A: 0.017, GIH A: 0.015
rs536381508	A>G	Intron-3	BEB G: 0.000, GIH G: 0.000
rs993226292	C>T	Intron-3	SAS T: 0.000
rs11349733	TTT>-, TTTTTT	Intron-3	SAS TTTTTTTTTTTTTTTTTT: 0.000
rs546904832	T>-	Intron-3	BEB TTTT: 0.017, GIH TTTT: 0.000
rs7914640	G>A	Intron-3	BEB A: 0.081, GIH A: 0.053
rs61566686	G>A	Intron-3	BEB A: 0.029, GIH A: 0.019
<b>rs57465155</b>	<b>C&gt;T</b>	<b>Intron-5</b>	<b>BEB T: 0.180, GIH T: 0.180</b>
rs72775101	C>T	Intron-5	BEB T: 0.052, GIH T: 0.019
rs902343218	T>-,TT,TTT	Intron-5	SAS TTTTTTTTTT: 0.001
rs1348122930	C>-	Intron-6	SAS CCCC: 0.000
rs537729618	C>G	Intron-7	BEB G: 0.012, GIH G: 0.015
<b>rs165531</b>	<b>C&gt;A,G</b>	<b>Intron-8</b>	<b>SAS C: 0.380 A: 0.000 G: 0.620</b>
rs1210283238	A>-,AA	Intron-9	Not available
rs11254468	C>T	Intron-9	BEB T: 0.064 , GIH T: 0.092
rs1458319927	T>-,TT	Intron-9	SAS TTTT: 0.000

NC\_000010.11 GRCh38 (17228241..17237593), BEB- Bengalis in Bangladesh, GIH- Gujarati Indians in Houston, MAF- minor allele frequency, SAS- South Asians, <sup>a</sup> 5'-UTR variant, <sup>b</sup> synonymous variant. The variants with MAF>0.1 are in boldface.

Of these, 90.91% were intronic, and 9.1% were exonic [4.55% in the 5'-UTR and 4.55% in the CDS] (**Figure 6.14A**). Further, 77.28% were substitutions and 22.72% were INDELS (**Figure 6.14B**). One SNP in the 5'-UTR, rs3758410 (MAF=0.28), located in the exon 2 was observed in the CDS of the *VIM* gene of the study subjects. One synonymous variant, rs531385322, was observed in the exon 2 (MAF=0.005). No SNPs were observed in the 3'-UTR of the *VIM* gene in the study subjects.

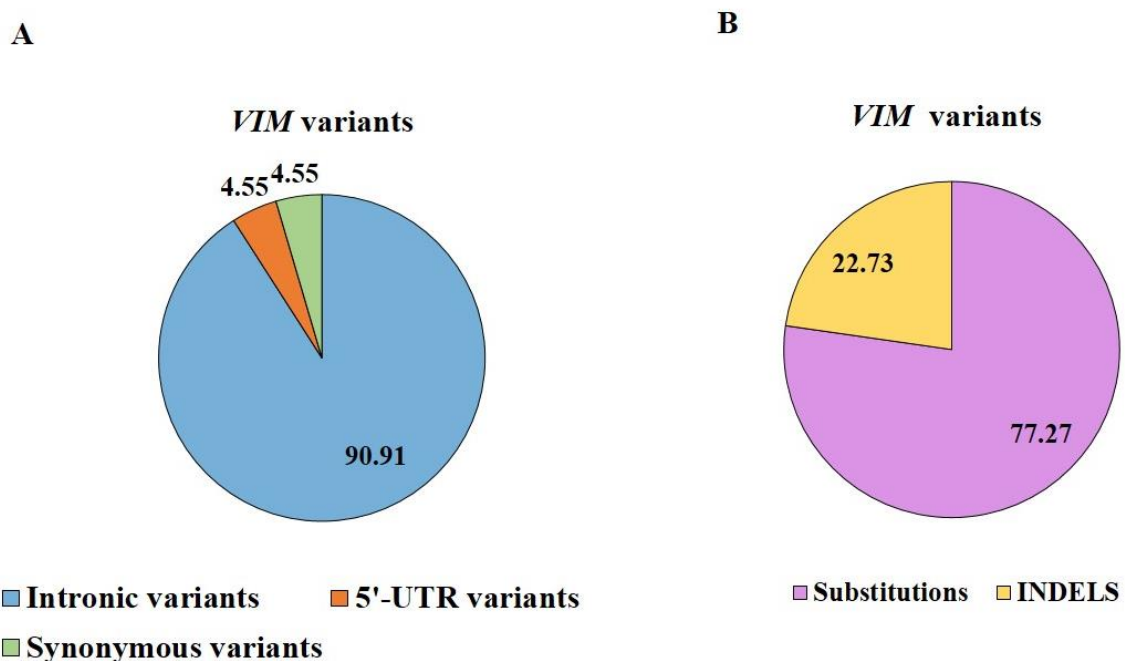


**Figure 6.14. Distribution of variants in *VIM* gene in controls, PEXS and PEXG. A.** Graphical representation showing the classification of the annotated variants. **B.** Graphical representation of the type of variants in the *VIM* gene.

A total of 7 variants with the alternate allele frequency equal to 0.01 were observed in PEX patients but not in controls. One of these variants, rs531385322, is located in the exon 2 of the gene and the rest of the variants are intronic. One variant, rs531385322 (substitution) was seen in only one PEXS subject. Of the 7 variants, 4 variants (3 substitutions- rs144610656, rs61566686, rs537729618; 1 INDEL- rs1348122930) were seen in only PEXG subjects and 2 variants (substitutions- rs41289325 and rs371414928) were seen in both PEXS and PEXG subjects.

We further analyzed the association of the 5'-UTR variant rs3758410 with PEX. The allele frequencies, odds ratio and statistical significance are presented in **Table 6.10. No significant difference in the allele frequencies was observed between PEX (p=0.79) and the controls for rs3758410.** Further, no significant difference in the genotype frequencies was observed between PEX (p=0.80). Even on segregation of the PEX group to PEXS and PEXG, no significant association was observed between PEXS (p=0.62) and control or PEXG (p=0.95) and control. No significant genotypic association was observed at rs7982 with either PEXS (p=0.48) or PEXG (p=0.74).

**Table 6.10.** Genetic association of rs3758410 with PEX, PEXS, and PEXG versus control

rs3758410 (G>C)	Allele freq.		OR (95%CI)	p- value	Genotype freq.			p- value
	G	C			GG	CG	CC	
Control (n=50)	0.90	0.10	0.95 (0.42-2.15)	0.90	0.82	0.16	0.02	0.80
PEX (n=94)	0.90	0.10			0.84	0.13	0.03	
PEXS (n=50)	0.94	0.06	0.57 (0.20-1.64)	0.29	0.90	0.08	0.02	0.48
PEXG (n=44)	0.87	0.13	1.42 (0.58-3.47)	0.43	0.78	0.18	0.04	0.74

Based on the results from sequencing of the fibulin-5, clusterin and vimentin genes, we have identified two exonic variants, rs7982 in the *CLU* gene and rs3758410 in the *VIM* gene that can be studied further in a larger sample size to establish their association with PEX.

## 6.4. Discussion

Identifying a robust biomarker that can help detect PEX at its early stages or even identify PEX patients with a risk of glaucoma will aid in preventing the debilitating effects of vision loss and ocular tissue damages accompanying PEXG Compared with the genetic risk

factors, biomarkers for PEX are less well characterized. Identifying the etiology and risk factors associated with PEX and developing novel biomarkers for the detection and prognosis of this disease at multiple stages of disease progression is, therefore, essential. There have been various attempts to identify biomarkers for PEX disease. Kondkar et al. showed that plasma levels of the cytokine TNF $\alpha$  have a 77.7% probability of distinguishing between PEXG and non-glaucomatous controls.<sup>270</sup> Demirdogen et al. evaluated the tear fluid and AH levels of CTGF in PEXS and PEXG. Although significant elevation of CTGF was observed in PEX patients, it was not found to be a good classifier for either PEXS or PEXG and thus, can't be used as a biomarker.<sup>271</sup> Multiple reports have suggested that the levels of various extracellular matrix (ECM) proteins and cytokines significantly differed in PEXG compared to PEXS (summarised in **Table 6.11**). The multifunctional cytokine, Transforming growth factor  $\beta$ , is consistently increased in PEX patients. TGF $\beta$ 1 performs various biological functions including ECM maintenance. It promotes the synthesis and secretion of matrix proteins and decreases matrix degradation. An aberrant increase of TGF $\beta$ 1 in PEX might result in an uncontrolled build-up of ECM components resulting in their aggregation in the exfoliative material.

**Table 6.11.** A sub-set of molecules that are differentially regulated in PEX

S. No.	Molecule	Function	Model and technique	Status in PEX
1.	Tumor growth factors (TGF $\beta$ )	It regulates ECM gene expression and contributes to tissue fibrosis.	Aqueous humor; ELISA  Aqueous humor; Multiplex bead system	TGF $\beta$ 1 is significantly increased in both PEXS and PEXG compared to controls. <sup>272</sup>  TGF $\beta$ 1, TGF $\beta$ 2, and TGF $\beta$ 3 are increased in both PEXS and PEXG compared to controls. <sup>113</sup>
2.	Other cytokines/chemokines	They aid in cell-cell communications. Pro-	Aqueous humor; multiplex bead immunoassay.	IL-6 and IL-8 increased in early PEXS compared to the controls, but no changes in PEXG

		inflammatory cytokines contribute to abnormal ECM production.		compared to controls. <sup>273</sup>
3.	Matrix metalloproteinases (MMPs)	They hydrolyze ECM components and contribute to ECM turnover.	Aqueous humor; enzyme immunoassays	MMP-2 and MMP-3 increased in PEXS and PEXG compared to controls. <sup>49</sup>
4.	Connective tissue growth factor	It is an inducer of ECM protein expression.	Aqueous humor; ELISA	Increased levels in PEXG compared to PEXS and controls. <sup>114,274</sup>
5.	Klotho	It is an anti-aging protein that has anti-oxidant properties.	Aqueous humor and serum; ELISA	Decreased in PEXS compared to controls and decreased in PEXG compared to both PEXS and PEXG. <sup>275</sup>
6.	Endothelin-1	It is a vasoconstrictor that regulates IOP.	Aqueous humor and serum; ELISA  Aqueous humor	Increased in PEXS and PEXG compared to controls. <sup>275</sup>  Increased in PEXG compared to PEXS. <sup>275</sup>

Although a cytoplasmic protein, VIM is secreted into the extracellular milieu during cell activation, apoptosis and stress among other scenarios.<sup>276,277</sup> The presence of higher levels of VIM in the aqueous humor of PEXS and PEXG individuals compared to controls is being reported for the first time with this study and might imply augmented cellular stress. The exact source of VIM in aqueous humor is unclear, but any tissue in contact with the AH could contribute to the increased levels of VIM in AH. Our study shows that the lens capsule tissue could be one source for the increased presence of VIM in AH. ROC analysis showed that VIM levels of AH have a 66.5% probability of distinguishing PEXS and a 76.6% probability of distinguishing PEXG from controls. AH VIM levels are a fair classifier of PEXG. Previously, Demirdogen et al. reported that the clusterin levels in AH were significantly higher in PEXG than in PEXS when compared to control and were seen to be a

good classifier to distinguish PEXG from PEXS.<sup>267</sup> However, accessing aqueous humor poses certain difficulties as it involves an invasive procedure, and is limited to subjects undergoing an intraocular surgery and can sometimes complicate the surgery if proper care is not taken.

Peripheral blood proves to be a minimally invasive source for detecting disease biomarkers, and plasma was seen to be more sensitive in detecting of biomarkers compared to serum.<sup>278</sup> Therefore, we checked the levels of VIM, CLU, and FBLN5 in the plasma of our study subjects. Fibulin-5 is a matricellular scaffold protein that deposits LOXL1 in the ECM and plays an important role in elastogenesis. We previously observed a decreased fibulin-5 in the lens capsule of PEXS individuals compared to the controls, which could contribute to a destabilized ECM in PEX patients.<sup>134</sup> Recently, Rebecca et al. observed increased fibulin-5 in the aqueous humor of PEXS and PEXG individuals through western blotting.<sup>77</sup> However, in this study, we did not observe any statistically significant differences in the plasma fibulin-5 levels in patients compared to the controls.

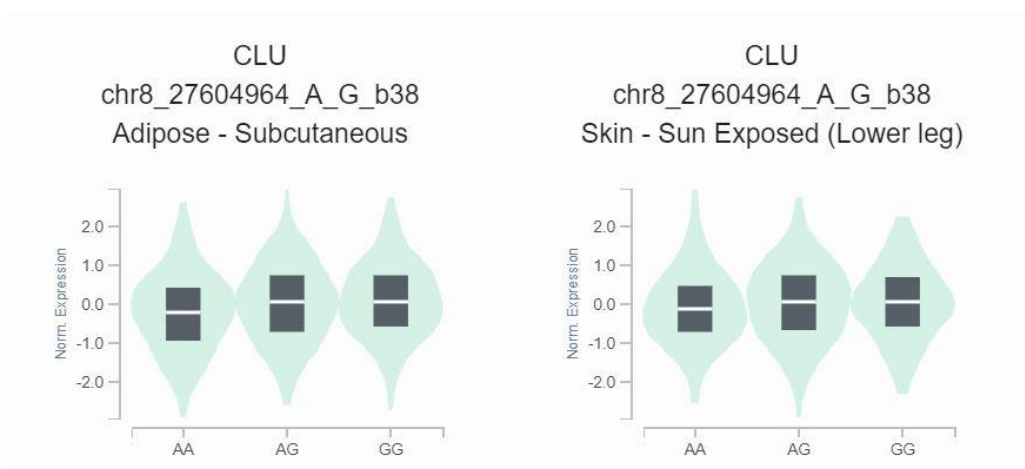
CLU plasma levels were significantly higher in PEXS but not in PEXG compared to the controls in this study. Previously, Yavrum *et al.* observed increased CLU levels in serum of PEXS and PEXG individuals compared to the controls. However, these differences were not found to be statistically significant.<sup>279</sup> Recently, Rebecca and co-workers reported increased clusterin in the lens capsule and aqueous humor of PEXS individuals.<sup>77</sup> Increased circulating CLU in the plasma in PEXS and its influx through the blood-aqueous barrier could contribute to the increased CLU deposits seen in XFM throughout the body, including the ocular tissues. However, this increase of CLU in PEXS did not prove to be a good diagnostic marker, as the AUC showed only a 60.2% probability of distinguishing PEXS from controls. Although we and others have reported increased CLU in the aqueous humor of PEXG, in this study, no significant difference in the levels of plasma CLU was observed

in PEXG compared to the controls.<sup>75,267</sup> However, surprisingly, the plasma levels of CLU were considerably higher in PEXS compared to PEXG, in contrast to what was observed in lens capsule and aqueous humor in previously reported studies.<sup>75,78</sup> This could be due to tissue-specific changes in the advanced stage of the disease which needs in-depth study. Tissue-specific regulatory mechanisms and differential gene expression in the early and advanced stages of PEX have been reported previously.<sup>273,280</sup> Also, differences in ethnicities could be another reason for the variations in results from different research groups.

We observed that the plasma VIM was significantly higher in both PEXS and PEXG compared to the controls. VIM levels in plasma have a 71.3% probability of distinguishing PEXS and an 87.7% probability of distinguishing PEXG from controls. Thus, plasma levels of VIM proved to be a fair and a good classifier of PEXS and PEXG, respectively. Further, plasma VIM levels were higher in PEXG than PEXS showing that plasma VIM levels have the potential to differentiate the severe stage of the disease, PEXG from PEXS with a 71.6% probability. VIM proves to be a robust classifier for PEX from controls with plasma serving as a better source than AH. This is the first study quantifying the levels of VIM in aqueous humor and plasma of pseudoexfoliation syndrome and pseudoexfoliation glaucoma patients. As VIM is induced under stress conditions, the substantial increase of its levels in both aqueous humor and plasma of the severe advanced stage of PEXG might be due to immense stress, such as impaired proteostasis and oxidative stress in PEXG.

This study might have some limitations pertaining to the number of subjects included for the analysis, which could not be avoided because of the limited availability of study subjects. However, owing to the significant differences between the groups analyzed, the power analysis showed that the sample size was sufficient to obtain statistically good results. A replication study with a larger sample size and in a greater number of populations should be conducted to gain more confidence in utilizing vimentin as a biomarker for PEXG.

We further initiated a pilot study to identify novel variants in *FBLN5*, *CLU*, and *VIM* genes that might be associated as risk factors with PEX. Complete gene sequencing of the three genes showed that the majority of variants were intronic and substitutions presided over insertions or deletions. We found a significant association of the synonymous variant, rs7982 with PEXS and PEXG. He *et al.* reported the genetic association of rs7982 with Alzheimer’s disease and showed an allele-specific expression of *CLU* in the temporal cortex of the AD brain.<sup>281</sup> Han *et al.* observed that rs7982 participates in alternate splicing and is associated with intron retention in different regions of the brain’s temporal lobe.<sup>282</sup> Further, rs7982 was found to be significantly associated with A $\beta$  deposition in cingulate, frontal cortex and standardized uptake value ratio of the AD brain. The subjects carrying the ‘GG’ genotype at rs7982 had the most A $\beta$  deposition than AG while those with ‘AA’ genotype showed the least A $\beta$  deposition.<sup>186</sup> The 1000 Genomes Project data on the Ensembl database recorded that the frequency of the risk allele ‘G’ at rs7982 is the highest in the East Asian population (79.0%), followed by South Asian (72.0%), American (66.0%), European (61.0%), and African (57.0%) populations. The eQTL data from the GTeX database showed a significant increase in clusterin expression in different tissues from individuals with the ‘GG’ genotype compared to those with the ‘AA’ genotype (**Figure 6.15**).



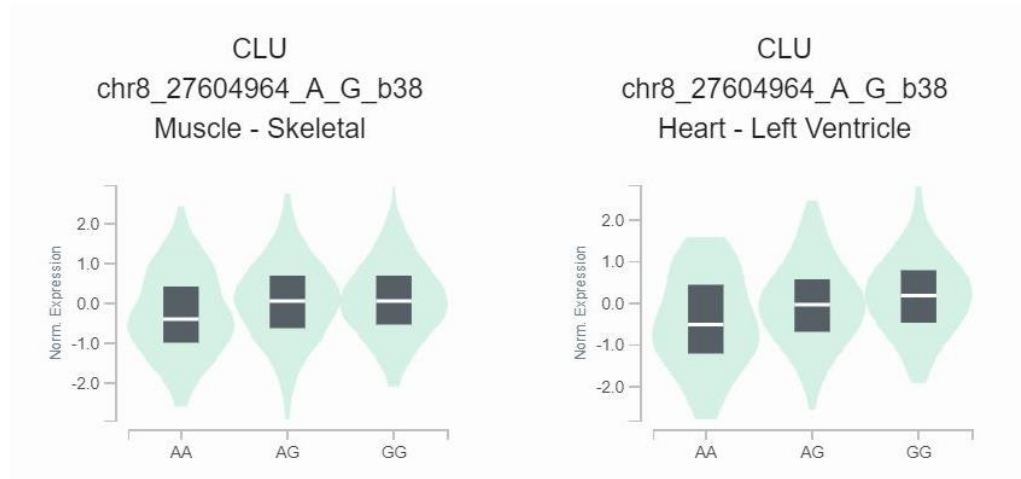


**Figure 6.15. rs7982 is an eQTL for CLU expression.** The eQTL violin plot obtained from the GTex portal shows that tissue with homozygous alternate genotype ‘GG’ at rs7982 shows increased CLU expression ( $p < 0.001$ ) compared to the homozygous reference genotype ‘AA’.

The complete sequencing of the *VIM* gene identified an exonic variant rs3758410 with a reported MAF > 0.1. With the limited sample size in our study we did not observe any significant difference in the allele frequencies at rs3758410 between PEX patients and controls. The 1000 Genomes Project data on the Ensembl database recorded that the frequency of the minor allele ‘C’ at rs3758410 is the highest in the African population (70.0%), followed by American (41.0%), East Asian (31%), European (31%), and South Asian (26.0%) populations. The eQTL data from the GTeX database showed a significant increase in vimentin expression in different tissues from individuals with the ‘CC’ genotype compared to those with the ‘GG’ genotype (**Figure 6.16**).

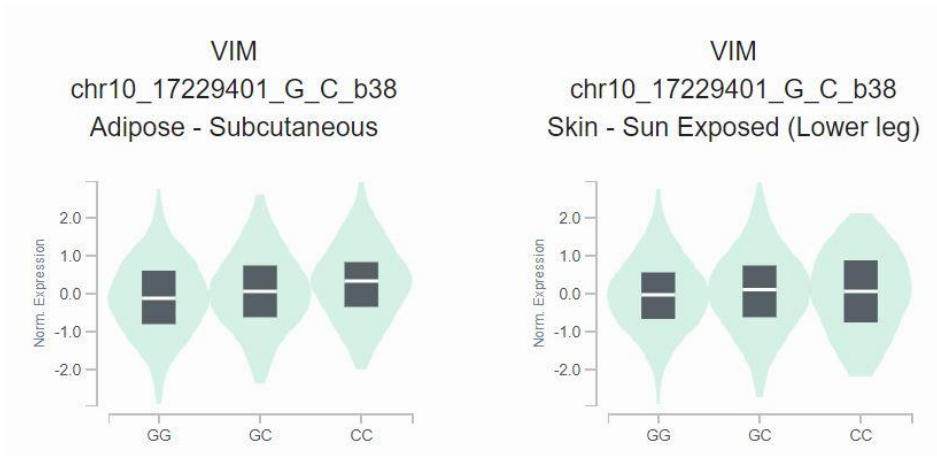


**Figure 6.16. rs3758410 is an eQTL for *VIM* expression.** The eQTL violin plot obtained from the GTex portal shows that tissue with homozygous alternate genotype ‘CC’ at rs3758410 shows increased *CLU* expression ( $p < 0.001$ ) compared to the homozygous reference genotype ‘GG’.

More number of samples needs to be added to the study to establish the genetic association of rs7982 and rs3758410 with the PEX pathology along with following up with other variants, and this work is in progress in the lab.

\*\*\*\*\*

## *Chapter 7*

# **Conclusions and future perspectives**

## 7. Conclusions and future perspectives

Pseudoexfoliation is a protein aggregopathy with multiple factors involved in its pathophysiology. Both genetic and epigenetic changes bring about the pathological phenotypes observed in PEX. This thesis reports the genetic and/or epigenetic regulation of four candidate genes, *FBLN5*, *CLU*, *GSTs*, and *VIM* in PEX pathology.

### 7.1. Role of fibulin-5 polymorphisms in pseudoexfoliation pathology

Fibulin-5 (FBLN5) is a matricellular protein crucial for the maintenance of the elasticity of the ECM. It is important for the activation of LOXL1 and the deposition of elastin fibrils for elastogenesis. FBLN5 knock-out mice exhibit numerous ECM defects and loss of elasticity due to dysregulation of FBLN5, leading to various elastinopathies such as pelvic organ prolapse, cutis laxa, and Charcot-Marie-Tooth disease. Missense mutations in fibulin-5 associated with cutis laxa or age-related macular degeneration have been reported to cause secretion defects.<sup>283</sup> Stone *et al.* have reported that missense variants in *FBLN5* are associated with age-related macular degeneration.<sup>145</sup> We previously reported downregulation of FBLN5 in PEXS lens capsule and novel genetic association of rs7149187 (5'-UTR) and rs929608 (10<sup>th</sup> intron) with PEXS and PEXG. These polymorphisms, however, did not exhibit an allele-specific regulatory effect.<sup>134</sup>

In the current study, we identified a genetic association of two polymorphisms, rs17732466 (4<sup>th</sup> intron) and rs72705342 (6<sup>th</sup> intron), with PEXG but not PEXS from a set of thirteen Tag SNPs, suggesting that these variants might contribute to the pathology of the advanced stage rather than to the onset of the disease. However, haplotypes of previously associated variants and the SNPs found to be associated with the disease from the current study were found to be associated with PEXS as well as PEXG. Thus, minor effects from these variants and other

known and unknown risk factors might synergistically manifest the disease. Luciferase reporter assays showed that alleles at rs72705342 could differentially regulate gene expression and, the risk allele at rs72705342 decreased *FBLN5* promoter activity compared to the protective allele. Also, this variant showed binding to two transcription factors, TFII I and GR- $\alpha$ . Although, *FBLN5* expression was not found to be decreased in PEXG, the allele-specific regulatory effect of rs72705342 suggests that this variant might affect the expression of distal genes that might contribute to the advanced glaucoma stage just as functional variants in other genes, such as, clusterin and *LOXLI* modulate the expression of distal genes.<sup>66,76</sup> This hypothesis, however, needs to be addressed in detail.

Further, a complete gene scan of the *FBLN5* gene in a subset of the study subjects identified 439 annotated variants. Besides the previously identified synonymous variant, rs2430347, no other CDS variants were identified in the current study set. Also, fibulin-5 plasma levels were not significantly different in PEX subjects compared to controls.

## **7.2. Regulatory mechanisms of clusterin in pseudoexfoliation pathogenesis**

Clusterin or Apolipoprotein-J is an extracellular molecular chaperone ubiquitously expressed in the tissues. Depending on the cellular conditions, CLU is either cytoprotective or cytotoxic and plays an important role in deciding the cell's fate. Dysregulation of CLU has been associated with various diseases, such as Alzheimer's, diabetes, cancers and pseudoexfoliation.<sup>177,284,285</sup> Previously, we observed a genetic association of rs2279590 (7<sup>th</sup> intron) and rs3087554 (3'-UTR) with PEX and increased levels of CLU were observed in AH of PEXG compared to controls.<sup>75</sup>

The current study reports the genetic association of two 3'-UTR variants, rs9331942 and rs9331949, with PEXS and PEXG. Both these variants are in linkage disequilibrium with the previously associated SNP, rs2279590. Both rs9331942 and rs9331949 exhibited an allele-

specific regulatory effect on gene expression. The risk alleles at rs9331942 and rs9331950 created binding sites for miR-223 and miR-1283, respectively. However, the risk alleles lead to decreased gene expression due to microRNA silencing, contrary to the increased CLU expression observed in PEX patients. We hypothesize that the expression of the target microRNAs is decreased in PEX patients leading to unchecked expression of CLU. A more robust regulatory mechanism might bypass the effect of these functional 3'-UTR variants in PEX. Also, to identify more regulatory SNPs, complete gene sequencing in a small subset of the study subjects was performed, which identified 75 annotated variants. The exonic variant rs7982 was found to be associated with PEXS and PEXG samples in the present study.

We found that the clusterin promoter is hypomethylated in PEX patients due to decreased DNA methyl transferase 1 expression resulting in increased clusterin expression in the blood cells and lens capsule of PEX patients. *In vitro* assays in human lens epithelial cells showed that hypomethylation of clusterin promoter facilitates enhanced binding of the transcription Sp1 which results in increased expression of clusterin. Thus, other than regulatory SNPs, epigenetic regulation of clusterin contributes to PEX pathogenesis.

Further, assessing the plasma clusterin levels revealed that the protein is significantly increased in the PEXS patients compared to controls. However, this increase was not found to have a diagnostic significance as it had less than a 70% probability of distinguishing between PEXS and controls accurately.

### **7.3. Regulation of glutathione-S-transferases in pseudoexfoliation**

Glutathione-S-transferases (GSTs) are enzymatic antioxidants crucial for detoxifying the cells. They are cytoprotective and aid in the reduction of oxidative stress. Glutathione-S-transferases are associated with various non-ocular and ocular diseases such as cancers, ARMD, ARC, and PEX.<sup>122,243,286</sup> We observed decreased expression of the GSTP1

isoenzyme in the LC of PEXS patients compared to controls. Increased oxidative stress has been observed in PEX eyes. The decreased GSTP1 in PEX results in impaired protective function against oxidative injury in PEXS eyes, possibly leading to an increase in reactive oxygen species that might subsequently damage the ocular tissues.

Decreased GSTP1 expression has been attributed to its promoter hypermethylation in various cancers and ocular diseases. Bisulfite sequencing to understand if the downregulation of GSTP1 in PEXS could be due to its promoter hypermethylation did not reveal any differential methylation status in PEXS versus controls in either blood or LC tissues. However, the sample size for the methylation analysis in tissues was limiting. Therefore, concluding that aberrant DNA methylation might not contribute to the reduced GSTP1 expression in PEX patients would be improper and warrants the investigation to be carried out with a larger sample size.

#### **7.4. Novel association of vimentin with pseudoexfoliation**

Vimentin (VIM) is a Type III intermediate filament whose role in PEX had not been elucidated. It supports the cytoskeleton and is also involved in maintaining protein homeostasis in a cell.<sup>198,218</sup> VIM is dysregulated in various cancers, and a missense mutation in VIM results in pulverized cataracts.<sup>190,199</sup>

In the present study, VIM was in the lens capsule and aqueous humor of PEX patients compared to the controls. We also observed increased protein aggregates in the LC of PEX patients correlated with an increased expression of the Wnt antagonist, Dickkopf-1 (DKK1). Overexpression of DKK1 in HLE B-3 cells resulted in increased protein aggregate formation. *In vitro* assays to understand the DKK1-VIM axis revealed that DKK1 regulated the VIM expression and protein aggregate formation via the Rho kinase, ROCK2.

Further, assessing the plasma and AH vimentin levels revealed that the protein is significantly increased in the PEXS and PEXG patients compared to controls. This increase was found to have a diagnostic significance. The AH VIM levels could distinguish the PEXG cases from controls with a 77% probability. Considering the limitation of accessing the AH, the analysis performed with plasma revealed that the VIM levels in plasma can distinguish both PEXS and PEXG from controls with good accuracy. The plasma VIM can distinguish PEXS from controls with a probability of 71% and PEXG with 88%. Furthermore, the plasma VIM levels were significantly higher in PEXG than in PEXS. This increase was also of diagnostic significance as the plasma VIM levels could differentiate PEXG from PEXS with a 71% accuracy. A positive correlation was observed in the plasma and AH VIM levels. These findings can help explore if plasma VIM can be a putative biomarker for PEX, as it could also differentiate between different stages of the disease.

Complete gene sequencing to identify any causal variants in vimentin revealed the presence of 22 annotated variants in a small subset of study subjects. The coding-region variants' frequency was very less ( $<0.02$ ). However, rs3758410 in the 5'-UTR was observed at a frequency of approximately 0.1 but it was not found to be genetically associated with either PEXS or PEXG with the current sample size.

## **7.5. Summary at a Glance**

Based on the findings from the current study, we propose a model (**Figure 7.1**) for PEX pathogenesis involving fibulin-5, clusterin, glutathione-S-transferase P1, and vimentin. In conclusion, this study reiterates the involvement of both genetic and epigenetic factors in PEX pathology and identifies novel risk factors and a potential biomarker for PEX.

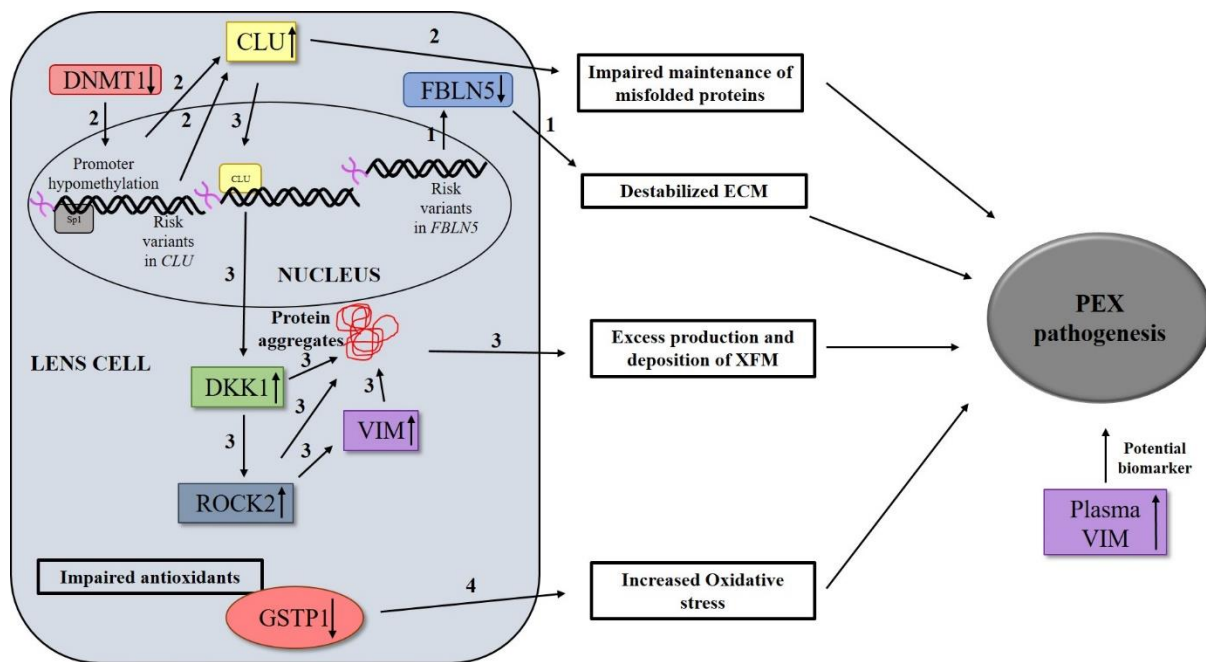


**Figure 7.1. A hypothetical model showing the factors contributing to pseudoexfoliation pathology.** Destabilized extracellular matrix (ECM) and proteotoxic stress are characteristic features of PEX. This study identified some regulatory mechanisms that might contribute to PEX pathogenesis. **(1)** The functional risk variants in fibulin-5 (*FBLN5*) affect its expression which results in a destabilized ECM. **(2)** Upregulation of clusterin might contribute to cytotoxicity by getting deposited in the exfoliative material resulting in the unavailability of the chaperone for maintaining proteostasis. Regulatory single nucleotide polymorphisms in clusterin (*CLU*) and promoter hypomethylation could be responsible for the increased expression of *CLU* in PEX pathogenesis. Hypomethylation of *CLU* promoter due to decreased expression of the DNA methyl transferase 1 (*DNMT1*) results in increased access of Sp1 to *CLU* promoter triggering its enhanced transcription. **(3)** The increased clusterin induces the expression of the Wnt antagonist Dickkopf-1 (*DKK1*), which ultimately produces toxic protein aggregates detrimental to the cell. Increase in *DKK1* results in an upregulation of the Rho kinase, *ROCK2*, which in turn regulates the expression of vimentin. This aberrant expression of these proteins contributes to the formation of exfoliative material. **(4)** In parallel, decreased expression of *GSTP1* in patients results in increased oxidative stress that adds to the impaired cytoprotective mechanisms in PEX pathogenesis.

## 7.6. Key findings from the study

- Two intronic variants, rs17732466 and rs72705342, within *FBLN5* are significantly associated with PEXG but not with PEXS.
- rs72705342 showed a significant allele-specific regulatory effect on gene expression.
- The 3'-UTR variants, rs9331942 and rs9331949 in *CLU*, are associated with PEXS and PEXG.

- Both rs9331942 and rs9331949 exhibit allele-specific regulatory effects on gene expression, and risk alleles at these variants create binding sites for miR-223 and miR-1283, respectively.
- Clusterin promoter is significantly hypomethylated in PEX patients compared to controls in blood and lens capsules which correlates with increased clusterin expression.
- CLU promoter hypomethylation correlates with decreased DNA methyl transferase 1 expression in PEX patients.
- Promoter hypomethylation facilitates enhanced binding of Sp1 to *CLU* promoter in human lens epithelial cells (HLE B-3).
- Vimentin levels are significantly higher in PEX patients compared to controls. Increased protein aggregates were observed in the LC of PEXS and PEXG compared to the controls.
- Overexpression of DKK1 leads to increased protein aggregation and ROCK2 and vimentin expression in HLE B-3 cells. DKK1 knockdown results in decreased expression of ROCK2 and vimentin. Inhibition of ROCK2 by the ROCK inhibitor, Y-27632, showed ROCK2-dependent downregulation of vimentin and decreased protein aggregates.
- GSTP1 is significantly downregulated in LC of PEXS compared to controls.
- Plasma CLU levels are significantly higher in PEXS than in the controls, but it is a poor classifier for distinguishing PEXS from controls.
- Vimentin levels in plasma and aqueous humor are significantly high in PEX patients compared to control. Plasma levels of vimentin are a good classifier for distinguishing PEXG from the controls, and a fair classifier for distinguishing PEXS from control and PEXG.

- Gene scans of fibulin-5, clusterin, and vimentin identified variants in the Indian population that can be studied further for association with PEX.

## **7.7. Future perspectives**

- Identification of novel regulatory SNPs in the fibulin-5 gene associated with PEX.
- Understand the detailed functional role of the 3'-UTR variants in the clusterin gene and the regulatory dynamics of the associated microRNAs in PEX.
- Identify more regulatory SNPs in clusterin gene associated with PEX.
- Assess the status of the GSTs in PEXG and study other regulatory epigenetic mechanisms, such as histone modifications and microRNA-mediated silencing on GSTP1 in PEX.
- Study the effect of DKK1 upregulation on other cellular pathways, such as apoptosis, autophagy, amyloid fiber formation through transcriptome analysis in DKK1 overexpressed cells.
- Identify novel regulatory SNPs in vimentin gene in association with PEX and study the association of rs7982 and rs3758410 with PEX in an extensive sample set.

\*\*\*\*\*

## *Chapter 8*

### **References**

## 8. References

1. Ritch, R. & Schlötzer-Schrehardt, U. Exfoliation syndrome. *Surv. Ophthalmol.* **45**, 265–315 (2001).
2. Ritch, R. Exfoliation syndrome and occludable angles. in *Transactions of the American Ophthalmological Society* vol. 92 845–944 (1994).
3. Ritch, R. & Schlo, U. Exfoliation ( pseudoexfoliation ) syndrome : toward a new Proceedings of the First International Think Tank. *Acta Ophthalmol Scand.* **79**, 213–217 (2001201).
4. Ringvold, A. A Preliminary Report on the Amino Acid Composition of the Pseudo-Exfoliation Material (PE Material). *Exp. Eye Res* vol. 15 (1973).
5. Zenkel, M. & Schlötzer-Schrehardt, U. The composition of exfoliation material and the cells involved in its production. *J. Glaucoma* **23**, S12–S14 (2014).
6. Challa, P. & Johnson, W. M. Composition of Exfoliation Material. *J. Glaucoma* **27**, S29–S31 (2018).
7. Ringvold, A. Ultrastructure of Exfoliation Material (Busacca deposits). *Virchows Arch. Abt.A Path. Anat* vol. 350 (1970).
8. Ritch, R., Otzer-Schrehardt, U. S. & Konstas, A. G. P. Why is glaucoma associated with exfoliation syndrome? *Progress in Retinal and Eye Research* vol. 22 (2003).
9. Tarkkanen, A. & Kivelä, T. John G. Lindberg and the discovery of exfoliation syndrome. *Acta Ophthalmol Scand.* **80**, 151-154 (2002).
10. Ariga, M., Nivean, M. & Utkarsha, P. Pseudoexfoliation syndrome. *Journal of Current Glaucoma Practice* vol. 7 118–120 (2013).
11. Gartaganis, S. P., Patsoukis, N. E., Nikolopoulos, D. K. & Georgiou, C. D. Evidence for oxidative stress in lens epithelial cells in pseudoexfoliation syndrome. *Eye* **21**, 1406–1411 (2007).
12. Naumann, G. O. H., Schlötzer-Schrehardt, U. & Kuchle, M. Pseudoexfoliation syndrome for the comprehensive ophthalmologist: Intraocular and systemic manifestations. *Ophthalmology* **105**, 951–968 (1998).
13. Kuchle, M., Nguyen, N.X., Hannappel, E., Naumann, G.O. The blood-aqueous barrier in eyes with pseudoexfoliation syndrome. *Ophthalmic Res.* **27**, 136-142 (1995).
14. Johnson, D. H. & Brubaker, R. F. Dynamics of aqueous humor in the syndrome of exfoliation with glaucoma. *Am. J. Ophthalmol.* **93**, 629–634 (1982).
15. Plateroti, P., Plateroti, A. M., Abdolrahimzadeh, S. & Scuderi, G. Pseudoexfoliation Syndrome and Pseudoexfoliation Glaucoma: A Review of the Literature with Updates on Surgical Management. *J. Ophthalmol.* **2015**, (2015).
16. Desai, M. A. & Lee, R. K. The medical and surgical management of pseudoexfoliation glaucoma. *International Ophthalmology Clinics* vol. 48 95–113 (2008).
17. Shazly, T. A., Farrag, A. N., Kamel, A. & Al-Hussaini, A. K. Prevalence of pseudoexfoliation syndrome and pseudoexfoliation glaucoma in Upper Egypt. *BMC*

- Ophthalmol.* **11**, (2011).
18. Ren, R. *et al.* Clinical signs and characteristics of exfoliation syndrome and exfoliative glaucoma in Northern China. *Asia-Pacific J. Ophthalmol.* **4**, 86–88 (2015).
  19. Rao, R. Q., Arain, T. M. & Ahad, M. A. The prevalence of pseudoexfoliation syndrome in Pakistan. Hospital based study. *BMC Ophthalmol.* **6**, 1–5 (2006).
  20. Bikbov, M. M. *et al.* Prevalence and Associated Factors of Pseudoexfoliation in a Russian Population: The Ural Eye and Medical Study. *Am. J. Ophthalmol.* **210**, 158–166 (2020).
  21. Miyazaki, M. *et al.* The Prevalence of Pseudoexfoliation Syndrome in a Japanese Population The Hisayama Study. *J. Glaucoma* **14**, 482-484 (2005).
  22. Lee, S. Y. *et al.* Prevalence of Pseudoexfoliation Syndrome in an Isolated Island Population of Korea: The Woodo Study. *J. Glaucoma* **26**, 730–734 (2017).
  23. Kim, S. *et al.* Prevalence of Pseudoexfoliation Syndrome and Associated Factors in South Koreans: The Korean National Health and Nutrition Examination Survey. *Ophthalmic Epidemiol.* **23**, 298–302 (2016).
  24. Thomas, R., Nirmalan, P. K. & Krishnaiah, S. Pseudoexfoliation in Southern India: The Andhra Pradesh eye disease study. *Investig. Ophthalmol. Vis. Sci.* **46**, 1170–1176 (2005).
  25. Arvind, H. *et al.* Pseudoexfoliation in south India. *Br. J. Ophthalmol.* **87**, 1321–1323 (2003).
  26. Jonas, J. B. *et al.* Pseudoexfoliation: Normative Data and Associations. The Central India Eye and Medical Study. *PLoS One* **8**, (2013).
  27. Gupta, R. K., Sharma, R., Gupta, R. K. & Sandhu, J. S. Prevalence and Ocular Manifestations of Pseudoexfoliation Syndrome Among Patients Scheduled for Cataract Surgery in a Teaching Hospital in North India. *Int. J. of Contemp. Med. Res.* **9**, B7-B12 (2022).
  28. Kaimbo Wa Kaimbo, D. Pseudoexfoliation syndrome in Congolese patients. *J. Fr. Ophthalmol.* **35**, 40–45 (2012).
  29. Rotchford, A. P., Kirwan, J. F., Johnson, G. J. & Roux, P. Exfoliation Syndrome in Black South Africans. *Arch. Ophthalmol.* **121**, 863-870 (2003).
  30. Olawoye, O. O. *et al.* Exfoliation syndrome in Nigeria. *Middle East Afr. J. Ophthalmol.* **19**, 402–405 (2012).
  31. Melese, E. K., Shibeshi, M. A. & Sherief, S. T. Prevalence of Pseudoexfoliation Among Adults and Its Related Ophthalmic Variables in Southern Ethiopia: A Cross-Sectional Study. *Clin. Ophthalmol.* **16**, 3951–3958 (2022).
  32. Hicks, P. M. *et al.* A global genetic epidemiological review of pseudoexfoliation syndrome. *Exploration of Medicine* vol. 2 527–543 (2021).
  33. Faulkner, H. W. Pseudo-exfoliation of the lens among the navajo Indians. *Am. J. Ophthalmol.* **72**, 206–207 (1971).
  34. Cashwell, L. F. & Shields, M. B. Exfoliation Syndrome Prevalence in a Southeastern

- United States Population. *Arch. Ophthalmol.* **106**, 335-336 (1988).
35. Hicks, P. M. *et al.* Pseudoexfoliation and Cataract Syndrome Associated with Genetic and Epidemiological Factors in a Mayan Cohort of Guatemala. **2**, 1–27 (2021).
  36. Arnarsson, Á. M. Epidemiology of exfoliation syndrome in the Reykjavik eye study. *Acta Ophthalmol.* **87**, 1–17 (2009).
  37. Aasved, H. The geographical distribution of fibrilloglucosaminoglycan: so-called senile exfoliation or Pseudoexfoliation of the anterior lens capsule. *Acta Ophthalmol.* **47**, 792–810 (1969).
  38. Yildirim, N., Yasar, E., Gursoy, H. & Colak, E. Prevalence of pseudoexfoliation syndrome and its association with ocular and systemic diseases in Eskisehir, Turkey. *Int. J. Ophthalmol.* **10**, 128–134 (2017).
  39. Alfaiate, M., Leite, E., Mira, J. & Cunha-Vaz, J. G. Prevalence and surgical complications of pseudoexfoliation syndrome in Portuguese patients with senile cataract. *J. Cataract Refract. Surg.* **22**, 972–976 (1996).
  40. Schlötzer-Schrehardt, U. & Naumann, G. O. H. Ocular and Systemic Pseudoexfoliation Syndrome. *Am. J. Ophthalmol.* **141**, (2006).
  41. Taylor, R. C. & Dillin, A. Aging as an event of proteostasis collapse. *Cold Spring Harb. Perspect. Biol.* **3**, 1–17 (2011).
  42. Ovodenko, B. *et al.* Proteomic analysis of exfoliation deposits. *Investig. Ophthalmol. Vis. Sci.* **48**, 1447–1457 (2007).
  43. Janciauskiene, S. & Krakau, T. Alzheimer's peptide: A possible link between glaucoma, exfoliation syndrome and Alzheimer's disease. *Acta Ophthalmol. Scand.* **79**, 328-329 (2001).
  44. Linnér, E. *et al.* The exfoliation syndrome in cognitive impairment of cerebrovascular or Alzheimer's type. *Acta Ophthalmol. Scand* **79**, 283–285 (2001).
  45. May, C. A. Specific Densified Regions in the Postlaminal Human Glaucomatous Optic Nerve. *Open Ophthalmol. J.* **9**, 20-24 (2015).
  46. Lee, R. K. The molecular pathophysiology of pseudoexfoliation glaucoma. *Curr. Opin. Ophthalmol.* **19**, 95-101 (2008).
  47. Schl, U. M. & Koca, M. R. Syndrome Systemic Ocular Manifestation of a. *Arch* **110**, 1752–2756 (1992).
  48. Schlötzer Schrehardt, U., Küchle, M. & Naumann, G. O. H. Electron-microscopic Identification of Pseudoexfoliation Material in Extrabulbar Tissue. *Arch. Ophthalmol.* **109**, 565–570 (1991).
  49. Schlötzer-Schrehardt, U., Lommatzsch, J., Küchle, M., Konstas, A. G. P. & Naumann, G. O. H. Matrix metalloproteinases and their inhibitors in aqueous humor of patients with pseudoexfoliation syndrome/glaucoma and primary open-angle glaucoma. *Investig. Ophthalmol. Vis. Sci.* **44**, 1117–1125 (2003).
  50. Scharfenberg, E., Rauscher, F. G., Meier, P. & Hasenclever, D. Pseudoexfoliation syndrome: analysis of systemic comorbidities of 325 PEX-positive patients compared with 911 PEX-negative patients. *Graefe's Arch. Clin. Exp. Ophthalmol.* **257**, 2471–

- 2480 (2019).
51. Schumacher, S., Schlötzer-Schrehardt, U., Martus, P., Lang, W. & Naumann, G. Pseudoexfoliation syndrome and aneurysms of the abdominal aorta. *Lancet* **357**, 359–360 (2001).
  52. Wirostko, B. M. *et al.* Risk for exfoliation syndrome in women with pelvic organ prolapse: A Utah Project on Exfoliation Syndrome (UPEXS) study. *JAMA Ophthalmol.* **134**, 1255–1262 (2016).
  53. Gökce, S. E. & Gökce, M. I. Relationship between pseudoexfoliation syndrome and erectile dysfunction: A possible cause of endothelial dysfunction for development of erectile dysfunction. *Int. Braz J Urol* **41**, 547–551 (2015).
  54. Yüksel, N. *et al.* Magnetic resonance imaging of the brain in patients with pseudoexfoliation syndrome and glaucoma. *Ophthalmologica* **220**, 125–130 (2006).
  55. Stein, J. D. *et al.* Geographic and climatic factors associated with exfoliation syndrome. *Arch. Ophthalmol.* **129**, 1053–1060 (2011).
  56. Kang, J.H., Loomis, S., Wiggs, J.L., Stein, J.D., Pasquale L.R. Demographic and geographic features of exfoliation glaucoma in 2 United States-based prospective cohorts. *Ophthalmology* **119**, 27-35 (2012).
  57. Kozobolis, V. P., Papatzanaki, M., Vlachonikolis, I. G., Pallikaris, I. G. & Tsambarlakis, I. G. Epidemiology of pseudoexfoliation in the island of Crete (Greece). *Acta Ophthalmol. Scand.* **75**, 726–729 (1997).
  58. Zenkel, M. *et al.* Regulation of Lysyl Oxidase-like 1 (LOXL1) and elastin-related genes by pathogenic factors associated with pseudoexfoliation syndrome. *Investig. Ophthalmol. Vis. Sci.* **52**, 8488–8495 (2011).
  59. Kang, J. H., Loomis, S. J., Wiggs, J. L., Willett, W. C. & Pasquale, L. R. A prospective study of folate, vitamin B6, and vitamin B12 intake in relation to exfoliation glaucoma or suspected exfoliation glaucoma. *JAMA Ophthalmol.* **132**, 549–559 (2014).
  60. Dewundara, S. & Pasquale, L. R. Exfoliation syndrome: A disease with an environmental component. *Current Opinion in Ophthalmology* vol. 26 (2015).
  61. Thorleifsson, G. *et al.* Common sequence variants in the LOXL1 gene confer susceptibility to exfoliation glaucoma. *Science (80-. )*. **317**, 1397–1400 (2007).
  62. Greene, A. G., Eivers, S. B., Dervan, E. W. J., O'Brien, C. J. & Wallace, D. M. Lysyl Oxidase Like 1: Biological roles and regulation. *Experimental Eye Research* vol. 193 107975 (2020).
  63. Aboobakar, I. F., Johnson, W. M., Stamer, W. D., Hauser, M. A. & Allingham, R. R. Major review: Exfoliation syndrome; advances in disease genetics, molecular biology, and epidemiology. *Exp. Eye Res.* **154**, 88–103 (2017).
  64. Fan, B. J. *et al.* LOXL1 promoter haplotypes are associated with exfoliation syndrome in a u.s. caucasian population. *Investig. Ophthalmol. Vis. Sci.* **52**, 2372–2378 (2011).
  65. Pasutto, F. *et al.* Pseudoexfoliation syndrome-associated genetic variants affect transcription factor binding and alternative splicing of LOXL1. *Nat. Commun.* **8**,

- (2017).
66. Berner, D. *et al.* The protective variant rs7173049 at LOXL1 locus impacts on retinoic acid signaling pathway in pseudoexfoliation syndrome. *Hum. Mol. Genet.* **28**, 2531–2548 (2019).
  67. Aung, T. *et al.* Genetic association study of exfoliation syndrome identifies a protective rare variant at LOXL1 and five new susceptibility loci. *Nat. Genet.* **49**, 993–1004 (2017).
  68. Schlötzer-Schrehardt, U. *et al.* LOXL1 deficiency in the lamina cribrosa as candidate susceptibility factor for a pseudoexfoliation-specific risk of glaucoma. *Ophthalmology* **119**, 1832–1843 (2012).
  69. Greene, A. G. *et al.* Differential Lysyl oxidase like 1 expression in pseudoexfoliation glaucoma is orchestrated via DNA methylation. *Exp. Eye Res.* **201**, 108349 (2020).
  70. Ye, H. *et al.* LOXL1 hypermethylation in pseudoexfoliation syndrome in the uighur population. *Investig. Ophthalmol. Vis. Sci.* **56**, 5838–5843 (2015).
  71. Pietrobon, D. CAV2.1 channelopathies. *Pflugers Arch. Eur. J. Physiol.* **460**, 374–393 (2010).
  72. Körtje, K. H., Schlötzer-Schrehardt, U., Naumann, G. O. H. & Erb, C. Energy-Filtering Transmission Electron Microscopy (EFTEM) in the elemental analysis of pseudoexfoliation material. *Investig. Ophthalmol. Vis. Sci.* **37**, 154–162 (1996).
  73. Burdon, K. P. *et al.* Genetic analysis of the clusterin gene in pseudoexfoliation syndrome. *Mol. Vis.* **14**, 1727–1736 (2008).
  74. Krumbiegel, M. *et al.* Exploring functional candidate genes for genetic association in german patients with pseudoexfoliation syndrome and pseudoexfoliation glaucoma. *Investig. Ophthalmol. Vis. Sci.* **50**, 2796–2801 (2009).
  75. Padhy, B. *et al.* Role of an extracellular chaperone, Clusterin in the pathogenesis of Pseudoexfoliation Syndrome and Pseudoexfoliation Glaucoma. *Exp. Eye Res.* **127**, 69–76 (2014).
  76. Padhy, B., Hayat, B., Nanda, G. G., Mohanty, P. P. & Alone, D. P. Pseudoexfoliation and Alzheimer's associated CLU risk variant, rs2279590, lies within an enhancer element and regulates CLU, EPHX2 and PTK2B gene expression. *Hum. Mol. Genet.* **26**, 4519–4529 (2017).
  77. Rebecca, M. *et al.* Increased desmosine in the lens capsules is associated with augmented elastin turnover in pseudoexfoliation syndrome. *Exp. Eye Res.* **215** (2022).
  78. Can Demirdögen, B., Demirkaya-Budak, S., Özge, G. & Mumcuoğlu, T. Evaluation of Tear Fluid and Aqueous Humor Concentration of Clusterin as Biomarkers for Early Diagnosis of Pseudoexfoliation Syndrome and Pseudoexfoliative Glaucoma. *Curr. Eye Res.* **45**, 805–813 (2020).
  79. Pasutto, F. *et al.* Association of LOXL1 common sequence variants in german and italian patients with pseudoexfoliation syndrome and pseudoexfoliation glaucoma. *Investig. Ophthalmol. Vis. Sci.* **49**, 1459–1463 (2008).
  80. Karaca, I. *et al.* Evaluation of CNTNAP2 gene rs2107856 polymorphism in Turkish

- population with pseudoexfoliation syndrome. *Int. Ophthalmol.* **39**, 167–173 (2019).
81. Malukiewicz, G., Lesiewska-Junk, H., Linkowska, K., Grzybowski, T. & Kaźmierczak, K. Analysis of CNTNAP2 polymorphisms in Polish population with pseudoexfoliation syndrome. *Acta Ophthalmol.* **90**, 1–2 (2012).
  82. Fountoulakis, N. *et al.* Tissue inhibitor of metalloproteinase 4 in aqueous humor of patients with primary open angle glaucoma, pseudoexfoliation syndrome and pseudoexfoliative glaucoma and its role in proteolysis imbalance. *BMC Ophthalmol.* **13**, (2013).
  83. Tsironi, E. E. *et al.* Evaluation of MMP1 and MMP3 gene polymorphisms in exfoliation syndrome and exfoliation glaucoma. *Mol. Vis.* **15**, 2890–2895 (2009).
  84. Mossböck, G. *et al.* Role of functional single nucleotide polymorphisms of MMP1, MMP2, AND MMP9 in open angle glaucomas. *Mol. Vis.* **16**, 1764–1770 (2010).
  85. He, M., Wang, W., Han, X. & Huang, W. Matrix metalloproteinase-1 rs1799750 polymorphism and glaucoma: A meta-analysis. *Ophthalmic Genet.* **38**, 211–216 (2017).
  86. Starikova, D., Ponomarenko, I., Reshetnikov, E., Dvornyk, V. & Churnosov, M. Novel Data about Association of the Functionally Significant Polymorphisms of the MMP9 Gene with Exfoliation Glaucoma in the Caucasian Population of Central Russia. *Ophthalmic Research* vol. 64 (2021).
  87. Vessani, R. M., Ritch, R., Liebmann, J. M. & Jofe, M. Plasma homocysteine is elevated in patients with exfoliation syndrome. *Am. J. Ophthalmol.* **136**, 41–46 (2003).
  88. Tranchina, L. *et al.* Levels of plasma homocysteine in pseudoexfoliation glaucoma. *Graefe's Arch. Clin. Exp. Ophthalmol.* **249**, 443–448 (2011).
  89. Zacharaki, F. *et al.* Plasma homocysteine and genetic variants of homocysteine metabolism enzymes in patients from central greece with primary open-angle glaucoma and pseudoexfoliation glaucoma. *Clin. Ophthalmol.* **8**, 1819–1825 (2014).
  90. Nilforoushan, N. *et al.* Lack of association between the C677T single nucleotide polymorphism of the MTHFR gene and glaucoma in Iranian patients. *Acta Med. Iran.* **50**, 208–212 (2012).
  91. Khan, M. I. *et al.* Association of tumor necrosis factor alpha gene polymorphism G-308A with pseudoexfoliative glaucoma in the Pakistani population. *Mol. Vis.* **15**, 2861–2867 (2009).
  92. Fakhraie, G., Parvini, F., Ghanavi, J., Saif, S. & Farnia, P. Association of IL-10 gene promoter polymorphisms with susceptibility to pseudoexfoliation syndrome, pseudoexfoliative and primary open-angle glaucoma. *BMC Med. Genet.* **21**, 1–8 (2020).
  93. Song, Y. *et al.* Identification of a compound heterozygote in LYST gene: A case report on Chediak-Higashi syndrome. *BMC Med. Genet.* **21**, 2–6 (2020).
  94. Trantow, C. M. *et al.* Lyst mutation in mice recapitulates iris defects of human exfoliation syndrome. *Investig. Ophthalmol. Vis. Sci.* **50**, 1205–1214 (2009).
  95. Chen, Y., Bedell, M. & Zhang, K. Age-related macular degeneration: Genetic and

- environmental factors of disease. *Mol. Interv.* **10**, 271–281 (2010).
96. Parsa, N. Environmental factors inducing human cancers. *Iran. J. Public Health* **41**, 1–9 (2012).
  97. Killin, L. O. J., Starr, J. M., Shiue, I. J. & Russ, T. C. Environmental risk factors for dementia: a systematic review. *BMC Geriatr.* **16**, 1–28 (2016).
  98. Pasquale, L. R. & Kang, J. H. Lifestyle, nutrition, and glaucoma. *J. Glaucoma* **18**, 423–428 (2009).
  99. Nickells, R. W. The cell and molecular biology of glaucoma: Mechanisms of retinal ganglion cell death. *Investig. Ophthalmol. Vis. Sci.* **53**, 2476–2481 (2012).
  100. Almasieh, M., Wilson, A. M., Morquette, B., Cueva Vargas, J. L. & Di Polo, A. The molecular basis of retinal ganglion cell death in glaucoma. *Prog. Retin. Eye Res.* **31**, 152–181 (2012).
  101. Hayat, B., Kapuganti, R. S., Padhy, B., Mohanty, P. P. & Alone, D. P. Epigenetic silencing of heat shock protein 70 through DNA hypermethylation in pseudoexfoliation syndrome and glaucoma. *J. Hum. Genet.* **65**, 517–529 (2020).
  102. Drewry, M. D. *et al.* Differentially expressed microRNAs in the aqueous humor of patients with exfoliation glaucoma or primary open-angle glaucoma. *Hum. Mol. Genet.* **27**, 1263–1275 (2018).
  103. Cho, H. kyung *et al.* MicroRNA profiles in aqueous humor between pseudoexfoliation glaucoma and normal tension glaucoma patients in a Korean population. *Sci. Rep.* **12**, 1–14 (2022).
  104. Kosior-Jarecka, E. *et al.* MicroRNAs in the aqueous humor of patients with different types of glaucoma. *Graefe's Arch. Clin. Exp. Ophthalmol.* **259**, 2337–2349 (2021).
  105. Tomczyk-Socha, M., Baczyńska, D., Przeździecka-Dołyk, J. & Turno-Kręcicka, A. MicroRNA-125b overexpression in pseudoexfoliation syndrome. *Adv. Clin. Exp. Med.* **29**, 1399–1405 (2021).
  106. Tomczyk-Socha, M., Kręcicka, J., Misiuk-Hojło, M. & Turno-Kręcicka, A. MicroRNA Expression in Pseudoexfoliation Syndrome with the Use of Next-Generation Sequencing. *Genes (Basel)*. **13**, (2022).
  107. Wiggs, J. L. *et al.* Common Variants at 9p21 and 8q22 Are Associated with Increased Susceptibility to Optic Nerve Degeneration in Glaucoma. *PLoS Genet.* **8**, e1002654 (2012).
  108. Hauser, M. A. *et al.* Genetic variants and cellular stressors associated with exfoliation syndrome modulate promoter activity of a lncRNA within the LOXL1 locus. *Hum. Mol. Genet.* **24**, 6552–6563 (2015).
  109. Schmitt, H. M. *et al.* Identification and activity of the functional complex between hnRNPL and the pseudoexfoliation syndrome-associated lncRNA, LOXL1-AS1 | Human Molecular Genetics | Oxford Academic. *Human Molecular Genetics* <https://academic.oup.com/hmg/advance-article-abstract/doi/10.1093/hmg/ddaa021/5731475?redirectedFrom=fulltext> (2020).
  110. Li, H. B. *et al.* Long Non-Coding RNA-MALAT1 Mediates Retinal Ganglion Cell

- Apoptosis Through the PI3K/Akt Signaling Pathway in Rats with Glaucoma. *Cell. Physiol. Biochem.* **43**, 2117–2132 (2018).
111. Xu, Y. & Xing, Y. Q. Long non-coding RNA GAS5 contributed to the development of glaucoma via regulating the TGF- $\beta$  signaling pathway. *Eur. Rev. Med. Pharmacol. Sci.* **22**, 896–902 (2018).
  112. Meng, X. M., Nikolic-Paterson, D. J. & Lan, H. Y. TGF- $\beta$ : The master regulator of fibrosis. *Nat. Rev. Nephrol.* **12**, 325–338 (2016).
  113. Garweg, J. G., Zandi, S., Gerhardt, C. & Pfister, I. B. Isoforms of TGF- $\beta$  in the aqueous humor of patients with pseudoexfoliation syndrome and a possible association with the long-term stability of the capsular bag after cataract surgery. *Graefe's Arch. Clin. Exp. Ophthalmol.* **255**, 1763–1769 (2017).
  114. Browne, J. G. *et al.* Connective Tissue Growth Factor Is Increased in Pseudoexfoliation Glaucoma. (2011) doi:10.1167/iovs.10.
  115. Zenkel, M. *et al.* Proinflammatory cytokines are involved in the initiation of the abnormal matrix process in pseudoexfoliation syndrome/glaucoma. *Am. J. Pathol.* **176**, 2868–2879 (2010).
  116. Jelodari-Mamaghani.
  117. Roodnat, A. W. *et al.* Genome-Wide RNA Sequencing of Human Trabecular Meshwork Cells Treated with TGF- $\beta$ 1: Relevance to Pseudoexfoliation Glaucoma. *Biomolecules* **12**, 1693 (2022).
  118. Forman, H. J. & Zhang, H. Targeting oxidative stress in disease: promise and limitations of antioxidant therapy. *Nat. Rev. Drug Discov.* **20**, 689–709 (2021).
  119. Tezel, G. *Oxidative stress in glaucomatous neurodegeneration: Mechanisms and consequences.* *Progress in Retinal and Eye Research* vol. 25 (2006).
  120. Dogru, M., Kojima, T., Simsek, C. & Tsubotav, K. Potential role of oxidative stress in ocular surface inflammation and dry eye disease. *Investig. Ophthalmol. Vis. Sci.* **59**, DES163–DES168 (2018).
  121. Koliakos, G. G. *et al.* Ascorbic acid concentration is reduced in the aqueous humor of patients with exfoliation syndrome. *Am. J. Ophthalmol.* **134**, 879–883 (2002).
  122. Zenkel, M. *et al.* Differential gene expression in pseudoexfoliation syndrome. *Investig. Ophthalmol. Vis. Sci.* **46**, 3742–3752 (2005).
  123. Zenkel, M., Kruse, F. E., Naumann, G. O. H. & Schlötzer-Schrehardt, U. Impaired cytoprotective mechanisms in eyes with pseudoexfoliation syndrome/glaucoma. *Investig. Ophthalmol. Vis. Sci.* **48**, 5558–5566 (2007).
  124. Yağci, R. *et al.* Oxidative stress and protein oxidation in pseudoexfoliation syndrome. *Curr. Eye Res.* **31**, 1029–1032 (2006).
  125. Yaz, Y. A. *et al.* Role of oxidative stress in pseudoexfoliation syndrome and pseudoexfoliation glaucoma. *Turkish J. Ophthalmol.* **49**, 61–67 (2019).
  126. Kondkar, A. A. *et al.* Increased Plasma Levels of 8-Hydroxy-29-deoxyguanosine (8-OHdG) in Patients with Pseudoexfoliation Glaucoma. *J. Ophthalmol.* (2019) doi:10.1155/2019/8319563.

127. Bleich, S. *et al.* Elevated homocysteine levels in aqueous humor of patients with pseudoexfoliation glaucoma. *Am. J. Ophthalmol.* **138**, 162–164 (2004).
128. Abu-Amero, K. K., Morales, J., Mohamed, G. H., Osman, M. N. & Bosley, T. M. Glutathione S-transferase M1 and T1 polymorphisms. *Mol. Vis.* **14**, 425–430 (2008).
129. Khan, M. I. *et al.* The association of glutathione S-transferase GSTT1 and GSTM1 gene polymorphism with pseudoexfoliative glaucoma in a Pakistani population. *Mol. Vis.* **16**, 2146–2152 (2010).
130. Jansson, M., Rada, A., Tomic, L., Larsson, L. I. & Wadelius, C. Analysis of the Glutathione S-transferase M1 gene using pyrosequencing and multiplex PCR-no evidence of association to glaucoma. *Exp. Eye Res.* **77**, 239–243 (2003).
131. Yilmaz, A. *et al.* Is GST gene polymorphism a risk factor in developing exfoliation syndrome? *Curr. Eye Res.* **30**, 575–581 (2005).
132. Lesiewska, H., Malukiewicz, G., Linkowska, K. & Grzybowski, T. Analysis of SOD1 polymorphisms in Polish population with pseudoexfoliation syndrome. *Acta Ophthalmologica* vol. 93 e322–e323 (2015).
133. Hayat, B., Padhy, B., Mohanty, P. P. & Alone, D. P. Altered unfolded protein response and proteasome impairment in pseudoexfoliation pathogenesis. *Exp. Eye Res.* **181**, 197–207 (2019).
134. Padhy, B., Kapuganti, R. S., Hayat, B., Mohanty, P. P. & Alone, D. P. De novo variants in an extracellular matrix protein coding gene, fibulin-5 (FBLN5) are associated with pseudoexfoliation. *Eur. J. Hum. Genet.* **27**, 1858–1866 (2019).
135. Fraga, M. F. *et al.* Epigenetic differences arise during the lifetime of monozygotic twins. *Proc. Natl. Acad. Sci. U. S. A.* **102**, 10604–10609 (2005).
136. Yanagisawa, H., Schluterman, M. K. & Brekken, R. A. Fibulin-5, an integrin-binding matricellular protein: Its function in development and disease. *Journal of Cell Communication and Signaling* vol. 3 337–347 (2009).
137. Papke, C. L. & Yanagisawa, H. Fibulin-4 and fibulin-5 in elastogenesis and beyond: Insights from mouse and human studies. *Matrix Biology* vol. 37 142–149 (2014).
138. Lee, Y. H., Albig, A. R., Regner, M., Schiemann, B. J. & Schiemann, W. P. Fibulin-5 initiates epithelial-mesenchymal transition (EMT) and enhances EMT induced by TGF- $\beta$  in mammary epithelial cells via a MMP-dependent mechanism. *Carcinogenesis* **29**, 2243–2251 (2008).
139. Chan, W. *et al.* Fibulin-5 regulates angiopoietin-1/Tie-2 receptor signaling in endothelial cells. *PLoS One* **11**, (2016).
140. Schluterman, M. K. *et al.* Loss of fibulin-5 binding to  $\beta$ 1 integrins inhibits tumor growth by increasing the level of ROS. *DMM Dis. Model. Mech.* **3**, 333–342 (2010).
141. Cheng, S. *et al.* Adult-onset demyelinating neuropathy associated with FBLN5 gene mutation. *Clin. Neuropathol.* **36**, 171–177 (2017).
142. Jung, H. J. *et al.* Changes in expression of fibulin-5 and lysyl oxidase-like 1 associated with pelvic organ prolapse. *Eur. J. Obstet. Gynecol. Reprod. Biol.* **145**, 117–122 (2009).

143. Orriols, M. *et al.* Down-regulation of Fibulin-5 is associated with aortic dilation: Role of inflammation and epigenetics. *Cardiovasc. Res.* **110**, 431–442 (2016).
144. Šafka Brožková, D. *et al.* Czech family confirms the link between FBLN5 and Charcot-Marie-Tooth type 1 neuropathy. *Brain* vol. 136 (2013).
145. Stone, E. M. *et al.* Missense Variations in the Fibulin 5 Gene and Age-Related Macular Degeneration. *N. Engl. J. Med.* **351**, 346–353 (2004).
146. Claus, S. *et al.* A p.C217R mutation in fibulin-5 from cutis laxa patients is associated with incomplete extracellular matrix formation in a skin equivalent model. *J. Invest. Dermatol.* **128**, 1442–1450 (2008).
147. Khadzhieva, M. B. *et al.* Fibulin-5 (FBLN5) gene polymorphism is associated with pelvic organ prolapse. *Maturitas* **78**, 287–292 (2014).
148. Wlazlinski, A. *et al.* Downregulation of several fibulin genes in prostate cancer. *Prostate* **67**, 1770–1780 (2007).
149. Manders, D. B. *et al.* Dysregulation of fibulin-5 and matrix metalloproteases in epithelial ovarian cancer. *Oncotarget* **9**, 14251–14267 (2018).
150. Hu, Z. *et al.* Fibulin-5 is down-regulated in urothelial carcinoma of bladder and inhibits growth and invasion of human bladder cancer cell line 5637. *Urol. Oncol. Semin. Orig. Investig.* **29**, 430–435 (2011).
151. Yue, W. *et al.* Fibulin-5 suppresses lung cancer invasion by inhibiting matrix metalloproteinase-7 expression. *Cancer Res.* **69**, 6339–6346 (2009).
152. Schiemann, W. P., Blobel, G. C., Kalume, D. E., Pandey, A. & Lodish, H. F. Context-specific effects of Fibulin-5 (DANCE/EVEC) on cell proliferation, motility, and invasion. Fibulin-5 is induced by transforming growth factor- $\beta$  and affects protein kinase cascades. *J. Biol. Chem.* **277**, 27367–27377 (2002).
153. Schlotzer-Schrehardt, U. Genetics and genomics of pseudoexfoliation syndrome/glaucoma. *Middle East Afr. J. Ophthalmol.* **18**, 30–36 (2011).
154. Want, A. *et al.* Autophagy and Mitochondrial Dysfunction in Tenon Fibroblasts from Exfoliation Glaucoma Patients. 1–21 (2016) doi:10.1371/journal.pone.0157404.
155. Wirostko, B. M. *et al.* Risk for exfoliation syndrome in women with pelvic organ prolapse: A Utah Project on Exfoliation Syndrome (UPEXS) study. *JAMA Ophthalmol.* **134**, 1255–1262 (2016).
156. Kozobolis, V. P. *et al.* Correlation between age-related macular degeneration and pseudoexfoliation syndrome in the population of Crete (Greece). *Arch. Ophthalmol.* **117**, 664–669 (1999).
157. Andley, U. P., Rhim, J. S., Chylack, L. T. & Fleming, T. P. Propagation and immortalization of human lens epithelial cells in culture. *Investig. Ophthalmol. Vis. Sci.* **35**, 3094–3102 (1994).
158. Kuang, P. P., Joyce-Brady, M., Zhang, X. H., Jean, J. C. & Goldstein, R. H. Fibulin-5 gene expression in human lung fibroblasts is regulated by TGF- $\beta$  and phosphatidylinositol 3-kinase activity. *Am. J. Physiol. - Cell Physiol.* **291**, (2006).
159. Kobayashi, N. *et al.* A comparative analysis of the fibulin protein family: Biochemical

- characterization, binding interactions, and tissue localization. *J. Biol. Chem.* **282**, 11805–11816 (2007).
160. Auer-Grumbach, M. *et al.* Fibulin-5 mutations link inherited neuropathies, age-related macular degeneration and hyperelastic skin. *Brain* **134**, 1839–1852 (2011).
  161. Hu, Q., Reymond, J. L., Pinel, N., Zobot, M. T. & Urban, Z. Inflammatory destruction of elastic fibers in acquired cutis laxa is associated with missense alleles in the elastin and fibulin-5 genes. *J. Invest. Dermatol.* **126**, 283–290 (2006).
  162. Farwick, A. *et al.* Variations in five genes and the severity of age-related macular degeneration: Results from the Muenster aging and retina study. *Eye* **23**, 2238–2244 (2009).
  163. Tang, S. M. *et al.* Association of the PAX6 gene with extreme myopia rather than lower grade myopias. *Br. J. Ophthalmol.* **102**, 570–574 (2018).
  164. Murphy, B. F., Kirszbaum, L., Walker, I. D. & d'Apice, J. F. Sp-40,40, a newly identified normal human serum protein found in the SC5b-9 complex of complement and in the immune deposits in glomerulonephritis. *J. Clin. Invest.* **81**, 1858–1864 (1988).
  165. Miners, J. S., Clarke, P. & Love, S. Clusterin levels are increased in Alzheimer's disease and influence the regional distribution of A $\beta$ . *Brain Pathol.* **27**, 305–313 (2017).
  166. Van Luijn, M. M. *et al.* Elevated expression of the cerebrospinal fluid disease markers chromogranin a and clusterin in astrocytes of multiple sclerosis white matter lesions. *J. Neuropathol. Exp. Neurol.* **75**, 86–98 (2016).
  167. Suuronen, T., Nuutinen, T., Ryhänen, T., Kaarniranta, K. & Salminen, A. Epigenetic regulation of clusterin/apolipoprotein J expression in retinal pigment epithelial cells. *Biochem. Biophys. Res. Commun.* **357**, 397–401 (2007).
  168. Shannan, B. *et al.* Challenge and promise: Roles for clusterin in pathogenesis, progression and therapy of cancer. *Cell Death Differ.* **13**, 12–19 (2006).
  169. Leskov, K. S., Klokov, D. Y., Li, J., Kinsella, T. J. & Boothman, D. A. Synthesis and functional analyses of nuclear clusterin, a cell death protein. *J. Biol. Chem.* **278**, 11590–11600 (2003).
  170. Giannakopoulos, P. *et al.* Possible neuroprotective role of clusterin in Alzheimer's disease: A quantitative immunocytochemical study. *Acta Neuropathol.* **95**, 387–394 (1998).
  171. Yerbury, J. J. *et al.* The extracellular chaperone clusterin influences amyloid formation and toxicity by interacting with prefibrillar structures. *FASEB J.* **21**, 2312–2322 (2007).
  172. Creasey, R. *et al.* Detecting protein aggregates on untreated human tissue samples by atomic force microscopy recognition imaging. *Biophys. J.* **99**, 1660–1667 (2010).
  173. Zenkel, M., Kruse, F. E., Jünemann, A. G., Naumann, G. O. H. & Schlötzer-Schrehardt, U. Clusterin deficiency in eyes with pseudoexfoliation syndrome may be implicated in the aggregation and deposition of pseudoexfoliative material. *Investig. Ophthalmol. Vis. Sci.* **47**, 1982–1990 (2006).

174. Szymanski, M., Wang, R., Bassett, S. S. & Avramopoulos, D. Alzheimer's risk variants in the clusterin gene are associated with alternative splicing. *Transl. Psychiatry* **1**, e18-7 (2011).
175. Lin, Y. L. *et al.* Genetic polymorphisms of clusterin gene are associated with a decreased risk of Alzheimer's disease. *Eur. J. Epidemiol.* **27**, 73–75 (2012).
176. Serrano, A. *et al.* Regulation of clusterin expression in human cancer via DNA methylation. *Tumor Biol.* **30**, 286–291 (2009).
177. Rauhala, H. E., Porkka, K. P., Saramäki, O. R., Tammela, T. L. J. & Visakorpi, T. Clusterin is epigenetically regulated in prostate cancer. *Int. J. Cancer* **123**, 1601–1609 (2008).
178. Yang, G. *et al.* Epigenetic and immunohistochemical characterization of the Clusterin gene in ovarian tumors. *Arch. Gynecol. Obstet.* **287**, 989–995 (2013).
179. Hellebrekers, D. M. E. I. *et al.* Identification of epigenetically silenced genes in tumor endothelial cells. *Cancer Res.* **67**, 4138–4148 (2007).
180. Xu, Z. & Taylor, J. A. SNPinfo: Integrating GWAS and candidate gene information into functional SNP selection for genetic association studies. *Nucleic Acids Res.* **37**, 600–605 (2009).
181. Gross, C. *et al.* Contribution of the transcription factors Sp1/Sp3 and AP-1 to clusterin gene expression during corneal wound healing of tissue-engineered human corneas. *Int. J. Mol. Sci.* **22**, (2021).
182. Jin, G. & Howe, P. H. Regulation of clusterin gene expression by transforming growth factor  $\beta$ . *J. Biol. Chem.* **272**, 26620–26626 (1997).
183. Doudevski, I. *et al.* Clusterin and complement activation in exfoliation glaucoma. *Investig. Ophthalmol. Vis. Sci.* **55**, 2491–2499 (2014).
184. Dubey, S. K. *et al.* Evaluation of Genetic Polymorphisms in Clusterin and Tumor Necrosis Factor-Alpha Genes in South Indian Individuals with Pseudoexfoliation Syndrome. *Curr. Eye Res.* (2015) doi:10.3109/02713683.2014.997884.
185. Wang, H. Z. *et al.* Validating GWAS-Identified Risk Loci for Alzheimer's Disease in Han Chinese Populations. *Mol. Neurobiol.* **53**, 379–390 (2016).
186. Tan, L. *et al.* Effect of CLU genetic variants on cerebrospinal fluid and neuroimaging markers in healthy, mild cognitive impairment and Alzheimer's disease cohorts. *Sci. Rep.* **6**, 1–12 (2016).
187. Yu, J. T. *et al.* Genetic variation in Clusterin gene and Alzheimer's disease risk in Han Chinese. *Neurobiol. Aging* **34**, 1921.e17-1921.e23 (2013).
188. Mullany, S. *et al.* RNA Sequencing of Lens Capsular Epithelium Implicates Novel Pathways in Pseudoexfoliation Syndrome. *Invest. Ophthalmol. Vis. Sci.* **63**, 26 (2022).
189. Su, L. *et al.* Role of vimentin in modulating immune cell apoptosis and inflammatory responses in sepsis. *Sci. Rep.* **9**, 1–14 (2019).
190. Satelli, A. & Li, S. Vimentin as a potential molecular target in cancer therapy Or Vimentin, an overview and its potential as a molecular target for cancer therapy. *Cell Mol Life Sci.* **68**, 3033–3046 (2011).

191. Handra-Luca, A. *et al.* Tumour epithelial vimentin expression and outcome of pancreatic ductal adenocarcinomas. *Br. J. Cancer* **104**, 1296–1302 (2011).
192. Liu, L. K. *et al.* Upregulation of vimentin and aberrant expression of E-cadherin/B-catenin complex in oral squamous cell carcinomas: Correlation with the clinicopathological features and patient outcome. *Mod. Pathol.* **23**, 213–224 (2010).
193. Wei, J. *et al.* Overexpression of vimentin contributes to prostate cancer invasion and metastasis via Src regulation. *Anticancer Res.* **28**, 327–334 (2008).
194. Zhao, W. *et al.* Clinical significance of vimentin expression and her-2 status in patients with gastric carcinoma. *Clin. Transl. Sci.* **6**, 184–190 (2013).
195. Kidd M.E., Shumaker D.K., Ridge K.M. The role of vimentin intermediate filaments in the progression of lung cancer. *Am. J. Respir. Cell Mol. Biol.* **50**, 1-6 (2014).
196. Kalyanasundaram, A. *et al.* Fibroblast-specific proteo-transcriptomics reveal distinct fibrotic signatures of human sinoatrial node in non-failing and failing hearts. *Circulation* **144**, 126-143 (2022).
197. Ostrowska-Podhorodecka, Z., Ding, I., Norouzi, M. & McCulloch, C. A. Impact of Vimentin on Regulation of Cell Signaling and Matrix Remodeling. *Front. Cell Dev. Biol.* **10**, 1–15 (2022).
198. Morrow, C. S. *et al.* Vimentin Coordinates Protein Turnover at the Aggresome during Neural Stem Cell Quiescence Exit. *Cell Stem Cell* **26**, 558-568.e9 (2020).
199. Müller, M. *et al.* Dominant cataract formation in association with a vimentin assembly disrupting mutation. *Hum. Mol. Genet.* **18**, 1052–1057 (2009).
200. Matsuyama, M. *et al.* Defect of mitotic vimentin phosphorylation causes microphthalmia and cataract via aneuploidy and senescence in lens epithelial cells. *J. Biol. Chem.* **288**, 35626–35635 (2013).
201. Lee, S. Y. *et al.* Increased glial fibrillary acid protein and vimentin in vitreous fluid as a biomarker for proliferative vitreoretinopathy. *Investig. Ophthalmol. Vis. Sci.* **61**, (2020).
202. Su, L. X. *et al.* Vimentin modulates apoptosis and inflammatory cytokine release by a human monocytic cell line (THP-1) in response to lipopolysaccharides in vitro. *Chin. Med. J. (Engl).* **132**, 1336–1343 (2019).
203. Zhang, L. *et al.* Hypoxia induces epithelial-mesenchymal transition via activation of SNAI1 by hypoxia-inducible factor -1 $\alpha$  in hepatocellular carcinoma. *BMC Cancer* **13**, 1 (2013).
204. Menet, R., Bourassa, P., Calon, F. & ElAli, A. Dickkopf-related protein-1 inhibition attenuates amyloid-beta pathology associated to Alzheimer's disease. *Neurochem. Int.* **141**, 104881 (2020).
205. Sellers, K. J. *et al.* Amyloid  $\beta$  synaptotoxicity is Wnt-PCP dependent and blocked by fasudil. *Alzheimer's Dement.* **14**, 306–317 (2018).
206. Killick, R. *et al.* Clusterin regulates  $\beta$ -amyloid toxicity via Dickkopf-1-driven induction of the wnt-PCP-JNK pathway. *Mol. Psychiatry* **19**, 88–98 (2014).
207. Dun, Y. *et al.* Inhibition of the canonical Wnt pathway by Dickkopf-1 contributes to

- the neurodegeneration in 6-OHDA-lesioned rats. *Neurosci. Lett.* **525**, 83–88 (2012).
208. Ren, C. *et al.* The role of DKK1 in Alzheimer’s disease: A potential intervention point of brain damage prevention? *Pharmacol. Res.* **144**, 331–335 (2019).
  209. Chu, H. Y. *et al.* Dickkopf-1: A Promising Target for Cancer Immunotherapy. *Front. Immunol.* **12**, 1–14 (2021).
  210. Bauer, P. O. *et al.* ROCK-phosphorylated vimentin modifies mutant huntingtin aggregation via sequestration of IRBIT. *Mol. Neurodegener.* **7**, 1–12 (2012).
  211. Meekins, L. C. *et al.* Corneal endothelial cell migration and proliferation enhanced by rho kinase (ROCK) inhibitors in in vitro and in vivo models. *Investig. Ophthalmol. Vis. Sci.* **57**, 6731–6738 (2016).
  212. Kamao, H., Miki, A. & Kiryu, J. ROCK Inhibitor-Induced Promotion of Retinal Pigment Epithelial Cell Motility during Wound Healing. *J. Ophthalmol.* **2019**, (2019).
  213. Lin, L. *et al.* ROCK inhibitor modified intraocular lens as an approach for inhibiting the proliferation and migration of lens epithelial cells and posterior capsule opacification. *Biomater. Sci.* **7**, 4208–4217 (2019).
  214. Menet, R., Bourassa, P., Calon, F. & ElAli, A. Dickkopf-related protein-1 inhibition attenuates amyloid-beta pathology associated to Alzheimer’s disease. *Neurochem. Int.* **141**, 104881 (2020).
  215. Sellers, K. J. *et al.* Amyloid  $\beta$  synaptotoxicity is Wnt-PCP dependent and blocked by fasudil. *Alzheimer’s Dement.* **14**, 306–317 (2018).
  216. Hartmann, S., Ridley, A. J. & Lutz, S. The function of rho-associated kinases ROCK1 and ROCK2 in the pathogenesis of cardiovascular disease. *Front. Pharmacol.* **6**, 1–16 (2015).
  217. Lam, T. T., Kwong, J. M. K. & Tso, M. O. M. Early glial responses after acute elevated intraocular pressure in rats. *Investig. Ophthalmol. Vis. Sci.* **44**, 638–645 (2003).
  218. Danielsson, F., Peterson, M., Caldeira Araújo, H., Lautenschläger, F. & Gad, A. Vimentin Diversity in Health and Disease. *Cells* **7**, 147 (2018).
  219. Tsubota, A. *et al.* IQGAP1 and vimentin are key regulator genes in naturally occurring hepatotumorigenesis induced by oxidative stress. *Carcinogenesis* **31**, 504–511 (2010).
  220. Gartaganis, S. P., Patsoukis, N. E., Nikolopoulos, D. K. & Georgiou, C. D. Evidence for oxidative stress in lens epithelial cells in pseudoexfoliation syndrome. *Eye* **21**, 1406–1411 (2007).
  221. Oltulu, P. & Oltulu, R. The Association of Cataract and Lens Epithelial Cell Apoptosis in Patients with Pseudoexfoliation Syndrome The Association of Cataract and Lens Epithelial Cell Apoptosis in Patients with. *Curr. Eye Res.* **00**, 1–4 (2017).
  222. Dmuchowska, D. A. *et al.* Metabolomics Reveals Differences in Aqueous Humor Composition in Patients With and Without Pseudoexfoliation Syndrome. *Front. Mol. Biosci.* **8**, 1–9 (2021).
  223. Vilaboa, N. E. *et al.* Heat-shock and cadmium chloride increase the vimentin mRNA and protein levels in U-937 human promonocytic cells. *J. Cell Sci.* **110**, 201–207

- (1997).
224. Zhang, L. *et al.* MicroRNA-30a Regulation of Epithelial-Mesenchymal Transition in Diabetic Cataracts Through Targeting SNAI1. *Sci. Rep.* **7**, 1–8 (2017).
  225. Levin, E. C. *et al.* Neuronal expression of vimentin in the Alzheimer's disease brain may be part of a generalized dendritic damage-response mechanism. *Brain Res.* **1298**, 194–207 (2009).
  226. Tapia-Rojas, C., Burgos, P. V. & Inestrosa, N. C. Inhibition of Wnt signaling induces amyloidogenic processing of amyloid precursor protein and the production and aggregation of Amyloid- $\beta$  (A $\beta$ )42 peptides. *Journal of Neurochemistry* vol. 139 (2016).
  227. Chakraborty, M., Sahay, P. & Rao, A. Primary human trabecular meshwork model for pseudoexfoliation. *Cells* **10**, (2021).
  228. Holmes, B. B. & Diamond, M. I. Cellular mechanisms of protein aggregate propagation. *Curr. Opin. Neurol.* **25**, 721–726 (2012).
  229. Wei, L., Surma, M., Shi, S., Lambert-Cheatham, N. & Shi, J. Novel Insights into the Roles of Rho Kinase in Cancer. *Archivum Immunologiae et Therapiae Experimentalis* vol. 64 259–278 (2016).
  230. Abe, H. *et al.* The Rho-kinase inhibitor HA-1077 suppresses proliferation/migration and induces apoptosis of urothelial cancer cells. *BMC Cancer* **14**, (2014).
  231. Waki, M., Yoshida, Y., Oka, T. & Azuma, M. Reduction of intraocular pressure by topical administration of an inhibitor of the Rho-associated protein kinase. *Curr. Eye Res.* **22**, 470–474 (2001).
  232. Zhong, Y. *et al.* The interaction of Lin28A/Rho associated coiled-coil containing protein kinase2 accelerates the malignancy of ovarian cancer. *Oncogene* **38**, 1381–1397 (2019).
  233. Bai, Y., Sha, J. & Kanno, T. The role of carcinogenesis-related biomarkers in the wnt pathway and their effects on epithelial–mesenchymal transition (EMT) in oral squamous cell carcinoma. *Cancers (Basel)*. **12**, (2020).
  234. Choi, S. H. *et al.* Dickkopf-1 induces angiogenesis via VEGF receptor 2 regulation independent of the Wnt signaling pathway. *Oncotarget* **8**, 58974–58984 (2017).
  235. Li, B. *et al.* Relationship between the altered expression and epigenetics of GSTM3 and age-related cataract. *Investig. Ophthalmol. Vis. Sci.* **57**, 4721–4732 (2016).
  236. Chen, J. *et al.* Aberrant Epigenetic Alterations of Glutathione-S-Transferase P1 in Age-Related Nuclear Cataract. *Curr. Eye Res.* **42**, 402–410 (2017).
  237. Shrishrimal, S., Kosmacek, E. A. & Oberley-Deegan, R. E. Reactive Oxygen Species Drive Epigenetic Changes in Radiation-Induced Fibrosis. *Oxid. Med. Cell. Longev.* **2019**, (2019).
  238. Valinluck, V. *et al.* Oxidative damage to methyl-CpG sequences inhibits the binding of the methyl-CpG binding domain (MBD) of methyl-CpG binding protein 2 (MeCP2). *Nucleic Acids Res* **32**, 4100–4108 (2004).
  239. Weitzman, S. A., Turk, P. W., Milkowski, D. H. & Kozlowski, K. Free radical adducts

- induce alterations in DNA cytosine methylation. *Proc. Natl. Acad. Sci. U. S. A.* **91**, 1261–1264 (1994).
240. Liu, A. *et al.* Low expression of GSTP1 in the aqueous humour of patients with primary open-angle glaucoma. *J. Cell. Mol. Med.* **25**, 3063–3079 (2021).
  241. Lee, W. H., Joshi, P. & Wen, R. Glutathione S-transferase pi isoform (GSTP1) expression in murine retina increases with developmental maturity. *Adv. Exp. Med. Biol.* **801**, 23–30 (2014).
  242. Zhu, X., Li, D., Du, Y., He, W. & Lu, Y. DNA hypermethylation-mediated downregulation of antioxidant genes contributes to the early onset of cataracts in highly myopic eyes. *Redox Biol.* **19**, 179–189 (2018).
  243. Chen, J. *et al.* Aberrant Epigenetic Alterations of Glutathione-S-Transferase P1 in Age-Related Nuclear Cataract. *Curr. Eye Res.* **42**, 402–410 (2017).
  244. Birben, E., Sahiner, U. M., Sackesen, C., Erzurum, S. & Kalayci, O. Oxidative stress and antioxidant defense. *World Allergy Organ. J.* **5**, 9–19 (2012).
  245. Wang, T., Arifoglu, P., Ronai, Z. & Tew, K. D. Glutathione S-transferase P1-1 (GSTP1-1) Inhibits c-Jun N-terminal Kinase (JNK1) Signaling through Interaction with the C Terminus. *J. Biol. Chem.* **276**, 20999–21003 (2001).
  246. Tew, K. D. & Townsend, D. M. Regulatory functions of glutathione S-transferase P1-1 unrelated to detoxification. *Drug Metab. Rev.* **43**, 179–193 (2011).
  247. Hadami, K. *et al.* Evaluation of glutathione S-transferase pi 1 expression and gene promoter methylation in Moroccan patients with urothelial bladder cancer. *Mol. Genet. Genomic Med.* **6**, 819–827 (2018).
  248. Krishnamoorthy, L., Shilpa, V., Bhagat, R., Premalata, C. & Pallavi, V. GSTP1 expression and promoter methylation in epithelial ovarian carcinoma. *Clin. Cancer Investig. J.* **3**, 487 (2014).
  249. Li, Q. F., Li, Q. Y., Gao, A. R. & Shi, Q. F. Correlation between promoter methylation in the GSTP1 gene and hepatocellular carcinoma development: A meta-analysis. *Genet. Mol. Res.* **14**, 6762–6772 (2015).
  250. Fang, C. *et al.* Aberrant GSTP1 promoter methylation is associated with increased risk and advanced stage of breast cancer: A meta-analysis of 19 case-control studies. *BMC Cancer* **15**, 4–11 (2015).
  251. Li, Y., Cai, Y., Chen, H. & Mao, L. Clinical significance and association of GSTP1 hypermethylation with hepatocellular carcinoma: A meta-analysis. *J. Cancer Res. Ther.* **14**, S486–S489 (2018).
  252. Martignano, F. *et al.* GSTP1 Methylation and Protein Expression in Prostate Cancer: Diagnostic Implications. *Dis. Markers* **2016**, (2016).
  253. Chan, Q. K. Y. *et al.* Promoter methylation and differential expression of  $\pi$ -class glutathione S-transferase in endometrial carcinoma. *J. Mol. Diagnostics* **7**, 8–16 (2005).
  254. Zhang, L. *et al.* piR-31470 epigenetically suppresses the expression of glutathione S-transferase pi 1 in prostate cancer via DNA methylation. *Cell. Signal.* **67**, 109501

- (2020).
255. Schnekenburger, M., Karius, T. & Diederich, M. Regulation of epigenetic traits of the glutathione S-transferase P1 gene: From detoxification toward cancer prevention and diagnosis. *Front. Pharmacol.* **5**, 1–7 (2014).
  256. Lo, H.W. *et al.* Identification and functional characterization of the human glutathione-S-transferase P1 gene as a novel transcriptional target of the p53 tumor suppressor gene. *Mol. Cancer Res.* **6**, 843–850 (2008).
  257. Karius, T. *et al.* Reversible epigenetic fingerprint-mediated glutathione-S-transferase P1 gene silencing in human leukemia cell lines. *Biochem. Pharmacol.* **81**, 1329–1342 (2011).
  258. Ahlemann, M. *et al.* Overexpression Facilitates mTOR-dependent Growth Transformation. *Mol. Carcinog.* **967**, 957–967 (2006).
  259. Uchida, Y. *et al.* MiR-133a induces apoptosis through direct regulation of GSTP1 in bladder cancer cell lines. *Urol. Oncol. Semin. Orig. Investig.* **31**, 115–123 (2013).
  260. Coles, B. F. & Kadlubar, F. F. Detoxification of electrophilic compounds by glutathione S-transferase catalysis: Determinants of individual response to chemical carcinogens and chemotherapeutic drugs? *BioFactors* **17**, 115–130 (2003).
  261. Sangal, N. & Chen, T. C. Cataract surgery in pseudoexfoliation syndrome. *Semin. Ophthalmol.* **29**, 403–408 (2014).
  262. Cheng, S. *et al.* Adult-onset demyelinating neuropathy associated with FBLN5 gene mutation. *Clin. Neuropathol.* **36**, 171–177 (2017).
  263. Jung, H. J. *et al.* Changes in expression of fibulin-5 and lysyl oxidase-like 1 associated with pelvic organ prolapse. *Eur. J. Obstet. Gynecol. Reprod. Biol.* **145**, 117–122 (2009).
  264. Janig, E. *et al.* Clusterin associates with altered elastic fibers in human photoaged skin and prevents elastin from ultraviolet-induced aggregation in vitro. *Am. J. Pathol.* **171**, 1474–1482 (2007).
  265. Wong, P. *et al.* Increased TRPM-2/clusterin mRNA levels during the time of retinal degeneration in mouse models of retinitis pigmentosa. *Biochem. Cell Biol.* **72**, 439–446 (1994).
  266. Jones, S. E., Meerabux, J. M. A., Yeats, D. A. & Neal, M. J. Analysis of differentially expressed genes in retinitis pigmentosa retinas Altered expression of clusterin mRNA. *FEBS Lett.* **300**, 279–282 (1992).
  267. Can Demirdöğen, B., Demirkaya-Budak, S., Özge, G. & Mumcuoğlu, T. Evaluation of Tear Fluid and Aqueous Humor Concentration of Clusterin as Biomarkers for Early Diagnosis of Pseudoexfoliation Syndrome and Pseudoexfoliative Glaucoma. *Curr. Eye Res.* **45**, 805–813 (2020).
  268. Lüdemann, L., Grieger, W., Wurm, R., Wust, P. & Zimmer, C. Glioma assessment using quantitative blood volume maps generated by T1-weighted dynamic contrast-enhanced magnetic resonance imaging: A receiver operating characteristic study. *Acta radiol.* **47**, 303–310 (2006).

269. Tests, D. Basic Principles of ROC Analysis. *Semin. Nucl. Med.* **VIII**, 283–298 (1978).
270. Kondkar, A. A. *et al.* Elevated levels of plasma tumor necrosis factor alpha in patients with pseudoexfoliation glaucoma. *Clin. Ophthalmol.* **12**, 153–159 (2018).
271. Can Demirdögen, B., Koçan Akçin, C., Özge, G. & Mumcuoğlu, T. Evaluation of tear and aqueous humor level, and genetic variants of connective tissue growth factor as biomarkers for early detection of pseudoexfoliation syndrome/glaucoma. *Exp. Eye Res.* **189**, 107837 (2019).
272. Schlötzer-Schrehardt, U., Zenkel, M., Kuchle, M., Sakai, L. Y. & Naumann, G. O. H. Role of transforming growth factor- $\beta$ 1 and its latent form binding protein in pseudoexfoliation syndrome. *Exp. Eye Res.* **73**, 765–780 (2001).
273. Zenkel, M. *et al.* Proinflammatory cytokines are involved in the initiation of the abnormal matrix process in pseudoexfoliation syndrome/glaucoma. *Am. J. Pathol.* **176**, 2868–2879 (2010).
274. Ho, S. L. *et al.* Elevated aqueous humour tissue inhibitor of matrix metalloproteinase-1 and connective tissue growth factor in pseudoexfoliation syndrome. *Br. J. Ophthalmol.* **89**, 169–173 (2005).
275. Ahoor, M. H., Ghorbanihaghjo, A., Sorkhabi, R. & Kiavar, A. Klotho and endothelin-1 in pseudoexfoliation syndrome and glaucoma. *J. Glaucoma* **25**, 919–922 (2016).
276. Frescas, D. *et al.* Senescent cells expose and secrete an oxidized form of membrane-bound vimentin as revealed by a natural polyreactive antibody. *Proc. Natl. Acad. Sci. U. S. A.* **114**, E1668–E1677 (2017).
277. Mor-Vaknin, N., Punturieri, A., Sitwala, K. & Markovitz, D. M. Vimentin is secreted by activated macrophages. *Nat. Cell Biol.* **5**, 59–63 (2003).
278. Yu, Z. *et al.* Differences between human plasma and serum metabolite profiles. *PLoS One* **6**, 1–6 (2011).
279. Yavrum, F., Elgin, U., Kocer, Z. A., Fidanci, V. & Sen, E. Evaluation of aqueous humor and serum clusterin levels in patients with glaucoma. *BMC Ophthalmol.* **21**, 1–7 (2021).
280. Pasutto, F. *et al.* Pseudoexfoliation syndrome-associated genetic variants affect transcription factor binding and alternative splicing of LOXL1. *Nat. Commun.* **8**, (2017).
281. He, L., Loika, Y. & Kulminski, A. M. Allele-specific analysis reveals exon- and cell-type-specific regulatory effects of Alzheimer’s disease-associated genetic variants. *Transl. Psychiatry* **12**, (2022).
282. Han, S., Nho, K. & Lee, Y. Alternative splicing regulation of an Alzheimer’s risk variant in CLU. *Int. J. Mol. Sci.* **21**, 1–8 (2020).
283. Lotery, A. J. *et al.* Reduced secretion of fibulin 5 in age-related macular degeneration and cutis laxa. *Hum. Mutat.* **27**, 568–574 (2006).
284. Woody, S. K. & Zhao, L. Clusterin (APOJ) in Alzheimer’s Disease: An Old Molecule with a New Role. in *Update on Dementia* (InTech, 2016). doi:10.5772/64233.
285. He, J. *et al.* Glomerular clusterin expression is increased in diabetic nephropathy and

protects against oxidative stress-induced apoptosis in podocytes. *Sci. Rep.* **10**, 1–11 (2020).

286. Güven, M. *et al.* Glutathione S-transferase M1, GSTT1 and GSTP1 genetic polymorphisms and the risk of age-related macular degeneration. *Ophthalmic Res.* **46**, 31–37 (2011).

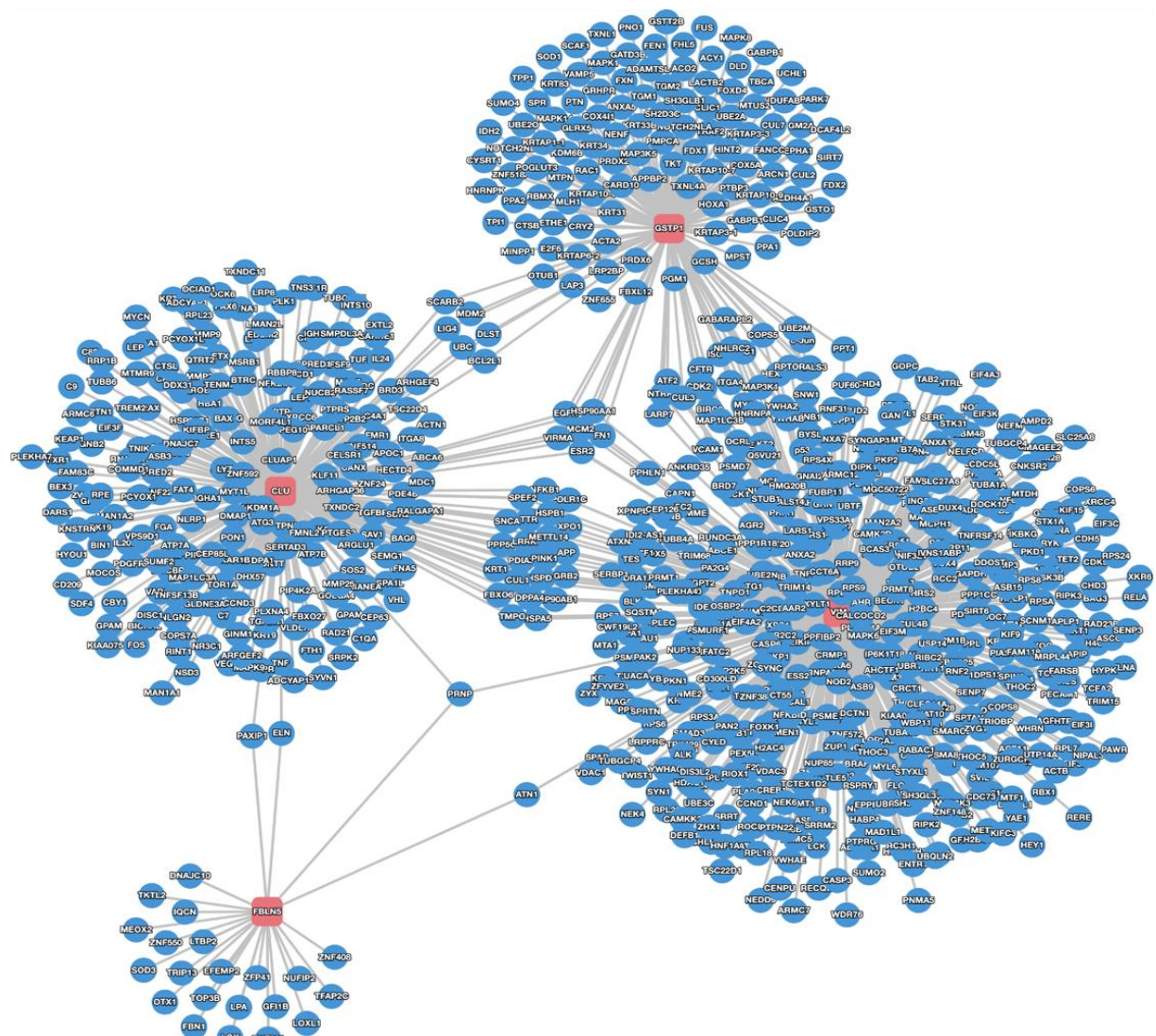
\*\*\*\*\*

## APPENDIX-I

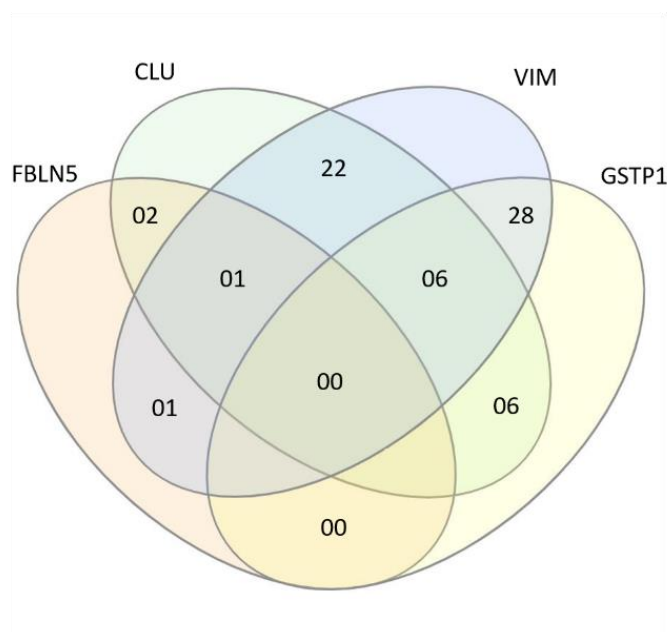
This appendix has no reference in the text.

### Network analysis between CLU, FBLN5, GSTP1 and VIM

To understand the interaction between the four candidate proteins, CLU, FBLN5, GSTP1 and VIM, a network analysis was done using the PINA (Protein Interaction Network Analysis) platform. Common interactors were identified for the proteins. All the four proteins did not have a common interactor. However, common interactors for two or more of the candidate proteins were identified.



The below chart shows the number of interactors between the proteins.



These interactors are listed in the below table.

Candidate Proteins	No. of interactors	Interactors	
		Symbol	Protein
CLU-FBLN5	02	ELN PAXIP1	Elastin PAX-interacting Protein 1
CLU-VIM	22	APP CUL1 DPPA-4 FBXO6 GRB2 HSP90AB1 HSPA5 HSPB1 HSPD1 KRT1 LRRK2 METTL14  NFKB1 PDIA3 PINK1 POLR1C PPP5C	Amyloid-beta precursor protein Cullin-1 Developmental pluripotency-associated protein 4 F-box only protein 6 Growth factor receptor-bound protein 2 Heat shock protein HSP 90-beta Endoplasmic reticulum chaperone BiP Heat shock protein beta-1 60 kDa heat shock protein, mitochondrial Keratin, type II cytoskeletal 1 Leucine-rich repeat serine/threonine-protein kinase 2 N6-adenosine-methyltransferase non-catalytic subunit Nuclear factor NF-kappa-B p105 subunit Protein disulfide-isomerase A3 Serine/threonine-protein kinase PINK1 DNA-directed RNA polymerases I and III subunit RPAC1 Serine/threonine-protein phosphatase 5

		SNCA SPEF2 TMPO TTR XPO1	Alpha-synuclein Sperm flagellar protein 2 Lamina-associated polypeptide 2, isoform alpha Transthyretin Exportin-1
CLU-GSTP1	06	BCL2L1 DLST  LIG4 MDM2 SCARB2 UBC	Bcl-2-like protein 1 Dihydrolipoyllysine-residue succinyltransferase component of 2-oxoglutarate dehydrogenase complex DNA Ligase 4 E3 ubiquitin-protein ligase Mdm2 Lysosome membrane protein 2 Polyubiquitin-C
FBLN5-VIM	01	ATN1	Atrophin-1
FBLN5-GSTP1	00	-	-
GSTP1-VIM	28	ATF2 BIRC3 CDK2 CFTR COPS5 CUL3 ENO1 GABARAPL 2 HEXIM1 HNRNFN ISG15 ITGA4 LARP7 LGALS3 MAP1LC3B  MAP3K1 MYC NHLRC2 NTRK1 PPT1 PRKN RPTOR TXN UBE2M VCAM1 YWHAB YWHAZ c-Jun	Cyclic AMP-dependent transcription factor ATF-2 Baculoviral IAP repeat-containing protein 3 Cyclin-dependent kinase 2 Cystic fibrosis transmembrane conductance regulator COP9 signalosome complex subunit 5 Cullin-3 Alpha-enolase Gamma-aminobutyric acid receptor-associated protein-like 2 Protein HEXIM1 Heterogeneous nuclear ribonucleoprotein A1 Ubiquitin-like protein ISG15 Integrin alpha-4 La-related protein 7 Galectin-3 Microtubule-associated proteins 1A/1B light chain 3B Mitogen-activated protein kinase kinase kinase 1 Myc proto-oncogene protein NHL repeat-containing protein 2 High affinity nerve growth factor receptor Palmitoyl-protein thioesterase 1 E3 ubiquitin-protein ligase parkin Regulatory-associated protein of mTOR Thioredoxin NEDD8-conjugating enzyme Ubc12 Vascular cell adhesion protein 1 14-3-3 protein beta/alpha 14-3-3 protein zeta/delta Transcription factor AP-1
CLU-FBLN5-VIM	01	PRNP	Major prion protein
CLU-GSTP1-	06	EGFR	Epidermal growth factor receptor

VIM		ESR2 FN1 HSP90AA1 MCM2 VIRMA	Estrogen receptor beta Fibronectin Heat shock protein HSP 90-alpha DNA replication licensing factor MCM2 Protein virilizer homolog
FBLN5- GSTP1-VIM	00	-	-
CLU-FBLN5- GSTP1-VIM	00	-	-

\*\*\*\*\*